Print edition ISSN 2615-5109
Electronic edition ISSN 2621-0541

Publisher:
Center of Technology, Fakultas Teknik, Universitas Hasanuddin

Address:
Engineering Faculty Campus, Hasanuddin University
Jl. Poros Malino km. 6, Bontomarannu
Kabupaten Gowa, Sulawesi Selatan, Indonesia, 92171
Email : epi-ije@unhas.ac.id
Website : cot.unhas.ac.id/journals/index.php/epiije
Telp/Fax : +62-(0)411-58601

EPI International Journal of Engineering

Foreword

We are pleased and delighted that we can present the EPI International Journal of Engineering (EPI-IJE) Volume 3 Number 2 August 2020. This edition is the second edition that we publish since the journal has been successfully accredited by the Ministry of Research and Technology/BRIN. The editorial team has always performed improvement in terms of management and manuscript content quality in order to pursue a higher accreditation level in the near future.

In this edition, 16 manuscripts are published which are divided into 6 topic categories. The first topic category is geology and mining engineering with 2 manuscripts. The first manuscript in this category studied the revenue estimation based on coal reference prediction at a mining company in East Kalimantan Province and the second manuscript investigated the petrophysical characterization of shale gas reservoirs in the Lower Indus Basin, Pakistan.

The second topic category is civil and environmental engineering which also contains 2 manuscripts. The first manuscript performed effluent quality enhancement on an anaerobic baffled reactor (ABR) with ozone and aerobic activated sludge for livestock wastewater treatment while the second manuscript conducted testing on nutmeg shells to produce a lightweight concrete material in terms of volume weight and compressive strength. The third topic category which is electrical and informatics engineering also has 2 manuscripts. They are about monitoring and predicting water quality in swimming pools and IoT based environmental surveillance network using 6 monopole elements array intelligent antennas.

The fourth topic which is mechanical and industrial engineering contains three manuscripts. The manuscripts in this category discussed construction and analysis of plastic extruder machine, utilization of gasoline fuel as an alternative fuel, and performance of a solar water heating system. In the fifth category which is naval architecture, ocean, and marine engineering, one manuscript conducted a study on beach sand filtrate as alternative gas fuel, 3 manuscripts are related to ships and submarine hull form and the last manuscript presented a study on the investment feasibility of a fishing boat.

The last topic category is architecture and urban & regional development engineering which contains 2 manuscripts. The first manuscript analyzed factors related to visitors' experience of orientation and disorientation at MTC Karebosi, Makassar while the last manuscript studied the performance of floating house substructure in Tempe Lake.

We are again deeply grateful for the manuscript contribution of all authors in this edition. Lastly, we also thank all people and institutions for the supports for the publication of this edition, including the continuous support from Prof. Yoshihiro Narita. We hope that the excellent manuscripts published in this edition could promote the development in the cutting-edge of science and technology.

Warm regards,

Prof. Baharuddin Hamzah
Editor-in-Chief of EPI-IJE

TABLE OF CONTENTS

EPI International Journal of Engineering
Volume 3, Number 2, August 2020, pp. 95-102
DOI: 10.25042/epi-ije.082020.01

*p*ISSN 2615-5109
*e*ISSN 2621-0541

Revenue Estimation of Pit Seam 14 Quarter Mine Block Sequence Design Based on Coal Reference Price Prediction at PT Alam Jaya Pratama, East Kalimantan Province

Rahmat Hidayat[a,*], Aryanti Virtanti Anas[b], Rizki Amalia[c], Muhammad Ramli[d], Nirmana Fiqra Qaidahiyani[e], Yoga Apri Disetia[f]

[a]Department of Mining Engineering, Engineering Faculty, Hasanuddin University. Email: rahmat_26@outlook.com
[b]Department of Mining Engineering, Engineering Faculty, Hasanuddin University. Email:aryantiv@unhas.ac.id
[c]Department of Mining Engineering, Engineering Faculty, Hasanuddin University. Email:rizkiamalia@unhas.ac.id
[d]Department of Mining Engineering, Engineering Faculty, Hasanuddin University. Email:ramli@unhas.ac.id
[e]Department of Mining Engineering, Engineering Faculty, Hasanuddin University. Email:nirmana.fiqra.q@unhas.ac.id
[f]Mine Planning Department, PT Alam Jaya Pratama, East Kalimantan Province.

Abstract

Seam 14 is one of coal prospects owned by PT Alamjaya Bara Pratama (PT ABP) with an estimated coal resources of ±4,022,458.63 tons which is will be produced in 2020 so that required a pit and mine sequence design used as a guideline in carrying out coal production activities. On the other hand, the uncertainty of coal prices caused the mine sequence design to be evaluated within a certain time as the coal reference price (HBA) was altered and company's production target. The model equation of coal reference price prediction in 2020 was carried out by using multiple linear regression method. Based on that model, prediction of coal reference price was obtained in CW 1 = $80.21, CW 2 = $81.47 and CW 3 = $82.50. The Pit 14 was designed with the consideration of company's geotechnical recommendation which is can be achieved on the conditions of stripping ratio (SR) of 6 and 7. The mine sequence was designed base on the evaluation of coal production in 2019 (CW 1 = SR > 3, CW 2 = 3 ≤ SR ≤ 6 and CW 3 = SR > 6). The calculation results of estimated revenue of Pit 14 with SR = 6 is CW 1 = US$40,131,297.12; CW 2 = US$36,431,457.31; and CW 3 = US$19,601,965.40. Estimated revenue of Pit 14 with SR = 7 is CW 1 = US$41,821,080.50; CW 2 = US$39,204,128.39; and CW 3 = US$31,715,767.60.

Keywords: Coal; coal getting; mine sequence; multiple linear regression; stripping ratio

1. Introduction

Seam 14 is one of the coal prospects owned by PT ABP with a large volume of resources which is estimated at 4,022,458.63 ton and will begin his production in 2020 thus it need a pit design that is used as a guidelines in carrying out that coal production activities [1]. The geometry of a pit design generally influenced by factors such as spatial characteristics of coal deposits, actual topography, geometry of safe slopes, and rates of profit in relation to the used value of stripping ratio (SR) [2].

Natural factors such as geological conditions (spatial deposits and geotechnical characteristics) are factors that occur beyond human control so that when designing the pit must adjust to that condition. On the other hand, the value stripping ratio was influenced by two main factors, namely amount of cost to be incurred to peel top soil and overburden and the coal reference price. The cost of mining operations is a factor that can be controlled by every mining company, but the magnitude of the coal price depends on global market conditions. In the last few years, coal price performance in global markets tends to fluctuate as coal demand decreases due to economic retarding in China, other Asian countries and Europe. In addition, increased coal production in South Africa, Colombia and Indonesia caused surplus coal stocks in global markets to increase [3].

Price prediction is an integral part of economic decision making. Specifically, somebody can use predictions to try to earn optimal income from speculative activities, determine optimal government policies, or to make business decisions [4].

Multiple linear regression model is one of the common methods used by academics in making a prediction model. Regression analysis relates to the study of the dependence of a variable called dependent variable on one or more variables (independent variables). Regression analysis aims to estimate and or predict the average value of the dependent variable if the value of the explaining variable is known [5].

The uncertainty of the coal price in the global market and the world economic conditions that have not been stable cause mining companies, especially in Indonesia,

*Corresponding author.
Jalan Poros Malino km. 6 Bontomarannu
Gowa, Indonsia 92171

difficult to choose the coal reference price as an input in designing a pit. On the other hand, coal price is one of the factors that need to be considered in determining the value of breakeven stripping ratio (BESR) as it can lead to the pit design which is made in the beginning of production year should be evaluated same as the mine sequence design also need to be evaluated in line with the change of coal price.

The prediction of coal reference price (HBA) is one of the solutions that can be done to get the approach value of coal reference price (HBA) in the future. Therefore, this research is done to predict the approach value of coal reference price (HBA) which can be used as consideration in determining the magnitude of break even stripping ratio (BESR), create a pit design of seam 14 coal prospects, create a block sequence design based on PT ABP coal production in 2019 and estimate the revenue of each sequence based on the coal reference price prediction.

2. Research Methods

Broadly, the research was conducted in three main phases, which is to predict the coal reference price using the econometrics model of multiple linear regression where the predicted result was used in calculating the break even stripping ratio (BESR), create a pit design with consideration of company's geotechnical recommendations, create mine block sequences design based on PT ABP coal production in 2019 and estimate the revenue of each sequence based on the coal reference price prediction.

2.1. Data collection

The coal reference price (HBA) prediction is done by using multiple linear regression models, the pit design and mine block sequences of coal mining requires some data to get the research activities can be done properly.

2.1.1. Coal reference price prediction data

Type of data that was used in predicting the coal reference price (HBA) by using the multiple linear regression is time series data, namely:

1. Coal Reference Price
   The coal reference price was issued monthly by the Ministry of Energy and Mineral Resources of the Republic of Indonesia. Coal reference price data in the time span of January 2009 until March 2019 was used in this research.
2. WTI Crude Oil Price
   The WTI crude oil price was derived from www.investing.com which provides information about the movement and magnitude of WTI coal price periodically. WTI crude oil price data in the time span of January 2009 until March 2019 was used in this research.
3. Coal Consumption for Electricity Generation
   The coal consumption was obtained from the monthly report issued by the U.S. Energy Information Administration. Coal consumption data in the time span of January 2009 until March 2019 was used in this research.
4. Renewable Energy Consumption
   The renewable energy consumption was obtained from the monthly report issued by the U.S. Energy Information Administration. Renewable energy consumption data in the time span of January 2009 until March 2019 was used in this research.
5. Natural Gas Price
   The natural gas price was derived from www.investing.com which provides information about the movement and magnitude of natural gas price periodically. Natural gas price data in the time span of January 2009 until March 2019 was used in this research.
6. Exchange Rate of Rupiah Against US Dollar
   The exchange rate was updated periodically by the Ministry of Trade of the Republic of Indonesia. Exchange rate data in the time span of January 2009 until March 2019 was used in this research.
7. Oil and Gas Commodity Price Projection for 2020 - 2025
   Oil and gas commodity price projection data was obtained from www.pubdocs.worldbank.com which is that website belongs to World Bank Institution.

2.1.2. Pit and mine block sequence design data

The required data in designing of pit and mine block sequence, namely:

1. Geological Drilling
   The geological drilling data was used in geological modelling of coal deposits (gridded seam model). Geological drilling data was obtained from the Geological Division of PT ABP.
2. Actual Topography Survey
   The actual topography survey is a data that indicating the changes of the topographical condition along with the mine progress in certain periods. Actual topography survey data was obtained from the Civil Engineering Division of PT ABP.
3. Bench Geometry Recommendation
   The bench geometry recommendation was issued by the Geotechnical Division of PT ABP based on geotechnical studies that was conducted in seam 14 coal prospects area. The recommended geometry is:
   a. Single slope angle (high wall) : 60º
   b. Bench width (high wall) : 5 meter
   c. Bench height (high wall) : 10 meter
   d. Maximum request level (RL) : 50 meter
   e. Overall slope angle (low wall) : 20º (based on seam 14 dip which is plan to be the pit floor)
   f. Ramp width : Based on Komatsu HD-785 dimension.
4. Mining Equipment Specification
   The largest mining equipment that will be used in seam 14 coal prospects area was the Komatsu HD-785 with the detail specification is written in the Komatsu Specification Handbook of HD-785.
5. Mining Operational Costs
   The mining operational costs was obtained from the Directorate General of Mineral and Coal of the Republic of Indonesia which was contained in the Kepdirjen Minerba No. 579.K/32/DJB/2015. Mining operational costs can be seen in Table 1.

Table 1. Mining operational costs

Costs Type	Description	Units	Costs Amount	Planned Costs
Direct Production Costs	Overburden Removal	US$/bcm	2.41	2.41
	Overburden Hauling	US$/ton/km	1.74	3.48
	Coal Getting	US$/ton	1.70	1.70
	Coal Transportation to the coal processing plant location	US$/ton/km	0.28	2.52
Indirect Production Costs	Coal Processing	US$/ton	1.98	1.98
	Amortization, land acquisition or land replacement and depreciation	US$/ton	6.88	6.88
General and Administration Costs	A. Utilization, management of reclamation and post-mining environments	US$/ton	0.55	0.55
	B. Occupational Health and Safety			
	C. Community Development			
	Overhead	US$/ton	2.07	2.07
	Fixed Dues	US$/ton	0.11	0.11
	Royalty	US$/ton	20.3%	4.41
	Margin	US$/ton	25%	6.53

2.2. Data processing and analysis

Data processing and analysis was conducted in the Mine Planning and Valuation Laboratory, Mining Engineering Department, Hasanuddin University. The data processing and analysis is done by using the Eviews 9 in creating the econometrics model of multiple linear regression to predict the coal reference price (HBA), MineScape 5.7 is use in designing the pit and block sequence, and Microsoft Excel 2010 is use in further output data processing from Eviews 9 and MineScape 5.7. The research stages are:

1. Creating an Econometric Model of Coal Reference Price Prediction
   Prediction of the coal reference price was carried out by using econometrics model of multiple linear regression. Coal reference price prediction equation was obtained from Eviews 9.
2. Econometric Model Validation of Coal Reference Price Prediction
   The validation of econometric model was carried out by using the Mean Absolute Percentage Error (MAPE) test.
3. Pit Limit Design
   The pit limit was designed base on company's geotechnical recommendation. MineScape 5.7 was used in designing the pit limit.
4. Pit Design
   Pit design was created based on geotechnical recommendation and ramp width calculation in straight and corner condition. MineScape 5.7 was used in designing the pit.
5. Calculation of Mineable Reserve
   The number of mineable reserve was obtained from the intersection of pit design and actual topography. The calculation was performed by using Microsoft Excel 2010.
6. Quarter Mine Block Sequence Design
   The quarter mine block sequence design was created base on evaluation of PT ABP coal production in 2019. Block sequence design was carried out by using MineScape 5.7.
7. Revenue Estimation of Quarter Mine Block Sequence
   Revenue estimation was calculated by multiplying the coal getting of pit design with coal reference price prediction using Microsoft Excel 2010.

3. Research Results

3.1. Multiple linear regression model and coal reference price prediction

Econometric model of multiple linear regression was obtained by interpreting the estimated outcome of the equation model generated by Eviews 9 (Table 2). The multiple linear regression equation model was used to perform the coal reference price prediction.

Before interpreting the equation of coal reference price prediction, previously the multiple linear regression need to be tested by the classic assumption test which is consists of normality test, heteroscedasticity test, multicollinearity test, autocolleration test, t-test, F-test, and coefficient determination test.

3.1.1. Normality test

Based on histogram of the models that shows a form like a bell and the value of Probability Jarque-Bera > 0.05 (α) (Fig. 1) it can be concluded that the model was distributed normally.

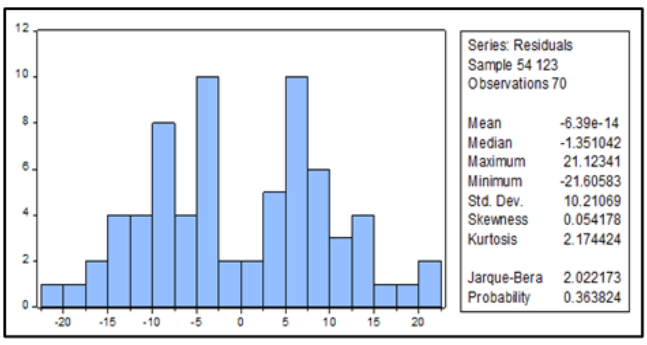

Figure 1. Histogram of econometric model

Table 2. Multiple linear regression model results

Variable	Coefficient	Std. Error	t-Statistic	Prob.
C	-164.5968	33.15924	-4.96383	0
NG	4.896968	2.915754	1.67949	0.0979
ERC	0.089055	0.019398	4.59107	0
ER	0.008979	0.001875	4.78846	0
COP	0.498939	0.108657	4.59187	0
CC	-1.45E-05	0.000153	-0.09477	0.9248
R-squared	0.601396	*Mean dependent var*		76.9076
Adjusted R-squared	0.570255	*S.D. dependent var*		16.1728
S.E. of regression	10.60204	*Akaike info criterion*		7.64179
Sum squared resid	7193.814	*Schwarz criterion*		7.83452
Log likelihood	-261.4625	*Hannan-Quinn criter.*		7.71834
F-statistic	19.31208	*Durbin-Watson stat*		0.45434
Prob(F-statistic)	0			

Table 3. Glejser heteroskedasticity test result

Heteroskedasticity Test: Glejser			
F-statistic	0.526809	*Prob. F(5,64)*	0.7551
*Obs*R-squared*	2.767102	*Prob.Chi-Square(5)*	0.7358
Scaled explained SS	1.719221	*Prob Chi-Square(5)*	0.8865

Table 4. VIF test result

Variable	Coefficient Variance	Uncentered VIF	Centered VIF
C	1099.535	684.7437	NA
NG	8.501624	55.27376	2.591778
ERC	0.000376	178.5108	1.592015
ER	3.52E-06	377.9009	2.499943
COP	0.011806	33.58642	3.373953
CC	2.35E-08	55.08977	2.007341

3.1.2. Heteroskedasticity test

Heteroskedasticity test was carried out by using Glejser Test (Table 3), it shows that the value of Probability F-Statistic is 0.7551 which is greater than 0.05 (α) thus it can be concluded that the model has no heteroscedasticity symptoms.

3.1.3. Multicollinearity test

Generally, the statisctic tool that was used to find out the multicollinearity symptomps in econometric model is variance inflation factor (VIF). Based on Table 4, it shows that the value of Centered VIF from all of the variable in model was lower than 10 so it can be concluded that there is no multicollinearity symptomps.

3.1.4. Autocolleration test

Autocolleration test can be done by using the Durbin-Watson Test, the criteria that used in making the decision from Durbin-Watson Test is:

1) D-W < -2 : Positive Autocolleration
2) D-W > +2 : Negative Autocolleration
3) 2 < D-W < +2 : No Autocolleration

Based on Table 2, it shows that the value of Durbin Watson Statistic is 0.45434 so it can be concluded that there is no autocolleration symptomps because the value of D-W Statistic had been meet the third criteria of Durbin Watson Test.

3.1.5. F test

The aim of F test is to find out the influence proportion of independent variable which is used in constructing econometric model simultaneously to the dependent variable. Based on Table 2, it shows that the value of Probability F-Statistic is 0 which is lower than 0.05 (α) thus it can be concluded that all the independent variable in equation model simultaneously influenced the dependent variable.

3.1.6. t test

The aim of F test is to find out the influence proportion of independent variable which is used in constructing econometric model partially to the dependent variable. Based on Table 2, it shows that almost all of the independent variable has value of t-Statistic lower than 0.05 (α) which is influenced the value of dependent variable partially except for natural gas and coal consumption.

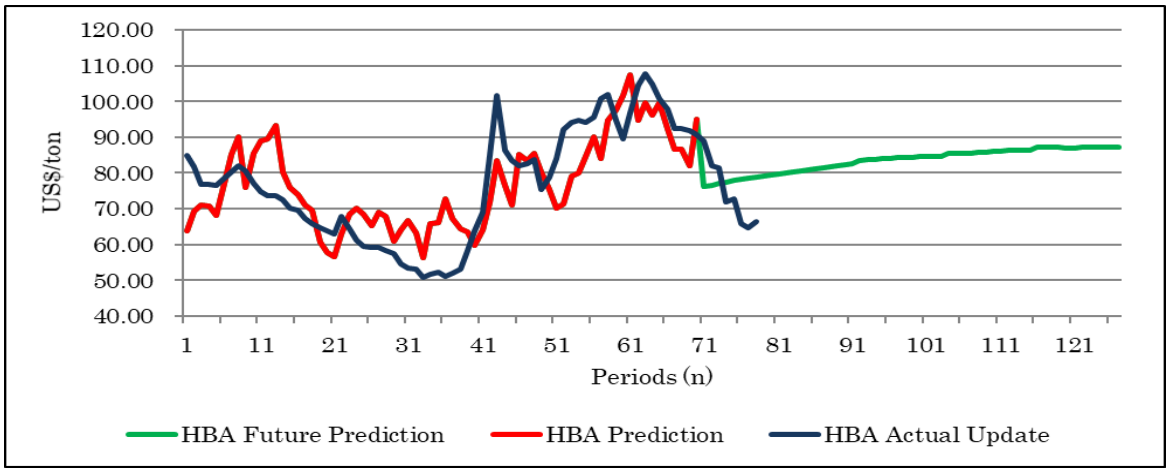

Figure 2. Comparative graphic of HBA actual and prediction

3.1.7. Coefficient determination test

The aim of coefficent determination test is to find out the influenced proportion of independent variable to dependent variable in percentage. Based on Table 2, it shows that the value of Adjusted R Square is 0.570255 so it can be concluded that the influenced proportion of independent variable is 57%.

3.1.8. Model validation and interpretation

Before interpreting the model equation of coal reference price prediction, previously the model must be validated using Mean Absolute Percentage Error (MAPE). Based on the validation result, the value of MAPE is 12.04% it means that the model has a good performance to use in predicting coal reference price. Deviation between predicted and actual value can be seen in Figure 2. Now, the model equation can be interpreted from Table 2 and the equation result is:

$$HBA = -164,5968 + \left[4,896968\left(NG\right)\right] + \left[0,089055\left(ERC\right)\right] + \left[0,008979\left(ER\right)\right] + \left[0,498939\left(COP\right)\right] - \left[0,0000145\left(CC\right)\right]$$

where

NG : Natural gas price
ERC : Renewable energy consumption
ER : Exchange rate of rupiah against dollar
COP : WTI crude oil price
CC : Coal consumption for electricity generation

Before predicting the coal reference price using the chosen model equation, previously the value of independent variable for prediction observations need to be known by using Simple Moving Average (SMA) Method for independent variable that had tendency to increased or decreased in certain period and for the value of independent variable that had tendency to fluctuate in certain period such as Natural Gas and WTI Crude Oil Price were determined from Oil and Gas Price Projection 2020 – 2025 by World Bank Institution. Prediction result of coal reference price can be seen in Table 5.

Table 5. Coal reference price prediction results (2020)

Periode	HBA (*Forecast*)
Januari - 20	79.43
Februari - 20	79.71
Maret - 20	79.96
April-20	80.21
Mei - 20	80.42
Juni - 20	80.72
Juli - 20	81.09
Agustus - 20	81.47
September-20	81.79
Oktober - 20	82.06
November-20	82.28
Desember - 20	82.50

3.2. Pit and quarter mine block sequence design

3.2.1. Estimated mining operational costs

Mining operational costs is one of the important factors that need to be considered in determining the value of break even stripping ratio based on coal reference price prediction (HBA). As can be seen in Table 1, the amount cost of overburden stripping is $2.41/bcm and total mining operation cost (exclude overburden stripping cost) is $30.22/ton.

3.2.2. Calculation of break even stripping ratio (BESR(2))

The minimum and maximum value of coal reference price prediction (HBA) were used in this research to find out the allowable value of stripping ratio (SR) in creating pit design. Based on coal price prediction (HBA) as a whole, the minimum value is $76,57/ton in Mei 2019 and the maximum value $87,31/ton in January 2023.

1. Value of BESR(2) if HBA Prediction is $76,57/ton
   Balance=HBA Prediction-Operational Mine Costs
   Balance=$76,57/ton-$30,22/ton
   Balance=$46,35/ton

   Furthermore, the calculation value of BESR (2) can be done by using the following equation:

〖BESR〗_((2))=Balance/(Overburden Stripping Cost)
〖BESR〗_((2))=($46,35/ton)/($2,41/bcm)=19,23≈20 bcm/ton

2. Value of BESR(2) if HBA Prediction is $87,31/ton
   Balance=HBA Prediction-∑Operational Mine Costs
   Balance=$87,31/ton-$30,22/ton
   Balance=$57,09/ton
   Furthermore, the calculation value of BESR(2) can be done by using the following equation:
   〖BESR〗_((2))=Balance/(Overburden Stripping Cost)
   〖BESR〗_((2))=($57,09/ton)/($2,41/bcm)=23,69≈24 bcm/ton

3.2.3. Pit limit design

Technical factors that affect the determining and designing of pit limit design is stripping ratio which is calculated with an approach to BESR(2), recommended bench geometry based on geotechnical study, actual topography and geological conditions. The pit limit design was done by using MineScape 5.7 and the result can be seen in Figs. 3 and 4.

3.2.4. Pit and disposal design

The calculation of mine haul road (ramp) geometry must be done before creating the pit design. Generally, the mine haul road geometry was calculated in two different conditions namely straight and corner condition. The mine haul road geometry must be adjusted to the largest equiopment that will operate in the pit location (Komatsu HD 785).

1. Ramp width (straight condition)
   The maximum width (Wt) of Komatsu HD 785 is 6.885 meters, thus the ramp width was calculated on a straight condition with two lanes (n) as follows.
   L_min=n .W_t+(n+1)(0,5 .W_t)
   L_min=2 .6,885 m+(2+1)(0,5 .6,885 m)
   L_min=24,0975 m ≈24,1 m

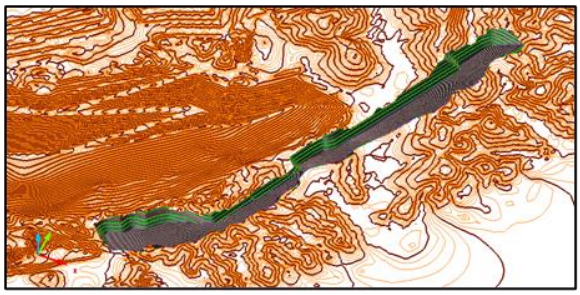

Figure 3. Pit Limit Design (SR = 6)

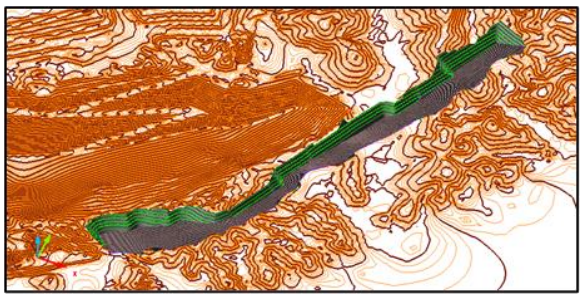

Figure 4. Pit Limit Design (SR = 7)

2. Ramp width (turn condition)
   Komatsu HD 785 has a trail width (U) at 1.716 meters, front tire width when making a turn (Fa) at 1.410 and rear tire width when making a turn (Fb) at 2.093 meters, and the width of roadside (Z) at 4.679 meters.
   W_min=2(U+F_a+F_b+Z)+C
   W_min=2(1,716 m+1,410 m+2,093 m+4,679 m)+4,679 m
   W_min=24,475 m ≈24,5 m

The disposal design that created in this research was designed by continuing the existed disposal area of Pit 7 (Eastern Disposal). This is done based on some technical consideration, such as to minimize the amount of run off water that flows direct to the pit. The pit design can be seen in Figs. 5 and 6.

3.2.5. Mineable coal reserve estimation

Determining the loss factor in estimating the mineable coal reserve is important because the result will become more realistic to the actual operational condition. The value of loss factor is 0.2, it means that 10 cm on roof and floor side of the coal seam wouldn't be included in estimation process. The minimum thickness of coal seam that will be included in estimating the coal reserve is 30 cm. The results of mineable coal reserve estimation can be seen in Table 6.

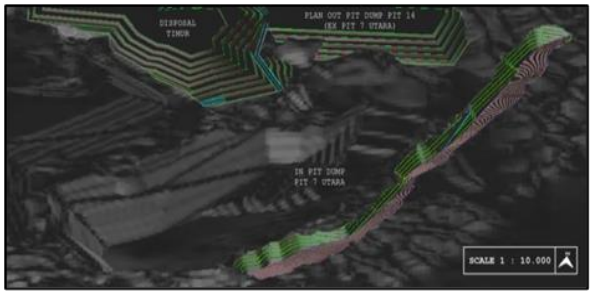

Figure 5. Pit 14 Design (SR = 6)

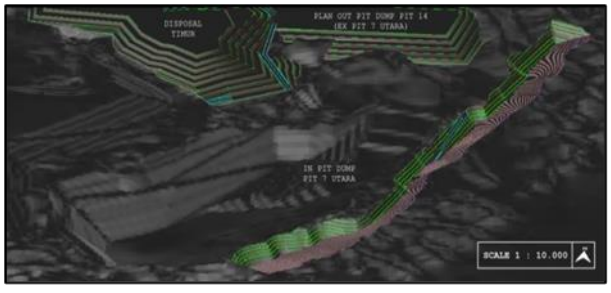

Figure 6. Pit 14 Design (SR = 7)

Table 6. Mineable coal reserve estimation results

Pit 14	OB Removal (bcm)	Coal Getting (ton)
SR 6	7,312,524.70	1,190,194.65
SR 7	9,602,251.09	1,391,812.52

3.2.6. Quarter mine block sequence design

The scenario of quarterly mine block sequence design was determined base on PT ABP coal production in 2019. Pit 7 North is one of the pit owned by PT ABP wiould be mined out at the end of the third quarter of 2019 with stripping ratio (SR = 3) and because of that PT ABP will be facing production deficit in the beginning of quarter 1 in 2020. Thus, Pit 14 was designed to avoid the production deficit and the mine block sequence scenario (Figures 7 and 8) that will be use is

1) Quarter 1 = SR < 3 (Blue Zone)
2) Quarter 2 = 3 ≤ SR ≤ 6 (Green Zone)
3) Quarter 3 = SR > 6 (Red Zone)

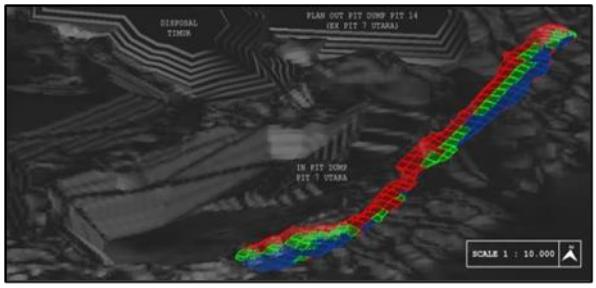

Figure 7. Pit 14 (SR = 6) mine block sequence

The estimated revenue of Pit 14 (SR = 6) and (SR = 7) block sequence as can be seen in Table 7 and 8 shows that there is a downtrend but on the other side the coal reference price prediction was increased until the end of quarter 3. It's happen because there is no synchronization between the amount of coal getting and the movement of coal reference price prediction which is cannot be controlled by using the mine block sequence method. The comparative histogram of Pit 14 estimated revenue can be seen in Figure 9.

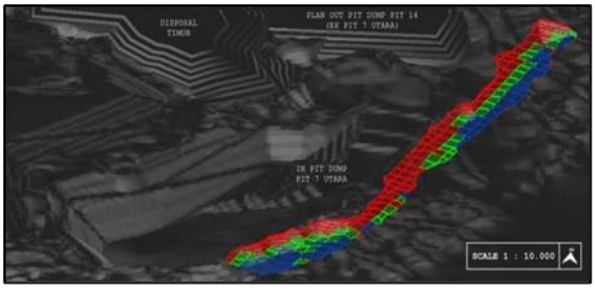

Figure 8. Pit 14 (SR = 7) mine block sequence

Table 7. Revenue estimation results of pit 14 (SR = 6) for 2020 production

Periods	Sequence Scenario	OB Removal (bcm)	Coal Getting (ton)	HBA ($/ton)	Estimated Revenue ($)	SR
CW 1	SR < 3	1,268,103	500,328	80.21	40,131,297	3
CW 2	3 ≤ SR ≤ 6	2,491,213	447,176	81.47	36,431,457	6
CW 3	SR > 6	3,541,863	237,600	82.50	19,601,965	15
Grand Total		7,301,180	1,185,104	-	96,164,720	-
Stripping Ratio			6			

Tabel 8. Revenue estimation results of pit 14 (SR = 7) for 2020 production

Periods	Sequence Scenario	OB Removal (bcm)	Coal Getting (ton)	HBA ($/ton)	Estimated Revenue ($)	SR
CW 1	SR < 3	1,332,526	521,395	80.21	41,821,081	3
CW 2	3 ≤ SR ≤ 6	2,796,084	481,209	81.47	39,204,128	6
CW 3	SR > 6	5,461,043	384,434	82.50	31,715,768	14
Grand Total		9,589,654	1,387,038	-	112,740,976	-
Stripping Ratio			7			

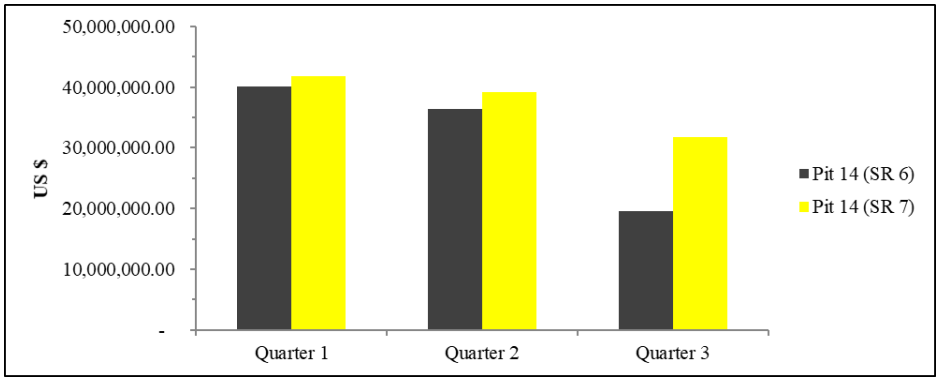

Figure 9. Estimated revenue comparison between Pit 14 SR 6 and SR 7

Table 9. Profit calculation results of pit 14 block sequence scenario

SR	Description		Production Cost		Estimated Prod. Cost ($)	Estimated Revenue ($)	Profit ($)
	OB (bcm)	Coal (ton)	OB ($/bcm)	Coal ($/ton)			
6	7,301,180	1,185,104	5.89	26.74	74,695,254	96,164,720	21,469,466
7	9,589,654	1,387,038	5.89	26.74	93,574,358	112,740,976	19,166,618

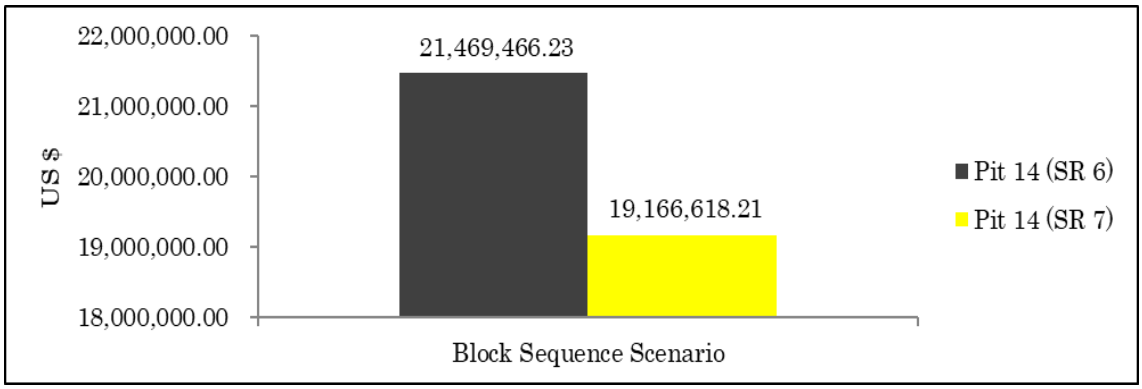

Figure 10. Profit Comparison Between Pit 14 SR 6 and SR 7

In choosing the best scenario between SR 6 and SR 7, it need to be validated by calculating the possible profit from that scenario. From that, the best possible scenario can be chosen. The profit calculation results can be seen in Table 9.

Based on Figure 10, it shows that the possible profit of Pit 14 SR 6 is $21,469,466.23 and Pit 14 SR 7 is $19,166,618.21. It can be concluded that Pit 14 SR 6 gives more profit than Pit 14 SR 7. The profit calculation was done by using Mining Operational Costs issued by Directorate General of Coal and Minerals on Kepdirjen Minerba No. 579.K/32/DJB/2015.

4. Conclusion

The coal reference price (in Indonesian: HBA) in the initial period was suffered a significant decrease of $76.57/ton (May 2019) which previously is $90.57/ton. After a significant decrease, the coal reference price (HBA) predicted to be increase at the maximum value of $87.31/ton (January 2023).

The optimal stripping ratio were obtained by trial and error and still considering the company's geotechnical recommendation is SR = 6 and SR = 7. Estimated revenue of Pit 14 (SR 6) for coal production in 2020 at Quarter 1 = $40,131,297.12, Quarter 2 = $36,431,457.31, and Quarter 3 = $19,601,965.40, whereas the estimated revenue of Pit 14 (SR 7) for coal production in 2020 at Quarter 1 = $41,821,080.50, Quarter 2 = $39,204,128.39, and Quarter 3 = $31,715,767.60.

Acknowledgements

The authors convey special gratitude to PT Alamjaya Bara Pratama for all support to this research.

References

[1] Engineering and Production Division. 2019. PT Alamjaya Bara Pratama.
[2] Hartman, H.L. 1987. Introductory Mining Engineering. Alabama: John Wiley & Sons.
[3] Aswandi, D dan Yulhendra, D. 2013. Redesain Rancangan Ultimate Pit dengan Menggunakan Software Minescape 4.118 di Pit S41 PT Energi Batu Hitam Kecamatan Muara Lawa dan Siduq Ngurai Kabupaten Kutai Barat Provinsi Kalimantan Timur. Jurnal Bina Tambang. Vol. 4, No. 1, 153-164.
[4] Ismail, Z., Yahya, A., Shabri, A. 2009. Forecasting Gold Prices Using Multiple Linear Regression Method. American Journal of Applied Sciences, Vol. 6, No. 8.
[5] Supranto, J. 2005. Ekonometri Buku Kedua. Jakarta: Ghalia Indonesia.

EPI International Journal of Engineering
Volume 3, Number 2, August 2020, pp. 103-107
DOI: 10.25042/epi-ije.082020.02

*p*ISSN 2615-5109
*e*ISSN 2621-0541

Petrophysical Characterizations of Shale Gas Reservoirs of the Ranikot Formation in the Lower Indus Basin, Pakistan

Kazunori Abe[a,*], Nouman Zobby[b], Hikari Fujii[c]

[a]Department of Earth Resource Engineering and Environmental Science, Faculty of International Resource Sciences, Akita University. Email: abe@mine.akita-u.ac.jp
[b]Department of Petroleum and Gas Engineering, Faculty of Engineering and Architecture, Baluchistan University of Information Technology Engineering and Management Sciences. Email: nauman.zobby@buitms.edu.pk
[c]Department of Earth Resource Engineering and Environmental Science, Faculty of International Resource Sciences, Akita University. Email:fujii@mine.akita-u.ac.jp

Abstract

The complex pore structure with nano-pores of shale gas reservoirs has an impact on the hydrocarbon storage and transport systems. We examined the pore structure of the shales of the Ranikot Formation in the Lower Indus Basin, Pakistan to investigate the full scaled pore size distributions by using a combination of techniques, mercury injection capillary pressure analysis and low pressure gas adsorption methods using N_2 and CO_2. Isotherm curves obtained N_2 and CO_2 adsorptions were interpreted using density functional theory analysis for describing the nano-scaled pore size distributions. The pore geometry of the shales was estimated to be slit-type from the isotherm hysteresis loop shape. The pore size distributions determined the density functional theory showed the dominant pore size of below around 10 nm. The Micro-scale effects such as slippage and adsorption/desorption also significantly influence the gas flow in nano-pore structure. The gas flow regimes in shales are classified into four types Darcy flow, slip flow, transition flow, Knudsen flow based on the value of the Knudsen number. Applying the specific reservoir conditions in Ranikot shale and pore size distribution to the Knudsen number, the gas flow regimes of the Ranikot shales were estimated mostly within the transition and slip flow.

Keywords: Knudsen number; petrophysical characterization; shale gas; pore structure; Ranikot formation

1. Introduction

Shale gas has become an increasingly important source of natural gas in the world and has been perceived as a potenial source of energy supplyment for decades. Shale is fine-grained clastic sedimentary rocks composed of clay minerals and a trace amount of fragments of quartz, feldspar and calcite. Shale rock is one of potential petroleum source rock The shale gas is natural gas trapped within shale formations, which consists of a large amount of lithified clays with organic material and detrital minerals. The organic matter is an integral constituent for a productive shale gas reservoir.

Recently in Pakistan, the Advanced Resources International Inc. estimated a total risked shale gas in-place of 586 trillion cubic feet (TCF) and the risked technically recoverable of 105 TCF [1]. The Ranikot Formations in the Lower Indus Basin in Pakistan is one of the potential source rock with a total organic carbon of about 2.0 % for gas-producing. The Ranikot Formation is 26,780 square miles, thickness of formation ranging from 1,000 to 3,000 feet with a net shale thickness of about 200 feet. The risked of Ranikot shale formation has shale gas in-place of 55 TCF [1]. However, the detailed petrophysical characterizations of the Ranikot shales formations have not been still conducted due to limited assets and techniques in the last decayed.

Characteristics of pore structure with nano-pores in shales was to elucidate the formation of a gas storage and gas flow in shale gas. Fluid invasion methods that have typically been used for pore structure to analyze characteristics of shale including a combination of mercury injection capillary pressure (MICP) and a low-pressure gas adsorption methods (LPA) [2-4]. MICP method is useful for characterizing mesopore (pore size in diameters between 2 nm and 50 nm) and macropore (pore size in diameters more than 50 nm), however, the pore structures are distortion in the pore size limit around 4 nm regarding to compressibility effects. On the other hand, LPA method using N_2 or CO_2 are commonly used to analyze the characteristics of the pore

*Corresponding author. Tel.: +81-18-889-3079
1-1 Tegata gakuen-machi, Akita, Akita, Japan, 010-8502

structure < 2 nm of pore size in diameter. Previous studies of pore structures in shale rocks from unconventional gas reservoirs have focused on Density Functional Theory (DFT) that DFT theory is used to interpret the potential source rocks technique by modern statistical thermodynamics [5] such as estimation of kerogen in the Barnett shales [6]. A rigorous methodology for characterizing pore structures and flow properties of tight gas sands was provided by Rushing et al. based on a rock-typing procedure [7].

The pore structures with nano-pores in shales have low permeability (nano-darcy) and transport systems acting at different scales; (1) surface diffusion of molecules adsorbed to kerogen and clay, (2) Knudsen diffusion and slip flow in micropore, mesopores, and lower macropores, (3) Darcy flow in macropores [8]. The gas flow regimes in shales are classified into four types such as Darcy flow, slip flow, transition flow, Knudsen flow by using the value of the Knudsen number [9]. Micro-scale effects such as slippage and adsorption/desorption also significantly influence the gas flow in nanopore structure. Therefore, the analysis of micropore structure can provide a better understanding of the gas storage and migration pathways in shale rock. Efficient depiction of the nanopore structure is critical for the quantification of producible resources and the evaluation of long term production behavior [4].

The aims of this research were to elucidate the characteristics of pore structures with nano-pores in the Ranikot shale formation to understand gas storage and gas flow by LPA and MICP methods on the basis of the Knudsen number.

2. Experimental Methods

2.1. Materials

The shale samples were collected from four area in the Ranikot Formations in the Lower Indus Basin, Pakistan. These shale sample were collected in different depth in each area such as 1,945-2,070 m from Dhodak area, 1,125-1,250 m from Bobi area, 1,190-1,290 m from Kadanwari and 485-838 m from Daru area. The shale samples were dried at temperature 333 K for 24 hours to expel solution such as water.

2.2. Low pressure gas adsorption methods (LPA)

Physisorption filling may be regarded as the primary physisorption process at the micropore scale and surface coverage takes place on the walls of mesopores or open macro-pores, which causes mono-multilayer adsorption and pore condensation [10]. LPA method is a well-established approach for the characterization of pore structures in shale. The shale rocks samples were treated in different temperature regarding to the LPA method using N_2 and CO_2 isotherm. In case of the LPA method using N_2 isotherm, the shale samples were treated at temperature of 77 K. On the other hand, the LPA method using CO_2 isotherm was treated the shale samples at temperature of 273 K. The analysis is performed the Autosorb iQ (Quantachrome Instruments), which the schematic diagram of the LPA method using N_2 is shown in Fig. 1. The samples were pre-dried and outgassed under a vacuum at temperature of 333 K for 3 hours. The nitrogen molecules were expelled water molecules and trace gas in micropores to degas and remove moisture contents before pore structure analysis. The isotherms are used to quantify the amount of gas adsorbed at relative pressure (P/P_0), where P is the absolute equilibrium pressure and P_0 is the saturated vapor pressure of each gas at laboratory conditions. N_2 adsorption via the physisorption filling of wide micropores still occurs at very low pressures. The pores with the minimum diameter of 1.3 nm can be explored by N_2 adsorption at 77 K. On the other hand, the relatively high boiling point (273 K) and high saturation vapor pressure (up to 3.5 MPa) of CO_2 make studying its adsorption at 273 K an acceptable method for investigating materials with very narrow micropores (about 0.33 nm) [2]. The maximum P/P_0 with CO_2 at 273 K is 0.03 (corresponding to ambient pressure). CO_2 adsorption can be found the maximum pore diameter of 2 nm. In this study, the DFT model was used for the PSD determination of shale samples included micropores through to lower macropores.

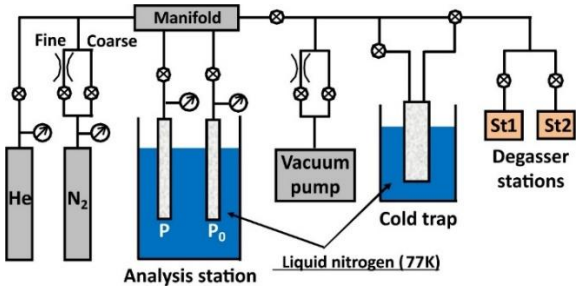

Figure 1. Schematic diagram of LPA using N_2

2.3. Mercury injection capillary pressure analysis (MICP)

MICP provides a wide range of information such as PSDs, total pore volume, bulk density and specific surface area [2]. The grain size of the shale samples is around 5 mm, and its sample weight are at least 0.4 gram. The mercury intrusion pressure values are converted to the pore size by using the Washburn equation [11]. The contact angle and mercury surface tension used in the Washburn equation for pore size calculations were 141 ° and 480 (mN/m), respectively. The MICP measurement was accomplished in a Thermo Electron Corporations porosimeter that attained a maximum instrusion pressure of 400 MPa. In this study, the pressures used for instruction were up to 200 MPa.

2.4. Flow regimes based on the Knudsen number

The gas flow regimes are calculated by the Knudsen number (K_n), which is defined as Eq.(1).

$$K_n = \frac{\lambda}{d_p} \tag{1}$$

where λ is the mean free path of a gas molecular (m), d_p is the diameter of the pore (m), which is given by Eq.(2).

$$\lambda = \frac{k_B T}{\sqrt{2}\pi p d^2} \quad (2)$$

where k_B is the Boltzmann constant (1.38×10^{-23}(J/K)), T is the temperature (K), p is the pressure (N/m^2), d is the diameter of the gas molecular (m).

For the Knudsen flow ($K_n > 10$), gas molecules collision frequently between gas molecular and pore wall is dominant. Therefore, the continuum assumption becomes invalid, and flow rate and pressure drop are no longer accurately predicted using Darcy's law. When $K_n < 0.01$, the Darcy flow is a dominant in the pore because the mean free path of gas molecules is negligible relative to the pore diameter. This intermediate zone ($0.01 < K_n < 10$) is divided into slip and transition flow regimes. For the slip flow, the effect of discontinuity appears near the pore wall, whereas fluid flow is based on the continuity far from the pore wall. The Knudsen number has an influence on the permeability of shales. For example, the permeability was underestimated than actual permeability under slip and early transition flow conditions [9]. Table 1 summarizes these four types of gas flow regimes and the driving forces [8].

3. Results and Discussion

Fig. 2 shows isotherm curves using N_2 adsorption at 77 K for the Ranikot shale samples. These sampling depths of each of fields, Dhodak, Bobi, Kadanwari and Daru are around 2,070 m, 1,250 m, 1,290 m and 838 m, respectively. The shapes of the isotherm curves suggest that the all shales contain narrow slit-like pores according to the International Union of Pure and Applied Chemistry (IUPAC) [12]. The micropores surface area and mesopores volume of Ranikot shale are domain of the pore structure. Fig. 3 shows the PSDs determined by using DFT model based on the isotherms obtained N_2 adsorptions for the Ranikot shales. The plots of the dV/d(logD) versus pore diameter is used to represent the PSD. Unimodal PSD of Dhodak field sample at the depth of 2,070 m shows pore modes at 1.40 nm, 1.69 nm and 3.79 nm. Kadanwari field sample at depth of 1,290 m revealed the strong pore peak at 3.79 nm and Bobi field sample at depth of 1,250m revealed 8.53 nm.

Table 1. Summary of flow regimes, Knudsen number, driving force [8]

Flow regime	Knudsen number	Driving force
Knudsen flow	$K_n > 10$	Total concentration gradient and molecular weight
Transition flow	$0.1 < K_n < 10$	Mostly Knudsen flow with some Darcy flow
Slip flow	$0.01 < K_n < 10$	Mostly Darcy flow with some Knudsen flow
Darcy flow	$0.01 > Kn$	Total pressure gradient

While the Daru field sample at depth of 838m shows the highest value at 3.79 nm. The PSD determined DFT model based on N_2 and CO_2 isotherms indicated that the nano-pores of Dhodak field samples were characterized ranges of 0.5-29 nm, Kadanwari field ranges of 3-29 nm, Bobi field ranges of 0.3-10 nm, and the Daru field ranges of 1.0-10 nm. Furthermore, the full scaled PSDs of the Dhodak sample at the depth of 2,070 were determined by using the combination of MICP, N_2 and CO_2 adsorption (Fig. 4). The MICP and CO_2 adsorption give more information about the macropores and ultra-micropores (pore diameters less than 2nm), respectively. The shale samples have a multi-modal distribution with the major peaks at approximately 0.57 - 0.82 nm, 3.78 nm in the micropores and mesopores. While the PSD based on the MICP shows the wide range PSD in the macropores.

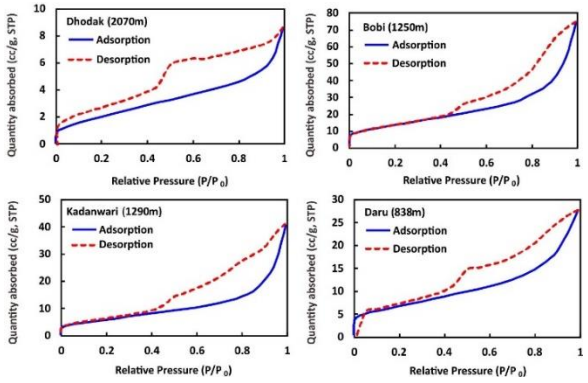

Figure 2. Adsorption and desorption isotherms of the Ranikot shales using N_2 adsorption. The sampling depths in each of the fields, Dhodak, Bobi, Kadanwari and Daru are around 2070m, 1250m, 1290m and 838m, respectively

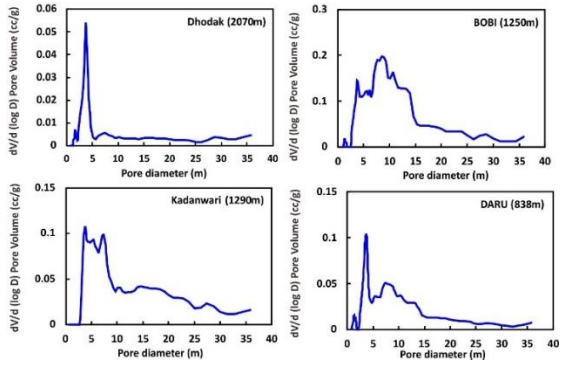

Figure 3. PSDs determined DFT analysis based on the isotherm obtained N_2 adsorption for the Ranikot shales, where the sampling depths in each fields of Dhodak, Bobi, Kadanwari and Daru are around 2070 m, 1250 m, 1290 m and 838m, respectively.

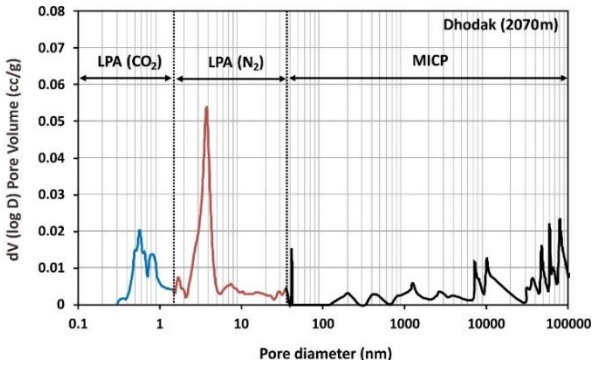

Figure 4. PSD determined by the combination of MICP, N_2 and CO_2 adsorption using DFT method for the Ranikot shales of Dhodak filed at the depths of 2070 m

Figure 5 shows the estimations of the flow regimes based on the Knudsen number for the Ranikot shale in each fields of Dhodak, Bobi, Kadanwari and Dara at each of sampling depths. For the calculations of the Knudsen number, d is used the molecular diameter for methane (0.38 nm) and the specific pressure and temperature at each of sampling depths [13]. The Dhodak and Daru shale samples exhibit the transition and slip flow mechanism, and the Kadanwari and Bobi field shale samples exhibit the Knudsen flow along with transitional and slip flow. The transportation of gas in Ranikot shale lies mostly within the transition and slip flow regimes.

4. Conclusion

In this work, the pore structure of the shale samples of the Ranikot Formation in the Lower Indus Basin, Pakistan have been investigated using MICP and LPA applying N_2 and CO_2. The pore geometry of all the shales were interpreted as narrow slit-like pores, as evidenced by shapes of the hysteresis loop according to IUPAC classification. The PSD determined DFT model based on N_2 and CO_2 isotherms indicated that the nano-pores of Dhodak field samples were characterized ranges of 0.5-29 nm, Kadanwari field ranges of 3-29 nm, Bobi field ranges of 0.3-10 nm, and the Daru field ranges of 1.0-10 nm. Combined the PSD based on the MICP, the shale samples have been had multi-modal wide PSDs. The flow regimes of the Ranikot shales are estimated based on the Knudsen number, applying specific temperature and pressure at the sampling depths. As a result, the Dhodak and Daru shale samples exhibit the transition and slip flow mechanism, and the Kadanwari and Bobi field shale samples exhibit the Knudsen flow along with transitional and slip flow. The gas regimes in Ranikot shales lies mostly within the transition and slip flow.

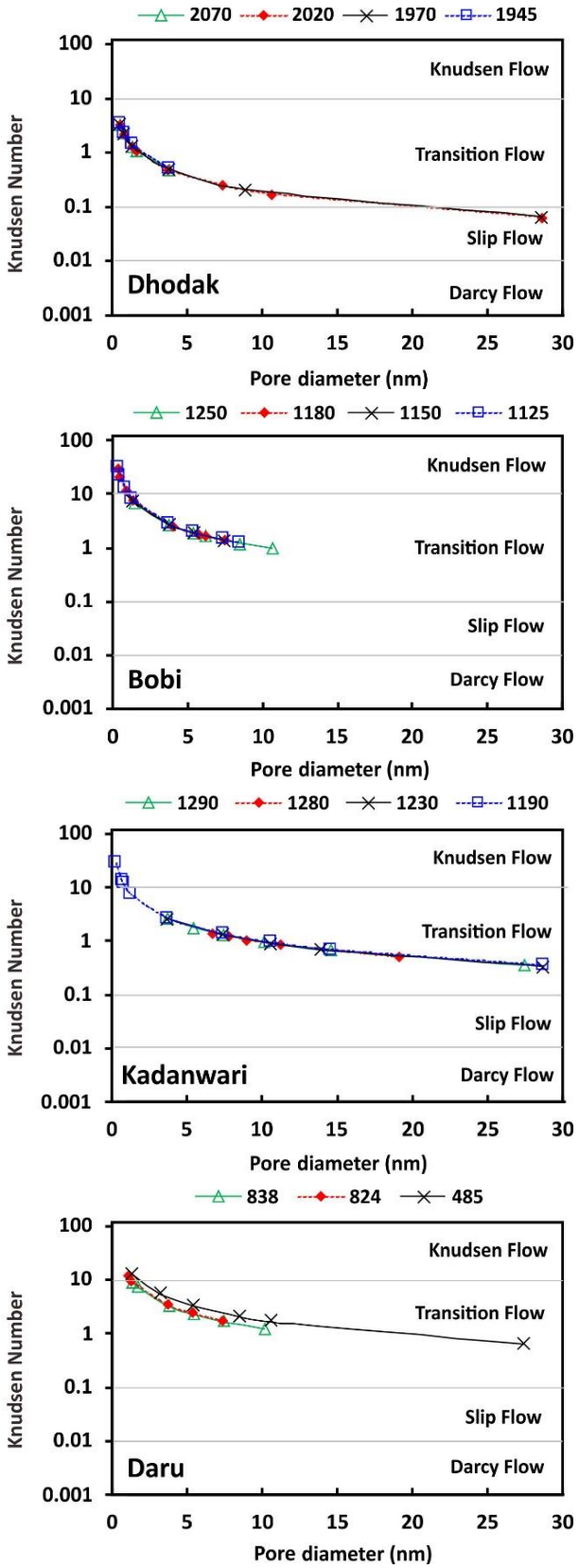

Figure 5. Estimations of the flow regimes based on the Knudsen number for the Ranikot shale in Dhodak, Bobi, Kadanwari and Daru fields at each of the sampling depths.

Acknowledgements

The authors would like to thank Japan International Cooperation Agency for supporting this research through the project on "In Country Training and Provision of Equipment for Baluchistan University of Information Technology Engineering and Management Sciences" and express our sincere gratitude to Directorate General of Petroleum Concession of Pakistan for providing samples. This work was supported by Akita University Support for Fostering Research Project.

References

[1] U.S. Energy Information Administration, World Shale Gas and Shale Oil Resource Assessment. Technically Recoverable Shale Oil and Shale Gas Resources: India and Pakistan. 2013.

[2] Matthias T, Katsumi K, Alexander VN, James PO, Francisco R-R, Jean R, Kenneth SWS. Physisorption of gases, with special reference to the evaluation of surface area and pore size distribution (IUPAC Technical Report). Pure Appl. Chem. 2015; 87 (9-10): 1051-1069.

[3] Jingqiang T, Brian H, Nicolaj M, Jinchuan Z, Christopher JB, Dorothee H, Ger VG, Bruce AT. Natural gas potential of Neoproterozoic and lower Palaeozoic marine shales in the Upper Yangtze Platform, South China: geological and organic geochemical characterization. International Geology Review. 2015; 57: 305-326.

[4] Mingming W, Li Z, Yongqiang X, Jinhua L, Ping'an P. Nanopore structure characterization for organic-rich shale using the non-local-density functional theory by a combination of N_2 and CO_2 adsorption. Microporous and Mesoporous Materials. 2016: 227: 88-94.

[5] Do DD, Do HD. Pore characterization of carbonaceous materials by DFT and GCMC simulations: A Review. Adsorption Science and Technology. 2003; 21(5): 389-423.

[6] Adelola GA, I. Akkutlu, Daniel ER, Chandra SR. Characterization of Barnet Shale Pore Size Distribution using DFT Analysis and Monte Carlo Simulations. Society of Petroleum Engineers. 2011; SPE-147397-MS.

[7] Jay AR, Kent EN, Thomas AB. Rock Typing – Key to understanding Productivity in Tight Gas Sands. Society of Petroleum Engineers. 2008; SPE-114164-MS.

[8] Rob H, John V, Mark Z. Experimental investigation of matrix permeability of gas shales. AAPG Bulletin. 2014; 98(5): 975-995.

[9] Ali SZ, Roberto A. Knudsen's Permeability Correction for Tight Porous Media. Transport in Porous Media. 2012; 91: 1: 239–260.

[10] Daniel JKR, Robert MB. The importance of shale composition and pore structure upon gas storage potential of shale gas reservoirs. Marine and Petroleum Geology. 2009; 26(6): 916-927.

[11] Edward WW. Note on a method of determining the distribution of pore sizes in a porous material. Proceedings of the National Academy of Science. 1921; 7: 115-116.

[12] Kenneth SWS. Reporting Physisorption Data for Gas/Solid Systems with Special Reference to the Determination of Surface Area and Porosity. Pure Appl. Chem. 1985; 57: 603-619.

[13] Breck DW. Zeolite Molecular Sieves: Structure, Chemistry, and Use. Wiley. 1974; ISBN 13: 9780471099857.

EPI International Journal of Engineering
Volume 3, Number 2, August 2020, pp. 108-112
DOI: 10.25042/epi-ije.082020.03

*p*ISSN 2615-5109
*e*ISSN 2621-0541

Enhanced Effluent Quality of Anaerobic Baffled Reactor (ABR) with Ozone and Aerobic Activated Sludge for Livestock Wastewater Treatment

Anshah Silmi Afifah[a,*], Muhammad Rizki Apritama[b], Yosef Adicita[c], I Wayan Koko Suryawan[d], Iva Yenis Septiariva[e]

[a]Department of Environmental Engineering, Faculty of Engineering, Universitas Universal, Batam. Email: silmi.kbub@gmail.com
[b]Department of Environmental Engineering, Faculty of Engineering, Universitas Universal, Batam. Email: rizkiapritama@outlook.com
[c]Department of Environmental Engineering, Faculty of Engineering, Universitas Universal, Batam. Email: yoseph_cita@yahoo.com
[d]Department of Environmental Engineering, Faculty of Infrastructure Planning, Universitas Pertamina, Jakarta.
Email: i.suryawan@universitaspertamina.ac.id
[e]Department of Civil Engineering, Faculty of Engineering, Universitas Sebelas Maret, Kota Surakarta. Email: ivayenis@staff.uns.ac.id

Abstract

ABR used to treat wastewater with high COD level such as livestock wastewater. ABR treatment consists of compartments which are limited by vertical bulkhead growth with attached bacteria. However, ABR treatment only capable degraded COD level by 50 – 53%. This value did not qualify to be discharged into the environment. Therefore, ABR treatment need further treatment with ozone treatment and aerobic activated sludge. There were two treatments in this study, which are ABR with ozone treatment and aerobic activated sludge (S1) and ABR with aerobic activated sludge (S2). COD degradation with ozone treatment showed low efficiency, 31.1 ± 1.5 % but BOD/COD level increased. Aerobic activated sludge with batch system showed efficiency of COD degradation as 95.3 ± 2.2 % (with ozone treatment) and 78.6 ± 4.5 % without ozone treatment. The final concentration effluent for livestock wastewater was 167.7 ± 62 mg/L. Aerobic activated sludge with continuous system was conducted to test that result and it average efficiency only decreased into 85%. This concentration was qualified to be discharged into environment.

Keywords: Activated sludge; anaerobic baffled reactor; livestock; ozone; wastewater

1. Introduction

Growing world population raise the demand livestock products [1]. The increasing of livestock wastewater in developing country due to high consumption of meat. Livestock wastewater majorly used as fertilizer, but it only degraded its organic matters. Whereas, its inorganic matters cannot be degraded properly and become residue that could threated environment especially water pollution like decreasing of water quality because of high nutrients. Livestock wastewater as organic waste that is consist of protein, carbohydrate, fat, mineral salt, can act as growth media and microbes breeding. Degradation process in wastewater makes the level of BOD, COD, NH_3, H_2S and pH changing and also raises bad odor like urea, Sulphur, and heavy metals. Heavy metals will affect leads to plant growth and heavy metals accumulation to plant [2, 3]. Besides that, the decreasing of DO level excessively can cause degradation of water quality. Generally, water body has capability to do self-purification, but with the increasing number of pollutants into water body caused autogenously purification of water body decrease. It is indicated with the changing of physical, chemical and biological in water body.

Anaerobic Baffled Reactor (ABR) is one of modification septic tank reactor with compartment addition [4]. ABR used to treat wastewater with high level COD like livestock wastewater. ABR treatment consists of compartments which are limited by vertical bulkhead growth with attached bacteria. Commonly, ABR consist of compartments that is arranged series. ABR combines sedimentation process with sludge decomposition partially in the same compartment, basically that compartment is sedimentation pond without moving parts or chemical materials adding. However, efficiency of COD degradation in ABR system still under 85% and yet qualified to standard quality [5, 6]. Hence, advanced treatment needs to be conducted to increase treatment's efficiency [7]. This study conducted ozone treatment and aerated activated sludge as advance treatment.

Plasma discharge technique is one of technic to produces ozone gas (O_3) as strong oxidation that is effective in wastewater treatment. Ozone can increase biodegradability of wastewater. Ozone including into strong oxidant after Fluor (F), but safe and environmentally friendly, because in the end of reaction,

*Corresponding author. +62-2277-4992
Jl. Teuku Nyak Arief, RT.7/RW.8, Simprug
Kec. Kebayoran Lama, Jakarta Selatan
Jakarta 12220

Table 1. Characteristics of livestock wastewater effluent

No	Parameters	Value	Unit
1	COD	9046 ± 193	mg/L
2	BOD_5	3479 ± 58	mg/L
3	TSS	1432 ± 189	mg/L
4	VSS	10575 ± 227	mg/L
5	NH_3-N	34.7 ± 0.7	mg/L
6	TKN	2589 ± 345	mg/L
7	pH	7.6-8.2	
8	BOD/COD	0.38	
9	C/N	4.02	

ozone (O_3) reform into oxygen (O_2). Some studies stated ozone is a process which increased biological treatment's efficiency [8, 9, 10]. Moreover, ozone appropriate as post-treatment in ABR method [11].

Ozone process cannot degrade all of organic materials chemically, so off the treatment can further with aerobic activated sludge treatment. The combination of ABR and aerobic activated sludge treatment had applied and successes to increase efficiency of organic materials removal [7, 12, 13]. This method requires air supply and it can maintain a high microbe concentration to absorb and accelerate the removal of organic matter.

The fact that ABR method's result yet still qualified into quality standard of wastewater, make this method need to be improved. Advanced processing that is used is ozone, aerated activated sludge and combined ozone and activated sludge. The objective of this study was to evaluate the performance of an anaerobic baffled reactor (ABR) with post treatment ozone, aerated activated sludge, and combined ozone and activated sludge in the treatment of livestock wastewater.

2. Materials and Methods

2.1. Livestock wastewater

Livestock wastewater sourced from farm in Denpasar, Bali. COD level of that livestock wastewater after treatment was high, 9046 ± 193 mg/L, and was difficult to treat with aerobic process and also requires high power. Nowadays, those livestock wastewater only treated by ABR process and its effluent not fulfilling the quality standard. The main physic-chemical and biological characteristics of livestock wastewater used in this study are shown in Table 1.

2.2. Reactor

In the ABR, wastewater is flowed continuously from raw wastewater tank by HRT 6 in 12 hours. ABR has a volume of 25 L and also 3 baffle compartments (Fig. 1). Next, wastewater is flowed into ozone reactor with a capacity of 10 L in the batch system. Ozone generator that is used have doses 1200 mg per hour. The procedure is continued by aerobic activated sludge with batch system and repeatedly. The aerobic system is classified into two, which are with ozone and without ozone.

2.3. Analysis procedure

The analysis parameters are DO, BOD_5, COD, pH, TKN and NH3-N established on standard method APHA AWWA. Essential parameter in this research is COD value that measured periodically. Each wastewater is retrieved as much as 20 mL from sampling port then analyzed based on each paramaters.

3. Results and Discussion

3.1. ABR treatment

The average characteristics of influent and effluent after the ABR treatment at 6 and 12 h HRTs are summarized in Fig. 2. The average effluent COD values at 6 h HRT were found to be around 4489.7 mg/L, respectively, while at 10 h HRT average COD values were of the order 4182 mg/L, respectively. At both HRTs COD removal averaged 50-53% indicating poor amount of removal.

The result of ABR treatment similar to the result of anoxic treatment of piggery wastewater which produced COD removal for 54.5% for anoxic activated sludge and 51-60% for ABR [14, 15]. As well as the result of NH_3-N, removal which merely produced 50-58% of value. This product is not complied the standard quality of wastewater of livestock industry.

The product of COD removal in process indicates low value compared to another research which produced more than 80% [16, 17]. The high removal fluctuation is produced by Pirsaheb et al.,with COD influent value of 15.000 mg/L by removal efficiency value of 43.01% and 95.13% respectively [18]. This matter is probably happened in consequence of highly NH3-N concentration in the wastewater. Much as ammonia is the essential nutrition for bacteria's growth, but if it is highly concentrated, it also can hinder methanogenesis during aerobic digestion process [19]. The after-process measurement result indicates COD/BOD value of 022±0.03, which is this value reveals the low biodegradability.

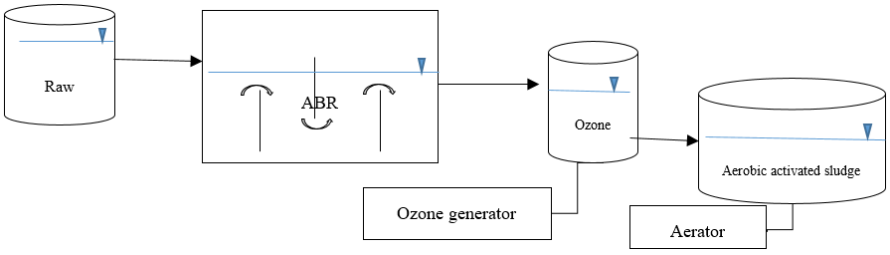

Figure 1. Flow chart of livestock wastewater treatment process

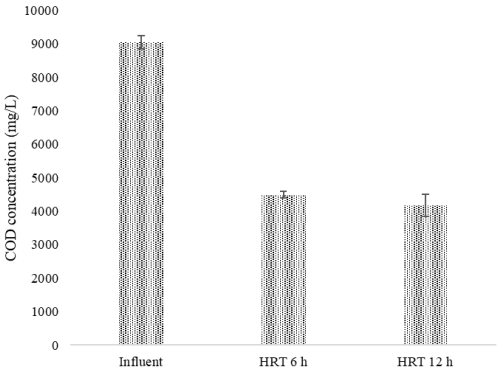

(a)

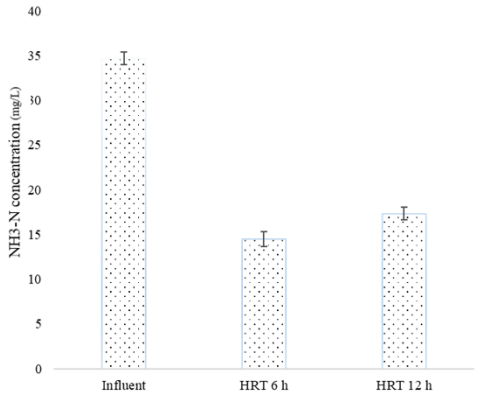

(b)

Figure 2. The results of livestock wastewater treatment with ABR tanks with different HRT (a) COD (b) NH_3-N

3.2. Ozone treatment

Indirect ozone reaction into $OH^{\cdot}$ radicals is dominantly functioning in the organic compound removal to produce higher quality of removal efficiency. This research stabilizes ozone mechanism is the method that can be used to remove organic material composition [8]. COD as organic removal (Fig. 3) and NH_3-N as nutrient removal indicates the quite low value of 31.1±1.5% and 19.2.1±2.1%. The result of BOD measurement indicates no difference with the average efficiency of 1%. There is a quite high increasing of BOD/COD value, from 0.25±0.02 to 0.37±0.01. Increasing the BOD/COD value showed in Fig. 4.

Some other parameter which determines the effectively of ozone mechanism is BOD as organic material indicator that can be degraded biologically. Another research that used UV/H_2O_2 oxidation process from effluent ABR increasing BOD/COD ratio of 0.4 to 0.6 [17]. NH_3-N also indicates poor effluent, which is 12.6±1.1 mg/L with efficiency value of 29.7±1.4 %. With reference to pH value in the ozone treatment, it indicates normal pH (7.2-7.5), where based on Khuntia et al., the optimum pH to be used in ammonia removal is up to 9 [19].

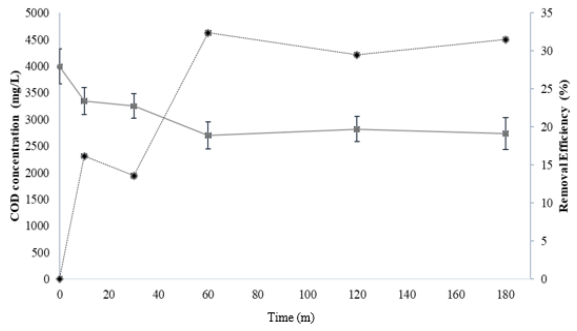

Figure 3. Degradation of COD as organic compounds with ozone pre-treatment

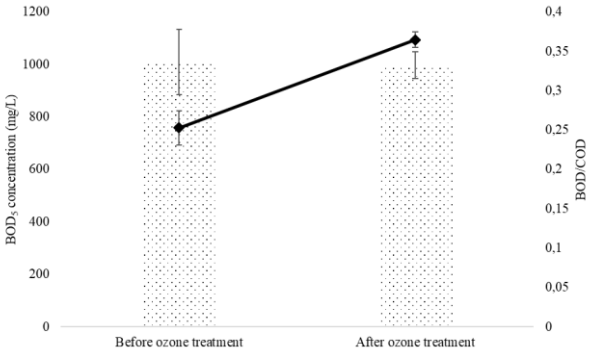

Figure 4. Changes in the value of BOD and biodegradability (BOD/COD) with ozone pre-treatment

3.3. Aerobic activated sludge treatment

In the aerobic activated sludge process, the used MLVSS concentration is about 831 mg/L at start-up. Which the sustained DO value is up to 4 mg/L to initiate the optimum aerobic processing [20]. The result can be viewed at the Fig. 5. COD removal efficiency with time detention of 60 days for S2 has reached the efficiency 95.3±2.2% with a value of 167.7±62 mg/L. NH_3-N removal only reached 52±6.2%.

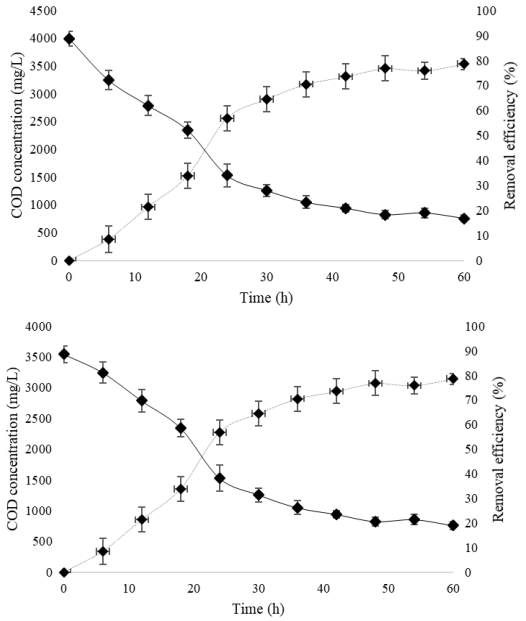

Figure 5. Removal of COD values by active sludge treatment process (S1= without ozone pre-treatment and S2 = with ozone pre-treatment)

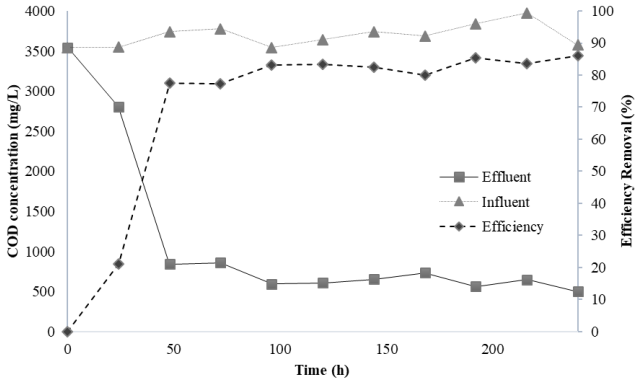

Figure 6. Removal of COD values by the active sludge treatment process in the continuous process with 48 hours HRT

In the meantime, the result of without-ozone process (S1) only produces COD and NH_3-N efficiency of 78.6±4.5% and 41.2±7.1%. Combined of activated sludge and ozone value have passed the threshold standard class in Indonesia. Next, the process output is tested by continually system with HRT 48 hours, which is the result reached the maximum COD efficiency 86% (Fig. 6) and NH_3-N efficiency only 39%.

This outcome of aerobic activated sludge treatment is established by another research which combined the ABR process with aerobic process that produces removal efficiencies 98% and 100% [21]. The result in continuous system is established by Pratiwi *et al.*, statement, the further decrease of HRT [10], the COD removal declined apparently. Another research also stated the combined anaerobic/aerobic process with HRT 19.7 and 1.22 days producing COD removal about 97% and 91% [22].

As a result of that matter, it needs the adjustment of HRT value in the treatment process of livestock wastewater. To remove the suspended particles can use bio flocculants which non-toxic and more eco-friendly solution [23]. For nutrient removal like NH_3-N can use phytoremediation or constructed wetland. Contracted wetland has ability to metabolize/absorb certain chemicals like NH_3-N [2, 24, 25].

4. Conclusions

The result of COD removal with ABR system is quite low, which is 50-53%. The results indicate that in the batch system, ozone can increase BOD/COD and decrease the COD only 31.1±1.5%. Significant removal of COD in both reactors occurs at the first hour, but reactor with ozone treatment has higher removal efficiency of COD than without ozone treatment. The removal efficiency of COD in the both reactors was 95.3±2.2%% and 78.6±4.5% respectively. In the continually process test (HRT 48 H) by ozone treatment, the COD removal maximum value is only 85%.

References

[1] Belay, G., and Negesse, T. (2019). Livestock feed dry matter availability and utilization in burie zuria district, North Western Ethiopia. Tropical and Subtropical Agroecosystems, 22: 55-70.

[2] Apritama, M. R., Suryawan, I. W. K., Afifah, A. S., and Septiariva, I. Y., (2020). Phytoremediation of effluent textile WWTP for NH3-N and Cu reduction using pistia stratiotes. Plant Archives, 20: 2384-2388.

[3] Johanto, A., Rosariastuti, R., and Cahyani, V. R. (2019). Effort to get safe rice for consumption through bioremediation technology in paddy field contaminated by lead. Tropical and Subtropical Agroecosystems, 22: 179-188.

[4] Bachman, A., Bread, V.L., and McCarty, P. L. (1985). Performance Characteristic of the Anaerobic Baffle Reactor. Water Research, 19(1): 99-106.

[5] Dyan, M. O., Putra, G. P., Budiyono, Sumardiono, S., and Kusworo T. J. (2015). The effect of pH and operation mode for COD removal of slaughterhouse wastewater with Anaerobic Batch Reactor (ABR). Waste Technology, 3(1): 7-13.

[6] Jürgensen L., Ehimen E.A., Born J., Holm-Nielsen J. (2016). Two-phase anaerobic digestion for biogas production from dairy effluent—CSTR and ABR in series. Proceedings of the 24th European Biomass Conference and Exhibition; insert date of conf.; place of conference, Publisher name, Place of publication, 1698-1702.

[7] Bodík, I., Kratochvíl, K., Gašpariková, E., and Hutňan, M. (2003). Nitrogen removal in an anaerobic baffled filter reactor with aerobic post-treatment. Bioresource Technology, 86(1): 79-84.

[8] Suryawan, I. W. K., Prajati, G., Afifah, A. S., & Apritama, M. R. (2020). NH3-N and COD reduction in Endek (Balinese textile) wastewater by activated sludge under different DO condition with ozone pretreatment. Walailak Journal of Science and Technology (WJST).

[9] Chaiprapat, A., and Laklam, T. (2011). Enhancing digestion efficiency of POME in anaerobic sequencing batch reactor with ozonation pretreatment and cycle time reduction. Bioresource Technology, 102(5): 4061-4068.

[10] Pratiwi R., Notodarmojo S., and Helmy Q. (2018). Decolourization of remazol black-5 textile dyes using moving bed bio-film reactor. The 4th International Seminar on Sustainable Urban Development (ISoSUD); August 9-10, 2017; Jakarta, Indonesia. In IOP Conf. Series: Earth and Environmental Science 106: 1-6.

[11] Marchioretto M. M., and Reali M. A. (2001). Ozonation followed by coagulation/flocculation and flotation as post-treatment of the effluent from an anaerobic baffled reactor treating domestic sewage. Water Science and Technology, 43(8): 99-106.

[12] Da Silva, G. H. R., Sarti, A., Maintinguer, S. I., Kaiser I. M., and da Silva, G. H. R. (2017). Performance of an anaerobic baffled reactor with an aerobic chamber treating low-strength wastewater. insert short title of journal,insert , Volume number(issue number): insert number of page.

[13] Tanikawa, D., Yakote, N., Nakahara, K., and Yamaguchi, T. (2016). Evaluation of process performance for lipid-rich wastewater treatment using a combination system of an anaerobic baffled reactor and an aerobic trickling filter. Journal of Water and Environment Technology, 14, 90–95.

[14] Suryawan, I. W. K., Afifah, A. S., and Prajati G. (2019). Degradasi bahan organik dan pertumbuhan biomassa konsorsium pada air limbah olahan babi dengan lumpur aktif anoksik. Jurnal Teknik Kimia dan Lingkungan, 3: 20-26.

[15] Suryawan, I. W. K., Prajati, G., Afifah, A. S., Apritama, M. R., & Adicita, Y. (2019). Continuous piggery wastewater treatment with anaerobic baffled reactor (ABR) by bio-activator effective microorganisms (EM4). Indonesian Journal of Urban and Environmental Technology, 3(1): 1-12.

[16] Aqaneghad, M., Moussavi, G., and Ghanbari, R. (2018). Anaerobic baffled reactor and hybrid anaerobic baffled reactor performances evaluation in municipal wastewater. Iranian Journal of Health, Safety and Environment, 5(3): 1027-1034.

[17] Cao, W., and Mehrvar, M. (2011). Slaughterhouse wastewater treatment by combined anaerobic baffled reactor and UV/H2O2 processes. Chemical Engineering Research and Design, 89(7): 1136-1143.

[18] Pirsaheb M., Rostamifar M., Mansouria, A. M., Zinatizadeh A. A. L., and Sharafief K. (2015). Performance of an anaerobic baffled reactor (ABR) treating high strength baker's yeast manufacturing wastewater. Journal of the Taiwan Institute of Chemical Engineers, 47: 137-148.

[19] Khuntia, S., Majumder, S. K., and Ghosh, P. (2013). Removal of ammonia from water by ozone microbubbles. Industrial & Engineering Chemistry Research, 52: 318–326.

[20] Djenar N. S., and Soeswanto B. (2005). Penyerapan polutan logam besi (Fe) dengan memanfaatkan tanaman eceng gondok. Jurnal Fluida, 4(1): 35-40.

[21] Sponza D. T., and Demirden, P. (2010). Relationships between chemical oxygen demand (COD) components and toxicity in a sequential anaerobic baffled reactor/aerobic completely stirred

reactor system treating Kemicetine. Journal of Hazardous Materials, 176(1-3): 64-75.

[22] Işık, M., & Sponza, D. T. (2008). Anaerobic/aerobic treatment of a simulated textile wastewater. Separation and purification technology, 60(1), 64-72.

[23] Czemierska, M., Szcześ, A., and Jarosz-Wilkołazka, A. (2015). Purification of wastewater by natural flocculants. BioTechnologia, 4: 272–278.

[24] Ziembińska-Buczyńsk, A., Wyszyńska, K., and Miksch, K. (2017). Detection and characteristics of sulfamethoxazole-resistant bacteria in constructed wetlands treating sulfamethoxazole-rich wastewater. BioTechnologia, 98 (1): 15-23.

[25] Suryawan I. W. K., Helmy, Q., and Notodarmojo S. (2020). Laboratory scale ozone-based post-treatment from textile wastewater treatment plant effluent for water reuse. The 5th International Conference on Technology and Vocational Teachers; October 5-6, 2019, Yogyakarta, Indonesia. In Journal of Physics: Conference Series 1456: 1-8.

EPI International Journal of Engineering
Volume 3, Number 2, August 2020, pp. 113-118
DOI: 10.25042/epi-ije.082020.04

*p*ISSN 2615-5109
*e*ISSN 2621-0541

Testing of Nutmeg Shell as a Lightweight Concrete Material in Terms of Volume Weight and Compressive Strength Value

Budiman[a,*]

[a]Department of Civil Engineering, Polytechnic State of Fakfak. E-mail: budiman@polinef.id

Abstract

Lightweight concrete can be defined as a type of concrete that includes an expanding agent in that it increases the volume of the mixture while giving additional qualities such as nailability and lessened the dead weight. The nutmeg shell has the characteristics of light and hard skin texture so that it has the potential to be used as a material for lightweight concrete. The purpose of this study is to determine the aggregate characteristic value and the compressive strength value of concrete using the DOE (design of experiment) method and referring to standards SNI. Variation of use nugmet shell toward the weight volume of concrete is 10%, 20%, 30%, 40%, and 50%. This research is sample-based laboratory research and analysis of aggregate characteristics and concrete compression test. The research result shows that the use of nutmeg skin as a coarse aggregate material in the concrete mixture affects the volume weight of the concrete. The weight of the concrete gets lighter along with the higher the percentage used. The average volume weight obtained was 1810.06 kg/m^3. Based on the weight of the concrete sample, it is classified as a light structure, includes concrete with low density and includes lightweight aggregate concrete. The compressive strength values for the characteristics of concrete at a composition of 10%, 20%, and 30% were obtained at 28.42 kg/cm^2, 31.65 kg/cm^{2,} and 32.68 kg/cm^2 which increased while the use of nutmeg shells at 40% and 50% compositions were obtained. values of 29.09 kg/cm^2 and 27.38 kg/cm^2 decreased at the age of 28 days. The increase in the value of the compressive strength of concrete (fck') occurred starting at the composition of 20% and 30% at 10.20% and 13.03% and begin to decrease at the composition of 50% by 3.65%. Lightweight concrete from nutmeg shells has a weight of 1810.06 kg/m^3 and a maximum compressive strength value of 3.2 MPa so that the concrete is in the category of lightweight structure.

Keywords: Compressive strength; lightweight concrete; nutmeg shell; volume weight

1. Introduction

Until now, Indonesia is one of the world's largest producers and exporters of mace and mace, with a market share of 75 percent. The main export destinations for Indonesian nutmeg are Vietnam, the United States, the Netherlands, Germany, and Italy. Indonesia's nutmeg production in 2011 reached 15,793 tonnes, which is produced from a production area of 118,345 hectares and involves 146,331 farmer family owners. Fakfak Regency is one of the main nutmeg producing areas in West Papua Province with production reaching 1,884 tons, 11 percent of Indonesia's total nutmeg production [1]. The production of this nutmeg is certainly comparable to the shell produced, the designation of the shell has not been used properly, it is only thrown away, burned, and piled up so that it becomes a pollutant for the environment.

The nutmeg shell has the characteristics of light and hard skin texture so that it has the potential to be used as a material for lightweight concrete. The use of nutmeg shell as a light aggregate has never been used, so it is interesting to study. The use of certain proportions may affect the behavior of lightweight concrete structures as a whole.

Concrete is a composite material that consists of a cement paste within which various sizes of fine and coarse aggregates are embedded. It contains some amount of entrapped air and may contain purposely-entrained air by the use of air-entraining admixtures both natural and artificial added ingredients (bamigboy). In concrete construction, the concrete represents a very large proportion of the total load on the structure, and there are clearly considerable advantages in reducing its density. One of the ways to reduce the weight of a structure is the use of lightweight aggregate concrete (LWAC) [2].

Lightweight concrete can be defined as a type of concrete that includes an expanding agent in that it increases the volume of the mixture while giving additional qualities such as nailability and lessened the dead weight [3]. It is lighter than the conventional concrete with a dry density of 300kg/m up to 1840 kg/m 87 to 23% lighter. It was first introduced by the Romans in the second century where 'The Pantheon' has been constructed using pumice,the most common type of aggregate used in that particular year [4]. From there on, the use of lightweight

*Corresponding author. Tel.: +62-812-7706-1052
Jalan TPA Imam Bonjol Atas Air Merah, Kelurahan Wagom Fakfak, Papua Barat, Indonesia 98611

concrete has been widely spread across other countries such as USA, United Kingdom, and Sweden.

In recent years, more attention has been paid to the development of lightweight aggregate concrete [5]. The specific gravity of concrete can be lowered either by using porous, therefore lightweight aggregates instead of ordinary ones, or introducing air into the mortar, or removing the fine fractions of aggregate and compacting concrete only partially. In all cases, the main goal is to introduce voids into the aggregate and the mortar or between mortar and aggregate. A combination of these methods can also be made in order to reduce further the weight of concrete. The use of lightweight aggregates is by far the simplest and most commonly used method of making a lightweight concrete [6].

The use of light aggregate from polystyrene material and the addition of 20% sludge of fire, to the sand aggregate produced a compressive strength value of up to 71 kg/cm^2, although the porosity of concrete can be reduced due to the substitution of sludge in concrete [7]. Lightweight concrete from PTE-type plastic waste produces a compressive strength value of 17.49 M of its use on unfavorable structures [8].

The main specialties of lightweight concrete are its low density and thermal conductivity. Its advantages are that there is a reduction of dead load, faster building rates in construction, and lower haulage and handling costs [4].

A porous lightweight aggregate of low specific gravity is used in this lightweight concrete instead of ordinary concrete. The lightweight aggregate can be natural aggregate such as pumice, scoria, and all of those of volcanic origin, and the artificial aggregate such as expanded blast-furnace slag, vermiculite, and clinker aggregate. The main characteristic of this lightweight aggregate is its high porosity which results in a low specific gravity [9].

This study utilizes natural aggregate from nutmeg shells as a substitute for coarse aggregate in lightweight concrete. The research was carried out in the laboratory material testing of Civil Engineering of Fakfak State Polytechnic. The research objective was to determine the effect of characteristics and values with a variety of nutmeg shell compositions of 10%, 20%, 30%, 40%, and 40% on the weight of the concrete volume.

2. Literature Review

2.1. Light concrete

Lightweight concrete has a density of not more than 1900 kg/m^3 [10] and has a compressive strength value of 0.35-6.90 MPa. while according to [11] lightweight concrete has a density between 1000-2000 kg/m^3. Types of lightweight concrete based on concrete weight and compressive strength [10] and Neville and Brooks [11] as shown in Tables 1 and 2.

Table 1. Types of lightweight concrete according to [10]

Weight concretes (kg/m^3)	Compressive strength (MPa)	Types lightweight concretes
240-800	0.35-6.9	Low-Density concretes
800-1440	6.9-17.3	Moderate Strength lightweight concretes
1440-1900	>17.3	Structural lightweight concretes

Table 2. Types of lightweight concrete according to [11]

Weight concretes (kg/m^3)	Compressive strength (MPa)	Types lightweight concretes
1400-1800	>17	Structural lightweight concretes
500-800	7-14	Masonry concretes
<800	0.7-7	Insulating concretes

Normal concrete is obtained by mixing Portland cement, water, and aggregate, while for lightweight concrete the constituent materials are very dependent on the type of lightweight concrete. According to [12] there are 3 types of lightweight concrete, namely lightweight aggregate concrete, foam concrete, and concrete without fine aggregate. The same thing was also conveyed by [13], several methods that can be used to reduce the weight of concrete include the following:

1. Making gas/air bubbles in the cement mix.
2. Using light aggregate, for example, fired clay, pumice stone, or artificial aggregate.
3. Making concrete without using fine aggregate grains (non-sand concrete).

Several parameters that affect the fine aggregate (sand) in determining the quality of the concrete are sludge content, moisture content, volume weight, absorption, specific gravity, fineness modulus, and organic content [14].

The level of sludge is the percentage of a size that passes filter No.200 according to ASTM and British Standards or 80 DIN (Germany) or standard filter hole size = 0.075 mm. Laboratory testing is generally carried out by the washing method according to ASTM C-117 (2000 Sieve in Mineral Aggregate by Washing) Standard Test Method for Materials. Tolerance for testing the fine aggregate sludge content is 0.2% - 6%.

The water content in the aggregate is greatly influenced by the amount of water contained in the aggregate. The bigger the difference between the original aggregate weight and the aggregate weight after oven drying, the more water is contained by the aggregate and vice versa. The tolerance of testing moisture content in fine aggregate is 3% - 5%.

The volume weight is the ratio between the dry aggregate weight and its volume. The aim is to determine the weight of the fine aggregate. The test tolerance for fine aggregate is 1.4 kg/ltr - 1.9 kg/ltr.

The absorption is the percentage by weight of water that can be absorbed by the material to the weight of dry aggregate. Tolerance of testing fine aggregate 0.2% - 2% and coarse aggregate 0.2% - 4%.

The specific gravity is the ratio between the weight of dry aggregate and the weight of distilled water whose content is the same as the aggregate content in a saturated state at a certain temperature. The test tolerance for fine aggregate is 1.6% - 3.3%.

The organic ingredients are materials contained in aggregates that can cause damage to concrete. The organic substances contained in fine aggregates generally come from destroyed plants, especially in the form of humus and organic sludge. Harmful organic substances include sugar, oil, and fat. Sugar can inhibit cement binding and the development of concrete strength, while oil and grease can

reduce cement binding capacity. The test tolerance for fine aggregates is less than a value of 3.

2.2. Compressive strength

Reference [15] provides an understanding of the compressive strength of concrete, which is the amount of load per unit area, which causes the concrete specimen to crumble when loaded with a certain compressive force, which is generated by a compression machine.

3. Research Methodology

3.1. Research stages

The stages of research consist of preparing tools and materials. The material consists of sand, cement, water, and nutmeg shells. Test the characteristics and characteristics of fine aggregate and count the combination of fine aggregate and nutmeg shell as coarse aggregate to get the suitable composition. Designing a concrete mix (mix design) with fck' 10 MPa. Making the composition of the concrete mixture with nutmeg shell variations of 10%, 20%, 30%, 40% and 50% of the weight of the concrete volume. Concrete maintenance for 3.7 and 28 days. Testing the compressive strength of concrete with a target of fck' 10 MPa.

3.2. Characteristic testing

Aggregate characteristic testing uses study literature as shown in Table 3 [15].

3.3. Compressive strength testing

Concrete compressive strength test results using compression machine test were analyzed by using compressive strength equation [15] :

$$fc = \frac{P}{A} \quad (1)$$

where

fc = compressive strength (kg/cm^2)
P = load (kg)
A = the weighted cross-sectional area (cm^2)

4. Result and Discussion

The results of testing the characteristics test of fine aggregate (sand) are shown in Table 4.

Table 3. Aggregate testing and method

No	Types of testing	Method
1	Filter Analysis	SNI 03-1968-1990
2	Specific Weight and Fine Aggregate Absorption	SNI 03-1970-1990
3	Specific Weight and Absorption of Coarse Aggregates	SNI 03-1969-1990
4	Water Content	SNI 03-1971-1990
5	Volume Weight	SNI 03-4804-1998

Table 4. The result of fine aggregate testing

No	Aggregate characteristics	Interval	Testing result	Description
1	Mud levels	Maks. 5%	4.00 %	Qualified
2	Water content	0.5 - 5%	2.33 %	Qualified
3	Volume weight	1.4 - 1.9 kg/liter	1.53	Qualified
4	Absorption	0.2 – 2%	1.01 %	Qualified
5	Specific weight			
	Real S.W	1.6 - 3.3	1.737	Qualified
	Dry-based S.W	1.6	1.768	Qualified
	Dry-surfaced S.W	1.6	1.754	Qualified
6	Roughness modulus	1.5 – 3.8	2.656	Qualified

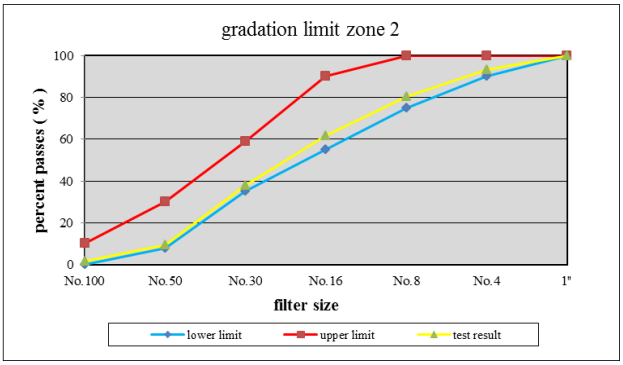

Figure 1. Graphic of fine aggregate gradation

The testing characteristics of fine aggregate, the value of sludge content is 4% and contains organic content which is suitable for use. According to [14] and [16], fine aggregate should not contain more than 5% sludge and not contain organic which can damage concrete. [17] A normal weight washed sand with a (4.75mm) maximum size is used as fine aggregates its use is to fill the space between coarse aggregates and provide discomfort. The graphic of the test results for fine aggregate grains is shown in Fig. 1.

Based on Fig. 1, the modulus of fineness of 2.656 meets the requirements for zone 2. According to [14] a very good sand for concrete mixtures is sand with a zone 2 grading limit.

To know the strength of the concrete quality that will be produced using fine aggregate (sand) and coarse aggregate from nutmeg shells by calculating the aggregate with the cement water factor planning (W/C) = 0.71 as shown in Tables 5 - 9.

Table 5. The results of concrete mix design with nutmeg shell 10%

Concrete material	Weight (kg/m^3)	Ratio to the amount of the cement (kg)	Weight for one sample (kg)	Weight for one sample (kg)
Water	198.626	0.742	1.263	11.371
Cement	267.605	1.000	1.702	15.321
Sand	699.955	2.615	4.452	40.076
CP 10%	21.990	0.082	0.139	1.259
Total	1.188		7.559	68.030

Table 6. The results of concrete mix design with nutmeg shell 20%

Concrete material	Weight (kg/m^3)	Ratio of the amount of the cement (kg)	Weight for one sample (kg)	Weight for one sample (kg)
Water	198.626	0.742	1.263	11.371
Cement	267.605	1.000	1.702	15.321
Sand	699.955	2.615	4.452	40.076
CP 20%	23.32	0.087	0.148	1.335
Total	1.189		7.567	68.106

Table 7. The results of concrete mix design with nutmeg shell 30%

Concrete material	Weight (kg/m^3)	Ratio of the amount of the cement (kg)	Weight for one sample (kg)	Weight for one sample (kg)
Water	198.626	0.742	1.263	11.371
Cement	267.605	1.000	1.702	15.321
Sand	699.955	2.615	4.452	40.076
CP 30%	34.98	0.130	0.222	2.002
Total	1.201		7.641	68.773

Table 8. The results of concrete mix design with nutmeg shell 40%

Concrete material	Weight (kg/m^3)	Ratio to the amount of the cement (kg)	Weight for one sample (kg)	Weight for one sample (kg)
Water	198.626	0.742	1.263	11.371
Cement	267.605	1.000	1.702	15.321
Sand	699.955	2.615	4.452	40.076
CP 40%	46.64	0.174	0.296	2.670
Total	1.212		7.716	69.441

Table 9. The results of concrete mix design with nutmeg shell 50%

Concrete material	Weight (kg/m^3)	Ratio of the amount of the cement (kg)	Weight for one sample (kg)	Weight for one sample (kg)
Water	198.626	0.742	1.263	11.371
Cement	267.605	1.000	1.702	15.321
Sand	699.955	2.615	4.452	40.076
CP 40%	58.30	0.217	0.370	3.338
Total	1.224		7.790	70.109

The calculation of the results of the design above, it is obtained that the difference in weight of light concrete with 10% nutmeg shells is obtained 1,188 kg/m^3, 20% of 1,189 kg/m^3, 30% of 1,201 kg/m^3, 40% of 1,212 kg/m^{3}and 50% of 1,224 kg/m^3. The weight value of the concrete shows that the use of nutmeg shells on the concrete affects the weight of the concrete itself and the compressive strength value of the concrete characteristics.

The results of testing the concrete mixture with nutmeg shells obtained an average correction water factor value of 0.30. The recapitulation of the volume weight of fresh concrete from the test results was analyzed by the average weight value of fresh concrete obtained divided by the volume of cylindrical specimens as in Table 10 and Fig. 2.

Table 10. The weight volume of freshly concrete

No	Sample	Volume of Freshly Concrete (kg/m^3)
1	Nutmeg shell concrete 10%	1865,6
2	Nutmeg shell concrete 20%	1837,3
3	Nutmeg shell concrete 30%	1792,4
4	Nutmeg shell concrete 40%	1780,2
5	Nutmeg shell concrete 50%	1774,8

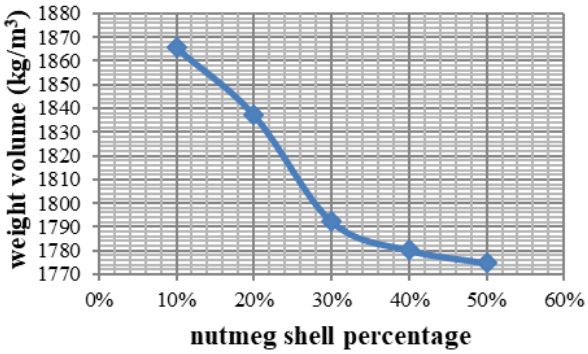

Figure 2. Weight volume

Based on Fig. 2 the weight of fresh concrete from 10% nutmeg is 1865.6 (kg/m^3) while for 50% it is obtained 1774.8 (kg/m^3), a decrease of 4.86%. The greater the percentage value of nutmeg shells used in the lightweight concrete design mixture, the lighter the volume weight of the fresh concrete. This practice will enable the attainment of the specified fresh and hard concrete properties [18]. As also emphasized by Goldbeck and Gray [19] the use of appropriate mix proportions of materials for on-site concrete production will allow suitable mix proportions for certain strength characteristics to be achieved rather than the usual procedure of using unapproved mix ratios for design strength targeted.

The results of the analysis of the test value of the compressive strength of concrete using nutmeg shells at the age of 28 days, shows that light concrete with the use of nutmeg shells as coarse aggregate in the concrete mixture affects the compressive strength of the concrete characteristics (fck'). The compressive strength values for the characteristics of concrete at a composition of 10%, 20%, and 30% were obtained at 28.42 kg/cm^2, 31.65 kg/cm^{2,} and 32.68 kg/cm^2 which increased while the use of nutmeg shells at 40% and 50% compositions were obtained. The values of 29.09 kg/cm^2 and 27.38 kg/cm^2 decreased at the age of 28 days as in Table 10 and Fig. 3.

Table 11. The compressive strength characteristics of concrete

No	Sample	Value fck' (kg/cm^2)
1	Nutmeg shell concrete 10%	28.42
2	Nutmeg shell concrete 20%	31.65
3	Nutmeg shell concrete 30%	32.68
4	Nutmeg shell concrete 40%	29.09
5	Nutmeg shell concrete 50%	27.38

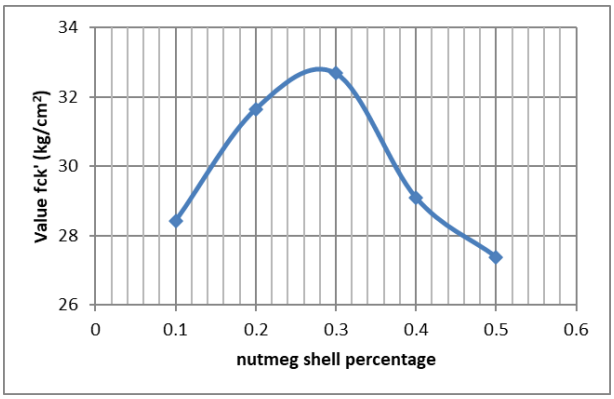

Figure 3. Value of fck'

As shown in Fig. 3 that the maximum concrete compressive strength (fck') value at the nutmeg shell composition is 30%. The increase in the value of the compressive strength of concrete (fck') was 13.03% and began to decrease in the composition of 40% and 50% of 3.65%. The decrease in the compressive strength value is influenced by the higher percentage of nutmeg shells that are used in the concrete mix, thereby reducing the volume of concrete that should be filled with cement paste. However, adding more nutmeg shells 40% and 50% of the volume of the concrete reduces the increase in compressive strength compared to 10%, 20%, and 30% remains higher and this is attributed to the inclusion of cavities in the mixture as the excessive fiber content of it can lead to reduced bonding. and disintegration [20].

Lightweight concrete according to [21] is concrete with a concrete weight below 1860 kg/m^3 with types of lightweight concrete consisting of structural, lightweight and very light structural concrete. Lightweight concrete from nutmeg shells has an average weight of 1810 kg/m^3 and a maximum compressive strength value of 3,26 MPa so that the concrete is in the lightweight structure category.

According to [10] and [11] lightweight concrete with low density has a concrete weight of 240 kg/m^3 - 800 kg/m^3 with a compressive strength value of 0.35-6.90 Mpa. The range of compressive strength values, lightweight concrete from nutmeg shell is included in the lightweight concrete category with low density, so it can be concluded that nutmeg shell has the opportunity to be used as a building material for lightweight concrete.

Classification of lightweight concrete based on the weight of concrete If referring to [12], then most of the weight of light concrete in this study is classified as light structure as an insulator, [10] includes concrete with low density, the classification of [11] includes heat-resistant lightweight concrete and [13] includes lightweight aggregate concrete.

5. Conclusion

The use of nutmeg skin as a coarse aggregate material in the concrete mixture affects the volume weight of the concrete. The weight of the concrete gets lighter along with the higher the percentage used. The average volume weight obtained was 1810.06 kg/m^3. Based on the weight of the concrete sample, it is classified as a light structure, includes concrete with low density and includes lightweight aggregate concrete. The compressive strength values for the characteristics of concrete at a composition of 10%, 20%, and 30% were obtained at 28.42 kg/cm^2, 31.65 kg/cm^{2,} and 32.68 kg/cm^2 which increased while the use of nutmeg shells at 40% and 50% compositions were obtained. values of 29.09 kg/cm^2 and 27.38 kg/cm^2 decreased at the age of 28 days. The increase in the value of the compressive strength of concrete (fck') occurred starting at the composition of 20% and 30% at 10.20% and 13.03% and begin to decrease at the composition of 50% by 3.65%.

Further research is needed to determine the appropriate composition for both lightweight concrete and normal concrete. Further research is needed using a smaller percentage interval and It is recommended to use nutmeg shell as coarse aggregate in light concrete with a low-density scale and intended for light structures, besides saving costs, it can also reduce waste that has an impact on the environment.

References

[1] ILO-PCdP2 UNDP, 2018. Report Development Program Community Based Fakfak District Phase II: Implementing Institutionalization of Sustainable Livelihood Development for Papuans.
[2] Mouli, M.& Khelafi, H. (2008). Performance characteristics of lightweight aggregate concrete containing natural pozzolan, Build. Environ. 43:31-36.
[3] Zakaria, M.L. (1978). Materials and Development, Language and Library Board.
[4] Samidi,M.R.(1997). First report research project on lightweight concrete, University Teknologi Malaysia, Skudai, Johor Bahru.
[5] Lo TY. Tang, WC. & Cui, HZ. (2007). The effects of aggregate properties on lightweight concrete, Build. Environ. 42: 3025-3029.
[6] Gündüz, L. & Uğur, I. (2005). The effects of different fine and coarse pumice aggregate/cement ratios on the structural concrete properties without using any admixtures, Cement Concrete Res. 35: 1859-1864.
[7] Fyzingsa., Dekarius Wiyan, Eka Selvi Elly Aggraeni, 2 009, Light Weight Making with the Addition of Lapindo Sludge and Artificial Aggregates in the Form of Polystiren, Thesis Engineering Study Program Sipil Inst itut Technology Sepuluh November, Surabaya.
[8] Pratikto, 2010, Lightweight Concrete Aggregated with PET (Polyetylene Terepthalate) Plastic Bottle Waste, National Seminar on Civil Engineering-2010, State Polytechnic of Jakarta, Jakarta.
[9] Lo, T.Y. & Cui, H.Z. (2004). "Effect of Porous Lightweight Aggregate on Strength of Concrete", Materials and Letters, Vol.58, pp. 916-919.
[10] Dobrowolski, A. J., 1998, *Concrete Construction Hand Book*, The Mc. Graw Hill Companies, Inc., New York.
[11] Neville, A.M. and Brooks, J.J., 1987, *Concrete Technology*, John Willey & Sons, New York.
[12] Raju, K.N., 1983, *Design of Concrete Mixes*, CBS Publishers & Distributors, 485, Jain Bhawan, Bhola Nath Nagar Shandra, Delhi-110032 (India).
[13] Tjokrodimuljo Kardiyono, 1996. "Concrete Technology", Department of Civil Engineering, Faculty of Civil Engineering, Gajah Mada University.
[14] National Standard Agency. 2002. Procedure for C Light Concrete Mixing with Light Aggregate SNI 03-3449-2002. Jakarta: National Standard Agency.
[15] SK SNI 03-1974-1990. Concrete Compressive Strength. National Standardization Body. 1990.
[16] Li, Z. Advanced concrete technology. New Jersey: John Wiley & Sons, 2011.
[17] Zinkaah, O. H. (2014). Influence of Steel Fibers on the Behavior of Light Weight Concrete Made from Crushed Clay Bricks. American Journal of Civil Engineering. Vol. 2, No. 4, 2014, pp. 109-116. doi : 10.11648/j.ajce.20140204.11
[18] Olusola, K. O., Babafemi, A. J., Umoh, A. A. and Olawuyi, B. J. Effect of batching methods on the fresh and hardened properties of concrete. *International Journal of Research and Reviews in Applied Sciences*, **13**(3), 2012, pp 7-12.

[19] Goldbeck, A. T and Gray, J. E. A method of proportioning concrete for strength, workability and durability. *National Crushed Stone Association, Engineering Bulletin* **11**, 1968, pp 1-37.

[20] Dawood, ET. & Ramli, M. (2009) "Study the effect of using palm fiber on the properties of high strength flowable mortar", CI Premier: 34th OWICs papers, Singapore. 2009; 93-101.

[21] Department of Public Works, 1994, Specification for Building Materials Part A (Non-Metal Building Materials), SNI 03-3449-1994, DPU of LPMB Foundation, Bandung.

EPI International Journal of Engineering
Volume 3, Number 2, August 2020, pp. 119-125
DOI: 10.25042/epi-ije.082020.05

*p*ISSN 2615-5109
*e*ISSN 2621-0541

Monitoring and Predicting Water Quality in Swimming Pools

Apriandy Angdresey[a], Lanny Sitanayah[b,*], Vandri Josua Abram Sampul[c]

[a]Department of Informatics Engineering, Faculty of Engineering, Universitas Katolik De La Salle, Manado - Indonesia.
Email: aangdresey@unikadelasalle.ac.id
[b]Department of Informatics Engineering, Faculty of Engineering, Universitas Katolik De La Salle, Manado - Indonesia.
Email: lsitanayah@unikadelasalle.ac.id
[c]Department of Informatics Engineering, Faculty of Engineering, Universitas Katolik De La Salle, Manado - Indonesia.
Email: 16013015@unikadelasalle.ac.id

Abstract

Water quality in public swimming pools affects human health. While changing the water too soon is wasteful, postponing changing the dirty water is not hygiene. In this paper, we propose an Internet of Things-based wireless system to monitor and predict water quality in public swimming pools. Our system utilizes an Arduino Uno, an ESP8266 ESP-01 WiFi module, a DS18B20 temperature sensor, a pH sensor, and a turbidity sensor. We predict the water quality using a data mining prediction model, namely the decision tree Iterative Dichotomiser 3 algorithm. We show by experiment that our sensor node and the wireless monitoring system work correctly. We also show by simulation using Weka that we can get 100% accuracy with a kappa statistical value of 1 and 0% error rate.

Keywords: Data mining; decision tree; iterative dichotomiser 3; Internet of Things

1. Introduction

Swimming is a kind of sport fancied by many people; not only children, but also adults. This sport makes our body healthy, because when we swim, we use almost all muscles in our body. Swimming is not only a sport, but also a recreational activity. Nowadays, there are many public swimming pools available for recreation or competition. As the pools are used by many people, water cleanliness triggers health issues. Swimming in a dirty pool can cause infectious diseases, such as skin diseases, diarrhea, eye irritation, and respiratory tract irritation.

In swimming pools, we can control disease-causing bacteria by adding chlorine in the water. Water acidic or the pH level is very important to determine how effective the disinfectant can kill germs. However, people can get eye or respiratory tract irritation due to the vapor from chloramine that is formed by chlorine and sweat or urine. Therefore, changing pool water regularly is necessary to improve water quality and hygiene. A simple solution is using a fixed schedule to change the water, for example once a week or every two weeks. However, if the water is still clean, it will be wasteful. If the water is too dirty, it is not hygiene until the next change schedule. Another solution is measuring the pH level and turbidity of the water manually, but this too is neither cost effective nor efficient as it may require several personnel visits to the pool.

Monitoring and predicting water quality in swimming pools can be done remotely thanks to the Internet of Things. The Internet of Things offer new platforms that enable physical objects equipped with sensor devices – with or without batteries [1] – to communicate and exchange information wirelessly without human intervention [2]. In this paper, we develop an Internet of Things-based wireless system to monitor and predict water quality in public swimming pools. Our contributions in this paper are two-folds:

1) Firstly, we design and implement a wireless system to monitor water quality in public swimming pools using an Arduino Uno, an ESP8266 ESP-01 WiFi module, a DS18B20 temperature sensor, a pH sensor, and a turbidity sensor.
2) Then, we utilize a data-mining prediction model to predict the quality of water in public swimming pools using the decision tree Iterative Dichotomiser 3 (ID3) algorithm.

The rest of this paper is organized as follows. Section 2 discusses the related works. Section 3 shows our system framework, such as hardware and software design and implementation. Section 4 describes our methods for water quality prediction. Section 5 reports our experiments and simulation results. Finally, Section 6 concludes this paper and suggests some future directions.

*Corresponding author. Tel.: +62-812-4365-9655
Universitas Katolik De La Salle
Manado, Indonesia

2. Related Works

The Internet of Things (IoT) enable physical objects equipped with smart sensors, *i.e.* from gas sensors [3] to medical sensors, to transmit data using wireless technology. One of the implementations of the Internet of Things is a Wireless Sensor Network-based monitoring and control system based on the use of electrical energy [4]. In this study, wireless sensor nodes are designed to measure electrical parameters of Alternating Current (AC) as effective voltage, effective current, active power, apparent power, power factor and total electrical energy consumption using the ESP8266 module as a link with WiFi. Power consumption monitoring through the Internet can show several electrical parameters with the same data from the data logger recap taken from an SD-Card installed in a wireless sensor node through an Android application and web browser.

In [5], the authors monitor the quality of lake water based on the parameters of acidity (pH), turbidity, dissolved oxygen (DO) and water temperature to provide an early warning when the lake water quality is approaching a given threshold, so that the loss of fish farmers in the lake can be minimized. The data of water quality measured by existing sensors is collected in a data logger and forwarded using a cellular network. The data is stored and displayed on a website and can be accessed from anywhere.

By using available and relevant data, data mining can generate several models to identify patterns among attributes that exist in a data-set. Some of the patterns can be predictive such as predicting the value or results that will occur on certain attributes. As in [6], the authors identify and predict the sex of tarantula using training data taken for almost one year. In addition, data mining can be implemented to conduct opinion mining, such as text document that crawls in social media that contains comments, criticism and reviews about presidential candidates of Republic Indonesia in 2019 [7].

There are several algorithms that can be applied in processing data mining; one of which is decision tree. Most of data mining algorithms are supervised learning. Decision tree uses a hierarchical structure for supervised learning. This algorithm performs the learning process based on the value of the target variable associated with the value of the predictor variables. By using this algorithm, the area of decision making, which was previously complex and very global, can be changed to be simple and specific.

There are several implementations of decision tree algorithms, such as in [8], the authors investigate an Android malware and detect it using decision tree algorithms. In [9], the study is about the influence on share price in accordance with financial fundamentals of a company. This paper builds a stock investment using the decision tree model through the ID3 algorithm. The results can provide decision support for future investments through the analysis of the current financial and market situation. The ID3 algorithm is also used in expert systems, such as in [10], where they develop an expert system that can predict whether a person is addicted to being vulnerable to drugs or not. Hence, they can control and be aware of any drug abuser as they can conduct the test repeatedly to cure them without hesitation.

3. System Design and Implementation

The wireless system for water quality monitoring in swimming pools is depicted in Fig. 1. Our system consists of one sensor node that periodically gathers data from a swimming pool and sends the data wirelessly via the Internet to the web server to be processed further. A user can then access the information using a web browser.

The main components of our sensor node are an Arduino Uno [11], an ESP8266 ESP-01 WiFi module [12], and three sensors, *i.e.* a DS18B20 temperature sensor, a pH sensor and a turbidity sensor. The three sensors and ESP8266 ESP-01 are connected to Arduino via wired connections. The sensor node design is shown in Fig. 2. Arduino periodically collects data from the three sensors and utilizes the WiFi module to send data wirelessly to the web server. We show the sensor node design in Fig. 2, the real image of the sensor node in Fig. 3 and the list of our hardware and software used in Table 1.

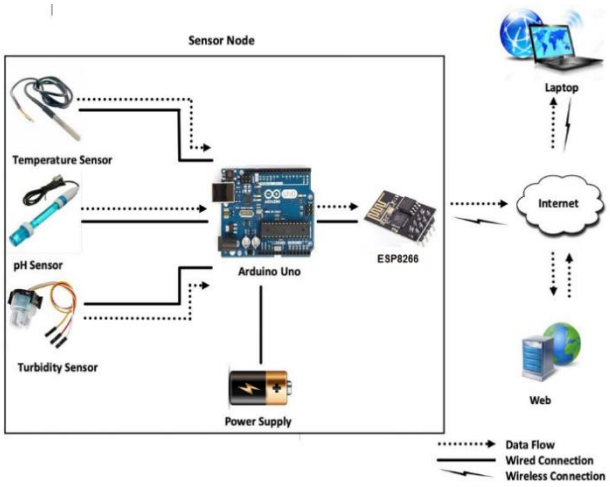

Figure 1. The monitoring system

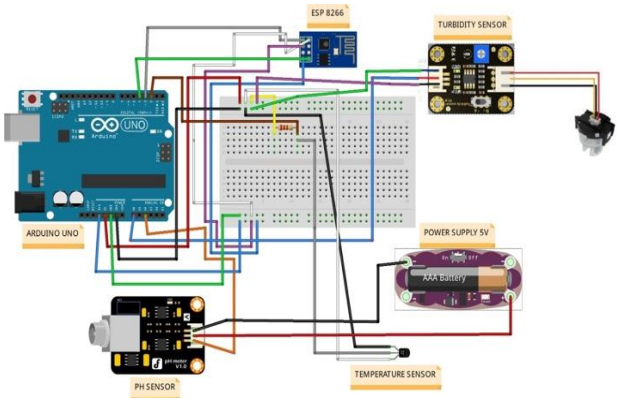

Figure 2. The sensor node design

Table 1. Hardware and software

Hardware/Software	Purpose
Arduino Uno	Collect, transform and send data.
ESP8266 ESP-01	WiFi module.
pH Sensor	Acidity sensor.
Turbidity Sensor	Turbidity sensor.
DS18B20 Sensor	Temperature sensor.
Laptop/Mobile Device	Access data from the web server.
Arduino Program	Collect, transform and send data.
PHP Program	Process data.

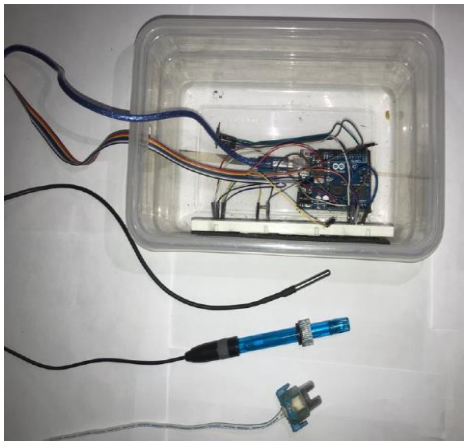

Figure 3. A sensor node consists of an Arduino Uno, a pH sensor, a turbidity sensor, a temperature sensor and an ESP8266 ESP-01

We implemented two programs to be used in our system for data collection, data transmission, and data processing. The first program is implemented using Arduino IDE and uploaded to the Arduino board. This program reads data from the three sensors, transforms and sends them using the WiFi module. The second program is implemented using Hypertext Preprocessor (PHP) for the web server. This program processes the data using machine learning techniques to produce useful information for users who can access it from a web browser.

Figure 4 shows processes in the client-side (sensor node). After system initialization, if an Internet connection is available, the sensor node gets readings from the three sensors, i.e. the temperature, pH, and turbidity sensors. Then, the raw data is transformed using predefined categories. For example, there are three categories for acidity, namely acidic, neutral, and alkaline. The two categories for turbidity are turbid and non-turbid, while temperature is categorized into hot, normal, and cold. The transformed data is sent to the server wirelessly, then the buffer is cleared. These processes occur repeatedly in a loop.

Figure 5 shows processes in the server-side, which also occur in a loop. Firstly, if the server is connected to the Internet, it can receive data sent by the sensor node. The data is then processed using the decision tree Iterative Dichotomiser 3 algorithm and stored in the database.

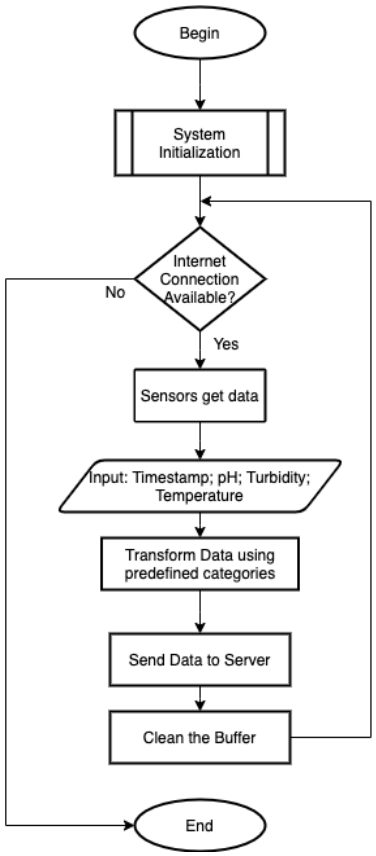

Figure 4. Client flowchart

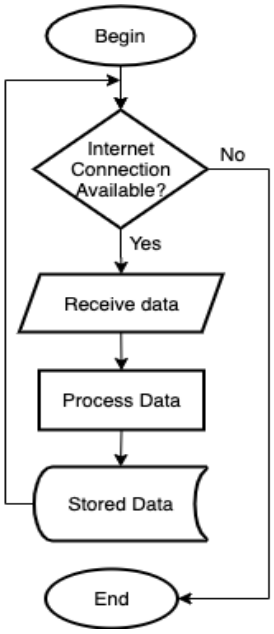

Figure 5. Server flowchart

4. Prediction Methods

In this section, we will discuss about the prediction methods, *i.e.* the decision tree methods with the ID3 algorithm on training data to predict water quality. The ID3 algorithm is an algorithm used to construct a decision tree that uses a hierarchical structure for supervised learning. The process of constructing the decision tree is done recursively.

The classification process is divided into two phases, namely learning and test. In the learning phase, most of the data that has been known its class of data are fed to model estimates. Moreover, in the test phase, the model formed from the learning phase is tested with most of other data to determine the accuracy of the model. This model is used for our prediction.

Historical data is presented in a table with attributes and records. Attributes declared as a parameter is created from the training data as a criterion in forming the tree, and the attribute values are called instances. In this study, we consider acidity, turbidity and temperature of water. Historical data is taken by existing sensors and is collected directly to web server. After that, the historical data is cleared and transformed. The value of each data obtained is numeric, so we change the data by categorizing it to show several different conditions. In this case, for acidity we have three categories, namely acidic (pH 0-6), neutral (pH 6.1-7.9) and alkaline (pH 8-14). Turbidity is divided into clear and cloudy. And for temperature, there are three categories, namely hot (less than 25 degrees), normal (25-35 degrees) and cold (more than 35 degrees). Entropy, as shown in Equation 3, defines the value of information gain, which is used to measure the effectiveness of an attribute in data classification. Entropy, defined in Equation 2, is the sum of probability of each label times the log probability of that same label. P_i, as shown in Equation 1, is the ratio of class i in the set S which is a set of attributes that are classified.

$$P_i = \frac{\sum_k^m X_k \in (i)}{S} \quad (1)$$

$$Entropy(S) = \sum_i^n -P_i Log_2(P_i) \quad (2)$$

$$Gain(S, A) = Entropy(S) - \sum_{\upsilon \in Values(A)} \frac{S\upsilon}{St} EntropySv \quad (3)$$

Where A is an attribute, S_v is declared number of samples for the value of v, and St is the total number of data samples. Meanwhile, entropy S_v is the entropy for samples that has value v. The following is an example to calculate entropy and gain. Suppose that the existing historical data have attributes such as Weather, Temperature, Humidity and Windy. Each attribute has a value. There are two classes: "play" and "not play". If the number of "play" class is 10 and the number of "not play" class is 4, then

$$Entropy(s) = (-(10/14)\ log_2(10/14) + (-(4/10)\ log_2(4/10)) = 0.863120569 \quad (4)$$

After getting the entropy of the whole case, one needs to perform analysis on each of the attributes and values and calculate the entropy. After getting the entropy value, the next step is to calculate the information gain value of each variable. *Gain(Weather)* = 0.863120569 - ((4/10) 0 + (5/14) 0.721928095 + (5/14) 0.970950594) = 0.258521037. Similarly, one needs to calculate *Gain(Temperature)*, *Gain(Humidity)*, and *Gain(Windy)*. The largest gain value will be the root node.

Furthermore, the quality of the classification rule will be evaluated using accuracy. Accuracy is the percentage of tuples that are covered and properly classified.

5. Evaluation and Result

We evaluate the wireless monitoring system by firstly showing that the sensor node and the system work correctly. Then, we show the result of our ID3 algorithm's simulation using data gathered from the sensor node.

(a)

(b)

Figure 6. Clean water test

(a)

(b)

Figure 7. Hot coffee test

5.1. Hardware evaluation

To test whether the sensor can sense correctly, firstly we test it by using spring water. We put spring water, which has neutral acidity, clear turbidity, and normal temperature, in a container as shown in Fig. 6(a). Then, we let the sensor detect the water quality and send the data to the web server to be processed and displayed at the web browser as depicted in Fig. 6(b). The second test uses hot coffee, which is acidic, not clear (cloudy), and hot, as shown in Fig. 7(a). This test too can be displayed correctly at the web browser as depicted in Fig. 7(b).

5.2. System evaluation

We evaluate our wireless monitoring system to show that the sensor node is able to capture acidity, turbidity and temperature data from a swimming pool, transform, send, and store the data correctly in our database. In our evaluation, the sensor node senses the environment every 10 minutes. However, for a better presentation in this paper, we only capture several chunks of data from the database that show different monitoring conditions. Note that in this system, the sensor node does not send numerical data, but only the transformed data.

Figure 8 shows the acidity transformed data, Figure 9 shows the turbidity transformed data, and Figure 10 shows the temperature transformed data, where one time unit is equivalent to 10 minutes. As we can retrieve this data from the database, it means our wireless monitoring system is able to collect data from the three sensors, transform, and send the data to the web server correctly. Table 2 shows the transformed data and the classes (clean and dirty) used in prediction.

Table 2. Transformed data

No.	Acidity	Turbidity	Temperature	Class
1	Neutral	Clear	Normal	Clean
2	Neutral	Clear	Normal	Clean
3	Neutral	Clear	Normal	Clean
…	…	…	…	…
21	Acidic	Clear	Normal	Clean
22	Acidic	Clear	Normal	Clean
79	Alkaline	Clear	Normal	Clean
80	Neutral	Clear	Normal	Clean
…	…	…	…	…
105	Alkaline	Clear	Normal	Clean
106	Acidic	Cloudy	Hot	Dirty
107	Acidic	Cloudy	Hot	Dirty
…	…	…	…	…
147	Acidic	Clear	Cold	Dirty
148	Acidic	Cloudy	Hot	Dirty
…	…	…	…	…
222	Alkaline	Clear	Cold	Dirty
223	Alkaline	Clear	Cold	Dirty
224	Alkaline	Cloudy	Cold	Dirty
…	…	…	…	…
340	Alkaline	Cloudy	Normal	Dirty
341	Alkaline	Cloudy	Normal	Dirty
342	Alkaline	Cloudy	Normal	Dirty

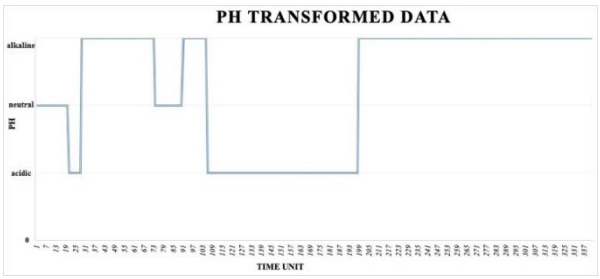

Figure 8. Acidity transformed data

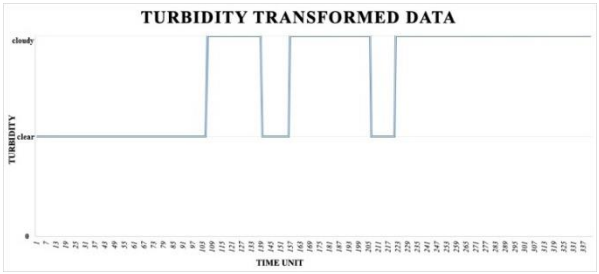

Figure 9. Turbidity transformed data

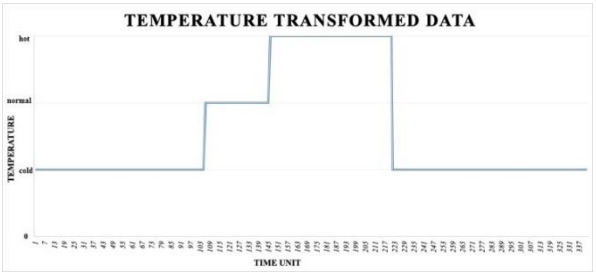

Figure 10. Temperature transformed data

5.3. ID3 simulation

In this phase, we conduct two trials. In the first trial, we build the water quality monitoring application. Users can see the sensor data in real time and make predictions using ID3, which is shown in Fig. 11.

Figure 11. The water quality monitoring application

The second trial use Weka to conduct simulations on learning data that we get to calculate the accuracy and kappa values. We divide the simulations into three different experiments. In the first experiment, we split the data into 80% learning data and 20% test data. In the second experiment, we split the data into 70% and 30%, then in the third experiment, we split it into 60% and 40%.

Figure 12 shows the results of the first experiment, Figure 13 shows the second experiment, and Figure 14 shows the third one. From these results, it can be seen that the accuracy value obtained from these three experiments is 100% with a kappa statistical value of 1 and 0% error rate. Figure 15 shows the comparison of execution time from the first experiment to the third experiment, where the second and the third experiments have better execution time.

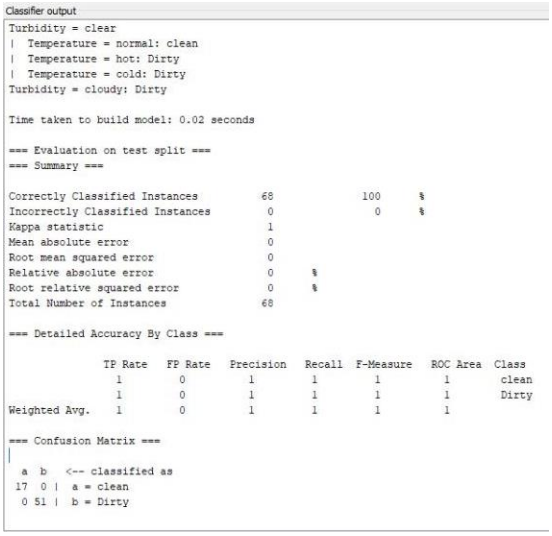

```
Classifier output
Turbidity = clear
|  Temperature = normal: clean
|  Temperature = hot: Dirty
|  Temperature = cold: Dirty
Turbidity = cloudy: Dirty

Time taken to build model: 0.02 seconds

=== Evaluation on test split ===
=== Summary ===

Correctly Classified Instances          68               100      %
Incorrectly Classified Instances         0                 0      %
Kappa statistic                          1
Mean absolute error                      0
Root mean squared error                  0
Relative absolute error                  0      %
Root relative squared error              0      %
Total Number of Instances               68

=== Detailed Accuracy By Class ===

               TP Rate   FP Rate   Precision   Recall  F-Measure   ROC Area  Class
                 1         0          1         1         1          1        clean
                 1         0          1         1         1          1        Dirty
Weighted Avg.    1         0          1         1         1          1

=== Confusion Matrix ===

  a  b   <-- classified as
 17  0 |  a = clean
  0 51 |  b = Dirty
```

Figure 12. Experiment 1

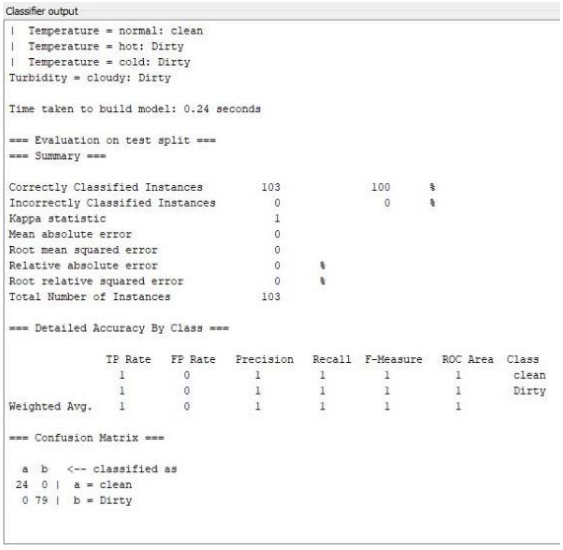

```
Classifier output
|  Temperature = normal: clean
|  Temperature = hot: Dirty
|  Temperature = cold: Dirty
Turbidity = cloudy: Dirty

Time taken to build model: 0.24 seconds

=== Evaluation on test split ===
=== Summary ===

Correctly Classified Instances         103               100      %
Incorrectly Classified Instances         0                 0      %
Kappa statistic                          1
Mean absolute error                      0
Root mean squared error                  0
Relative absolute error                  0      %
Root relative squared error              0      %
Total Number of Instances              103

=== Detailed Accuracy By Class ===

               TP Rate   FP Rate   Precision   Recall  F-Measure   ROC Area  Class
                 1         0          1         1         1          1        clean
                 1         0          1         1         1          1        Dirty
Weighted Avg.    1         0          1         1         1          1

=== Confusion Matrix ===

  a  b   <-- classified as
 24  0 |  a = clean
  0 79 |  b = Dirty
```

Figure 13. Experiment 2

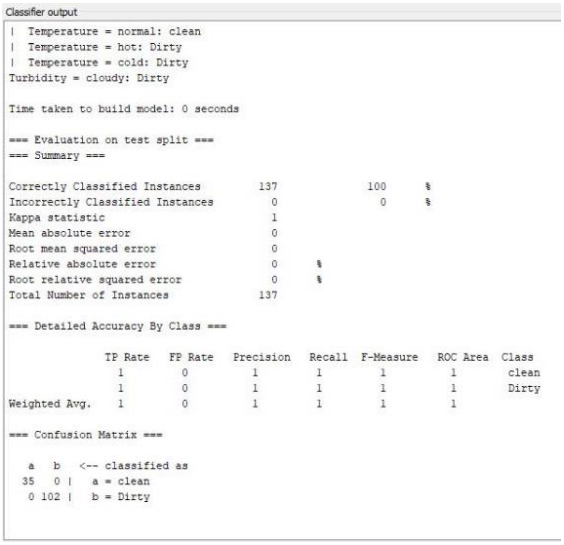

```
Classifier output
|  Temperature = normal: clean
|  Temperature = hot: Dirty
|  Temperature = cold: Dirty
Turbidity = cloudy: Dirty

Time taken to build model: 0 seconds

=== Evaluation on test split ===
=== Summary ===

Correctly Classified Instances         137               100      %
Incorrectly Classified Instances         0                 0      %
Kappa statistic                          1
Mean absolute error                      0
Root mean squared error                  0
Relative absolute error                  0      %
Root relative squared error              0      %
Total Number of Instances              137

=== Detailed Accuracy By Class ===

               TP Rate   FP Rate   Precision   Recall  F-Measure   ROC Area  Class
                 1         0          1         1         1          1        clean
                 1         0          1         1         1          1        Dirty
Weighted Avg.    1         0          1         1         1          1

=== Confusion Matrix ===

   a   b   <-- classified as
  35   0 |   a = clean
   0 102 |   b = Dirty
```

Figure 14. Experiment 3

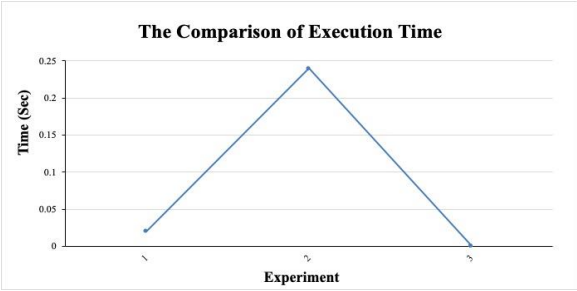

Figure 15. Execution time comparison

6. Conclusion and Future Work

In this paper, we propose a wireless solution based on the Internet of Things to monitor and predict water quality in public swimming pools. Our system consists of one sensor node that periodically sends temperature, pH, and turbidity conditions to a web server for further processing. We utilize the Decision Tree method, namely Iterative Dichotomiser 3, to predict the water quality. We show by experiment that our sensor node and the wireless monitoring system work correctly. Then, based on the Weka simulations, we show that the experiments achieve 100% accuracy with a kappa statistical value of 1 and 0% error rate.

Currently, our monitoring system has only one sensor node. In the future, we plan to add more sensor nodes and deploy them at different places in a pool. We also plan to utilize more sensors, so we can get more variables for prediction. As our current system can only monitor and predict water quality, we would like to incorporate automation capability into the system. For example, adding chlorine automatically to improve the pool's water quality.

References

[1] J. Hester, N. Tobias, A. Rahmati, L. Sitanayah, D. Holcomb, K. Fu, W. Burleson, and J. Sorber. Persistent clocks for batteryless sensing devices. *ACM Transactions on Embedded Computing Systems*, 15:1–28, Aug. 2016.

[2] F. Balo. Internet of things: A survey. International Journal of Applied Mathematics, Electronics and Computers, pages 104–110, Dec. 2016.

[3] J.B. Sanger, L. Sitanayah, and V.D. Kumenap. Detection system for cigarette smoke. In *4th International Conference on Information Technology, Information Systems and Electrical Engineering (ICITISEE)*, pages 145–149, 2019.

[4] I. Giriantari, I. Eka Putra and L. Jasa. Monitoring penggunaan daya listrik sebagai implementasi internet of things berbasis wireless sensor network. *Majalah Ilmiah Teknologi Elekt*ro, 16(3):50–55, 2017.

[5] D. Sudirman and N. Hidayatullah. Aplikasi sistem monitoring kualitas air danau sebaga mitigasi kebencanaan berbasis IoT. *Jurnal Poli-Teknologi*, 18(2), 2019.

[6] A. Angdresey and M. Wongkar. Identification of the reproductive apparatus of tarantula genus brachypelma using linear discriminant analysis method. *In International Conference on Electrical Engineering and Computer Science (ICECOS)*, pages 409–414, 2018.

[7] M. Wongkar and A. Angdresey. Sentiment analysis using naïve bayes algorithm of the data crawler: Twitter. *In Fourth International Conference on Informatics and Computing (ICIC)*, pages 1–5, 2019.

[8] A. Utku, I.A. Do ̆gru, and M.A. Akcayol. Decision tree based android malware detection system. *In 26th Signal Processing and Communications Applications Conference (SIU)*, pages 1–4, 2018.

[9] C. Chen. The apply of ID3 in stock analysis. *In 6th International Conference on Computer Science Education (ICCSE)*, pages 24–27, Aug. 2011.

[10] Kaur and R.K. Bawa. Implementation of an expert system for the identification of drug addiction using decision tree ID3 algorithm. *In 3rd International Conference on Advances in Computing, Communication Automation (ICACCA) (Fall)*, pages 1–6, Sep. 2017.

[11] Arduino. Available at https://components101.com/ microcontrollers/arduino-uno. [22 February 2020].

[12] Getting Started With the ESP8266 ESP-01. Available at https://www.instructables.com/id/Getting-Started-With-the-ESP8266-ESP-01/. [22 February 2020].

EPI International Journal of Engineering
Volume 3, Number 2, August 2020, pp. 126-131
DOI: 10.25042/epi-ije.082020.06

*p*ISSN 2615-5109
*e*ISSN 2621-0541

6 Monopole Elements Array Intelligent Antennas for IoT Based Environmental Surveillance Network

Elyas Palantei[a,*], Arif Hidayat[b], Wardi[c], Intan Sari Areni[d], Sunarno[e], Eko Setijadi[f], Dewiani Jamaluddin[g], Merna Baharuddin[h], Ahmad Khatami[i], Muhammad Sabirin Hadis[j], Akbar Hendra[k], Nurfitri Kaharuddin[l], Priska Wina[m], Mainsuri[n], Vickyarnoldo Wantura[o] and Mulyadi[p]

[a]Department of Electrical Engineering, Faculty of Engineering, Hasanuddin University. Email: elyas_palantei@unhas.ac.id
[b]LAPAN Pare-Pare, South Sulawesi. E-mail: arif.hidayat81@gmail.com
[c]Department of Electrical Engineering Faculty of Engineering, Hasanuddin University. Email: wardi@unhas.ac.id
[d]Department of Electrical Engineering Faculty of Engineering, Hasanuddin University. Email: intan_sariareni@unhas.ac.id
[e]Department of Nuclear and Physics Engineering, Universitas Gadjah Mada (UGM), Yogyakarta. Email: sunarno@ugm.ac.id
[f]Department of Electrical Engineering, Institut Teknologi Sepuluh Nopember (ITS), Surabaya. Email: e_setijadi@ee.its.ac.id
[g]Department of Electrical Engineering Faculty of Engineering, Hasanuddin University.
[h]Department of Electrical Engineering Faculty of Engineering, Hasanuddin University. Email: merna@unhas.ac.id
[i]Center of Excellence for Applied Intelligent Technology, Faculty of Engineering, Hasanuddin University
[j]PT. Balla Cerdas Teknologi and STMIK AKBA, Makassar. Email: muhammadsabirinhadis@gmail.com
[k]PT. Balla Cerdas Teknologi and STMIK AKBA, Makassar. Email: akbarhendra842@gmail.com
[l]Center of Excellence for Applied Intelligent Technology (CEAIT), Faculty of Engineering, Hasanuddin University.
E-mail : nurfitri3003@gmail.com
[m]Department of Electrical Engineering Faculty of Engineering, Hasanuddin University. Email: winapriska@gmail.com
[n]Department of Electrical Engineering Faculty of Engineering, Hasanuddin University. Email: mainsuri.postel@gmail.com
[o]Center of Excellence for Applied Intelligent Technology Faculty of Engineering, Hasanuddin University. Email: vickyarnoldo9@gmail.com
[p]Department of Electrical Engineering Faculty of Engineering, Hasanuddin University. E-mail: muliadi7404@unm.ac.id

Abstract

Three types of 6 monopoles array intelligent antennas was numerically and practically examined. The main purposes of the investigation is to guarantee that those designed antennas are feasible to implement and to install in a particular IoT based environmental surveillance network configuration. The basic differences of the three intelligent antennas lied on the frequency operations (i.e. 433 MHz, 875-915 MHz and 2.5 GHz) and the actual environment operations (whether for indoor or outdoor). The extreme differences of such frequency operations, of course, affecting the differences on the whole antenna physical dimension. The higher the frequency operation determined then the smaller the physical size of the designed antennas produced. However, the deep intelligent antenna evaluations presented in the paper is the one that operated on frequency band of 875 -915 MHz. The intelligent electronic part of six monopole wire elements arrayed on a circular ground plate was composed of LoRa chip module, Android Uno microcontroller, and the switching network part. The three parts determined whole antenna operation throughout the IoT network. The results of whole antenna examinations are thoroughly discussed in the paper.

Keywords: Environmental surveillance; monopole array; intelligent antennas; IoT network

1. Introduction

In fact, the classical problems in wireless-based IoT networks such as the effects of multipath propagation fading between the transmitter and receiver units, the noise effects, the limitations of the narrow and expensive bandwidth-spectrum resources and the limitations of RF power could appear as the most serious and critical issues required to overcome. The quality of the IoT network that is built by adopting data / information connectivity techniques such as those that are widely applied in traditional wireless communication networks is largely determined by these important and critical factors [1-20].

*Corresponding author. Tel.: +62-812-829-15003
Komplek Perumahan Dosen UNHAS Tamalanrea Blok P1, No.4 Makassar 90245, South Sulawesi Indonesia

In general, there are several methods that are very broadly applied to overcome various technical problems in wireless communication networks and which will be widely studied and updated in building and maintaining the quality of IoT networks that are proposed in ongoing research and development (R&D) activities. 3 types of techniques such as robust adaptive computing algorithms, sophisticated signal processing and adaptive space filtering by optimizing various smart antenna technology innovations (i.e. switched parasitic element configuration category and phased array) will be widely utilized to obtain the more optimum IoT network configuration [5-16], [18], and [20].

A relatively powerful and simple computing algorithm to mitigate the multipath propagation effects that traditionally encounter throughout the wireless IoT

Table 1. The physical parameters of the six monopoles array intelligent antennas operated at 875 – 915 MHz

Antenna Elements Dimension	Prototype-I	Prototype-II
Length of monopole size (mm)	77.81	77.81
Ground plane diameter (mm)	330	330
Monopole distance from center of the ground plane (mm)	280.13	80
Conducting layer thickness of ground plane (mm)	0.8	0.8
Monopole wire outer radius (mm)	3	3

surveillance networks was extensively studied in the current scientific paper submission. In practical construction the monopole elements array of a single RF feed positioned on top of circular ground plane as suggested in [1-16], [16], [18] and [20] were slightly altered by removing the center feeder and applied computing algorithm to allow all the remaining monopole wires array to become the active elements for a certain operation time interval. The developed intelligent computing algorithm was programmed into an Arduino Uno microcontroller device to steer each monopole wires via the insertion of lumped switching network located exactly underneath of each feeder. The experimental testing of the applied RF-computing method to mitigate the multipath propagation "fading" phenomena in the wireless IoT sensor network is thoroughly analyzed and presented on the following paragraphs.

2. Numerical Computing and Characterization

The most common technique adopted to construct various types of the targeted antenna system for any intended applications such as modern communication network, satellite relay system, wireless sensor network and several IoT based wireless applications, is preliminary running the early designed antenna through a numerical computing. Usually, a programmed antenna design has to run, to assess, to characterize and to modify for several number of computing stages so-called the numerical computing optimization processes.

There were three kinds of 6 monopoles array intelligent antennas was practically feasible to implement and to install in order to support whole IoT based environmental surveillance network configured at the new smart campus of the Faculty of Engineering, Universitas Hasanuddin located at Bontomarannu, Gowa regency, South Sulawesi, Indonesia. The basic differences of the three intelligent antennas lied on the frequency operations (i.e. 433 MHz, 875-915 MHz and 2.5 GHz) and the actual environment operations (whether for indoor or outdoor). However, the constructed antenna systems and their corresponding discussion for 433 MHZ and 2.5 GHz IoT network applications are not included in the current paper content.

2.1. The intelligent antennas optimization

In the current research and development, monopoles array intelligent antennas operated at 875 – 915 MHz frequency band was designed in such manner to consider the physical parameters tabulated in Table 1. It is clearly shown that the optimized computing process may have several difference output of the targeted antenna numerical design by altering a single monopole planar array, i.e. the distance of the monopole position from the center point of circular ground plane varied from 280.13 mm to 80 mm. In this case, two types of intelligent monopoles array antennas have been generated through the sequential running of the programmed computing machine. These are called prototype antenna-I and prototype antenna-II, respectively. The two antenna set-up are to resemble and to characterize the impacts of the distance between monopole elements on the planar array configuration to whole antenna system operation performance.

2.2. Electrical properties comparisons

The numerical models of the 6 monopole wires planar array configured on top of the circular ground plane sized 330 mm as visualized in Fig. 1 were schematically drawn and run using a licensed-3D CST software package. Various difference of the computing results were generated and very interesting to analyze further for the purpose of prototype-I and prototype-II electrical properties comparisons.

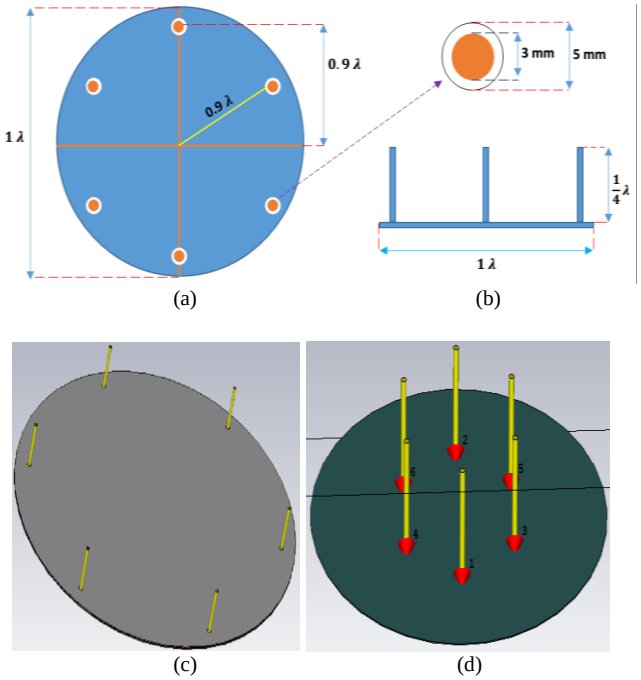

Figure 1. Two types of 6 monopole wires array configured on top of the circular ground plane sized 330 mm (a) Top view of prototype antenna-I; (b) Side view of prototype antenna-I; (c) 3D-planar model of prototype antenna-I; and (d) 3D-planar model of prototype antenna-II

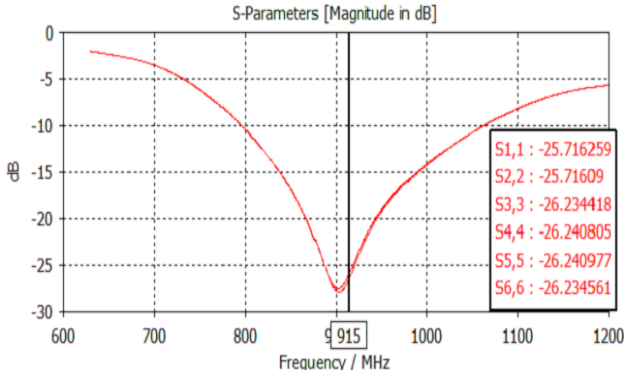

Figure 2. A prototype antenna-I reflection coefficient performance S_{11} (dB) versus operation frequencies (MHz)

The numerical constructed prototype antenna-I has a pretty excellent reflection coefficient parameter while it operated from 800 MHz up to 1100 MHz. It appeared that the identical S_{11} properties were also generated fon all RF-feeding ports, i.e. S_{11} Port-1 is almost the same to other ports. The broadband frequency could be potentially provided was approximately 300 MHz. The recorded VSWR performance of the designed prototype antenna-I appears to have a stable value about 1.1 at all feeding ports while it operates on the frequency 915 MHz.

The power radiation pattern of 6 monopoles array intelligent antennas 915 MHz designed to support a typical IoT based environmental surveillance network is depicted in Fig. 4. It is obviously that the -3 dB Beamwidth power pattern is in average 98.8 degree. This is quite broad pattern could be provided during the transmission of various data from the sensor node to reach the server terminal. Both pattern in the front direction and in the back direction is almost the same. FTBR is quite small value and it is around few dBi. This also resembles the potential to connect and to monitor more sensor nodes inside the operated network remotely through the base station server terminal.

When the six monopoles position were set-up to more close each other and to approach the center point of the circular ground plane (see Fig. 1. (d)) than the previous prototype antenna-I the unsatisfied electrical properties of the prototype antenna-II were generated. Both the S11 and VSWR profiles tends to have the poor values (see Fig.s 5 and 6). At the operation frequency 915 MHz all ports only produced about – 9 dB. This is equivalent to 2.2 Voltage Standing Wave Ratio (VSWR).

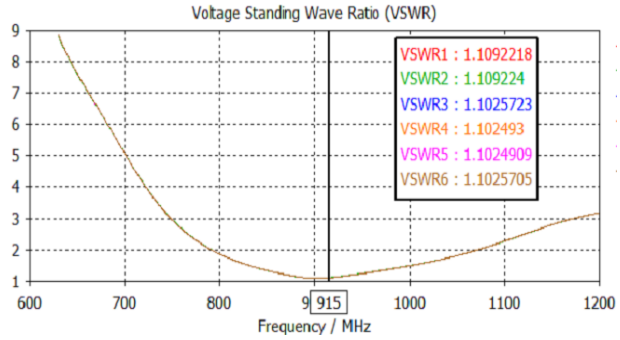

Figure 3. A prototype antenna-I VSWR property versus operation frequencies (MHz)

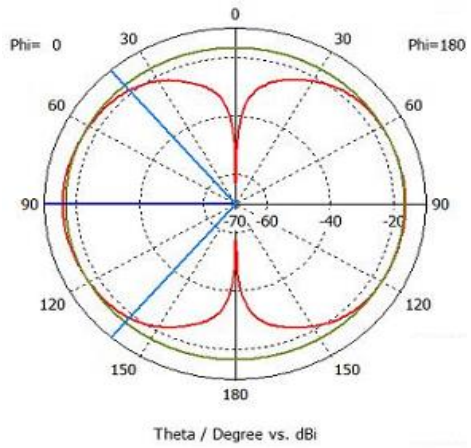

Figure 4. The prototype antenna-I power radiation pattern of 6 monopoles array intelligent antennas 915 MHz

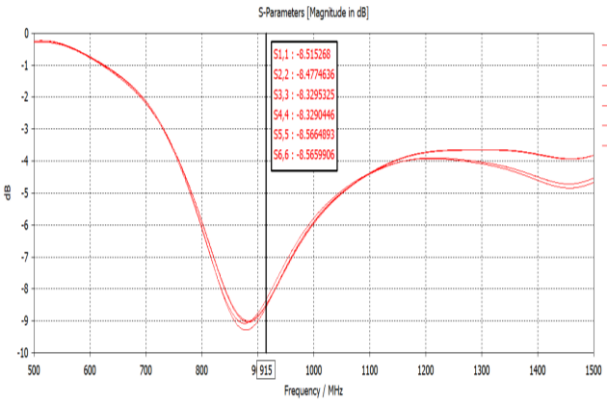

Figure 5. A prototype antenna-II reflection coefficient performance S_{11} (dB) versus operation frequencies (MHz)

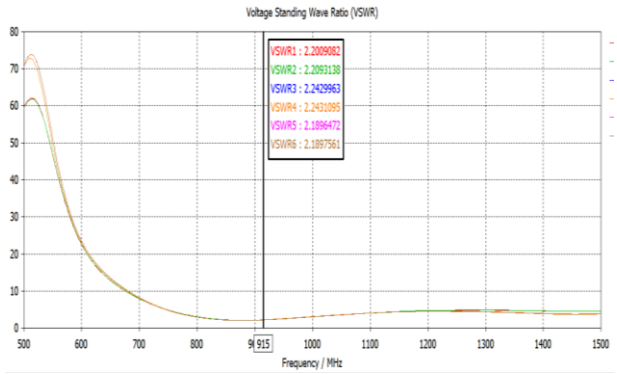

Figure 6. A prototype antenna-II VSWR property versus operation frequencies (MHz)

Despite the destroyed S11 and VSWR electrical properties generated as the distance range amongst the monopole wires of prototype antenna-II to set-up smaller than another antenna type, however, the interested power pattern were produced as one monopole wire activated and others 5 elements inactivated (floating status). Two identical power patterns illuminated from two different ports were activated on two different sequential operation times. These are shown in Fig. 7. The probability of other ports to have the similar power pattern but in the different main lobe directions are relatively high depending on the accuracy of each monopole wires placement on the conducting ground plane during the computation.

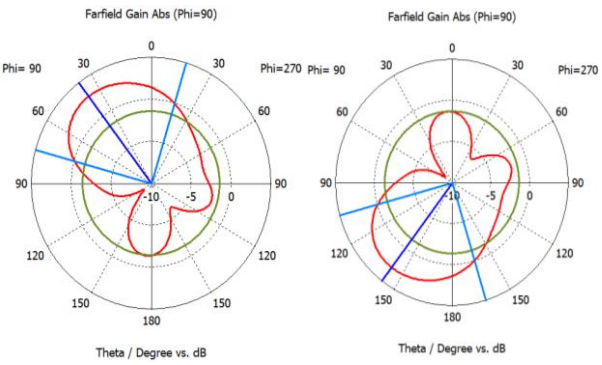

Figure 7. The prototype antenna-II power radiation pattern of 6 monopoles array intelligent antennas 915 MHz

Both the FTBR and the -3 dB Beamwidth power pattern produced by the prototype antenna-II are better than the prototype antenna-I has generated. FTBR produced is almost 5 dBi. While, the -3 dB Beamwidth power pattern is approximately 91.5 degree.

3. Manufacturing, Testing and Evaluating

A fabricated 6 monopole wires planar array intelligent antenna incorporated into a particular wireless IoT based environmental surveillance network is described in Fig. 8. The physical size of the constructed antennas placed on both the transmitting and the receiving parts was set-up according the parameters listed in Table 2. The antennas will maintain the quality of both signals transmission and reception throughout the operated IoT network to combat the multipath fading effects.

In principle the typical wireless IoT based environmental sureveillance configured as visualized in Figure 8 will collect all data from the connected sensors and further processed in the transmitting electronic part. The adaptive transmitter unit consists of an array of the environmental sensors, Arduino Uno microcontroller device, LoRa module chip and the transmitting antenna. Meanwhile, in the intelligent receiving electronic part some processing units (i.e. receving antenna, LoRa chip module and Arduino Uno microcontroller) were connected each other in order to reprocessed the received data and to feed forward to a PC/ laptop server unit.

The main purpose of the measurement configuration set-up for an indoor 915 MHz IoT network environment as described in Fig. 9 is to compare the performance of a conventional single monopole wire antenna that usually attached inside the LoRa module with the performance of the constructed 6 monopole wires planar array intelligent antennas. One of the interesting practical testing result on the performance of an indoor IoT based surveillance system employed 6 monopole wires array intelligent antennas is portrayed in Fig. 10.

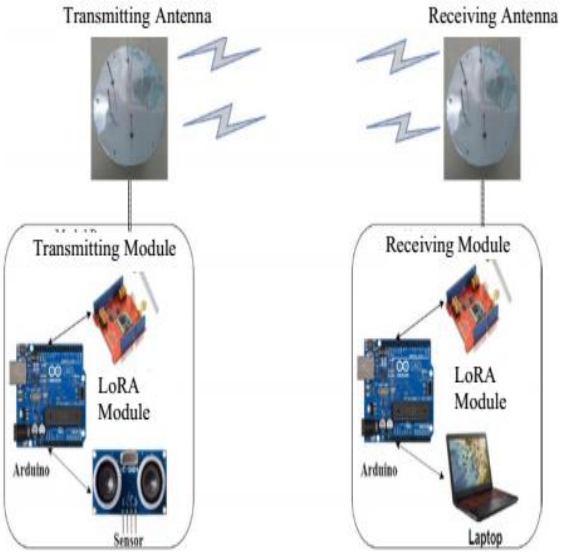

Figure 8. The 6 monopole wires planar array intelligent antenna incorporated into a particular 915 MHz wireless-IoT based environmental surveillance network

Table 2. The physical parameters of the six monopoles array intelligent antennas operated at 875 – 915 MHz frequency band

Antenna Elements	Dimension (mm)
Length of monopole	80
Ground plane diameter	330
Monopole distance from center of the ground plane	82.5
Distance separation between each monopole wire elements	82.5
Conducting layer thickness of ground plane	0.8
Monopole wire outer radius	3

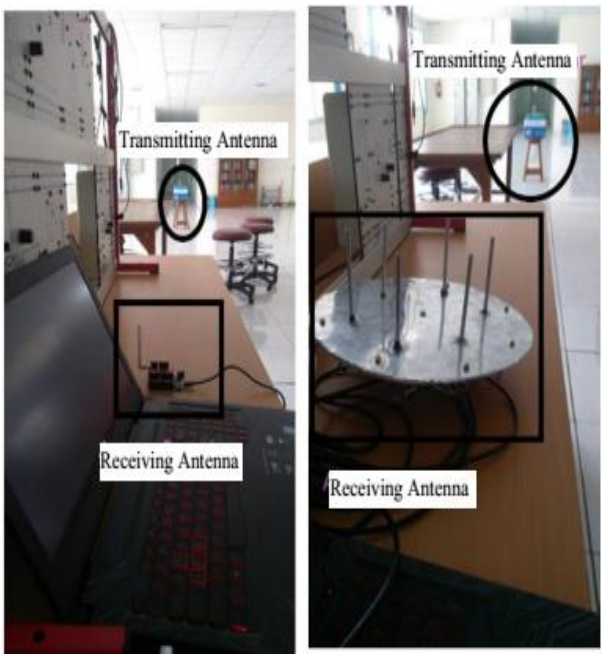

Figure 9. The measurement configuration set-up in the indoor 915 MHz IoT network environment

It is obviously that, as described in Fig. 10., the deployment of the constructed antennas on both the transmitting part and the receiving part might significantly maintaining on the stable power reception of approximately – 60 dBm while the mobile sensor nodes removing. It is contradicted with the installed single monopole antenna opponent which the quality of the signal receptions appeared unstable while the sensor node module was repositioned away from the base server station terminal. The fluctuated signal receptions of approximately 60 dB power might encountered throughout the IoT network while using this antenna during the operational period.

Another interesting experimental examination obtained during the trial mobile testing in the outdoor environmental operation of IoT based surveillance system was demonstrated in Fig. 11. On this practical testing the sensor node was removed away up to several hundred meters outside the building of LAPAN Pare-Pare remote sensing office. Only the constructed 6 monopole wires planar array intelligent antennas were installed on both two transceiver parts and one sensor node part was positioned inside a carried box.

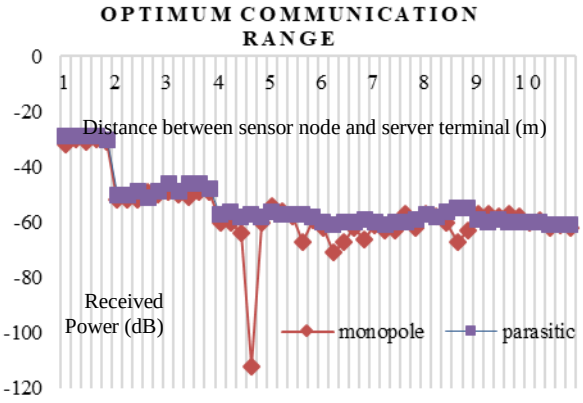

Figure 10. The measurement configuration set-up in the indoor 915 MHz IoT network environment

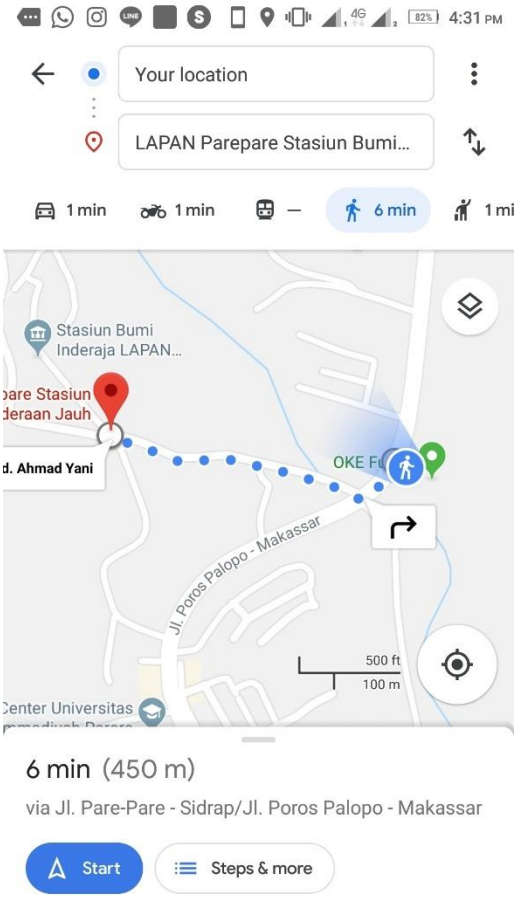

Figure 11. The outdoor measurement set-up of the IoT transceiver in a particular sub urban environment located in Pare-Pare city, South Sulawesi province

The observer is then moving to follow the below figure of the walking track. Based on the experimental activity described in Fig. 11, it is clearly seen that the maximum communication distance between the mobile IoT based sensor node and the operated fix position of central collected server inside LAPAN office building is no more than 450 meters distance. Over that distance range the more failure data and connection problem encountered during the actual measurement and data recording.

4. Concluding Remarks

The 6 monopole wires array intelligent antennas was numerically and practically constructed and characterized to be suitable employed in the 875-915 MHz wireless IoT based environmental surveillance. The manufactured switched parasitic antenna was incorporated into IoT network and was tested for both the indoor and outdoor environments. Both for the two operation environments the designed intelligent antennas outperformed the conventional single monopole antenna in terms the stability of signal reception. The smart parasitic antenna has also had the better read/communication range between the sensor node and the server terminal than using the single monopole antenna. The longest communication distance recorded no more than 450 meter. Over this range more failure data receptions encountered along the free space communication link.

Acknowledgements

Authors would like to thanks to the Ministry of Research and Technology/ BRIN, Republic of Indonesia for providing the sufficient funding to allow the ICT R&D group at Universitas Hasanuddin together with others collaborator higher education institutions such as UGM and ITS, and other national research and industry partners (PT. Lapan Pare-Pare and PT. Balla Cerdas Teknologi) to implement various ICT R&D products focusing on the smart antennas development since 2019. Authors would also like to extend our sincere thanks to any people who are indirect or directly contributing for many achievements gained during the R&D process period.

References

[1] S.L. Preston, D.V. Thiel, T.A. Smith, S.G.O'Keefe, and J.W. Lu, 1998. "Base Station Tracking in Mobile Communications Using a Switched Parasitic Antenna Array". IEEE Transactions on Antennas and Propagation. Vol. 46. No.6. June 1998. pp. 841-844.

[2] S.L. Preston, D.V. Thiel and J.W. Lu, 1999. "A Multibeam Antenna Using a Switched Parasitic and Switched Active Elements for Space Division Multiple Access Applications". IEICE Transactions on Electronics. Vol. E82-C. No.7. July 1999. pp. 1202-1210.

[3] D. V. Thiel and S. Smith, Switched Parasitic Antennas for Cellular Communications, Artech House, Inc., 2002.

[4] R.W. Schlub, and D.V. Thiel., 2004. "Switched Parasitic Antenna on a Finite Ground Plane with Conductive Sleeve". IEEE Trans. Antennas and Propagation, Vol.52, (5), pp. 1343-1347, May 2004.

[5] E. Palantei and D.V. Thiel, "Electronically Switched Parasitic Smart Antenna for Wireless Communication", Conference Digest of the 9th Australian Symposium on Antennas, Sydney, Australia, pp.24, 16-17 Feb. 2005.

[6] E. Palantei and D.V. Thiel, "An Investigation of an Electronically Switched Beam Smart Antenna: Numerical and Empirical Approaches." Digest of Microelectronic Engineering Research Conference (MERC) 2005, South Bank, Brisbane, Australia, 2-3 November 2005.

[7] E. Palantei and D.V. Thiel, "Controller Algorithms for Single Feed Switched Parasitic Antennas," IEEE AP-S International Symposium, USNC/URSI National Radio Science and AMEREM Meetings, Albuquerque, New Mexico, USA, 9 -14 July 2006: pp.378.

[8] E. Palantei and D.V. Thiel, "Current Variations of Parasitic Monopoles: Its Impact on the Performance of Switched Beam Smart Antenna", Asia-Pacific Symposium on Applied Electromagmetics and Mechanics (APSAEM) 2006, University of Technology Sydney (UTS), Sydney, Australia, 20-21 July 2006.

[9] E. Palantei and D.V. Thiel, "Symmetry Problems in Switched Parasitic Smart Antennas", IEEE Antennas and Propagation-Society(APS)International Symposium, Honolulu, HI, USA, 10-15 June 2007: pp. 3360-3363.

[10] E. Palantei and D.V. Thiel, "The Impact of Bias Voltage on the Performance of a P.I.N. Diode Loaded Smart Antenna," Journal of the Japan Society of Applied Electromagnetics and Mechanics (JSAEM),Vol.15, No.3, September 2007, pp.274-277.

[11] E. Palantei and D.V. Thiel, "Dual Frequency Plug and Play of Steerable Antenna for ISM band Communication," International Conference on Electrical Engineering and Informatics (ICEEI) 2007, Institut Teknologi Bandung, Bandung, Indonesia, 17-19 June 2007.

[12] E. Palantei, D. V. Thiel, and S.G. O'Keefe, "Reconfigurable Intelligent Antennas using a Switched Constellation of Parasitic Elements," Digest of GSERC 2007 conference, Logan Entertainment Centre, Qld, Australia, 29-30 October 2007.

[13] E. Palantei, D. V. Thiel, and S.G. O'Keefe, "Rectangular Patch with Parasitic Folded Dipoles: A Reconfigurable Antenna," Proceedings of the IEEE International Workshop on Antenna Technology (IEEE iWAT) 2008: Small Antennas and Novel Metamaterials, 4-6 March 2008, Chiba, Japan.

[14] E. Palantei and D. V. Thiel, "Comments on A Novel Planar Switched Parasitic Array Antenna with Steered Conical Pattern," IEEE Transactions on Antennas and Propagation, Vol. 56, No.9, September 2008, pp.3084.

[15] E. Palantei and D.V. Thiel, "Circular Monopole Array Antenna with Intelligent Electronic Circuit at the Bottom Side of Cylindrical Ground Structure" to be submitted to IEEE Transactions on Antennas and Propagation.

[16] E. Palantei, S. Kanata, N.K.Subaer, Adnan, Z.B. Hasanuddin, D. Djamaluddin, I.S. Areni, Indrabayu, Wardi, and D.V Thiel, "Prototyping Plug and Play Smart Antenna untuk Aplikasi Generasi Lanjut Sistem Komunikasi Nirkabel," Research Report of Program Dukungan R&D Produk Telekomunikasi, Research Grant awarded by General Directorate of Post and Telecommunication, Ministry of Communication and Information, Republic of Indonesia, 2007-2009.

[17] D. V. Thiel, "Progress in Wireless Sensor Design and Networking," Proceedings of 1st Macassar International Conference on Electrical Engineering and Informatics (MICEEI), Macassar, South Sulawesi, Indonesia, 13-14 November 2008.

[18] E. Palantei, S. Syarif, A. Hidayat dan STA. Munawar, "Low-Cost Switched Array- Wide Band Antenna for Search and Rescue Disaster," The 3rd IEEE-International Conference on Science and Technology, Yogyakarta, Indonesia, 11-12 July 2017.

[19] P. Guillemin, P. Friess, O Vermesan, M. Hrrison, H. Vogt, K. Kalaboukas, M. Tomasella, K. Wouters, S. Gusmeroli, dan S. Haller, "Internet of Things: Strategic Research Roadmap," CERPIoT SRA version European Commission (EC) DG INFSO-D4 Unit for the European and International IoT stakeholders 15 September 2009.

[20] E Palantei, "Switched Parasitic Smart Antenna: Design and Implementation for Wireless Communication Systems," PhD Thesis, Griffith University, Brisbane, Australia, May 2012.

EPI International Journal of Engineering
Volume 3, Number 2, August 2020, pp. 132-137
DOI: 10.25042/epi-ije.082020.07

*p*ISSN 2615-5109
*e*ISSN 2621-0541

Construction and Analysis of Plastic Extruder Machine for Polyethylene Plastic Waste

Muhammad Luthfi Sonjaya[a,*], Muh. Farid Hidayat[a,b]

[a]Department of Agro Industrial Manufacturing Engineering, ATI Polytechnic of Makassar. Email: mluthfi.sonjaya@gmail.com
[b]Department of Mechanical Engineering, Engineering Faculty, Hasanuddin University. Email: faridhidayat006@gmail.com

Abstract

Polyethylene plastic waste is such hazard object in the world, while the benefits of this plastic rubbish are prodigious. An extruder machine is one of the great ways to reduce huge amounts of plastic waste not only to the manufacturing companies which recycle the plastic waste but also to the small society. This extruder machine was created to overcome the problems faced by all countries about plastic waste in land or in ocean. The results of extruded plastic waste were solid filament that can be utilized for some valuable stuff made by plastic. From this study, experimental test was applied by heating the plastic waste with different temperatures of 150, 160, 170, 180, 190, 200, 210, 220, and 230°C. As a result, the best temperature to heat the polyethylene plastic waste is 190°C according to surface roughness test and digital caliper measurement.

Keywords: Extruder machine; polyethylene plastic waste; surface roughness

1. Introduction

Plastic is material that has many functions in human's life. Firstly, most of our packaging for food uses plastic to cover the food. Many fast food restaurants, for instance, take advantage of using plastic in order to serve the meal. Secondly, household dishes are made by plastic because they are simple to utilize. Lastly, the furniture companies begin to produce family's needs in terms of chairs, desks, cupboards and others.

However, plastic becomes one of the environmental issues in the world because some people have not been able to use it wisely. [1] Still lots of plastic garbage lay strewn across the street in some parts of world. In addition, [2] plastic is also extremely dangerous for the ocean because plastic rubbish goes all the way to the sea for the last destination. The impact is a hazard to marine life. Million tons of plastic garbage are currently entering to the ocean every year from land through river mostly located in Asia [3]. On other impacts of plastic waste, it affects the condition on coral reefs which increase diseases that can threaten them [4].

Plastic extruder is a machine to recycle the plastic garbage to be something that is more valuable. The process of this machine is to extrude the plastic by heating process. The purpose of this machine is to reduce plastic garbage in the world and recycle plastic waste.

*Corresponding author. Tel.: +62-852-2446-0409
Jalan Sunu No. 220
Makassar, Indonesia, 90152

2. Literature Review

Plastic extruder mechanism consists of 5 mm threaded lead screw (worm screw). The plastic is fed from the hopper, letting it fall on the thread. As indicated by the direction, the plastic is going forward. With the help of the heater pad, it melts as it moves forward. The heater pad is heated to 350 ° C. The molten plastic is moved forward and from the nozzle it is collected [5], [6].

There are plenty of things that extruder machine can create from plastic waste. Brick is one example of utilizing plastic garbage. [7], [8] By using different kinds of plastic with various combinations to create different kinds of bricks, researchers believe the different properties of bricks through conducting different tests on them. The most popular test performed on bricks involves compression and water absorption testing.

In addition, Due to the extreme quick emergence of this innovation, leaps have been created towards enhancing manufacturing. Ideally, the invention of screw extrusion would open doors to new 3d printing concepts. Screw extrusion would allow people to access a larger range of high-resolution products for their 3D printed parts [9].

In the field including researchers, manufacturers, designers, engineers and scientists, 3D printing technology is becoming famous each day, and FDM is the most commonly utilized 3D printing technology. The purpose of the project was to design and develop a Bowden Extruder based on FDM. Researchers built a Bowden extruder that was simple and user-friendly.

Researchers found that the prints are almost consistent with the extruder [10].

In the research, [11] a model feedback control system has been developed and experimentally tested to regulate the temperature and pressure of the component in a single screw extruder. Through a simple yet effective control architecture focused on two separate external SISO loops and seven identical internal SISO loops for local temperature control, actual-time temperature and pressure regulation was effectively accomplished.

Based on Labview and Matlab/ Simulink, the plastic extruder's constructed semi-physical actual-time simulation system for temperature control was implemented. The study proved that even in the plastic extruder production line, the HIL simulation technique and our designed temperature control computer program had an amazing effect [12]. The discover through simulation also expressed the potential to complement many other determinations by means of extended analytics; affective synchronization and in-situ identification such as injection fill time; packing injection ramp speed, operating temperatures, reliability, etc. [13]. The simulation method can be commonly used in the design of the process control system, it can not only shorten the development cycle and cost, increase the design quality of the control system, but also provide a solution for the real-time display of the controller [12].

Indicators of extruded plastic waste have been studied. Mechanical and chemical parameters of recycling solid plastic waste have been researched [14], [15], [16]. The laminates of textile cotton waste plastic were researched in order to understand characterization of tensile and fatigue [17], [18]. The properties of low-isotacticity polypropylene elastomeric fibers with purpose of spinning were inscribed [19], also plastic bag waste to use ecofriendly polyethylene fiber was studied [20].

The result of plastic extruder machine should be analyzed by the measurement of surface roughness. This aims to determine best results of the machine according to the temperature tested. Surface roughness test for plastic composites by applying an optical method was measured [21]. Furthermore, plastic pipes that were used for irrigation were calculated experimentally using internal surface roughness test [22].

3. Design and Procedure of Machine

The tools used in this research as shown in Fig. 1 are: electrical welding machine, safety goggles, welding gloves, heat resistant gloves, mechanical tools (wrench, pliers, and hammer), measuring tools (ruler, varnier caliper, micrometer, surface roughness test and dial indicator), conventional machines (turning, milling, grinding, drilling, and shaping), computer set, power supply, and CNC milling machine.

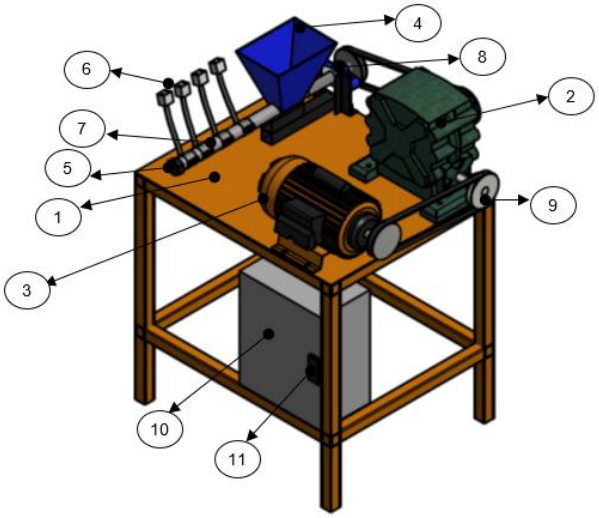

1) Frame
2) Reducer
3) Motor
4) Hopper
5) Nozzle screw
6) Band heater
7) Barrel set
8) Bearing
9) Pulley – belt transmision
10) Electrical box
11) Thermostat

Figure 1. Design of Plastic Extruder Machine

The main function of this machine is to heat the plastic to become filament extruded. A part to heat the plastic is barrel that is connected with hopper. The material that is used for barrel is steel. In order to drive the plastic out, screw is paired up inside barrel. In Fig. 2 (c), nozzle is a part to mold the extruded plastic after heating the plastic. The size of nozzle circle is Ø4 mm. it means the size result of solid filament should be around 4 mm in diameter.

In this study, the average of motor rotation is 30 RPM. This is from AC motor with ¼ HP. Before motor connected to screw driver, there is reducer 1:20 to decrease the rotation from AC motor. Pulley –belt transmission is applied in this machine. The heat source of barrel is band heater. There are 3 band heaters used with the distance among band heaters 32 mm. To control the temperature, thermocouple and thermostat are attached. The function of thermocouple is to measure the temperature of barrel while thermostat is to set the temperature.

The steps in order to operate this extruder machine is (1) Connect electrical box to power supply, (2) switch MCB on from electrical box, (3) set temperature by using thermostat, (4) wait until the temperature reaches the maximum set, (5) after reaching the temperature, turn on motor to rotate barrel screw, (6) enter plastic shredded from shredder machine into the hopper, (7) prepare a container to place the result of extruding.

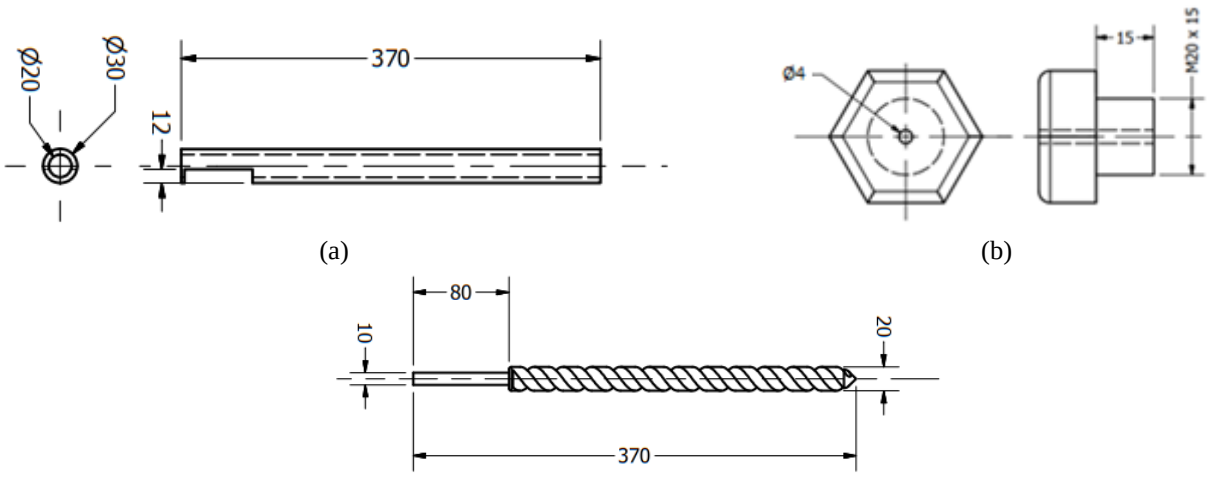

Figure 2. Design of (a) barrel (b) screw (c) nozzle

4. Result and Discussion

4.1. Construction and operation result of plastic extruder machine

The frame of plastic extruder machine in Fig. 3 is assembled by electrical welding machine. The position of main tools of this machine is on the frame while the electrical box is on one side of the frame. Miniature circuit breaker is inside the electrical box. It has function to run the machine with red lamp as a sign.

There were two buttons on the electrical box in its front door. A left button is for running AC motor and a right button for turning off AC motor. On front door of electrical box, thermostat was available in order to show the temperature of barrel.

In the experimental test, polyethylene plastic waste was tested. Each experiment contained 30 gram plastic waste of polyethylene. The variation of this research was from temperature 150, 160, 170, 180, 190, 200, 210, 220, and 230°C. In order to get the time to melt plastic, estimated time was counted by using stopwatch. It started from pouring plastic waste to melting the plastic out from the nozzle. It was noted that while pouring waste plastic into the hopper, motor was on to rotate screw driver. In order to describe the result of filament, molten results were taken into two categories. One category is *solid* which means if the samples are extruded well or no, and another is *continue* which means whether the samples are consistent or inconsistent.

Table 1 shows the data of extruding plastic waste with various hot temperatures. According to the experimental test, the filament with temperatures of degree 150 and 160 was not melted at all due to low heat from the barrel as heater of plastic waste. While the filament samples with higher temperature (170, 180, 190, 200, 210, 220 and 230°C) were melted. However, some samples of filament such as the temperature of 210, 220 and 230°C were inconsistent in extruding process. The high temperatures also produced darker filament results of extruding process (see Fig. 4). It occurred because heat of the barrel was too high. Furthermore, a sample of 230°C produced not only unstable extruded plastic but also liquid plastic that are different with other samples.

(a) (b)

Figure 3. Construction of plastic extruder machine (a) top view (b) front view

Table 1. Data of extruding process on plastic waste

No.	Temperature (°C)	Time from Pouring Plastic to Melting Plastic (Minute)	Molten Result		Total Time (Minute)	Annotation
			Solid	Continue		
1.	150	-			600	No Molten Plastic
2.	160	-			600	No Molten Plastic
3.	170	204	Yes	Yes	1616	
4.	180	150	Yes	Yes	1048	
5.	190	125	Yes	Yes	896	
6.	200	70	Yes	Yes	558	
7.	210	88	Yes	No	473	
8.	220	55	Yes	No	363	
9.	230	41	No	No	297	

Table 1 shows the data of extruding plastic waste with various hot temperatures. According to the experimental test, the filament with temperatures of degree 150 and 160 was not melted at all due to low heat from the barrel as heater of plastic waste. While the filament samples with higher temperature (170, 180, 190, 200, 210, 220 and 230°C) were melted. However, some samples of filament such as the temperature of 210, 220 and 230°C were inconsistent in extruding process. The high temperatures also produced darker filament results of extruding process (see Fig. 4). It occurred because heat of the barrel was too high. Furthermore, a sample of 230°C produced not only unstable extruded plastic but also liquid plastic that are different with other samples.

Duration of the time from pouring the plastic waste into the hopper to melting plastic waste was measured. This aims to know plastic which melts slower and faster by different heating temperature with similar weight of plastic (30 gr). It can be shown from Table 1 that a temperature of 170°C was slower than other temperature. On the other hand, a temperature of 230°C was the most rapid to heat the plastic. It means that the hotter barrel is, the faster melting time is. Total time needed in melting plastic was also measured. From the study, experiments with temperatures of 170, 180, and 190°C needed longer time to finish 30gr-plastic waste. While samples heated on temperatures of 200, 210, 220 and 230°C only needed no more than 600 minutes.

4.2. Analysis of filament size

Various heating temperature causes the size change of filaments. In this research, Digital caliper Mitutoyo CD-6'' ASX with serial number of B17012083 was used to get real inspection in measuring. The caliper measuring range is up to 150mm with minimum indication of 0.01mm. As explanation above, the size of each sample should be around 4mm in diameter because of nozzle circle size 4mm. From Table 2, samples which have suitable size with nozzle pit are 180, 190 and 200°C. The average size value of the samples is more than 4mm which means that plastic waste extruded fully, while samples with temperature of 170, 210 and 220°C were partially melted due to less size of 4mm in average.

Figure 4. Result of melting by different temperature
(a) 170°C (b) 180°C (c) 190°C (d) 200°C (e) 210°C (f) 220°C (g) 230°C

Table 2. Data of filament size

Temperature (º)	Measuring (Times)	Diameter of Solid Filament (mm)		Temperature (º)	Measuring (Times)	Diameter of Solid Filament (mm)	
		Value	Mean			Value	Mean
	1	3.15			1	4.67	
170	2	3.58	3.29	200	2	4.15	4.34
	3	3.13			3	4.19	
	1	4.19			1	4.18	
180	2	4.76	4.36	210	2	3.89	3.79
	3	4.14			3	3.30	
	1	4.98			1	4.93	
190	2	4.85	4.88	220	2	2.95	3.60
	3	4.81			3	2.93	

4.3. Analysis of surface roughness test

In order to survey the result of melted plastic waste, analysis of roughness surface from filament is important to measure. Portable surface test machine SJ-310 Mitutoyo (Fig. 5) was operated in this study. The surface roughness was used after the filament has been got from the extruder machine. Roughness measurements were repeated into three times with different surface of each sample to rise up the reliability. Values of surface roughness measurements were recorded by Ra and Rq where; Ra is the deviation of arithmetic average from the samples analyzed in µm, and Rq is the root mean square average of the profile heights over the evaluation length in µm. The standard of measurement used in the surface roughness test was ISO1997. The speed of detector to take the data was 0.5mm/second. Sampling length of the test was 0.8 mm.

Table 3 shows parameters of surface roughness test on all samples with various temperatures. Data taken from this study were mean roughness value (Ra) and root mean square average (rq). In this experimental test, three times tests were required in different surfaces to get the reliability. From test 1 to test 3 for all the samples, Ra and Rq value were not overly far. This means that the surfaces on all samples were almost similar.

Figure 6 presents comparison of Ra data from surface roughness test. It can be seen that the average better value of *Ra* surface roughness from all the samples was the sample with temperature of 190°C, followed by samples of 180 and 170°C, while samples of 200 and 210°C got higher arithmetic deviation in average. However, the sample of 220°C had average low *Ra*. This was because the extruding process was inconsistent.

(a) (b)

Figure 5. (a) Portable surface roughness testing machine SJ-310 Mitutoyo
(b) detector of surface roughness attached by dial indicator base

Table 3. Data of surface roughness test

Temperature (°C)	Testing (times)	Ra (µm)		Rq (µm)	
		Value	Mean	Value	Mean
150					
160					
	1	0.914		1.253	
170	2	1.007	0.999	1.463	1.383
	3	1.077		1.433	
	1	1.028		1.233	
180	2	0.898	0.940	1.187	1.173
	3	0.895		1.101	
	1	0.545		0.698	
190	2	0.565	0.586	0.707	0.731
	3	0.648		0.788	
	1	3.674		5.170	
200	2	3.638	3.317	5.139	4.498
	3	2.640		3.185	
	1	3.890		4.818	
210	2	3.285	3.895	4.140	4.870
	3	4.510		5.654	
	1	0.845		1.124	
220	2	0.912	0.828	1.179	1.083
	3	0.728		0.947	
230					

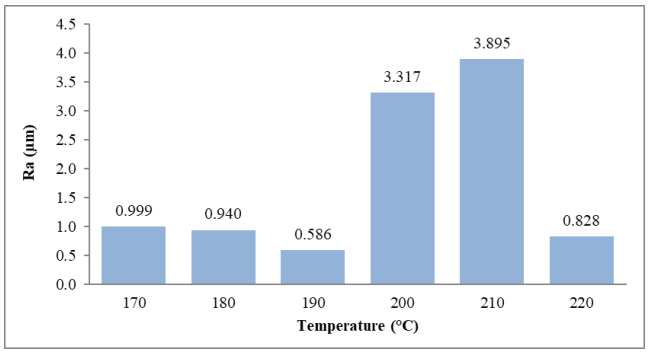

Figure 6. Comparison of arithmetic average deviation (Ra) among the temperatures of 170, 180, 190, 200, 210 and 220°C

5. Conclusion

In this research, the mechanical design and the construction of an extruder machine were built to reduce polyethylene plastic waste. The result of this machine was solid filament from polyethylene plastic waste that can be used for some valuable stuff such as furniture, household appliances or other things made from plastic. In order to get better solid filament, digital caliper measurement and surface roughness test were applied with different samples from various temperatures of barrel as heater of plastic waste. According to the research, a sample with temperature of 190°C had the greatest value of surface roughness test and showed solid size with constant diameter.

Acknowledgements

The authors would like to thank to the Edinburgh University for the grant of the research under Global Challenges Research Fund Project.

References

[1] R. C. Thompson, S. H. Swan, C. J. Moore, and F. S. Vom Saal, "Our plastic age," *Philos. Trans. R. Soc. B Biol. Sci.*, vol. 364, no. 1526, pp. 1973–1976, 2009.

[2] J. R. Jambeck, Q. Ji, Y.-G. Zhang, D. Liu, D. M. Grossnickle, and Z.-X. Luo, "Plastic waste inputs from land into the ocean," *Science (80-.).*, vol. 347, no. 6223, pp. 764–768, 2015.

[3] L. C. M. Lebreton, J. Van Der Zwet, J. W. Damsteeg, B. Slat, A. Andrady, and J. Reisser, "River plastic emissions to the world's oceans," *Nat. Commun.*, vol. 8, pp. 1–10, 2017.

[4] G. Bidegain and I. Paul-Pont, "Commentary: Plastic waste associated with disease on coral reefs," *Front. Mar. Sci.*, vol. 5, no. JUL, pp. 26–29, 2018.

[5] L. B. Variya, M. Bhavik, P. Harshil, P. Jenish, and G. Hardik, "Plastic Extruder Machine," vol. V, no. 02, pp. 53–54, 2018.

[6] H. Janeschitz-Kriegl, J. Schijf, and J. A. M. Telgenkamp, "A temperature probe for flowing polymer melts," *J. Sci. Instrum.*, vol. 40, no. 8, pp. 415–419, 1963.

[7] R. S. Kognole, K. Shipkule, and K. S. | M. P. | L. P. | U. Survase, "Utilization of Plastic waste for Making Plastic Bricks," *Int. J. Trend Sci. Res. Dev.*, vol. Volume-3, no. Issue-4, pp. 878–880, 2019.

[8] J. P. Modak, V. V. Sohoni, and H. V. Aware, "Manually powered manufacture of keyed bricks," *Build. Res. Inf.*, vol. 25, no. 6, pp. 354–364, 1997.

[9] M. H. Wankhade and S. G. Bahaley, "Design and Development of Plastic Filament Extruder for 3D Printing," *IRA-International J. Technol. Eng. (ISSN 2455-4480)*, 2018.

[10] M. Hoque, H. Kabir, and M. H. Jony, "Design and Construction of a Bowden Extruder for a Fdm 3D Printer Uses 1.75Mm Filament," *Int. J. Tech. Res. Sci.*, vol. 3, no. VIII, 2018.

[11] F. Previdi, S. Savaresi, and A. Panarotto, "Design of a feedback control system for real-time control of flow in a single-screw extruder," *IFAC Proc. Vol.*, vol. 16, pp. 454–459, 2005.

[12] J. Xu, G. Zuo, J. Chen, and M. Wan, "A rapid control prototyping system design for temperature control of plastic extruder based on labview," in *2011 International Conference on Electronics, Communications and Control, ICECC 2011 - Proceedings*, 2011.

[13] M. Lakkanna, G. C. Mohan Kumar, and R. Kadoli, "Computational design of mould sprue for injection moulding thermoplastics," *J. Comput. Des. Eng.*, vol. 3, no. 1, pp. 37–52, 2016.

[14] K. Ragaert, L. Delva, and K. Van Geem, "Mechanical and chemical recycling of solid plastic waste," *Waste Manag.*, vol. 69, pp. 24–58, 2017.

[15] C. L. Wu, M. Q. Zhang, M. Z. Rong, and K. Friedrich, "Tensile performance improvement of low nanoparticles filled-polypropylene composites," *Compos. Sci. Technol.*, vol. 62, no. 10–11, pp. 1327–1340, 2002.

[16] J. Z. Liang and Q. Q. Yang, "Mechanical properties of carbon black-filled high-density polyethylene antistatic composites," *J. Reinf. Plast. Compos.*, vol. 28, no. 3, pp. 295–304, 2009.

[17] R. Petrucci *et al.*, "Tensile and fatigue characterisation of textile cotton waste/polypropylene laminates," *Compos. Part B Eng.*, vol. 81, pp. 84–90, 2015.

[18] J. J. Hwang, T. Adachi, T. Kuwabara, and W. Araki, "Laminate model expressing mechanical properties of polypropylene foams having non-uniform cell-shape distributions," *Mater. Sci. Eng. A*, vol. 487, no. 1–2, pp. 369–376, 2008.

[19] Y. Kohri, T. Takebe, Y. Minami, T. Kanai, W. Takarada, and T. Kikutani, "Structure and properties of low-isotacticity polypropylene elastomeric fibers prepared by sheath-core bicomponent spinning: Effect of localization of high-isotacticity component near the fiber surface," *J. Polym. Eng.*, vol. 35, no. 3, pp. 277–285, 2015.

[20] A. S. Soekoco, Noerati, M. Komalasari, Kurniawan, and A. Hananto, "Characterization of ecofriendly polyethylene fiber from plastic bag waste," *AIP Conf. Proc.*, vol. 1868, 2017.

[21] N. Duboust *et al.*, "An optical method for measuring surface roughness of machined carbon fibre-reinforced plastic composites," *J. Compos. Mater.*, vol. 51, no. 3, pp. 289–302, 2017.

[22] H. S. Da Rocha, P. A. A. Marques, A. P. De Camargo, J. A. Frizzone, and E. Saretta, "Internal surface roughness of plastic pipes for irrigation," *Rev. Bras. Eng. Agric. e Ambient.*, vol. 21, no. 3, pp. 143–149, 2017.

EPI International Journal of Engineering
Volume 3, Number 2, August 2020, pp. 138-142
DOI: 10.25042/epi-ije.082020.08

*p*ISSN 2615-5109
*e*ISSN 2621-0541

Utilization of Gasoline Fuel as an Alternative Fuel for LPG Substitution

Asril Mallombasang[a], Zuryati Djafar[b,*], Wahyu Haryadi Piarah[c]

[a]Department of Mechanical Engineering, Faculty of Engineering, Universitas Hasanuddin. Email: mallombasangchito@gmail.com
[b]Department of Mechanical Engineering, Faculty of Engineering, Universitas Hasanuddin. Email: zuryatidjafar@unhas.ac.id
[c]Department of Mechanical Engineering, Faculty of Engineering, Universitas Hasanuddin. Email: wahyupiarah@unhas.ac.id

Abstract

The subsidized gasoline conversion to LPG 3 kg in 2007 became the Indonesian Government's policy to reduce reliance on fuel oil. The increasing LPG consumption and obstacle distribution have been the scarcity of the LPG in all regions of Indonesia. The gasoline fuel stove has overcome from the LPG scarcity. So, this research has conducted by comparing the consume rate between both Pertalite and Pertamax of gasoline types to fuel LPG at the boiling process 1 litre of water which has used the quantum gas stove, with several pressure variations from 1.5 kPa to 2.5 kPa. Test results showed that the highest fire temperatures for Pertalite 430 °C fuel, Pertamax 530 °C fuel and LPG 578 °C fuel. Fuel consumption for Pertalite 0.025 kg, Pertamax 0.027 kg and LPG 0.061 kg. While the distribution time is 682 s for Pertalite, 669 s Pertamax and 503 s for LPG. The least compaction efficiency value occurs at 1.5 kPa pressure, for Pertalite 6.136 %, Pertamax 7.730 % and LPG 9.018 %. The higher the pressure hence greater the fuel efficiency, instead the fuel consumption and water boiling time are reduced. The cost used to boil water on Pertalite is 236 Rupiah, Pertamax 251 Rupiah, and LPG is 309 Rupiah.

Keywords: Air pump; efficiency; pertalite; stove; tube reactor

1. Introduction

Indonesia is one of the countries which have abundant natural resources like petroleum. Natural resources have been processed and used in supporting daily activity such as industrial field, transportation, household but the main problem of petroleum resources is scarcity. Indonesian's Government has exhibited the issue policy to replace kerosene usage to LPG gas. The purpose of this policy is reducing consume rate of kerosene continuously [1].

LPG gas is a fuel taken from natural gas contained in the earth and processed into gas that can be used by the community as an innovation in the utilization of natural resources in Indonesia.

If the kerosene conversion to LPG gas is a success, the Indonesian Government is saving 15 to 20 trillion fuel oil subsidized every year [2]. The target of conversion of kerosene to LPG gas is to households and micro-enterprises. For household criteria that get it is a user of pure kerosene, does not have an LPG stove, earns less than 1.5 million every month and is a native of the area. While the criteria of micro-enterprises are consuming kerosene to production process [3].

The role of fuel oil (BBM) in this modern era is usefully significant that almost all activity has been using fuel oil. This energy source has been used as long as thousands of years due to its flexible nature. As a simple example of using BBM in daily life is the use of an oil stove for cooking. Of course, we remember the government's efforts to replace kerosene stoves with gas stoves on the grounds of increasing efficiency. Some cases of fire that occur in Indonesia has caused by gas stoves because of the very flammable fuel of the LPG. When LPG gas became scarce, some of people returned to using kerosene and even firewood, but some also tried gasoline as an alternative to LPG gas.

Alkarim, et al., [4] in their research using a reactor tube containing Pertalite connected to an aerator (air pump) as an air supply as well as a Pertalite evaporation aid. So, Ridhuan and Darma [5] used a stove with premium fuel, This is to determine the variation in the number of holes and the diameter of the stove burner on premium fuel consumption. Another related research has been revealed by Sukandi and Porawati [6] that has used a reactor tube as a storage container of hydrogen gas as stove fuel.

2. Fundamental Theory

2.1. Pertalite fuel

Pertalite is an oil fuel issued by Pertamina company with Research Octane Number (RON) 90, an announcement in May 2015, and green bright in color characteristics [7]. The rule of the mixture used for manufacturing Pertalite is Naphtha where has RON 65 - 70. Enhance the quality of RON becomes RON 90 can be conducted by mixed with *High Octane Mogas Component*

*Corresponding author. Telp. +62-812-8047-7465
Jalan Poros Malino km. 6, Bontomarannu,
Gowa, South Sulawesi, Indonesia 92171

(HOMC), and EcoSAVE additives have also added to make the engine smoother, cleaner, and more efficient [8].

2.2. Pertamax fuel

Pertamax was first launched in 1999 to replace the premium mixture (premix 98) because it contains Methyl Tertiary Butyl Ether (MTBE) compound that is not environment friendly. Pertamax is a recommendation for vehicles produced after 1990, especially those that have used technology equivalent to electronic fuel injection (EFI) and catalytic converters (catalytic converters). Pertamax is produced by Pertamina base on the decision of the Directorate General of Oil and Gas No. 3674/K24/DJM/2006, dated 17 March 2006 concerning specifications for gasoline, 91 [9].

2.3. LPG (Liquified Petroleum Gases)

LPG stands for Liquified Petroleum Gas, which means gas that is liquefied at any pressure and has obtained from fractionated petroleum. The types of LPG based on its specifications have mixed LPG, propane LPG and butane LPG. Whereas currently circulating in the community based on the Decree of the Director-General of Oil and Gas Number: 25K/36/DDJM/1990 is a type of mixed LPG. To reduce the risk of explosion and find out the gas leak in the tube, Pertamina has added mercaptan gas that has a distinctive odor and has nose piercing properties [10].

2.4. Calorific value

The heating value is a property of a fuel which states the energy magnitude of the fuel. Determination of the calorific value of the fuel can be done by testing or by estimating based on the raw components of the fuel [11]. Meanwhile, low heating value (LHV) is the heating value where it has assumed that water and hydrogen are in the vapor phase [12]. The calorific value, density and fuel price of Pertalite, Pertamax and LPG can be seen in Table 1.

2.5. Maturity Efficiency

Maturity efficiency is the ratio between the useful heat needed to heat water a certain amount from the initial temperature until mature with the heat provided by the fuel [15].

The method used is to boil 1 (one) liter of water to a temperature between 95 ºC to 99 ºC on the one eye stove using gasoline types Pertalite, Pertamax, and 3 kg LPG fuel. The measured water volume and the mass of gasoline (Pertalite and Pertamax) and LPG fuel that has used, so that the heating efficiency has calculated by the following formula.

Table 1. Calorific value (LHV), density and price of fuels [9], [13], [14]

Type of fuel	Calorific value (LHV) (kJ/kg)	Density (kg/m^3)	Price (Rp.)
Pertalite	44260	732.9	7,850
Pertamax	44791	768.7	9,200
LPG	47089.29	1.5	17,000

$$m_{bb} = m_a - m_{ak} \quad (1)$$

$$\dot{m}_{bb} = \frac{m_{bb}}{t} \quad (2)$$

where

m_{bb} = mass of fuel consumed (kg)
m_a = initial fuel mass (kg)
m_{ak} = final fuel mass (kg)
$\dot{m}_{bb}$ = fuel mass flow rate (kg/s)
t = boiling time (s)

Combustion Power (P_{in}) is the heat energy contained in the fuel multiplied by the mass flow rate (ṁ) used in the boiling process.

$$P_{in} = \dot{m}_{bb} \cdot LHV \quad (3)$$

where

P_{in} = net power to raise the water temperature (kW)
LHV = the lowest calorific value of fuel (kJ/Kg)

Output power(P_{out}) is the ratio of the energy used to heat water to the length of time which it takes to reach its boiling point [16].

$$P_{out} = \frac{m_{air} \cdot cp_{air} \cdot \Delta T_{air} + m_{panci} \cdot cp_{panci} \cdot \Delta T_{panci}}{t} \quad (4)$$

where

P_{out} = nett power (kW)
m_{air} = water density (kg)
Cp_{air} = specific heat of the water (kJ/kg °C)
m_{panci} = the mass of pan (kg)
Cp_{panic} = specific heat ofpan (kJ/kg °C)
ΔT = difference in temperature (°C)

The heating efficiency (η) is ratio between net power that isused to boil water and the combustion power of the fuel.

$$\eta = \frac{P_{out}}{P_{in}} \times 100\% \quad (5)$$

The initial conditions of the study in the form of air density and specifications of other research materials can be seen in Table 2.

2.6. Economic value

The economic value of the use of petroleum fuel types Pertalite and Pertamax and LPG fuel is the number of fuel costs used to boil 1 (one) liter of water. There are two parts economic value such as fix cost likely stove and its installation, and change cost likely consume rate of fuel in the boiling process of a litre of water with the time required in the boiling process.

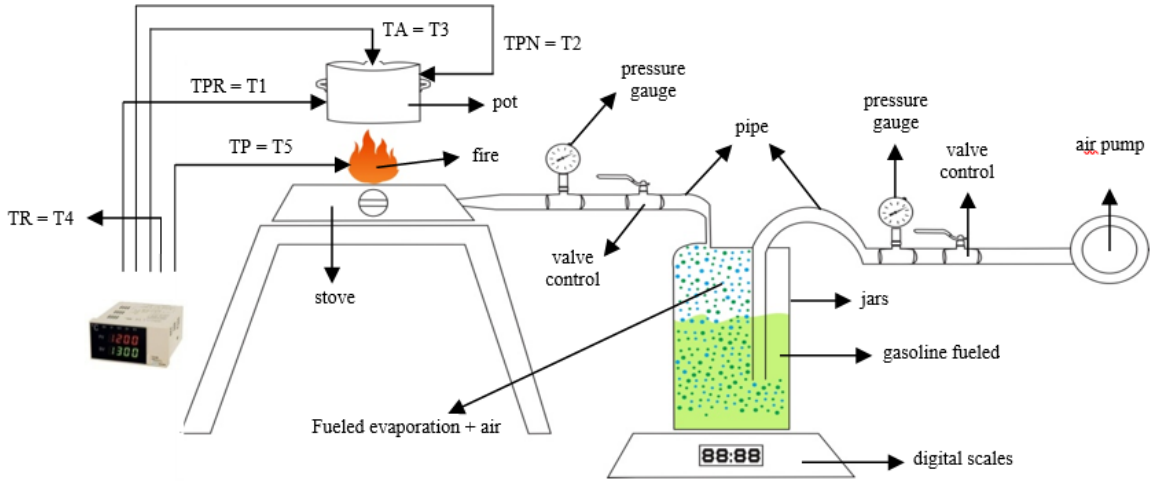

Description

TPR	= T1	= Wall temperature of left pot	TR	= T4	= Room temperature
TPN	= T2	= Wall temperature ofright pot	TP	= T5	= Fire temparature
TA	= T3	= Water temperature			

Figure 1. Testing sketch of boiling water

Table 2. Initial condition of research [14], [16], [17]

Initial Condition	Magnitude
Water mass	0.968 kg
Pan mass	0.219 kg
Cp (specific of water)	4.1866 kJ/kg °C
Cp (specific of pan)	0.9 kJ/kg °C
Air density (ρ)	1.2 kg/m^3

$$B_{bb} = m_{bb} \cdot H_{bb} \quad (6)$$

where

B_{bb} = fuel cost (Rp)
m_{bb} = consume rate of fuel (liter)
H_{bb} = price of fuel (Rp)

3. Research Methodology

3.1. Research tools and materials

- Materials of Research
  a. Water
  b. Pertamax
  c. Pertalite
  d. LPG 3 kg
- Tools of Research
  a. Termokopel
  b. Digital scales
  c. Stopwatch
  d. Manometer
  e. Measuring glass
  f. Stove
  g. Air pump
  h. Pot
  i. Jars

3.2. Testing method

The testing method has conducted by using one eye stove for boiling a litre of water. Gasoline fuel in the reactor tube pumped with air pump, and at the same time use to vaporize gasoline fuel such as revealed in Fig. 1.

4. Result and Discussion

4.1. Analysis of maturity characteristic

Testing has conducted on this research so we can analyze the relation of two variables that is pressure and fire temperature (shown in Fig. 2).

Figure 2 has revealed a firing temperature for Pertalite fuel reach out 349 °C at 1,5 kPa of pressure and reach out the highest temperature at 430 °C on 2.5 kPa of pressure. For Pertamax fuel, the fire temperature at 1.5 kPa is 416 °C and the highest temperature is 530 °C at 2.5 kPa. Meanwhile, for LPG fuel, the firing temperature at 1.5 kPa of pressure is 483 °C, and the highest temperature in 578 °C at 1.8 kPa of pressure. There were fluctuations at several pressure points up to a pressure of 2.2 kPa to 2.5 kPa for Pertalite and Pertamax fuels, the fire temperature continued to increase.

Figure 3 has reveals the relationship between pressure and consume rate of fuel. Figure 3 has shown that the higher pressure, the lower the fuel consumption. The highest of fuel consumption rate is used LPG fuel. by pressure variation has used among 0.054 kg to 0.066 kg. Rate fuel consumption pertamax and pertalite fuel is relatively between from 0.021 kg to 0.033 kg. Figure 4 revealed relationship between pressure and boiling time of water.

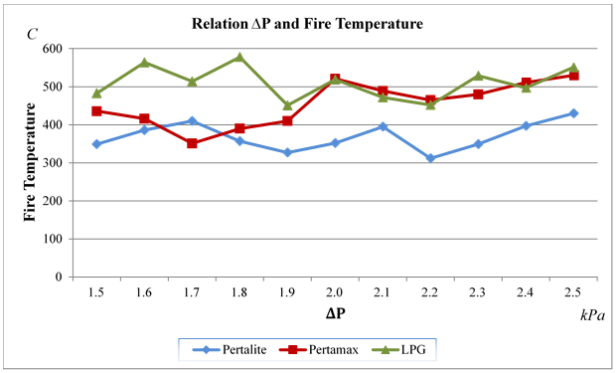

Figure 2. Relation of pressure (ΔP) to fire temperature (ºC) at gasoline fuel (Pertalite, Pertamax) and LPG fuel

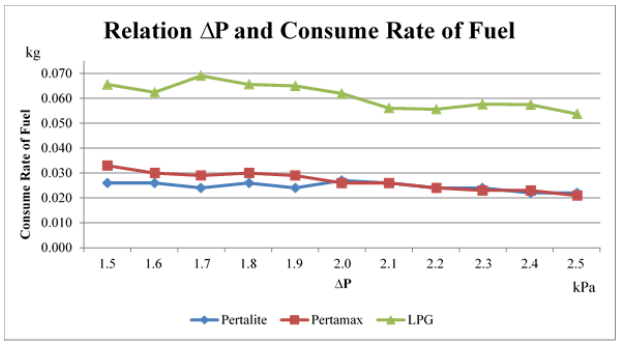

Figure 3. Pressure (ΔP) to consume rate of fuel the gasoline fuel (Pertalite, Pertamax) and LPG fuel

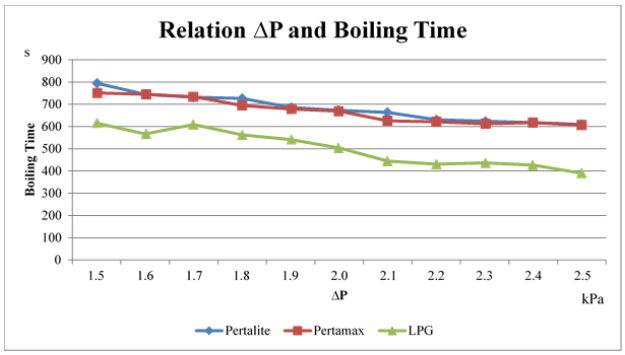

Figure 4. Pressure (ΔP) with boiling time in the gasoline (Pertalite, Pertamax) and LPG fuels

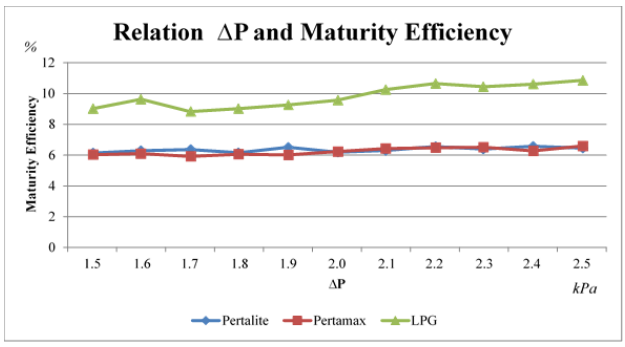

Figure 5. Pressure (ΔP) to Maturity Efficiency in the gasoline (Pertalite, Pertamax) and LPG fuels

Figure 4 shows that the fastest boiling time has used LPG fuel that its time among 391 seconds to 616 seconds. Pertamax and Pertalite fuel reveal relatively equal in the time and magnitude value that is the higher pressure, the shorter the simmering time required from 607 seconds to 795 seconds.

Figure 5 shows relationship between pressure and maturity Efficiency in the gasoline fuel. Figure 5 reveals that the efficiency value of pertalite and pertamax fuels is relatively constant on ranges between 6.359 % and 8.020 %. For LPG fuel, there is enhance efficiency as long as increased pressure. The highest value of efficiency on 2.5 kPa (10.857 %), 1.5 kPa (9.018 %). This shows that the greater the pressure applied, the greater the tomaturity efficiency value.

4.2. Maturity cost analysis

The cost comparison parameter used is operational costs. For costs of investment are considered relatively the same because they is use the same stove despite using

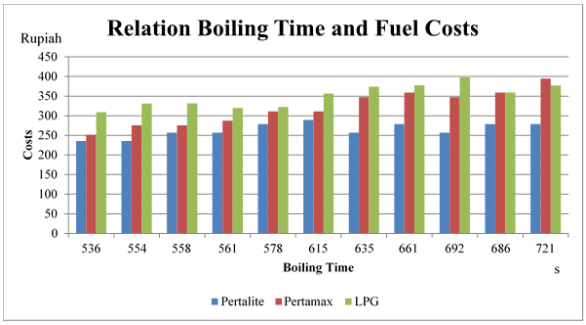

Figure 6. Boiling Time to Cost of Gasoline (Pertalite, Pertamax) and LPG fuels

different fuel containers. Figure 6 shows that greater the time, and greater operational cost. It also appears that the lowest operating costs are pertalite fuel then pertamax and finally LPG.

To boil water 1 litre of water with pertalite fuel at a pressure of 2.5 kPa, it costs 236 Rupiah and for pertamax fuel of 251 Rupiah. As for LPG fuel amount to 309 Rupiah. For low pressure (1.5 kPa), it costs 278 Rupiah for Pertalite, 395 Rupiah for Pertamax and 377 Rupiah for LPG.

5. Conclusion

The highest fire temperatures for Pertalite fuel are 430℃, Pertamax fuel 530℃ fuel and LPG 578 ℃ fuel. Fuel consumption at 2.5 kPa for Pertamax 0,021 kg fuel, Pertalite fuel 0.022 kg, and LPG fuel 0.054 kg. For the fastest discharge time occurs at a pressure of 2.5 kPa, for LPG fuel takes 391 seconds, Pertamax 607 seconds fuel and Pertalite fuel time is 610 seconds. While the fuel efficiency value at 2.5 kPa has obtained for Pertalite fuel is 6.136%, Pertamax fuel, 7.730% and LPG fuel 9.018%. The cost required to boil 1 (one) litre of water is Pertalite fuel amounting to Rp. 236,- Pertamax fuel Rp. 257,- and LPG fuel of Rp. 309,-. This research should be a reference for household users to overcome the scarcity of LPG.

References

[1] Ahmad Hidajat Effendi, “Fire Safe and Energy Saving Stove Performance Study (AHE Stove),” Settlement Journal, vol. 3, no. 1, May 2008.

[2] Diah Krisnatuti Pranadji, Muhammad Djemdjem Djamaludin, Nuriza Kiftiah, “Behavior Analysis of Household Use of LPG in Bogor City,” vol. 3, no. 2, p. 173 – 183, ISSN : 1907 – 6037, August 2010.

[3] Nur Ikhwani, “Community Acceptance of the Use of LPG Gas in Dusun Tua Village, Kelayang District, Indragiri Hulu Regency,” JOM FISIP, vol. 6, Riau University, 2019.

[4] Bayu Maidi Alkarim, R. Hengki Rahmanto, M. Irham Mahfud, “Effect of Air Pressure on Gasoline Stoves on Combustion Performance with the Evaporation Method,” Mechanical Engineering Scientific Journal, vol. 6, no. 2, August 2018, Islamic University 45 Bekasi.

[5] Kemas Ridhuan dan Ervan Septa Darma, “Variations in The Number of Holes and The Size of The Burner Diameter of The Premium Stove on Fuel Consumption,” Journal of Mechanical Engineering, Muhammadiyah Metro University, vol. 5, no. 2, p – ISSN : 2301 – 6663, e – ISSN : 2477 – 250 X, 2016.

[6] Sukardi dan Hilda Porawati, “Reactor Tube Design on Used Canned Fuel Stove,” Journal of Innovators, vol. 2, no. 2, 2019.

[7] Rayyan, Abdul Wahab, Margianto, “Comparison of the use of Pertalite and Pertamax Turbo fuels against carbon residue and performance on 2013 Yamaha Byson motorbikes”.

[8] P. Nara Wiryawan, G. Widayana, Rihendra Dantes, "The Comparative Effect of Using Pertalite Oil and LPG Fuel on The Performance of a 4-Stroke Gasoline Motorbike on a Honda Supra Fit," Journal of The Department of Mechanical Engineering Education, vol. 8, no. 2, Ganesha University of Education, 2017.

[9] Tri Susilo Wirawan, Ikram Anugrah, Suryanto, Musrady Mulyadi, "Analysis of Gasoline Fuel on the Performance and Economic Value of the CM 11 Gasoline Motor," Proceedings of the Research Results Seminar (SNP2M), pp. 12 – 17, 978-602-60766-4-9, 2018.

[10] Joko Triyatno, "Comparison of the Use of Natural Gas to LPG in Meeting Household Needs in Bontang," Al Ulum Science and Technology, vol. 4, no. 1, STTIB Bontang, November 2018.

[11] Wahyudi, "Research of Calorific Value of Biomass: Comparison of Test Results and Calculation Results," Semesta Teknika Scientific Journal, vol. 9, no. 2, 2006.

[12] Dian Marya Novita dan Enri Damanhuri, "Calculation of Heating Value Based on The Composition and Characteristics of Urban Waste in Indonesia in The Concept of Waste to Energy," Journal of Environmental Engineering, vol. 16, no. 2, October 2010.

[13] Dwi Yuliyanto, Edi Widodo, "Effect Against Fuel type viscosity and TBN Lubricant SAE 10 W - 30 On Motor Fuel 125 cc," Manufacturing Energy Engineering Journal, vol. 3, no. 1, 2018.

[14] Agung Sugeng Widodo," Increased Heating System Efficiency with The Addition Of A Grid To A Pertorated Burner" Journal of Mechanical Engineering, vol. 7, no. 1, ISSN 2477 – 6041, 21 – 25, 2016.

[15] Sudarno dan Fadelan, "Increasing the Efficiency of the LPG Stove Using the Fire Element," Semesta Teknika Scientific Journal, vol. 19, no. 2, November 2016.

[16] Arif Mulyanto, Mirmanto, Muhammad Athar, "Effect of Height of Air inlets of Biomass Combustion Furnaces on Performance," Mechanical Engineering Dynamics, vol. 6, no. 1, June 2016, p. ISSN: 2088 - 088X, e. ISSN : 2502 - 1729.

[17] Maula Nafi, "Hardness Analysis of AL - 6061 COR Results with Double Quenching Heat Treatment," Mechanics - Journal of Mechanical Engineering, vol. 2, no. 2, 2016.

EPI International Journal of Engineering
Volume 3, Number 2, August 2020, pp. 143-149
DOI: 10.25042/epi-ije.082020.09

*p*ISSN 2615-5109
*e*ISSN 2621-0541

Performance Analysis of Solar Water Heating System with Plate Collector Integrated PCM Storage

Andi Syahrinaldy Syahruddin[a], Jalaluddin[b,*], Azwar Hayat[c]

[a]Department of Mechanical Engineering,Engineering Faculty, Hasanuddin University. Email:a.syahrinaldy@gmail.com
[b]Department of Mechanical Engineering,Engineering Faculty, Hasanuddin University. Email: jalaluddin_had@yahoo.com
[c]Department of Mechanical Engineering,Engineering Faculty, Hasanuddin University. Email:azwarhayat@unhas.ac.id

Abstract

Availability of solar energy as a renewable energy source is very abundant and inexhaustible. Solar water heater is an equipment that utilizes solar energy as a source of energy. The thermal performance of a solar water heater system using absorber plate with phase change material (PCM) as thermal energy storage is presented in this study. Two design of solar water heater collectors with absorber plate variations, i.e. an absorber plate with PCM storage and absorber plate without PCM storage were investigated experimentally and numerically simulation. First, the material properties of paraffin wax as PCM storage was analized analyticaly. Every shape model of solar water heater systems were imported and simulated at three variations of constant solar radiation, i.e. 400 W/m^2, 700 W/m^2, and 1000 W/m^2. The simulation using a computational fluid dynamic (CFD) fluent software. The results showed that the average collector efficiency between absorber plate with and without PCM storage is 70.98 % using experimental study and 67.73 % using numerical simulation study.

Keywords: Computational Fluid Dynamic (CFD); Fluent software; solar water heater system; Phase Change Material (PCM)

1. Introduction

The availability of solar energy as a renewable energy source is very abundant and inexhaustible. A solar water heater is an equipment that utilizes solar energy as a source of energy and has been used in various countries around the world. However, because there were still many shortcomings of existed solar water heater, various research on it were carried out. Research on solar water heating systems is considered very important because it is expected to be able to improve the efficiency and effectiveness of solar water heating technology. Previous research is an experimental study of solar water heater system with V-shaped plate absorber [1], two solar water heater systems were installed and tested at a low flow rate of 0.5 L/min and a high flow rate of 2 L/min. The results showed that the solar water heater system with a V-shaped plate absorber had a 3.6-4.4% better performance compared with that of the system with a flat-plate absorber.

On another side, a high temperature on the V-shaped plate surface causes heat losses to the collector surface to become large too, so needed thermal energy storage which can maximize the performance of the solar collector. Experimental performance investigation of a solar phase change material (PCM) has been presented and discussed by Pisut Thantong [2] in a tropical climate. The experiment has proved that the solar phase change material is energy efficient in terms of heat gain reduction and energy saving. Palacio [3] has presented a comparative experimental analysis of a conventional flat plate solar collector and an identical prototype with thermal storage system by PCM and the results indicate that the selection of the PCM and the contact conduction between the absorber and PCM are key factors to increase the collector performance respect to conventional flat plate solar collector.

Study towards improving charge/discharge rate of latent heat thermal energy storage has been studied by Yanping Du [4] has a result that the temperature of PCM-metal foams composite/case study of paraffin became more uniform, while the cold discharge rate was improved by approximately 8 times. Optimization of melting and solidification processes of PCM integrated collector storage solar water heater has been analyzed by Allouhi [5] with result optimize obtained when a mass flow rate of 0.0015 kg/s is used with a PCM thickness of 0.01 m and set the temperature of 313 K.

A study about simulated solar water heaters has been investigated by Badiei and Eslami [6] with a solar flat plate collector integrated with a layer of PCM and the resulting temperature distributions are analyzed during two different summer and winter days in Shiraz, Iran. Results show that although the system with PCM has lower output temperatures in the morning, hot water can be supplied in a longer duration in the evening while discharging.

In this study, a solar water heater that integrated a PCM storage as thermal energy storage (TES) with a thermosyphon system was simulated and investigated experimentally. Two modelings of solar water heater systems with two different heat collectors, i.e. an absorber

*Corresponding author. Tel.: +62 821-9226-7077
Jalan Poros Malino km. 6 Bontomarannu
Gowa, Indonesia
92171

plate with and without PCM storage was modeled and their performances were simulated numerically.

2. Literature Review

Solar water heater collectors are heat exchangers that convert solar radiation energy into thermal energy in water. Solar radiation was absorbed by a collector plate and transferred to the water. The water in the pipe flowed through the collector by inlet pipe which connected with storage water before. The water in the pipe of the collector was heated by heat transfer that happened of the collector [7]. Due to a temperature difference of water in the pipe, the water with higher temperature automatically goes up to the top collector and then flows to the storage water back, this matter called thermosyphon system. There are several factors that impact the system performance among others thermal insulation, the tilt angle of the collector, absorber plate and its design, selective coating, and working fluid. A schematic layout of a typical thermosyphon solar water heater is shown in Fig. 1.

In this study an absorber plate of solar water heater made from a thin metal sheet whose surface is black painted to maximize the solar radiation absorbed. Furthermore, a transparent glass sheet is used as covering the collector to transmit the short wave of solar radiation to the absorber plate and prevent heat escape from the collector. Due to the large amount of heat loss from the absorber plate to the glass surface, hence the solar water heater was integrated with phase change material (PCM) as thermal energy storage.

Experimental study about solar water heater thermosyphon system whose integrated with PCM has been done by Nadjib [8] using paraffin wax as the PCM, which the results indicate that the utilization of PCM effective enough as thermal energy storage. Due to its costs and physicochemical properties, paraffin wax is used in low water boiling point requirement applications, such as drying, heating, and household water heating. The main disadvantage is its low thermal conductivity, about 0.2 W/mK. The solution for this to mix PCM with high thermal conductivity materials, such as aluminum, copper, or carbon [9]. The properties of paraffin wax are shown in Table 1. Meanwhile, lists of thermal properties of some paraffin shown in Table 2.

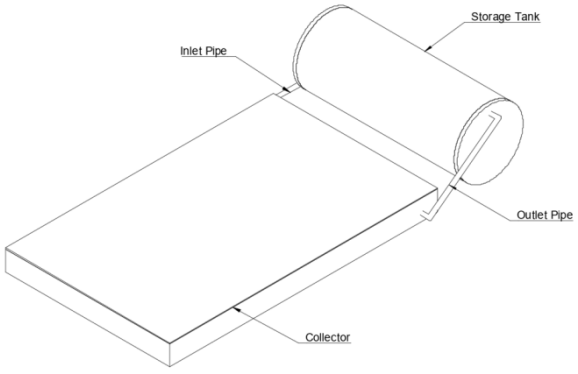

Figure 1. Schematic layout of a typical thermosyphon solar water heater

Table 1. Properties of paraffin wax

Property	Value	
	Solid	Liquid
Density, g/cm^3	0.861	0.778
Specific Heat, J/kgK	1900	2300
Melting Point, *Co*	55	
Latent Heat, kJ/kg	200 ± 10	

Table 2. Physical properties of some paraffin

Paraffin	Freezing Point / range (^{0}C)	Heat of fusion (kJ/kg)
6106	42-44	189
P116[c]	45-48	210
5838	48-50	189
6035	58-60	189
6403	62-64	189
6499	66-68	189

Along with the times, solar water heater systems today use a thermosyphon principle. The experimental and simulations of the solar thermal system have been presented by Ka-Kui Tse [10] and the results reveal that the overall efficiency of the solar thermal system can be improved by further physical design optimization. As for validated between the mathematical method and experimental method indicated that the maximum temperature of hot water occurred at 4:00 p.m as 65.25^{0}C, 71.19^{0}C, and 69.46^{0}C, respectively [11]. Garnier [12] have been presented a computational fluid dynamic (CFD) analysis of internal flows and heat transfer regimes within the new collector configuration and compares its performance against previously developed prototypes using empirical testing.

From the studies discussed previously, it can be concluded that numerical simulation with a computational fluid dynamic (CFD) analysis is more important to do before presented the prototype of a product.

3. Research Methodology

In this research, the used methodology is the experimental method and numerically simulation method. In the experimental method, two designs of solar water heater thermosyphon systems with an absorber plate with and without PCM storage have been presented and tested their performances with dimensions shown in Fig. 2.

The experimental study scheme is shown in Fig. 3 where 2 solar water heater thermosyphon systems with an absorber plate with and without PCM storage have been tested their performances using a thermocouple to measure the amount of temperature and a weather station to measure the amount of solar radiation from 9 AM to 8 PM.

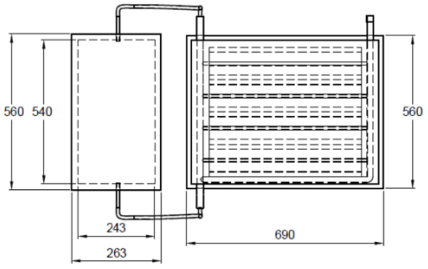

Figure 2. The dimensions of the thermosyphon system

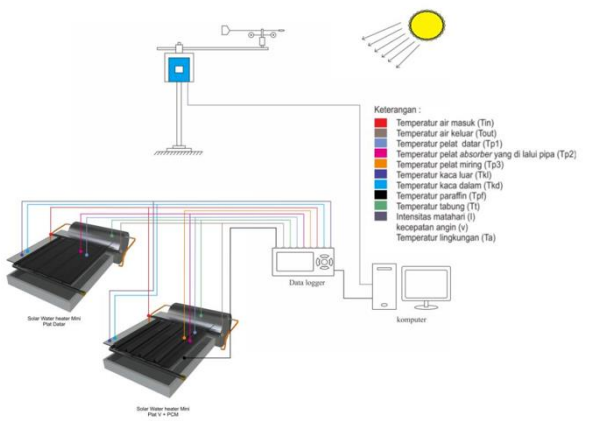

Figure 3. The experimental study schematic

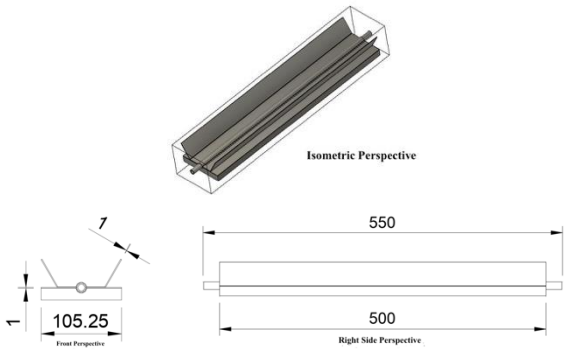

a) Absorber plate with PCM storage

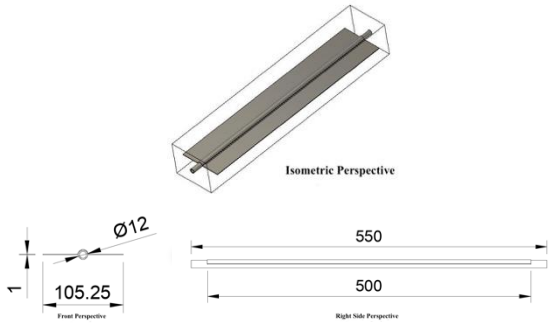

b) Absorber plate without PCM storage

Figure 4. The dimensions of the thermosyphon system

Meanwhile, the numerical simulation uses a set computer with windows 10 pro 64 bit, processor core i7-7700, and RAM 32 GB specification and capable of running a CFD fluent software and geometry modeling software i.e. an ANSYS Fluent and Autodesk Fusion 360, respectively. The simulation method, two shape model of the solar water heater thermosyphon system which will be simulated with one series, i.e. pipe, absorber plate with or without PCM, water flow in a pipe, glass, and two sides symmetry on the left and right side with the dimensions as shown in the Fig. 4.This is done because one series considered to be typical with others.

The simulation scheme as shown in Fig. 5 where an absorber plate with and without PCM modeling has given water inlet and constant radiation variations i.e. 400 W/m^2, 700 W/m^2, and 1000 W/m^2. A different temperature between inlet and outlet will be shown by contours

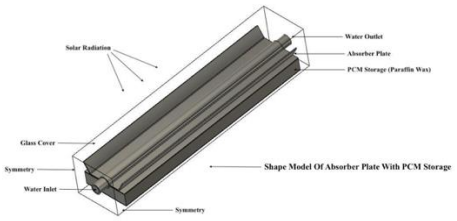

a) Absorber plate with PCM storage

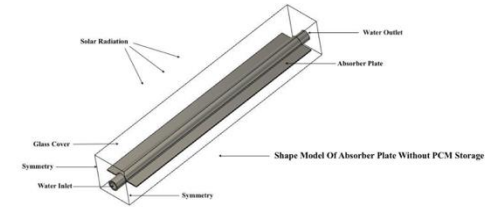

b) Absorber plate with PCM storage

Figure 5. The numerical simulation schematic

variations as a result of the simulation, likewise a contours temperature of the absorber plate, PCM, and water in the pipe.

Generally, the simulation run out based project schematic of fluid flow (fluent) from ANSYS Fluent, and each step be marked by the correct sign when done. The first step of the simulation is to draw or to import the geometry from another drawing software, provided that the file format of the geometry is compatible with ANSYS Fluent software (.iges or .step file) [13].

The simulation test kit consists of two shape model that was meshed of solar water heater collectors with absorber plate variations: a) Absorber plate with PCM storage and b) Absorber plate without PCM storage as shown in Fig. 6.

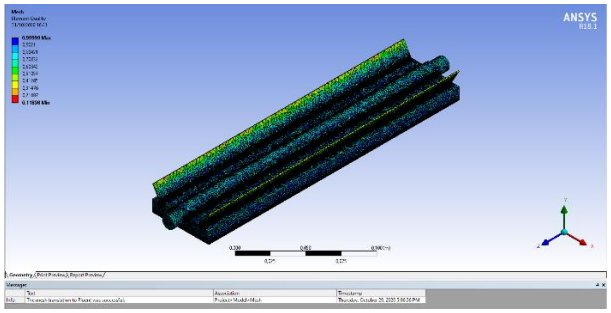

a) Absorber plate with PCM storage

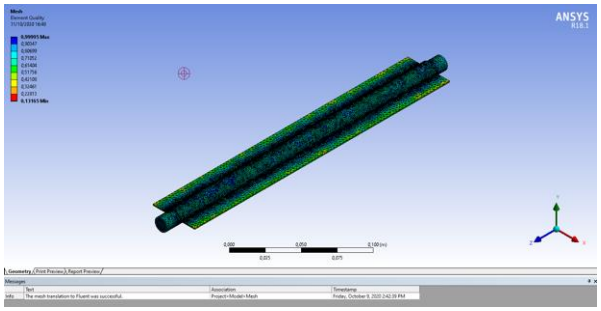

b) Absorber plate with PCM storage

Figure 6. Meshed shape model of the absorber plate

The numerical calculation study i.e includes calculating the collector efficiency by comparing the useful energy with the product of surface area and solar radiation, as shown in Eq. 1 :

$$\eta = \frac{Qv}{Ac\,.I\tau} \qquad (1)$$

Where $I\tau$ is solar radiation (W/m^2) and Ac is collector surface area (m^2), meanwhile, the useful energy was calculated based on the simulation results of inlet and outlet water temperature at a certain flowrate. The useful energy Qv was defined by Eq.2 :

$$Qv = m.Cp.\Delta T \qquad (2)$$

Where m is flowrate (kg/s), Cp is the specific heat of water (J/kg.K), and ΔT is the temperature difference of inlet and outlet of water (℃).

A simulation study of shapes model plate absorber with and without PCM storage was conducted under the same methods. Water flowed through a copper tube by inlet water with uniform 1 m/s velocity. Figure 7 shows (a) Setup model simulation; (b) Solution methods and solution control; and (c) Run calculation processes.

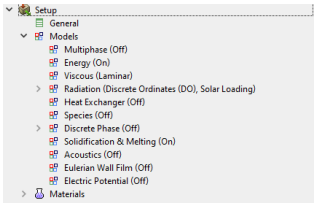

a.) Setup model simulation

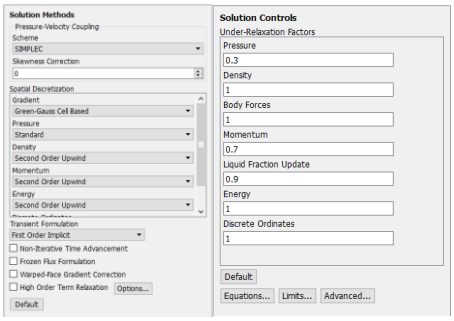

b.) Solution method and control

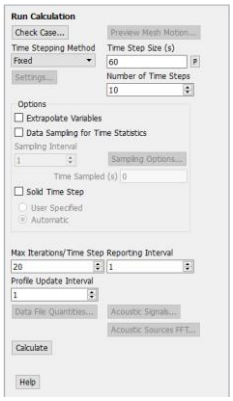

c.) Run calculation processes

Figure 7. Used Simulation method

4. Result and Discussion

The research was conducted at the Renewable Energy Laboratory of the Mechanical Engineering Department, Hasanuddin University, Gowa. Experimental and numerical simulation tests of two design solar water heater collectors using an absorber plate with and without PCM storage.

The results of the experimental study that have been done of the absorber plate with and without PCM storage at the same time of day and condition i.e. October 11-13, 2020 are shown in Fig. 8. However, as a valid data with numerically simulation study, solar radiation has been chosen which ranges between 400 W/m^2, 700 W/m^2, and 1000 W/m^2 as a sample of solar radiation at three times a day i.e. morning or afternoon; before or after daylight; and the daylight.

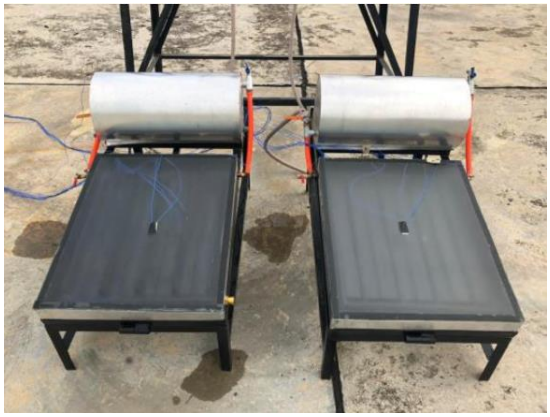

Figure 8. Absorber plate with PCM storage (left side) and without PCM storage (right side)

Figure 9 shows a comparison of inlet and outlet water temperature, plate temperature, and paraffin wax temperature as a PCM storage at three solar radiation variations as the results of an experimentally study. The outlet temperature from the absorber plate with PCM storage is higher than the absorber plate without PCM storage which the highest outlet water temperature of the absorber plate with PCM storage is 52.36 ^{0}C when compared with the absorber plate without PCM storage that is 50.97 ^{0}C. But in reverse with a maximum temperature of plate surface which the temperature of absorber plate without PCM storage is higher than absorber plate with PCM storage, which the maximum temperature of plate surface on absorber plate without PCM storage is 74.47 ^{0}C, while the maximum temperature of plate surface on absorber plate with PCM storage is only about 72.03 ^{0}C.

Meanwhile, the results of the simulation can access by contours, a difference temperature shown in contours of temperature. A temperature contours of absorber plate with and without PCM storage on constant radiation 400 W/m2 (a); A temperature contours of absorber plate with and without PCM storage on constant radiation 700 W/m2 (b); and A temperature contours of absorber plate with and without PCM storage on constant radiation 1000 W/m2 (c) is shown in Fig. 10.

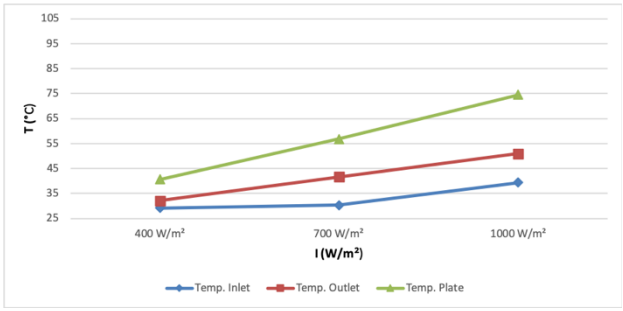

a) Absorber plate without PCM storage

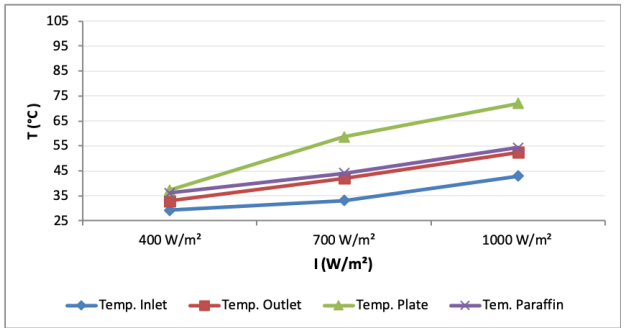

b) Absorber plate with PCM storage

Figure 9. Inlet and outlet water temperature, plate, and PCM temperature

A temperature contours of water on absorber plate with and without PCM storage on constant radiation 400 W/m^2 (a); A temperature contours of water on absorber plate with and without PCM storage on constant radiation 700 W/m^2 (b); and A temperature contours of water on absorber plate with and without PCM storage on constant radiation 1000 W/m^2 (c) shown in Fig. 11.

The temperature contours of paraffin wax on an absorber plate with PCM storage are shown in Fig. 12. In this study, simulation has given constant direct solar radiation too i.e. 400 W/m^2, 700 W/m^2, and 1000 W/m^2. Then it was obtained of a temperature comparison of water on every shape model was simulated.

Figure 13 shows a comparison of constant direct solar radiation variations on each simulated model and the results of the numerical simulation study. The water temperature from absorber plate without PCM storage is higher than absorber plate with PCM storage which the maximum water temperature of absorber plate without PCM storage is 102.04 ^{0}C on 1000 W/m^2 constant radiation when compared with absorber plate with PCM storage that is 73.85 ^{0}C on the same condition of the constant radiation. However, the heat was absorbed by the plate absorber with PCM storage was transferred to PCM storage partially.

As shown in Fig. 13 where the average paraffin wax temperature as PCM storage even higher than the maximum paraffin temperature is 70.21 ^{0}C on 1000 W/m^2 constant radiation. So as the collector efficiency of the absorber plate with PCM storage is better than the absorber plate without PCM storage.

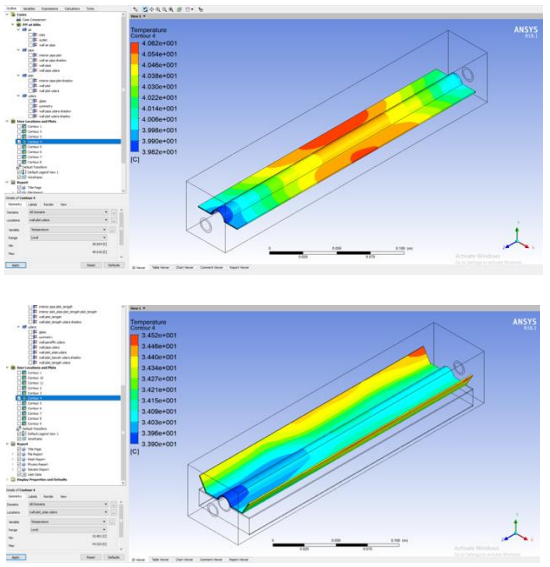

a) Temperature contours of absorber plate on radiation 400 W/m^2

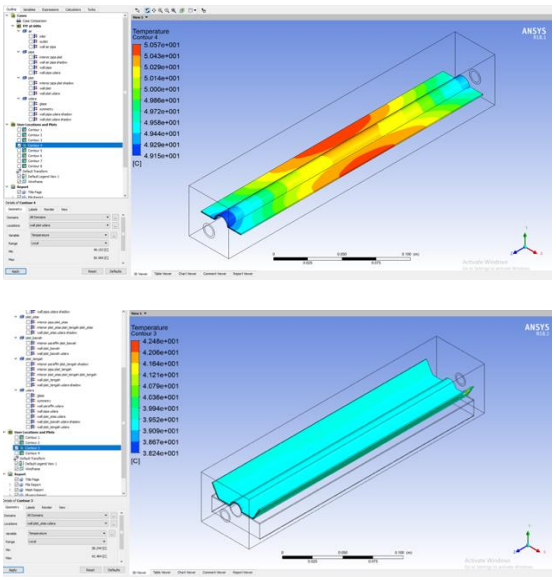

b) Temperature contours of absorber plate on radiation 700 W/m^2

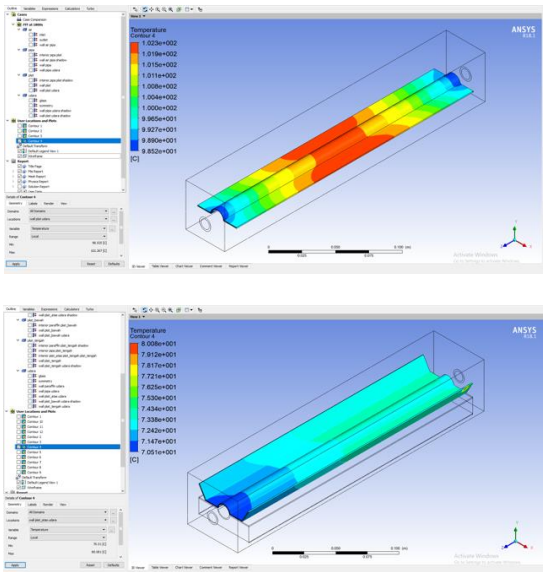

c) Temperature contours of absorber plate on radiation 1000 W/m^2

Figure 10. Temperature contours of the absorber plate

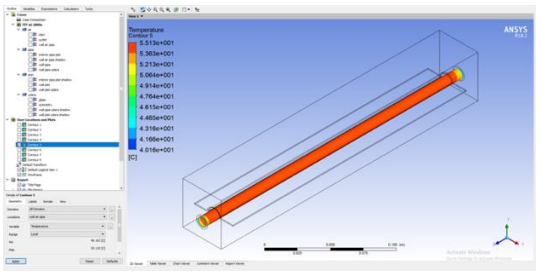

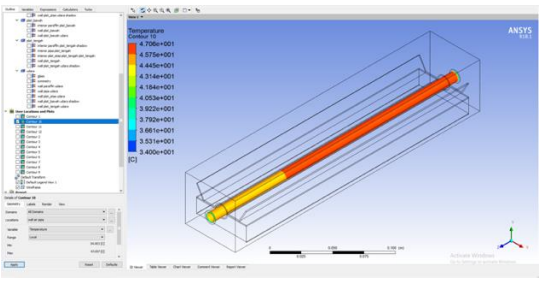

a) Temperature contours of water on radiation 400 W/m^2

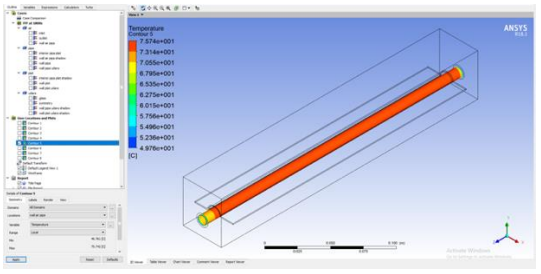

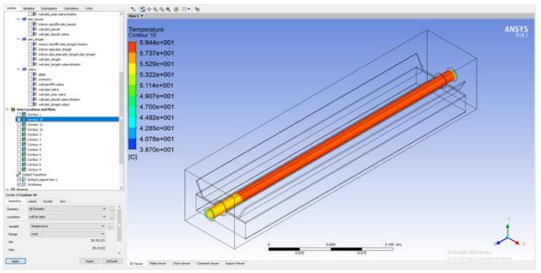

b) Temperature contours of water on radiation 700 W/m^2

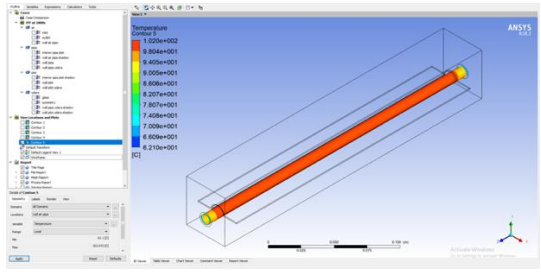

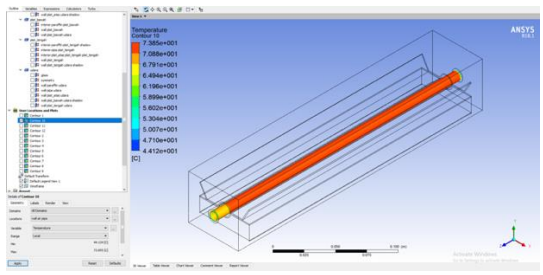

c) Temperature contours of water on radiation 1000 W/m^2

Figure 11. Temperature contours of water on absorber plate

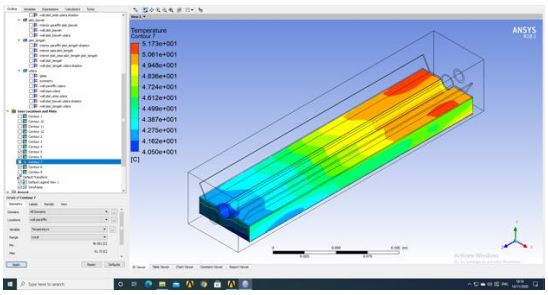

a) Temperature contours of paraffin wax on radiation 400 W/m^2

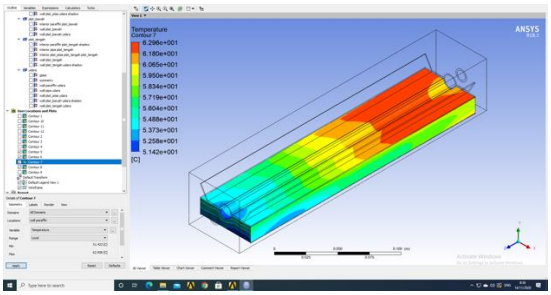

b) Temperature contours of paraffin wax on radiation 700 W/m^2

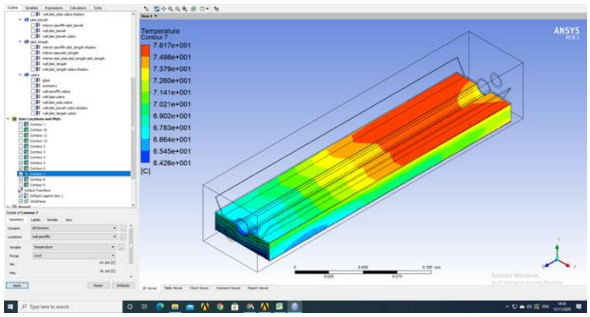

c) Temperature contours of paraffin wax on radiation 1000 W/m^2

Figure 12. Temperature contours of paraffin wax

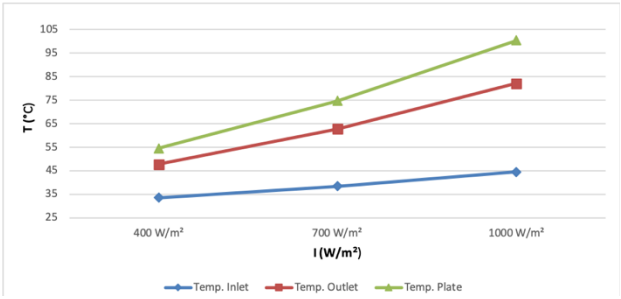

a) Absorber plate without PCM storage

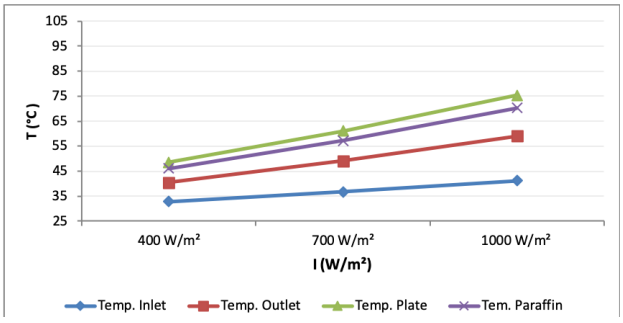

b) Absorber plate with PCM storage

Figure 13. Inlet and outlet water temperature, plate, and PCM temperature

Figure 13 shows a comparison of inlet and outlet water temperature, plate temperature, and paraffin wax temperature as a PCM storage at three constant solar radiation variations as the results of a numeric simulation study. The average water temperature from the absorber plate without PCM storage is higher than the absorber plate with PCM storage which the highest average outlet temperature of the absorber plate without PCM storage is 82.06 ^{0}C when compared with the absorber plate with PCM storage that is 58.99 ^{0}C. Likewise with the average plate surface temperature which 75.29 ^{0}C for absorber plate with PCM storage, lower than absorber plate without PCM storage as much as 100.39 ^{0}C.

Based on experimentally and numerically simulation study at the high constant solar radiation, the efficiency collector by absorber plate with and without PCM storage is shown in Fig. 14. The difference in collector efficiency using a simulation method tended to lower than using an experimental method. Using the experimental method, the collector efficiency was 70.36 % for the absorber plate without PCM storage and 71.61 % for the absorber plate with PCM storage. While using the simulation method, the collector efficiency was 67.14 % for the absorber plate without PCM storage and 68.33 % for the absorber plate with PCM storage. So, the average collector efficiency between absorber plates with and without PCM storage was 70.98 % using an experimental study and 67.73 % using a simulation study. Based on an experimental and numerical simulation study, the average collector efficiencies were 68.75 % for absorber plate without PCM storage and 69.97 % for absorber plate with PCM storage, so the absorber plate with PCM storage had a better performance than the absorber plate without PCM storage.

5. Results and Discussion

The absorptivity of the absorber plate with and without PCM storage was investigated. It was shown that the absorber plate with paraffin wax as PCM storage had better absorptivity if compared with the absorber plate without PCM storage. The absorber plate with PCM storage was applied in the experimental and numerical simulation study.

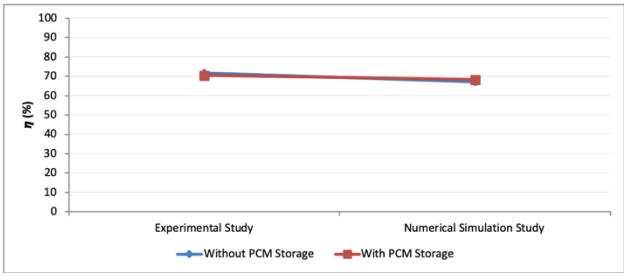

Figure 14. Collector efficiency of absorber plate with and without PCM storage

Two designs of solar water heater thermosyphon system with different absorber plate, i.e. absorber plate with PCM storage and absorber plate without PCM storage were investigated experimentally and numerically simulation. The results show that the solar water heater with a PCM storage absorber plate had a better performance. The average collector efficiency between absorber plates with and without PCM storage was 70.98 % for experimental and 67.73 % for numerical simulation. Applying for the absorber plate with PCM storage in a solar water heater thermosyphon system increases its performance due to the increased absorptivity of its absorber plate.

Acknowledgments

This research is supported and financed by the Institute of Research and Community Service (LP2M) Hasanuddin University.

References

[1] Jalaluddin., Effendy, Arif., Rustan, Tarakka., *Experimental Study of a SWH System with V-Shaped Plate*, J.Eng. Technol, 48, pp. 2337-5779, 2016.

[2] Thantong, Pisut., Chantawong, Preeda., *Experimental Study of Solar – Phase Change Material Wall for Domestic Hot Water Production under the Tropical Climate*, Energy Procedia, 138, pp. 38-43, 2017.

[3] Palacio, Mario., Rincon, Anggie., Carmona, Mauricio., *Experimental Comparative Analysis of Flat Plate Solar Collector With and Without PCM*, Solar Energy, 206, pp. 708-721, 2020.

[4] Yanping Du., Ding, Yulong., *Towards Improving Charge / Discharge Rate of Latent Heat Thermal Energy Storage (LHTES) by Embedding Metal Foams in Phase Change Materials (PCMs)*, Chemical Engineering and Processing, 108, pp. 181-188, 2016.

[5] Allouhi, A., Msaad, A.Ait., Amine, M.Benzakour., Saidur, R., *Optimization of Melting and Solidification Processes of PCM : Application to Integrated Collector Storage Solar Water Heaters (ICSSWH)*, Solar Energy, 171, pp. 562-570, 2018.

[6] Badiei, Z., Eslami, M., Jafarpur, K., *Performance Improvements in Solar Flat Plate Collectors by Integrating with Phase Change Materials and Fins: A CFD Modeling*, Energy, 19, pp.32414-4, 2019.

[7] Fregah, B., *Design , Development And Optimisation Of A Novel Thermo-Syphon System For Domestic Applications*, 2016.

[8] Nadjib, Muhammad., *Paraffin Wax As a Thermal Energy Storage Of Solar Water Heater Thermosyphon System*, Vol. 18, No. 3, Pp. 76–85, 2016.

[9] A. Reyes., L. Henriquez-Vargaz., J. Rivera., F. Sepulveda., *Theoritical and Experimental Study of Alluminium Foils and Paraffin wax Mixtures As Thermal Energy Storage Material*, Renewable Energy, 101: 225-235: 2017.

[10] Tse, Ka-Kui., Chow, Tin-Tai., *Dynamic Model and Experimental Validation of an Indirect Thermosyphon Solar Water Heater Coupled with a Parallel Circular Tube Rings Type Heat Exchange Coil*, Solar Energy, 114, pp. 114-133, 2015.

[11] Wannagosit., Sakulchangsatjatai., *Validated Mathematical Models of a Solar Water Heater System with Thermosyphon Evacuated Tube Collectors*, Case Studies in Thermal Engineering, 12, pp. 528-536, 2018.

[12] Garnier, Celine., Muneer, Tariq., Currie, John., *Numerical and Empirical Evaluation of a Novel Building Integrated Collector Storage Solar Water Heater*, Renewable Energy, 18, pp.30352-5, 2018.

[13] Ansys, Inc., *ANSYS Fluent Single-Window, Task Based Workflow for Better CFD Simulation*, Application Brief, 2020.

EPI International Journal of Engineering
Volume 3, Number 2, August 2020, pp. 150-153
DOI: 10.25042/epi-ije.082020.10

*p*ISSN 2615-5109
*e*ISSN 2621-0541

Beach Sand Filtrate as an Alternative Gas Fuel

Hasdinar Umar[a,*]

[a]Department of Ocean Engineering, Faculty of Engineering, Universitas Hasanuddin. Email: hasdinarumar@unhas.ac.id

Abstract

The golden age of the oil business in Indonesia is over and now petroleum is even a burden. As oil producing countries prepare themselves to start the second phase of the golden era of oil, Indonesia is heading towards an era of energy crisis. Renewable energy is needed as an alternative to meet the community's fuel needs. Beach sand is one material that can be used to help the biomass gasification process. Small particles of sand are filled into a container and gas is flowed from below and suppresses the flow of each particle which is useful for the biomass decomposition process. When using beach sand, we can also utilize heat energy optimally in coastal areas to make gasification reactions easier. This study aims to examine the groups contained in the TMS (Tetramethylsilan) spectrum of the beach sand filtrate fluid by paying attention to the CH3 compounds which are arranged in TMS. FTIR (Fourier Transform Infrared Spectroscopy) test results show that the beach sand filtrate fluid gives an illustration that from wavelengths of 3000 to 3500 the sharpness of the amount of nitrogen and hydrogen in the sand beach filtrate liquid solution can be used as ammonia gas (a fuel). Nitrogen and Hydrogan when bound with Hydroxide will form ammonium hydroxide which can function as a fuel (heating).

1. Introduction

The golden age of the oil business in Indonesia was over and now it was petroleum instead it becomes a burden. Renewable energy, such as solar cells, wind power, biomass, etc. were attracting the attention of various parties, mainly because the use of these various energies did not increase concentration carbon dioxide in the air. Biomass was a potential source of energy, its use was quite varied, so it was very important. Biomass was a concept that views biota bodies quantitatively. This concept also includes agricultural products including biomass. As oil producing countries prepare to start the second golden era of oil, Indonesia was heading for an era of energy crisis [1]. The products of nanotechnology are nanomaterials, where nanosilica synthesis is currently being developed which is very widely used in the electronics field. The largest silica content is found in coastal sand [2].

One of them observed in this study is that sea sand from Lampung Province has the characteristics of coarse grains and varying gradations and has a content of chloride (Cl) and sulfate (SO4) salts not exceeding the specified limit [3]. Previous research stated that beach sand originated from corals which had weathered and eroded turned out to have a lot of mineral and ion content, one of which is S4 (sulfate). Sulfate itself is one of the main components of the clay / red soil that we know together can be used as a catalyst in the gasification process of sawdust. With that, we can make So4 Compound as a reference to make beach sand as a catalyst in the gasification process.

*Corresponding author. Telp.: +62-811-416-5078
Jalan Poros Malino km. 6, Bontomarannu,
Gowa, South Sulawesi, Indonesia 92171

In addition, coastal sand is mostly composed of silisium dioxide, so that it can be used as raw material for silisium production. Silisium itself in the process of processing silisium dioxide into silisium or metal materials that are gray can be used energy that is environmentally friendly and is provided by nature, namely wind energy or energy from sunlight. Silisium is a non-toxic material and has energy content such as carbon, which is the core of fossil energy. The energy in silisium is stored safely because of chemical bonds, and can be moved to other places safely. When the process of producing silisium into silicon is obtained by-product liquid, Tetramethylsilan (TMS) which has a fuel energy of gasoline from petroleum. If this TMS is burned, it will produce less energy and CO2 gas compared to gasoline and clean sand. Thus, this TMS can be used as an alternative fuel for the future.

The FTIR (Fourier Transform Infrared Spectroscopy) testing of Kuri Ca 'in the Maros Regency shows that beach sand has a CH3 group in the TSM spectrum, which proves that beach sand has fuel energy [4]. FTIR was a way of characterizing a functional group of a sample. If infrared light was passed through a sample of an organic compound, then there were a number of frequencies that were absorbed and some were transmitted or transmitted without being absorbed. The absorption of light by molecules was dependent on the electronic structure of the molecule. The molecules that absorb that energy there were changes in vibrational energy and changes in the level of rotational energy [5]. The FTIR method has the advantage of being accurate and fast, while requires minimal sample preparation even suitable for in situ analysis by using a portable FTIR spectrometer [6]. FTIR is very effective at identifying these forms of silica,

whereas microscopy and X-ray diffraction (XRD) are still powerless to distinguishes non-crystallized forms. FTIR spectroscopy is numerous used for identification of silica forms [7].

2. Experimental Setup

This research was conducted at the Chemistry Department Laboratory of FMIPA Unhas.

1. Material of experiment
   a) Liquid yield from the Sand filtrate
   b) Natriumsulfate (Na2SO4)
2. Experimental Tool
   a) Test tube (Fig. 1)
   b) FTIR (Fourier-transform infrared spectroscopy) test (Fig. 3)
   c) Circle plat (Fig. 2)
   d) Crystal and solid NaCl
   e) Aluminium Foil
3. Experimental Process
   a) Pour the liquid filtrate from the beach sand with methanol into the test tube as much as 5 drops.
   b) Add 5 grams of Natriumsulfat into the test tube consisting of beach sand filtrate liquid so that the liquid in the tube can be solid.
   c) Cover the test tube with aluminum foil then shake the test tube so that the filtrate solution can be fused with natriumsulfate.
   d) After that the sample will be put into a circular plate mold which is coated with NaCl which has been dense which is useful for removing the remnants of water contained and so that infrared rays can penetrate the liquid filtrate that has been compacted.
   e) Then the circular plate will be tested through the FTIR tool the content of the TSM from the white sand filtrate liquid extracted with methanol

Figure 1. Test Tube

Figure 2. Sample in a Circular Plat

Figure 3. FTIR Test

4. How to read FTIR spectra as shown in Fig. 3.
   a) Find the X-axis and Y-axis of the spectrum. The x-axis of the IR spectrum was labeled as "wave number" and the numbers range from 400 on the far right to 4,000 on the far left. The X-axis provides the absorption number. The Y axis was labeled as "Percent transmittance" and the numbers range from 0 at the bottom to 100 on the top.
   b) Determine the characteristics of the peaks in the IR spectrum. All infrared spectrum contains many peaks. Next look at the functional group area data needed to read the spectrum.
   c) Determine the region of the spectrum where the characteristic peaks were present. The IR spectrum can be separated into four regions. The first region ranges from 4,000 to 2,500. The second region ranges from 2,500 to 2,000. The three regions range from 2,000 to 1,500. The fourth region ranges from 1,500 to 400.
   d) Determine the functional group absorbed in the first region. If the spectrum has a characteristic peak in the 4,000 to 2,500 range, the peaks correspond to the absorption caused by the single NH, CH and OH bonds.
   e) Determine the functional group absorbed in the second region. If the spectrum has a characteristic peak in the range of 2,500 to 2,000, the peaks correspond to the absorption caused by the triple bond.

f) Determine the functional group absorbed in the third region. If the spectrum has a characteristic peak in the 2,000 to 1,500 range, the peaks correspond to the absorption caused by a double bond such as C = O, C = N and C = C. 7. Compare the peak in the fourth region to the peak in the other fourth region of the IR spectrum. The fourth was known as the fingerprint region of the IR spectrum and contains a large number of absorption peaks which account for a wide variety of single bonds. If all the peaks in the IR spectrum, including those in the fourth region, were identical to the peaks of the other spectrum, then you can be sure that the two compounds were identical.

3. Experimental Results

The results of the Sand Filtrate Fluid were tested using a FTIR (Fourier-transform infrared spectroscopy) tool aimed at examining how much nitrogen and hydrogen content contained in TMS is already in liquid form (Fig. 5 and Table 2). As is known that TMS (Tetramethylsilan) is a polar compound that is soluble in water and therefore the solvent used to dissolve it is methanol. Methanol is known as a semi-polar compound, which when combined with beach sand will dissolve all polar compounds contained in beach sand. When viewed from the FTIR chart prove that the wavelength of 3000 to 3500 (Table 1) shows the sharpness of the many elements of nitrogen and hydrogen in liquid solutions that can be used as ammonia (a fuel). Nitrogen and Hydrogan when bound with Hydroxide will form ammonium hydroxide which can function as a fuel (heating) as shown in Fig.4.

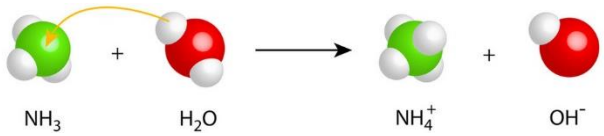

Figure 4. Chemical reaction of nitrogen and hydrogen bound with hydroxide

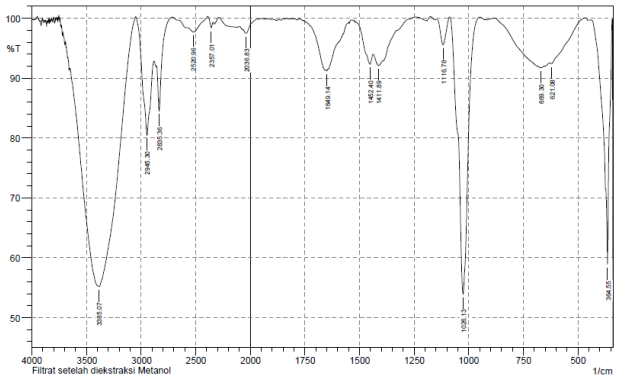

Figure 5. FTIR test result of filtration beach sand

Table 1. Functional area on IR [8]

Bond	Compound Tipes	Regional Frequency	Intensity
C – H	Alkana	2850 - 2970 1340 - 1470	Strong Strong
C – H	Alkena	3010 – 3095 675 - 995	Medium Strong
	H C === H		
C – H	Alkuna	3300	Strong
C – H	Cincin Aromatik	3010 – 3100 690 – 900	Medium Strong
O – H	Fenol, Monomer alcohol, alcohol ikatan hydrogen, fenol	3590 – 3650 3200 – 3600 3500 – 3650	Fluctuate Fluctuate Sometimes it widen
	Monomer asam karboksilat, ikatan hydrogen asam, karboksilat	2500 - 2700	Medium Widen
N – H	Amina, Amida	3300 – 3500	Medium
C ==== C	Alkena	1610 – 1680	Fluctuate
C ==== C	Cincin Aromatik	1500 – 1600	Fluctuate
C ≡≡≡ C	Alkuna	2100 – 2260	Fluctuate
C – N	Amina, Amida	1180 – 1360	Strong
C ≡≡≡ N	Nitril	2210 – 2280	Strong
C – O	Alkohol, Eter, Asam Karboksilat, Ester	1050 – 1300	Strong
C ==== O	Aldehid, Keton, Asam Karboksilat, Ester	1690 - 1760	Strong
NO_2	Senyawa Nitro	1500 – 1570 1300 – 1370	Strong

Besides the sharpness of the elements of alkenes, and alkenes in the Coastal Sand Filtrate Liquid graphs tested using FTIR (Fourier-transform infrared spectroscopy) so that compounds for fuel produced at TSM (Tetramethylsilan) will be more numerous.

4. Conclusion

Based on the results of testing using FTIR shows that :

a) Wavelengths of 3000 to 3500 show the sharpness of the many elements of nitrogen and hydrogen in the liquid sand beach filtrate solution which can be used as ammonia gas (a fuel).
b) The Alkene and Alkuna elements in the FTIR test chart for Sand Beach filtrate fluid are sharper, which shows that there are more fuel compounds produced at the TMS.

Table 2. Data of FTIR test result

No	Peak	Intensity	Corr.Intensity	Base (H)	Base (L)	Area	Corr. Area
1	364.55	58.894	40.993	441.7	343.33	6.288	6.215
2	621.08	92.421	0.498	628.79	487.99	2.68	0.245
3	669.3	91.728	0.269	682.8	653.87	1.07	0.021
4	1026.13	53.974	46.229	1085.92	948.98	11.61	11.73
5	1116.78	95.57	4.459	1145.72	1087.85	0.54	0.547
6	1411.89	92.112	2.649	1436.97	1240.23	2.899	0.629
7	1452.4	92.328	2.569	1516.05	1438.9	1.54	0.396
8	1649.14	91.212	0.443	1653	1573.91	1.991	0.002
9	2036.83	97.489	0.116	2040.69	1957.75	0.426	-0.052
10	2357.01	98.412	1.248	2389.8	2339.65	0.146	0.105
11	2520.96	97.688	1.289	2574.97	2389.8	1.039	0.535
12	2835.36	84.543	8.697	2856.58	2717.7	3.161	1.13
13	2945.3	80.487	15.119	3049.46	2883.58	7.923	5.315
14	3385.07	55.215	40.229	3651.25	3051.39	84.967	73.908

Acknowledgements

The authors would like to thank to LP2M Universitas Hasanuddin for the grant of PDPA 2019, Chemical Laboratory, Faculty of Science, Universitas Hasanuddin and Coastal Engineering and Environmental Laboratory, Department of Ocean Engineering, Faculty of Engineering, Universitas Hasanuddin.

References

[1] Indirasardjana, Pria. 2014. *2020 Indonesia Dalam Bencana Krisis Minyak Nasional*. Jakarta: Gramedia.

[2] Alimin et.al, 2016, *Analisis Kandungan Mineral Pasir Pantai Losari Kota Makassar Menggunakan XRF dan XRD*, CHEMICA: Jurnal Ilmiah Kimia dan Pendidikan Kimia, Vol. 17 No. 2, 2016.

[3] Fuad, I.S. 2015, *The Effect of Using River Sand with Sea Sand Against the Press Strength and Bending of Concrete Quality K-225*. Journal of Technology Desimination, Volume 3 No. 1, January 2015 Palembang: Civil Engineering Study Program, Faculty of Engineering, University of Tridinanti.

[4] H.Umar, et.al, 2019, *The Content and Function of Electrical Energy Sources from Silisium which are contained by the Sand of Kuri Ca'di Beach in Maros Regency*. J. Phys : Conf. Ser, 1341 052002.

[5] Soleh, Mohamad. 2014. *Ekstrasi Silika dari Sekam Padi dengan Metode Pelarutan dan Pengendapan Silika serta Analisis EDX dan FTIR* [skripsi]. Bogor: Institut Pertanian Bogor.

[6] Gil, M.I.A., Luna, M., Zarzuela, R., & García-Moreno, M.V 2020, 'Quantitative Determination of the Penetration of a Silica-Based Consolidant in a Limestone by FTIR Spectroscopy', Vibrational Spectroscopy, vol. 110, doi: 10.1016/j.vibspec.2020. 103109.

[7] Salih and Zaher, 2019, *Investigation of silica polymorphs stratified in siliceous geode using FTIR and XRD methods*, Material Chemistry and Physics 228, Elsevier, 2019.

[8] Skoog, et.al, 1998, *Principles of Instrument Analysis*, Saunders College Pub, 1998.

EPI International Journal of Engineering
Volume 3, Number 2, August 2020, pp. 154-159
DOI: 10.25042/epi-ije.082020.11

*p*ISSN 2615-5109
*e*ISSN 2621-0541

Investigating the Performance of a Ship by Matching the Stern Hull Form to Propeller and Engine Power

Andi Dian Eka Anggriani[a,*], Suandar Baso[b]

[a]Department of Naval Architecture, Faculty of Engineering, Hasanuddin University. Email: a.dianeka@unhas.ac.id
[b]Department of Naval Architecture, Faculty of Engineering, Hasanuddin University. Email: s.baso@eng.unhas.ac.id

Abstract

Designing the form of the ship stern hull could have some impacts on the efficiency of ship propeller and the requirement of the ship speed. Therefore, stern hull form of a ship matched to its propeller and engine power is important consideration in preliminary ship design stage. The main objective of this study is to investigate ship performance by matching the stern hull shape to the propeller diameter and engine power toward high speed. This study was conducted by free running model test and Maxsurf Resistance application. The stern forms were employed U-shape and V-shape. In addition, the fixed pitch propeller (FPP) with three blades was used and the diameter is varied into three sizes 0.032 m, 0.040 m, and 0.048 m. The results show the increase of propeller diameter increases model's speed for both U-shape and V-shape stern and the effect of the propeller diameter on the speed could be described by using the equations of second-order polynomial. The optimum propeller diameter could be determined taking into account stern hull form, stern shape, tip clearance, and proper speed where then propeller diameter related to draft is given by 0.79T with tip clearance 10%Dp for both U-shape and V-shape. The ship resistances of U-shape stern at Fr 0.221 and V-shape at 0.208 are obtained approximately 89.797 KN and 77.10 KN respectively. Furthermore, the powers of ship for both U-shape and V-shape at those Fr are obtained 904,374 KW and 726,807 KW respectively. Finally, the best stern hull form matched to propeller diameter and engine power is selected and given by U-shape stern.

Keywords: Stern hull form ; U-shape ; V-shape

1. Introduction

All ship owners need the good performance for their ship in actual sea and the one of aspect is the proper service speed. This impacts on cost and time operation. Therefore, a ship must be design properly to achieve a proper service speed. Correspondingly, some parameters of ship hydrodynamic must be investigated and considered completely associated with hull form, engine power, and propulsion system.

Although, a stern form of a ship design is obtained in good shape, however the proper determination of main engine power and propeller diameter are also important things in ship design. This must be noted that a ship hull form should match to propulsion system. Particularly in the stern form, the shape of stern contour is mostly related with propulsion performance, therefore a stern form of a ship must be matched to propeller diameter as well. For stern form design, a number of factors such as hydrodynamic efficiency, construction simplicity and flow patterns must be considered. The design of ship stern shape must ensure uniform flow of water around the hull and good hull efficiency coefficient and then these indicate on that mitigate the stern waves and improve the flow into the propeller.

Some studies related with hull form of a ship matched to propulsion system have been conducted widely. Stapersma and Woud [1] discussed the basic matching problem of a propulsion engine to the propulsor and its influences and they also applied their calculation method to evaluate design and off design conditions. Ukon et al. [2] developed the ship hulls and optimum propellers to concretely solve some serious hydrodynamic problems on a high-speed and high-powered ship with a large diameter single screw propeller. Lin et al. [3] proposed a process to design ship-engine-propeller simultaneous matching where the ship-propeller subsystem and the engine-propeller subsystem in which relationships between rotational speed of the propeller and advancing speed that were expressed N-V curves. Ogar et al. [4] proposed the design analysis to use for optimal matching of controllable pitch propeller to the hull and diesel engine. In order to make the wake field more uniform, the stern frame from above the shaft line was shifted to the stem and the stern bulb sectional area was increased and the gravity center of the area was made lower. Ren et al. [5] proposed a procedure development of the combination of the system matching theory and Energy Efficiency Design Index (EEDI) calculation, which can provide the matching results of ship–engine–propeller as well as the corresponding EEDI value. Nurhadi et al. [6] studied engine propeller matching and discussed EPM on a high speed vessel that uses Gawn series propeller type.

The stern of a ship has several forms or shapes such as V–shape, the U–shape, transom etc. Each shape has

*Corresponding author. Tel.: +6285255325548
Jalan Poros Malino km.6 Gowa
Sulawesi Selatan 92171

individually its own advantages and disadvantages. The choice of the shape of the top side stern section should be decided on the basis of Froude number. The design hull form of a ship taking into account proper speed have been studied such as Lu et al. [7] proposed an innovative methodology of synchronous local optimization of ship bow and stern hull form considering the whole ship speed range. Ghasemi and Zakerdoost [8] proposed design methodology that represents a comprehensive approach to optimize the hull–propeller system simultaneously wherein the well-known evolutionary algorithm based on NSGA-II was employed to handle the multi-objective problems, where the main propeller and hull coefficients are the unknown and are considered as design variables.

The different types of propellers are classified by blade number and blade pitch. However, the number of propeller blade has little agreement for the best options. The effectiveness of a propeller depends upon several factors, but diameter is one of the most important.

Johannsen [9] investigated the performance of three-bladed propeller with varying diameters for the ship. For all variants the radial pitch and camber distribution was reevaluated to achieve best wake adaptation and the three-bladed propeller gained up to 3.5% in power requirement.

Based on the explanation above, this study describes the container ship performance which was investigated by matching the stern hull form to propeller and engine power. Then, the investigation was conducted by free running model test where the U-shape and V-shape of stern form were matched to varied propeller size and engine power based on resistance results generated by U-shape and V-shape. The resistance of ship was predicted by using Maxsurf Resistance [10].

2. Methods

Here, the ship performance was investigated by conducting the free running model test and using Maxsurf Resistance [10]. The stern shapes were matched to varied propeller diameters and engine power. Then, this study steps are shown in Fig. 1.

Ship type which was employed in this study is container. Then, ship main particulars are provided in Table 1 and body lines plan are shown in Fig. 2. This ship has previously U-shape in the stern part along hull ship which has a body lines plan as shown in Fig. 2a. Furthermore, it was re-designed becoming V-shape particularly in stern part (in section areas 1 to 3) and the body lines plan is shown in Fig. 2b. While re-design process, the hydrostatic parameters were verified and then they must be similar as provided in Table 2. The 3-dimensional shape both U-shape and V-shape is shown in Fig. 3. In addition, ship models were made with scale 1:100 and the ship models for both shapes are shown in Fig. 4. In addition, the fixed pitch propeller (FPP) with three blades was used and the propeller diameter (Dp) is varied into three sizes 32 mm (0.032 m), 40 mm (0.040 m), and 48mm (0.048 m) as shown in Fig. 5.

The purpose of free running model test is to obtain model speed with varieties of stern shape and propeller diameters. Free running model test was conducted at towing tank, Ship Hydrodynamic Laboratory, Naval Architecture Department, Faculty Engineering, Hasanuddin University. The towing tank sizes are 60 m in length, 4 m in width, and 4 m in depth. In order to measure model speed, the model was run freely along 25 meters at towing tank. For test set-up, some tools and devices were provided such as electric motor (1400KV), servo motor (Torque 15kg.cm), electronic speed control (ESC), rudder, universal joint (dia. in 3.17mm, out 4mm), radio control remote (2.4GHz), shaft (dia. 4mm), stopwatch, tachometer, battery (4000mAh). The tools and devices are shown in Fig. 6 and they were attached and installed on models. The revolution per minutes (RPM) in shaft was measured by using tachometer that is 1088.

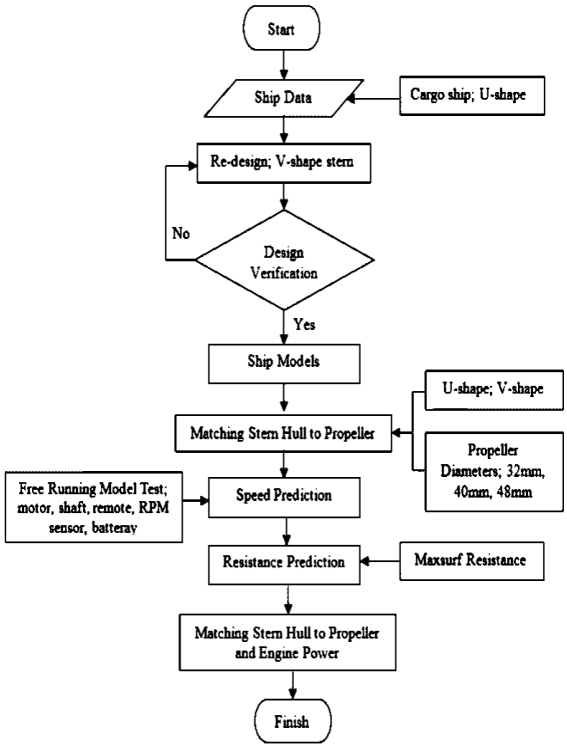

Figure 1. The systematical study steps

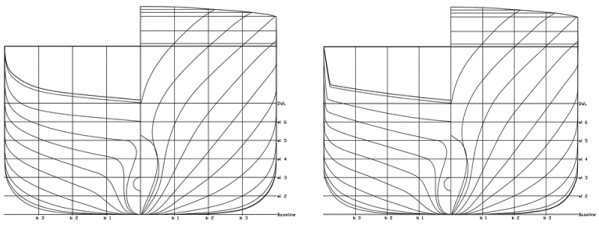

a b

Figure 2. Body lines plan; a). U-shape, b). V-shape

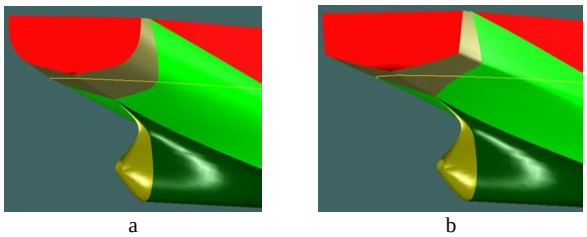

a b

Figure 3. The 3-dimensional stern hull form; a). U-shape, b). V-shape

a b

Figure 4. Ship models; Stern form a). U-shape, b). V-shape

Figure 5. Propeller models FPP;
Diameter a). 32 mm, b). 40 mm, c). 48 mm

Figure 6. Tools and devices for the set-up of free running model test

Table 1. Ship main particulars

Description	Value
Lenght overall (Loa)	80.00 m
Length between perpendiculars (Lbp)	74.43 m
Length water line (Lwl)	76.29 m
Breath (B)	15.00 m
Depth (H)	9.24 m
Draft (T)	6.15 m
Block coefficient	0.602
Displacement	4343 ton

Meanwhile, ship resistances for both shapes were predicted by using software application Maxsurf Resistance. The propulsive coefficient is overall efficiency that are propulsor efficiency, hull efficiency, relative rotative efficiency, appendage coefficient and the shaft transmission losses. Then, the efficiency was specified by assuming total efficiency for container ship, the same efficiency is used to calculate the power over the whole speed range. Nevertheless, wave contours for both shapes were predicted as well to predicted water flow particularly in stern region.

Table 2. The hydrostatic parameters after re-designed process particularly in the stern part

Description	Value	
	U-shape	V-shape
Displacement (ton)	4343	4343
Displaced volume (m^3)	4237.02	4237.02
Immersed depth (m)	6.15	6.15
Water line length (m)	76.29	76.29
Beam max extents on water line (m)	15.00	15.00
Prismatic coeff. (Cp)	0.628	0.627
Block coeff. (Cb)	0.602	0.602
Max section area coeff. (Cm)	0.959	0.961
Water plane area coeff. (Cwp)	0.84	0.838
Length centre bouyancy/LCB (m) from after peak point	37.24	37.30
Keel to bouyancy point/KB (m)	35.24	35.17

Accordingly, stern hull forms which were matched to propeller and engine power were obtained based on investigation results. Regardless, this study investigated the best selected stern shape as well.

3. Results and Discussion

The free running model test was successfully performed at towing tank as show in Fig. 7. The test was performed in keeping the straight forward movement only. The revolution per minutes (RPM) of model's shaft without attached propeller was measured by using tachometer and then it was obtained 1088. This RPM was measured in full power of electric motor. In this test, full power was used each test. Then, the shaft's RPM was in the same condition with other tests where test was performed three times on each case. The investigation of speed characterized by Froude number (Fr) in matching stern shapes to varied propeller diameters was conducted. The test data for both stern hull form (U-shape and V-shape) and three propeller diameters were obtained as provided in Table 3. The increase of propeller diameter increases model's speed for both stern forms. The increase of model's speed is significantly high from propeller diameter 0.032 m to 0.040 m and then it tends to increase slightly from propeller diameter 0.040 m to 0.048 m as shown in Fig. 7. The increase speeds from propeller diameter 0.032 m to 0.040 m and then 0.040 m to 0.048 m are approximately 18.6% and 10.3% respectively.

Meanwhile, Figure 8 shows the trendlines of the relation between propeller diameters and Froude number (Fr) in matching to stern hull forms by using the equations of second-order polynomial with R-squared value (R) 1.0. This equation describes the propeller diameter affects significantly on the speed. By using the trendlines derived by those equations as shown in Fig. 9, the peak speeds for U-shape and V-shape are at Fr 0.227 and 0.212. for propeller diameter 0.058 m and 0.056 m respectively.

Figure 7. The free running model test performed at towing tank

Table 3. The average speed model achieved by matching stern shapes to varied propeller diameters

Stern Form	Propeller Dia. (m)	Averaged Speed (m/sec.)
U-shape stern	0.032	0.431
	0.040	0.530
	0.048	0.593
V-shape stern	0.032	0.411
	0.040	0.505
	0.048	0.561

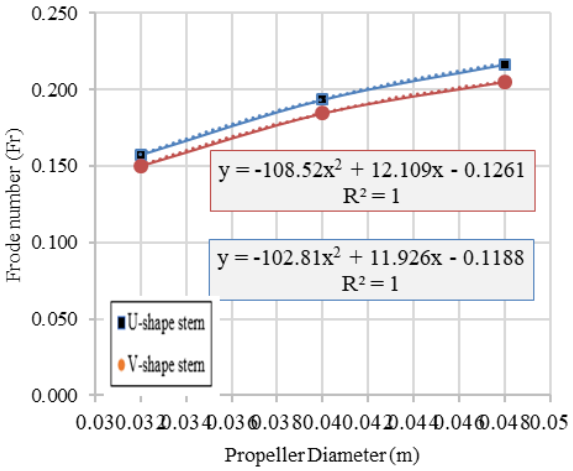

Figure 8. The relation between propeller diameter and Fr for both stern form U-shape and V-shape

The speed decreases gradually after reaching the peak speed and this is because of the high impact on hull pressure induced by the interaction between stern form, propeller and wake inflow and outflow. This impact is similar on both stern hull forms which were matched to varied propeller diameters.

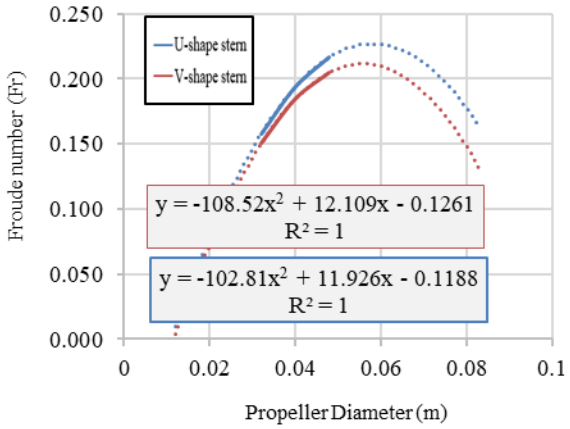

Figure 9. The relation between propeller diameter and Fr given by the quadratic function

In determining the propeller diameter, the propeller diameter could be obtained based on open water tests of systematic propeller series, numerical simulation, computational fluid dynamic (CFD), statistical analysis, or empirical method. For a simple method, a propeller diameter of a ship is determined as given by 0.70 of design draft and it was adopted as a standard in the LCB and geometrical variation series [11]. The approximations of the propeller diameter/design draft ratio (d/T) for container ship can be given 0.74 [12]. Also, the approximations of diameter propeller can be used as function of the maximum draft given by statistical analysis that is 0.623Tmax – 0.16 by Kristensen and Lutzen [13].

As defined on previous explanations, the maximum speed could be determined in this study based on function of propeller diameter and draft. Then, it is given by the ratio of propeller and draft which is approximately 0.94 and 0.91 for U-shape and V-shape respectively. However, the propeller diameter is not only depended on stern shape, propeller blade number, and maximum speed but also on stern design and propeller tip clearance.

Bensow and Gustafsson [14] investigated the clearances between the propeller tip and a generic hull with tunnel configuration with similar propeller diameter that were 0.7%Dp, 5%Dp, and 20%Dp. Then, the predicted impact on hull pressure is very large, with the maximum amplitude differing an order of magnitude between the small clearance case and the one with normal clearance. Moreover, some practical rules use 10%Dp to 30%Dp.

The small propeller tip clearance generates propeller-hull vortex cavitation and vibration, in contrast high clearance have a little impact on propeller performance, however it is affected on low speed. Therefore, the wake dynamics is caused by propeller tip clearance. The wave contour along ship for both shapes at a few Froude number are shown in Fig. 10. The wave contour is resulted in different magnitude comparing between low and high Froude number. In addition, the wake induced by stern shape and propeller diameter in inflow and outflow region could be distinguished. The wake discrepancies between U-shape and V-shape at the same Fr seems slight as depicted in Fig. 11.

Figure 12 shows stern hull form, propeller diameter and propeller tip clearance for both U-shape and V-shape. The propeller diameter which is 4.8 m (actual ship dimension) or 0.048 m (model dimension) has a propeller tip approximately 0.62 m (0.0062 m for model) according to stern hull design. Referring to this propeller tip clearance, it is given 12.9%Dp.

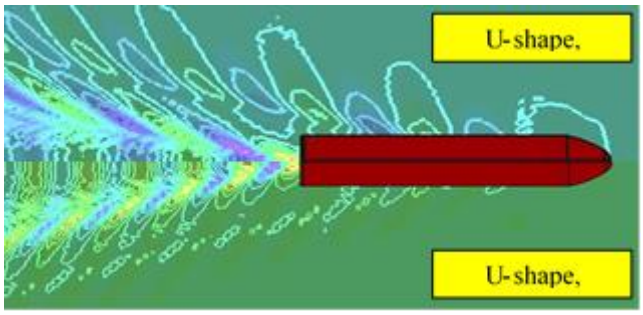

Top view

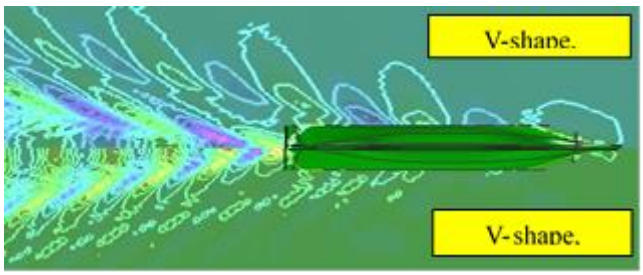

Bottom view

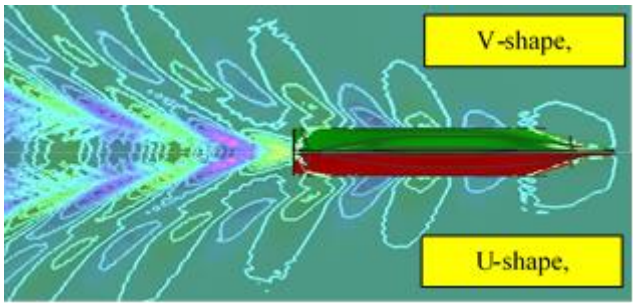

Bottom view

Figure 10. Wave contour along ship for both U-shape and V shape

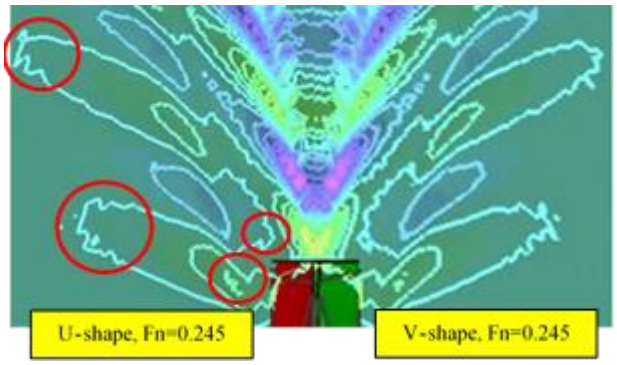

Figure 11. The discrepancies of wake surface between U-shape and V shape at Fn=0.245

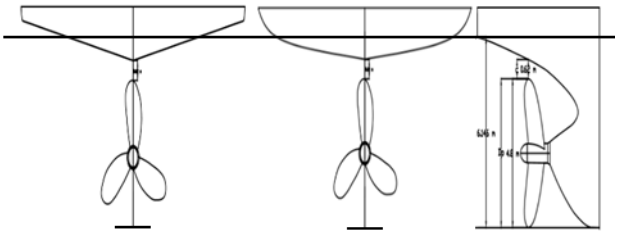

Figure 12. Stern hull forms and propeller tip clearance for both U-shape and V-shape

This must be noted that the determination of propeller diameter considers the stern hull design and propeller tip clearance although the greater propeller diameter it produces higher speed. Therefore, the optimum propeller diameter could be determined in this study taking into account stern hull form, stern shape, tip clearance, and proper speed where then propeller diameter related to draft is given by 0.79T with tip clearance 10%Dp for both U-shape and V-shape. However, those propeller diameters produce in different speed (Fr) for both U-shape and V-shape that are approximately 0.221 (11.69 Knot) and 0.208 (11 Knot) respectively.

The ship resistances for both U-shape and V-shape were obtained by using Maxsurf resistance application by using Holtrop method [15] as shown in Fig. 13. Here, these resistances are without propeller and rudder attachments and total efficiency was given 0.60. Based on Fig. 10, the higher ship is produced by U-shape comparing with V-shape in the same resistance. The ship resistances of U-shape stern at Fr 0.221 and V-shape at 0.208 are obtained approximately 89.797 KN and 77.10 KN respectively. Furthermore, the powers of ship for both U-shape and V-shape at those Fr are obtained 904,374 KW and 726,807 KW respectively as shown in Fig. 14.

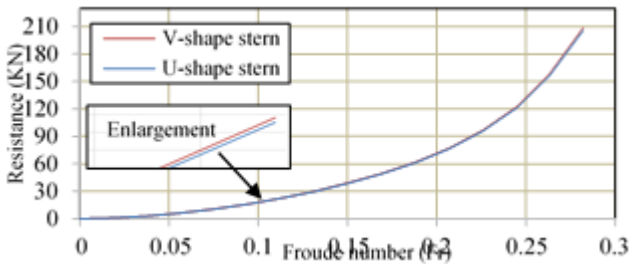

Figure 13. The ship resistances for both U-shape and V-shape

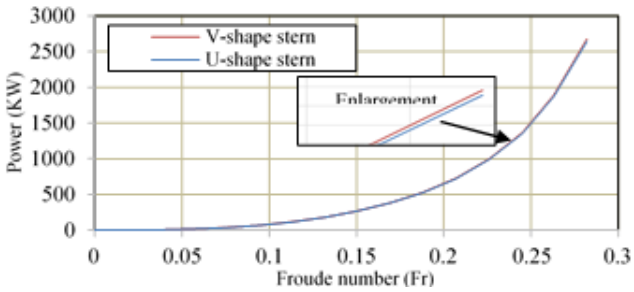

Figure 14. The ship engine power for both U-shape and V-shape

Accordingly, the best stern hull form matched to propeller diameter and engine power is selected and obtained that is U-shape stern with suitable propeller diameter 0.79T, propeller tip clearance 10%Dp, engine power 904,374 KW, and propeller shaft 1088 RPM. This matching condition could be produced ship speed approximately 11.69 Knot or Fr 0.221.

4. Conclusions

Herein the investigation of the performance of a ship by matching the stern hull form to propeller and engine power was successfully conducted and then the method could be proposed to implement in preliminary ship design.

The increase of propeller diameter increases model's speed for both U-shape and V-shape stern. the trendlines of the relation between propeller diameters and Froude number (Fr) in matching to stern hull forms by using the equations of second-order polynomial with R-squared value (R) 1.0. The effect of the propeller diameter on the speed could be described by using the equations of second-order polynomial. The peak speeds for U-shape and V-shape are at Fr 0.227 and 0.212. for propeller diameter 0.058 m and 0.056 m respectively. The speed decreases gradually after reaching the peak speed and this is because of the high impact on hull pressure induced by the interaction between stern form, propeller and wake inflow and outflow.

This must be noted that the determination of propeller diameter considers the stern hull design The optimum propeller diameter could be determined in this study taking into account stern hull form, stern shape, tip clearance, and proper speed where then propeller diameter related to draft is given by 0.79T with tip clearance 10%Dp for both U-shape and V-shape. The ship resistances of U-shape stern at Fr 0.221 and V-shape at 0.208 are obtained approximately 89.797 KN and 77.10 KN respectively. Furthermore, the powers of ship for both U-shape and V-shape at those Fr are obtained 904,374 KW and 726,807 KW respectively. Finally, the best stern hull form matched to propeller diameter and engine power is selected and obtained that is U-shape stern with suitable propeller diameter 0.79T, propeller tip clearance 10%Dp, engine power 904,374 KW, and propeller shaft 1088 RPM.

Acknowledgements

We gratefully acknowledge to undergraduate students, Ship Hydrodynamic Laboratory, Naval Architecture Department, Engineering Faculty, Hasanuddin University namely Ardedi Yusuf and C.J.V. Sitorus who supported to perform experimental work for this research.

References

[1] D. Stapersma and H. Woud, "Matching propulsion engine with propulsor," *J. Mar. Eng. Technol.*, 2005.

[2] Y. Ukon *et al.*, "Research on Improvement of Propulsive Performance of a High-Speed Ship Equipped with a High-Powered Propeller," *Natl. Marit. Res. Inst.*, vol. 8, no. 1, pp. 51–82.

[3] S. Lin, J. Sun, and D. Xie, "Design of ship-engine-propeller simultaneous matching and development of a propeller and engine selecting system," in *MARINE 2015 - Computational Methods in Marine Engineering VI*, 2015.

[4] O. B. Ogar, S. Nitonye, and I. John-Hope, "Design Analysis and Optimal Matching of a Controllable Pitch Propeller to the Hull and Diesel Engine of a CODOG System," *J. Power Energy Eng.*, 2018.

[5] H. Ren, Y. Ding, and C. Sui, "Influence of EEDI (Energy efficiency design index) on ship-engine-propeller matching," *J. Mar. Sci. Eng.*, 2019.

[6] N. Nurhadi, H. Zen, and S. Sumarsono, "Study of Engine Propeller Matching for High-Speed Vessel with Gawn Series Propeller," *EPI Int. J. Eng.*, 2018.

[7] Y. Lu, X. Chang, X. Yin, and Z. Li, "Hydrodynamic Design Study on Ship Bow and Stern Hull Form Synchronous Optimization Covering Whole Speeds Range," *Math. Probl. Eng.*, 2019.

[8] H. Ghassemi and H. Zakerdoost, "Ship hull-propeller system optimization based on the multi-objective evolutionary algorithm," *Proc. Inst. Mech. Eng. Part C J. Mech. Eng. Sci.*, 2017.

[9] Christian Johannsen, "Three blades for reduced fuel consumption A new generation of optimum performance propellers for tanker and bulker," *HSVA Newswave*, Hamburg, p. 1, 2007.

[10] Maxsurf, "Maxsurf Resistance." Bentley Software, 2014.

[11] Todd F.H, *Series 60 Methodical Experiments with Models of Single-screw Merchant Ships*. 1963.

[12] MAN Diesel &Turbo, "Basic Principles of Ship Propulsion," 2011.

[13] H. O. Kristensen and M. Lützen, "Prediction of resistance and propulsion power of ships," *Proj. no. 2010-56, Emiss.*, 2012.

[14] Rickard E Bensow and Robert Gustafsson, "Effect of Propeller Tip Clearance on Hull Pressure Pulses," in *5th International Symposium on Marine Propulsors*, 2017.

[15] J. Holtrop and G. G. J. Mennen, "APPROXIMATE POWER PREDICTION METHOD.," in *International Shipbuilding Progress*, 1982.

EPI International Journal of Engineering
Volume 3, Number 2, August 2020, pp. 160-164
DOI: 10.25042/epi-ije.082020.12

*p*ISSN 2615-5109
*e*ISSN 2621-0541

Hull Form Factor Prediction of Mini Submarine Model Using Prohaska Method

Mahendra Indiaryanto[a], Ahmad Syafi'ul Mujahid[b,*], Taufiq A Setyanto[c], Navik Puryantini[d]

[a]Indonesian Hydrodynamics Laboratory, Agency for the Assessment and Application of Technology (BPPT) Indonesia.
Email: indiaryanto@gmail.com
[b]Indonesian Hydrodynamics Laboratory, Agency for the Assessment and Application of Technology (BPPT) Indonesia.
Email: aaf2k3li@gmail.com
[c]Indonesian Hydrodynamics Laboratory, Agency for the Assessment and Application of Technology (BPPT) Indonesia
Email: taufiq.setyanto@gmail.com
[d]Indonesian Hydrodynamics Laboratory, Agency for the Assessment and Application of Technology (BPPT) Indonesia
Email: navik.puryantini@gmail.com

Abstract

The resistance on mini-submarines is certainly different from the type of surface vessels in general. This is related to differences in the shape of the sub's hull when compared to the surface ship. In addition to the differences in the shape of the hull, the operational area of the ship is also different, where the submarine's hull operates at full water depth, while the surface ship hull partly operates at sea level. If the submarine model is tested then the value of the coefficient of resistance will be very different. Where the component of the coefficient of resistance (CT) consists of the coefficient of friction (CF), form factor (1+K), and correlate allowance (CA). Because the hull shape is different from the surface ship, then the hull form factor coefficient is the focus of this study. The prediction of the hull form factor can be searched by using Prohaska method. This method is implemented using a mini-submarine model test. Using the known value of the hull form factor, then it can be used to find the value of the coefficient of resistance and the resistance of the ship can be obtained.

Keywords: Hull form factor; Prohaska method; resistance coefficient

1. Introduction

In the past decade, the Agency for Assessment and Application Technology (BPPT) as one of the State research institutions has conducted several studies on submarines. Surely the design of this submarine hull matches the geographical conditions of Indonesia which is an archipelagic country and has many straits. Indirectly with many straits in Indonesia, submarine hulls are needed to operate in shallow water.

So based on these considerations, a submarine hull design with an efficient and suitable form to operate in Indonesian waters is chosen. Based on several literature studies that studied both the area of operation and the capability of cruising mini-submarines, it was decided to design the submarine hull with a length of 22m.

Based on these considerations then Laboratory for Hydrodynamics Technology (BTH) - BPPT tried to design a 22m mini-submarine hull for its research in 2014 because the main task and function of BTH is research in hydrodynamics, submarine hull design must meet the hydrodynamic aspects, especially on the efficiency of the resistance value of the mini-submarine hull to be designed. Because an efficient resistance value will reduce Brake Horse Power (BHP) which will be installed into a 22m mini-submarine.

Some researchers have conducted studies on submarine characteristics and hull form factor, that are: Dhana [1] studied about hull form factor analysis that obtained difference of result value between ship and model hydrostatics data must be less than 2% in order both of them have not different characteristic significantly. Kusuma [2] has studied the powering calculation especially resistance calculation of the submarine using the MIT method and sister ship for calculating the Admiral coefficient. Syafiul [3] has studied the analysis of the effect of speed changes on one component of the submarine resistance force using computational fluid dynamics. Nugroho [4] studied the characteristics of the submarine hull against the fluctuate of hydrodynamics pressure dives from the ocean surface to a depth of operational and back to the surface again causing the submarine to change the burden of recurrent (repeated load) which contribute substantially to the structure of the submarine hull. Adin [5] studied the characteristics of the fluid along with the resistance components upon the ship, the scaling of the ship was used for model testing. The model of the ship that was in a 3-dimensional object was determined to find out the form factor, the value of the resistance. To estimate the

*Corresponding author. Tel.: +6285655617011
Jalan Hidrodinamika, Gd. BPPT, Komplek ITS Surabaya 60112

value of form factor (1 + k), experimental ship model at low speeds less than 0.2 Froude number obtained to collect data so that the wave resistance (CW) can be assumed to be zero.

2. Basic Theory

The design of surface ship hulls in general and submarine hulls are very different, the characteristics of the resistances between surface and submarines are also very different. Based on references from the book Submarine Hydrodynamic by Martin Renilson [6], a very basic distinction between the surface ship resistance and the submarine is in the wave resistance. Where on the surface ship obtained wave resistance, while submarines in diving conditions do not obtain wave resistance. Some number of resistance components while the submarine is sinking are as follows:

- Surface friction between fluid and hull occurs in all wet surface areas and the length of submarines.
- The frictional force of the fluid with some forms of foil on the wing and submarine rudder causes flow differences due to the shape of the foil itself.
- Drag resistance from the blunt shape of the front of the submarine hull.
- Induced drag is produced by the submarine hull component which produces lift for the capability of heaving and pitching movements.

From all of the resistance components described above then it is not necessary to be entirely modeled in an experiment, but just approaching by a mini-submarine hull model test at the BTH-BPPT Towing Tank facility. By testing the model, it needs to found some coefficient of resistance for the extrapolation process from the resistance value of the submarine model to the actual resistance value of the submarine by using the International Towing Tank Conference (ITTC) method.

The coefficient that needs to be sought is the value of the coefficient of resistance (CT). Where the resistance coefficient equation can be explained as follows [7]:

$$CT = CTm - (1+k)\cdot(CFs - CFm)\cdot CA \qquad (1)$$

$$CFs = \frac{0.075}{(\log 10Rn - 2)^2} \qquad (2)$$

$$CA = 0.006(Lwl + 100)^{-0.16} - 0.00205 \qquad (3)$$

$$CTm = \frac{RTm \cdot 9,81}{0,5\rho SV^2} \qquad (4)$$

where

CT = Coefficient of ship resistance
CTm = Coefficient of model resistance
(1+K) = Form factor
CFs = Coefficient of ship friction
CFm = Coefficient of model friction
CA = Tolerance allowance
Rn = Reynold Number
LWL = Length of ship's waterline (m)
RTm = Model resistance value (kg)
ρ = Water density (Kg/m^3)
S = Wetted surface area (m^2)
V = Ship speed (m/s)

From some of the coefficients above, the hull form factor is very influential in calculating the coefficient of resistance. Because the shape of a mini-submarine hull is very different from surface ship type.

The most famous empirical formula to determine the form factor value is by using the Watanabe formula [8]. To find out the approach of Form factor values can also be calculated using equations from Holtrop, 1 + k) value at the graphic in Fig. 1 can be calculated by using the least-square method [9]:

$$1 + k = 1 + k_1\left[1 + k_2 - (1 + k_1)\right]\frac{Sapp}{Stot} \qquad (5)$$

where

$1+K_1$ = Form factor bare hull
$1+K_2$ = Form factor appendages
Sapp = Ship appendages area (m^2)
Stot = Ship wetted surface area (m^2)

The explanation of equations $1 + K_1$ and $1 + K_2$ can be seen in the book Principle Naval Architecture Vol. 2 [11]. Meanwhile, to find the hull form factor on a mini-submarine, the equation above cannot be used, and the prediction value of the hull form factor is much different from the data in Table 1. To find out the value of the hull form factor and the resistance value of the model, model testing is needed. To find out the value of the mini-submarine hull form factor, the Prohaska method can be used. This method is based on ship model testing, where a mini-submarine model is towed in a towing tank at the Laboratory for Hydrodynamics Technology (BTH) by the value of Froude Number (Fn) below 0.2.

Table 1. Form factor approach of surface ships [10]

L/V $^{1/3}$	Monohull (1+*k*)	Catamarans (1+b*k*)
6.3	1.35	1.48
7.4	1.21	1.33
8.5	1.17	1.29
9.5	1.13	1.24

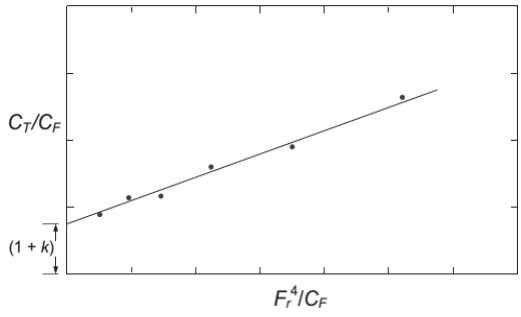

Figure 1. Form factor (1 + k) using the Prohaska method

In Fig. 1, it can be seen that the Y-axis on the graph of the Prohaska method is a *CTm/CFM* coefficient comparison, while on the X-axis is the *Fn4/CFm* coefficient ratio. To find the value of Froude Number (Fn) the equation below can be used [12].

$$Fr = \frac{V}{\sqrt{Lwl \cdot g}} \quad (6)$$

where

Fn = Froud number
V = Ship speed (m/s)
Lwl = Length of ship's waterline (m)
g = Gravity acceleration (9.81 m/s^2)

3. Methods

Data and design of mini-submarine hull shapes are shown in Table 2 and Fig. 2. Furthermore, preparations for testing mini-submarine models in Towing Tank facilities are carried out such as setting up instrumentation tools and mechanical equipment on submarines. To obtain the *CTm* and *CFM* coefficients then submarine model testing is required to obtain the resistance value at Froude Number (Fn) below 0.2 [10]. Measurement of the resistance in the submarine model is conducted by measuring the total of the resistance component (Rtm) by using a load cell transducer which is installed in-line with the centerline of the ship [13]. Before testing the resistance, measurement of the water temperature at the towing tank pool is aimed to determine the level of water viscosity in the pool expressed in kinematic viscosity. For submarine speed variations, it is shown in Table 3 and the process of testing a 22m mini-submarine model is shown in Fig. 3.

4. Result and Discussion

From the measurement of the water temperature at the towing tank pool before testing the submarine model is obtained a temperature of 28ºC. The viscosity kinematic value is 0.83572 x 10^{-6} m^2/sec at 28ºC. So the Reynold Number (Rn) value on each variation of the ship speed can be calculated.

Table 2. The main dimension of the 22m mini-submarine model with scale 1:7 [11]

Parameter	Full Scale	Scale	Unit
Lwl	22	3.143	m
D total	5.133	0.733	m
D press hull	3.000	0.428	m
Vol Δ	113.8	0.331	m^3
S	151.4	3.089	m^2

Figure 2. Model of a 22m mini-submarine with scale 1: 7

Table 3. Test speed variation of mini-submarine models with scale 1:7

Vs	*Vm*	*Fn*	*RTm*
Knots	(m/s)		Kg
2.5	0.468	0.091	-
3.0	0.583	0.109	-
3.5	0.681	0.127	-
4.0	0.778	0.145	-
4.5	0.875	0.164	-
5.0	0.972	0.182	-

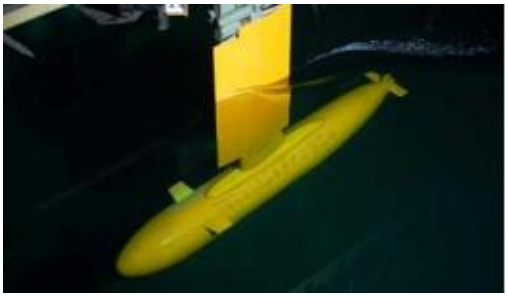

Figure 3. Testing process of the 22 m mini-submarine model with scale 1:7

The mini-submarine model testing is carried out on the mini-submarine model which is submerged approximately 1 m from the water surface of the pool as shown in Fig. 3. By using the speed variation data in Table 3, resistance testing is carried out to find the value of the total resistance (*RTm*) of the mini-submarine model. From the resistance testing, the resistance graph of the mini-submarine model tends to increase significantly on each speed variation as shown in Fig. 4. This is considered reasonable because the resistance testing of the mini-submarine model measures the entire area of mini-submarine components consisting of the hull, fins, and rudders.

After the resistance value of the submarine model is obtained, the coefficient of model resistance (*CTm*) can be calculated using Eq. 4 and the coefficient of the friction model (*CFm*) can be calculated using Eq. 2 based on the parameters of the mini-submarine model with scale 1:7. From the results of the resistance test of a 22-meter mini-submarine model, a table can be made for the graph of the Prohaska method as shown in Table 4, while the form factor (*1 + k*) graph by using the Prohaska method from the test results is shown in Fig. 5.

From Table 4, a Prohaska graph can be made by plotting the results of the *CTm/CFm* comparison on the *Y*-axis and the results of the *Fn4/CFm* comparison on the *X*-axis. And the linear line equation $y = ax + b$ is made. In Fig. 5, it is obtained the linear equation $y = 25.073x + 6.3818$ with an *R*-squared value of 0.9402. From this line equation then can be determined the value of form factor *(1 + k)* by substituting the value $x = 0$ in the linear equation. So the *Y* value is obtained 6.3818. Thus the value obtained from the form factor *(1 + k)* on the mini-submarine is 6.3818.

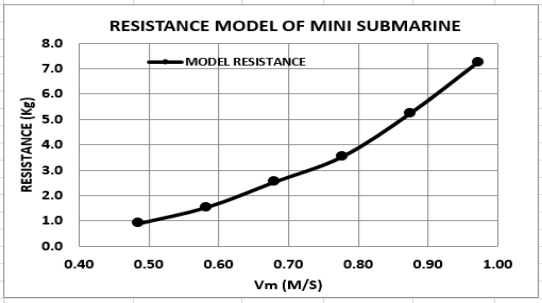

Figure 4. The resistance of the 22m mini-submarine model

Table 4. Coefficient calculations for Prohaska chart

Rn	*CTm*	*CFm*	*CFm/ CTm*	*Fn4/ CFm*
1.70E+06	0.468	0.024	0.0042	5.813
2.03E+06	0.583	0.029	0.0040	7.127
2.37E+06	0.681	0.035	0.0039	8.886
2.71E+06	0.778	0.037	0.0038	9.727
3.05E+06	0.875	0.043	0.0037	11.645
3.39E+06	0.972	0.049	0.0037	13.323

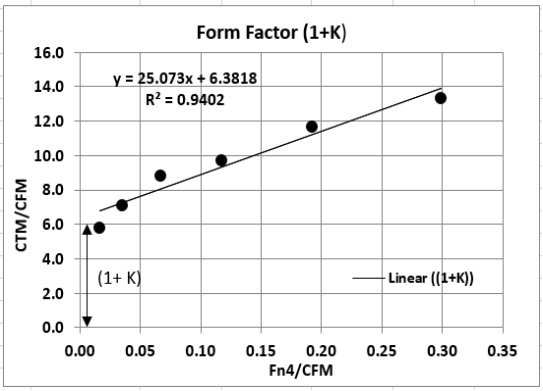

Figure 5. The form factor *(1 + k)* using Prohaska method from the test results

The difference in form factor values between mini-submarines and surface ship is much different where the value of form factors on surface vessels is 1.13 to 1.35 as shown in Table 1, while the form factor values on mini-submarines reach 6.38. However, the form factor on this mini-submarine is considered appropriate when referring to Table 5.

From Table 5, it can be ascertained that the hull shape of the 22m mini-submarine model is Parallel Middle Body Hull (PMB) because the value of the form factor produced is 6.38. Because this form factor is a fixed coefficient, then the coefficient value remains the same if the submarine is made into the full-scale form [14].

If the form factor value is known then it can be used to calculate the coefficient of resistance of mini-submarines in full scale *(CTs)* using equation 1 above. Next, the extrapolation process is calculated from model resistance to full-scale mini-submarine resistance because the value of submarine coefficient *(CTs)* has been obtained.

Table 5. Submarine form factor based on hull shape [15]

Description	**ζhull**
Teardrop shape	3
Modern submarine shape	4 ~ 5
PMB hull from	6

5. Conclusion

From the research that has been conducted, it can be seen that the difference in form factor values is quite significant between the surface ship type and the 22m mini-submarines. By the form factor value of 6.38, it can be ascertained that the shape of the submarine model is based on the Parallel Middle Body (PMB) hull concept. The hull shape of this submarine type provides advantages because the hull shape is wider when compared to the concept of the hull type of teardrop shape. But with a little area of the shape, this submarine's hull can also increase the coefficient of skin drag fiction and total drag on the mini-submarine hull.

Acknowledgments

The authors highly appreciate a research grant from the Agency for the Assessment and Application of Technology to conduct this study.

References

[1] Dhana, F. R. (2018). *Analisis Alternatif Hull Form Self-Propelled Barge Untuk Meningkatkan Performa Hidrodinamika*. Tesis. Fakultas Teknologi Kelautan: Institut Teknologi Sepuluh Nopember..

[2] Kusuma, Cahya. (2017). *Desain Propeller Kapal Selam 29 Meter dengan Menggunakan Propeller B-Series*. Jurnal Wave Volume 11 Nomor 1, Juli 2017: Hal: 1-6.

[3] Syafiul, Ahmad. dan Ridwan Utina. (2017). *Analisa Pengaruh Variasi Kecepatan Terhadap Tekanan pada Model Kapal Selam dengan Menggunakan Simulasi Numerik*. Jurnal Wave Volume 11 Nomor 2, Desember 2017: Hal: 17-24.

[4] Nugroho, Wibowo h. dan Ahmad Syafiul. (2015). Prediksi umur kelelahan struktur badan tekan kapal selam karena pengulangan perubahan beban hidrostatik. Jurnal MIPI (Majalah Ilmiah Pengkajian teknologi). Vol 9, No 3. BPPT. Jakarta.

[5] Aden. (2020). *Analisis estimasi dan prediksi form factor berbagai bentuk lambung kapal berdasarkan data uji model dan simulasi CFD*. Final Project. Department of Naval Architecture. Faculty of Marine Technology. Sepuluh Nopember Institute of Technology. Surabaya.

[6] Martin Renilson *(2015*), *Submarine Hydrodynamics*. Launceston TAS, Australia.

[7] ITTC (2008). *Uncertainty Analysis in Resistance Towing Tank Tests*. In: Proceeding of 25th ITTC. Fukuoka, (pp. 1-16). .

[8] Larsson, L., Raven, H.C. (2010). *The Principles of Naval Architecture Series Ship Resistance and Flow*. New Jersey: The Society of NavalArchitects and Marine Engineers..

[9] Prohaska, C.W. (1966). *A Simple Method for the Evaluation of the Form Factor and Low-Speed Wave Resistance*. In: Proceedings of 11th ITTC. Society of Naval Architects of Japan, Tokyo, (pp 65–66).

[10] Molland, A.F., Turnock, S.R., dan Hudson, D.A. (2011). *Ship Resistance and Propulsion: PracticalEstimation of Ship Propulsive Power*, Cambridge University Press, New York, USA.

[11] Edward V. Lewis. (1988) Principles of Naval Architecture Second Revision. Volume II. Resistance, Propulsion and Vibration. The Society of Naval Architects and Marine Engineers 601 Pavonia Avenue Jersey City, NJ.

[12] Martin, R. (2015). *Submarine Hydrodynamic*. Springer Briefs in Applied Sciences and Technology.,

[13] Andi Jamaluddin & Dewi Kentjanawati, (2013), *Eksperimental Studies Viscous Form Factor on Resistance Catamaran Vessels,* Jurnal Wave Volume. 7 Nomor 1, Juli 2013: Hal 1 -6.

[14] Renilson MR, Ranmuthugala D (2012) The effect of proximity to Free surface on the optimum length/diameter ratio for a submarine. In: First international conference on submarine technology and marine robotics (STaMR 2012), Chennai, 13–14 Jan 2012.

[15]Warren CL, Thomas MW (2000) Submarine hull form optimization case study.Naval Eng J112 (6).

EPI International Journal of Engineering
Volume 3, Number 2, August 2020, pp. 165-171
DOI: 10.25042/epi-ije.082020.13

*p*ISSN 2615-5109
*e*ISSN 2621-0541

Analysis of Form Coefficient for Measuring Gross Tonnage of Wooden Ship Compared with Domestic Measurement Method of Indonesia

Habibi Amal[a], Syamsul Asri[b], Andi Ardianti[c,*], Suandar Baso[d]

[a]Department of Naval Architecture, Engineering Faculty, Hasanuddin University, Gowa, Indonesia. Email: abichoy@gmail.com
[b]Department of Naval Architecture, Engineering Faculty, Hasanuddin University, Gowa, Indonesia. Email: sa_tanri_kapal83@yahoo.com
[c]Department of Naval Architecture, Engineering Faculty, Hasanuddin University, Gowa, Indonesia. Email: aardianti@gmail.com
[d]Department of Naval Architecture, Engineering Faculty, Hasanuddin University, Gowa, Indonesia. Email: s.baso@eng.unhas.ac.id

Abstract

Most of the gross tonnage (GT) of the traditional wooden ship in Sinjai and Bone Regencies were measured using the domestic measurement method. By this measurement method, sometimes shipowners who belonged boats with sizes <30 GT think the disadvantaged matters in terms of policies, permits, landing fees, subsidized fuel rations, etc. The objectives of this study are to determine the characteristics of the main dimension and shape of traditional wooden ships affected on the GT calculation, to compare the GT of the traditional wooden ship between the real body calculation with the domestic measurement method, and to compile the formula in determining the value of the ship volume factor *f* based on the main dimensions for the calculation of the GT. The data were processed by using the Slovin technique with the sample number of the traditional wooden ship of 49 ship units. The results show that the traditional wooden ships in Sinjai and Bone Regencies have quite the same geometric characteristics. The GT between the real body and the domestic measurement method seems a difference wherein the GT of cargo ship using the real body is higher than the domestic measurement method, in contrast, for the fishing boat, the GT using the real body is smaller than the domestic measurement method. For small fishing boat <7 GT, the difference of the GT is approximately 40%. The correlation between the volume factor *f* with non-dimensional of volume $LBH^{1/3}$ expresses the high correlation. By an algorithmic equation, the volume factor *f* can be determined by using a function. Using the obtained formula, it can be a reference for a responsible person in charge of the GT measurement to obtain the proper GT.

Keywords: Form coefficient; gross tonnage; ship measurement; traditional wooden ship

1. Introduction

Geographically, Sinjai and Bone Regencies consist of coastal areas, lowlands, and highlands with an altitude between 0-2.871 meters above sea level (masl) of the groundwater level (GW). The two Regencies are contiguous and in the bay of Bone [1]. In general, the coastal communities of Sinjai and Bone Regencies work as fishermen and entrepreneurs. In their daily lives, they use the traditional wooden boat to carry out their activities [2].

Before operating a new ship, the ship has to obligated for being measured in order to obtain the physical identification of the ship such as main dimensions of length, breadth, and height, gross tonnage (GT), and net tonnage (NT). The purpose of the measurement is to fulfill the requirements for registration and issuance of a ship's nationality as well as safety requirements [3].

Most of the gross tonnage (GT) of the traditional wooden ships are measured using the domestic measurement method issued by the Regulation of the Minister of Transportation of the Republic of Indonesia Number PM 8 of 2013 concerning Ship Measurement. To calculate the GT of the traditional wooden ship using the domestic measurement method, it is obtained by multiplying the coefficient of 0.25 by the total volume of the space below the deck and the volume of all rooms above the closed deck [4].

There are several problems related to GT measurement results measured using the domestic measurement method wherein many ship GT do not match the physical themself. Usually, the ship's GT on the document is smaller than the GT of the physical ship wherein this problem is stated commonly as markdown [5], especially, the ships with initial size are less than 30 GT. The difference of GT measurement is the average of up to 111% between the new and old GT measurement result [3]. This happens on a fishing boat with an avoiding mode to obtain fishing permits (SIPI), fisheries business permits (SIUP), and fish transportation ship permits (SIKPI) issued by the head office of the Ministry of Marine Affairs and Fisheries [6], For this reason, many shipowners who belonged the

*Corresponding author. Tel.: +62-813-1849-9282
Andi Caco Barat, Pangkajene Kepulauan,
Sulawesi Selatan, Indonesia, 99611

traditional wooden boat with size <30 GT decline verification or re-measurement for their ships because the GT results by the verification or re-measurement have increased significantly from the previous GT [7]. Shipowners think the consequence of obtaining the disadvantaged matter in terms of policies, permits, landing fees, subsidized fuel rations, and etc.

By the problem mentioned above, it is very detrimental for the government wherein it can affect the inaccurate data and loss in terms of Non-Tax State Revenues (PNBP). The amount of PNBP is determined from the GT size stated in the ship's document. In addition, the shipowner also experiences loss in the form of assistance, insurance receipts when the shipowner makes a loan with a ship as collateral. As known, the assistance, insurance, and collateral depend on the amount of GT in the documents they have [8].

Correspondingly, the objectives of this study are to determine the characteristics of the main dimensions and shape of traditional wooden ships affected on the GT calculation, to compare the calculation results of the GT of the traditional wooden boat between the real body shape calculation with the domestic measurement methods, and to compile the equation in determining the value of the ship volume factor based on the main dimensions of the traditional boat for the calculation of the GT. The traditional wooden ship as the sample of this present study is in Sinjai and Bone Regencies.

2. Research Method

The locations of the traditional wooden ship are in two locations, namely the Cappa Ujung Port in Sinjai Regency and the Tuju-Tuju Port in Bone Regency, South Sulawesi Province. Both ports are under working area of the Class III Sinjai Port Administration Unit Office.

In this present study, the sample of the measurement documents of the traditional wooden ships are 49 ship units. The traditional wooden ship as a sample is the type of cargo and fishing boat operated at the Cappa Ujung Port and the Tuju-Tuju Port. For the first, the data were processed by using the Slovin technique to obtain a minimum number of sample.

Furthermore, the characteristics of hull and upperdeck on the traditional wooden ship were observed directly on site. Then, the geometry characteristics of the traditional wooden ships were defined by the ratios of L/B, B/H and L/H.

The GT was calculated based on the real body and domestic meaurement method. The real body means the body lines of a ship was directly measured and then it was described by dividing into 12 sections wherein each bow and stern parts are divided by four sections. Then, the real body is divided into five waterplanes wherein the bottom part is divided into two section because of extreme form. This method is used for obtaining the ship volume. For the GT based on the domestic measurement, the calculation of GT is followed Permenhub RI Number PM 8, 2013. Here, By using this domestic measurement method, the GT is applied for a ship with the length of less than 24 meters. The ship length used in the GT calculation is defined by 96% of the length of the length of waterline (LWL) at 85% of the ship height. By this definition of the ship length, it can be considered for using the domestic measurement method if the ship length meets less than 24 meters.

The total volume consists of the volume under the measuring deck (V_1) and the volume of the rooms above the closed deck (V_2). The volume under the measuring deck is defined by multiplying the main dimensions of the ship with a volume factor (f) regarding the ship form [4].

Finally, to determine the volume factor f, the correlation between the volume factor f with non-dimensional of volume defined by $LBH^{1/3}$ are expressed by using several equations such as linear equation, logarithmic equation, power expression equation, and exponential equation. The coefficient of determination (R Square) which gives the greatest influence is formulated in a mathematical equation [9]. Therefore, the equation with the highest determination coefficient becomes the equation of the volume factor used for the GT calculation.

3. Results and Discussion

3.1. Characteristics of traditional wooden ship buildings

3.1.1. General description

The traditional wooden ship is a transportation vehicle and supporting welfare for coastal communities. Generally, this kind of ship is constructed based on knowledge acquired from generation to generation based on tradition in the field and instincts in adapting to their environment [10]. The adaptation process is influenced by the local wisdom of the local area. The local wisdom of an area determines the various forms of traditional wooden ships, both in terms of variations in size and style [11]. The kinds of traditional wooden ship operating in the Regencies of Sinjai and Bone can be seen in Figs. 1 and 2.

Figure 1. Traditional wooden boat in Sinjai Regency

Figure 2. Traditional wooden boat in Bone Regency

3.1.2. Hull characteristics

Most of the traditional wooden ship operating in Sinjai and Bone Regencies are fishing boats and cargo ships. These ships are directly related to the livelihoods of the majority of the population living in coastal areas, who generally work as fishermen and entrepreneurs. There are differences in shape and size between traditional wooden ship operating near the coast and in offshore. However, most of the traditional wooden boat has the same shape characteristics only on the hull that is the bottom shape. The bottom shape is almost semicircular. The hull form of the traditional wooden ship operated in the Regencies of Sinjai and Bone [12,13] can be seen in Figs. 3 and 4.

3.1.3. Characteristics of upper deck

The building of traditional wooden ship operated in Sinjai and Bone Regencies have the characteristics of the upper deck divided into two characteristics of the deckhouse based on the type of ship. A cargo ship generally only has a maximum of two deck houses arranged at the rear wherein the deckhouse is usually used for the crew room, wheelhouse, map room, and radio communication room. The cargo hold is located in the middle part. On the other hand, the fishing boat generally has one deckhouse located in the rear or middle and used for the navigation room, and several fish cargo hatches. The characteristics of the upper deck of the traditional wooden ship operated in the Regencies of Sinjai and Bone are shown in Figs. 5 and 6.

Figure 3. Characteristics of ship hulls in Sinjai Regency

Figure 4. Characteristics of ship hulls in Bone Regency

Figure 5. Characteristics of upper deck of the traditional wooden boat in Sinjai Regency

Figure 6. Characteristics of upper deck of the traditional wooden boat in Bone Regency

3.2. Analysis of geometry characteristics of traditional wooden ships

The number of ship samples operated at the Ports of Cappa Ujung and Tuju-Tuju is 49 units. The data were processed using the Slovin technique with the error of 15%. After the data processing, the minimum number of ship samples was considered 23 units. By the 23 ship units, eight ships are the cargo type and 15 ships are the fishing type.

Moreover, the minimum number of ship sample was further used to analyze the geometric characteristics of traditional wooden ships by using the ratio of main dimensions as follows:

$$\frac{L}{B} = \frac{Length}{Breadth} \tag{1}$$

$$\frac{B}{H} = \frac{Breadth}{Length} \tag{2}$$

$$\frac{L}{H} = \frac{Length}{Height} \tag{3}$$

As the results, the ratio of main dimensions is shown in Table 1 and then the tendency of the main dimension ratio of cargo ship and fishing boat is shown in Figs. 7 and 8 respectively. In those figures, the *x*-axis is defined by *n* ship where *n* is ordered from the small to large ship dimension.

Table 1. The ratio of the main sizes of traditional wooden ship

Type of Ship	L/B	B/H	L/H
Cargo	3.56 – 5.93	2.03 – 3.24	7.77 – 13.43
Fishing Boat	4/42 – 7.25	1.86 – 3.25	9.97 – 20.50

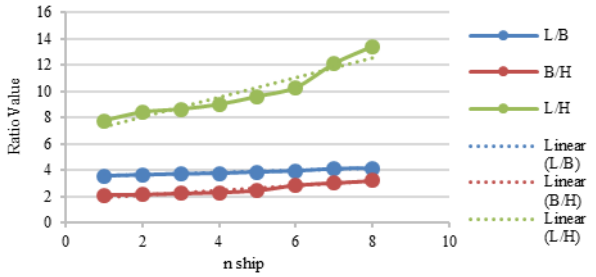

Figure 7. The tendency of the ratio of main dimensions of cargo ship

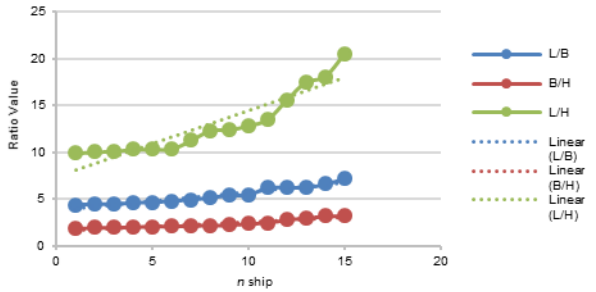

Figure 8. The tendency of the main dimension ratio of the fishing boat

Based on Fig. 7, for the cargo ship, the ratio of L/B is the range of 3.56 to 5.93 and it is obtained in the range of ship length from 20.19 to 27.0 m and ship breadth in the range of 4.75-6.90 m. The overall ratio L/B is an average of 3.86. The ratio of B/H is in the range of 2.03 to 3.24 for the height range 1.55-3.09 m. The overall ratio B/H is an average of 2.56. Moreover, the ratio of L/H is the range of 7.77-13.43. Then, the overall ratio L/H is an average of 9.91.

Based on Fig. 8, for the fishing boat, the ratio of L/B is the range of 4.42-7.25 and it is obtained in the range of ship length from 11.60-21.70 m and ship breadth in the range of 1.85-4.85 m. The overall ratio L/B is an average of 5.42. The ratio of B/H is in the range of 1.86-3.25 for the height range 0.60-1.97 m. The overall ratio B/H is an average of 2.41. Moreover, the ratio of L/H is the range of 9.97-20.50. Then, the overall ratio L/H is an average of 13.05.

As known, the ratios of L/B and B/H characterize the ship stability and resistance. Meanwhile, the ratio of L/H characterize the longitudinal ship strength. In future work, the influence of the main dimension ratios should be analyzed on ship hydrodynamics and strength because the geometry of the traditional wooden ship is quite different with the modern ship.

3.3. Calculation and comparison of gross tonnage (GT)

3.3.1. Direct measurement of the ship main dimensions of the ship

The main dimensions of the wooden ships were measured directly in Sinjai and Bone Regencies and the main dimensions are shown in Table 2. The direct measurement was carried out to the conformity of the main dimensions of the wooden ship stated in the ship document. In fact, the direct measurement of the main dimensions for five traditional wooden ships is larger than stated in ship document. These direct measurement results are used for the GT calculation followings.

Table 2. Main dimensions of traditional wooden ship

Ship Name	Type of Ship	Main Dimensions (m)					
		Ldeck	B	H	LOA	LWL	LBP
Ship A	Cargo	26.00	6.90	3.05	27.18	23.93	21.44
Ship B	Cargo	25.85	5.02	2.12	26.78	22.58	21.07
Ship C	Fishing Boat	19.00	4.06	1.68	19.00	17.05	15.60
Ship D	Fishing Boat	14.70	2.44	1.29	14.70	13.23	12.36
Ship E	Fishing Boat	13.60	2.06	1.10	13.60	12.25	11.44

Table 3. The GT of real ship body

Ship Name	Type of Ship	V under deck (V_1)	V upper deck (V_2)	V ($V_1 + V_2$)	GT
Ship A	Cargo	298.68	68.46	367.14	92
Ship B	Cargo	155.20	45.44	200.64	49
Ship C	Fishing Boat	7.63	17.03	88.66	21
Ship D	Fishing Boat	25.74	0	25.74	5
Ship E	Fishing Boat	16.61	0	16.61	3

3.3.2. GT calculation of the actual main dimensions and shape (real body)

The GT calculations of the actual main dimensions as result of the direct measurement mentioned previously were conducted. Here, the ship body were divided by the large number of sections to obtain the real body of the traditional wooden ship because the body form of the traditional is generally different and almost parallel bodies are less [14]. The calculation method using the real body is almost same method with the international measurement method. By the difference of body form, the real body is considered to be divided into 12 sections wherein each bow and stern parts are divided by four sections. Then, the real body is divided into five waterplanes wherein the bottom part is divided into two section because of extreme form. This method is used for obtaining the ship volume. As the results, the GT for the five traditional wooden ships is shown in Table 3.

3.4. GT calculation based on domestic measurement method

Here, the GT calculation is referred to the Regulation of Transportation Ministry of Republic of Indonesia Number PM 8, 2013. By using this domestic measurement method, the GT is applied for a ship with the length of less than 24 meters. The ship length used in the GT calculation is defined by 96% of the length of the length of waterline (LWL) at 85% of the ship height. By this definition of the ship length, it can be considered for using the domestic measurement method if ship length meets less than 24 m.

The total volume consists of the volume under the measuring deck (V_1) and the volume of the rooms above the closed deck (V_2). The volume under the measuring deck is defined by multiplying the main dimensions of the ship with a volume factor (f) regarding the ship form [4]. The volume factor f is here used that are 0.50 and 0.70 mentioned in the measurement documents. Correspondingly, the GT of a ship is obtained by multiplying a coefficient K_1 of 0.25 with the total volume (V). Therefore, the GT are obtained for the five sample vessels as shown in Table 4.

Table 4. The GT using the domestic measurement method

Ship Name	Type of Ship	Length (L)	Breadth (B)	Height (H)	85% H (T)	LOA	LWL	96% LWL	LBP	*f*	V_1	V_2	V (V_1+V_2)	GT
Ship A	Cargo	26.00	6.90	3.05	2.59	27.18	23.93	22.97	21.44	0.50	273.59	68.46	342.05	85
Ship B	Cargo	25.85	5.02	2.12	1.80	26.78	22.58	21.68	21.07	0.50	137.55	45.44	182.99	45
Ship C	Fishing Boat	19.00	4.06	1.68	1.43	19.00	17.05	16.37	15.60	0.70	90.72	17.03	107.75	26
Ship D	Fishing Boat	14.70	2.44	1.29	1.10	14.70	13.23	12.70	12.36	0.70	32.39	0.00	32.39	8
Ship E	Fishing Boat	13.60	2.06	1.10	0.94	13.60	12.25	11.76	11.44	0.70	21.57	0.00	21.57	5

Table 5. The GT using the real body and the domestic measurement method

Comparison of GT Real Body (RB) vs Domestic	Ship A		Ship B		Ship C		Ship D		Ship E	
	Cargo		Cargo		Fishing Boat		Fishing Boat		Fishing Boat	
	RB	Domestic	RB	Domestic	RB	Domestic	RB	Domestic	RB	Domestic
Length (L)	26.00	26.00	25.85	25.85	19.00	19.00	14.7	14.7	13.6	13.6
Breadth (B)	6.90	6.90	5.02	5.02	4.06	4.06	2.44	2.44	2.06	2.06
Height (H)	3.05	3.05	2.12	2.12	1.68	1.68	1.29	1.29	1.1	1.1
85% H (T)	2.59	2.59	1.80	1.80	1.43	1.43	1.1	1.1	0.94	0.94
LWL	23.93	23.93	22.58	22.58	17.05	17.05	13.23	13.23	12.25	12.25
96% LWL	22.97	22.97	21.68	21.68	16.37	16.37	12.7	12.7	11.76	11.76
LBP	21.44	21.44	21.07	21.07	15.60	15.60	12.36	12.36	11.44	11.44
V_1	298.68	273.59	155.20	137.55	71.63	90.72	25.74	32.39	16.61	21.57
V_2	68.46	68.46	45.44	45.44	17.03	17.03	0	0	0	0
V (V_1 + V_2)	367.14	342.05	200.64	182.99	88.66	107.75	25.74	32.39	16.61	21.57
GT	**92**	**85**	**49**	**45**	**21**	**26**	**5**	**8**	**3**	**5**
f	**0.55**	**0.50**	**0.56**	**0.50**	**0.55**	**0.70**	**0.56**	**0.7**	**0.54**	**0.7**

Table 6. The difference in GT using the real body and the domestic measurement method

Ship Name	Type	GT	GT	Difference (%)	Description
		RB	Domestic		
Ship A	Cargo	92	85	7.61	RB > Domestic
Ship B	Cargo	49	45	8.16	RB > Domestic
Ship C	Fishing Boat	21	26	19.23	RB < Domestic
Ship D	Fishing Boat	5	8	37.50	RB < Domestic
Ship E	Fishing Boat	3	5	40.00	RB < Domestic

Table 7. The GT using the same *f* for the real body and domestic measurement method

Comparison of GT Real Body (RB) vs Domestic	Ship A		Ship B		Ship C		Ship D		Ship E	
	Cargo		Cargo		Fishing Boat		Fishing Boat		Fishing Boat	
	RB	Domestic	RB	Domestic	RB	Domestic	RB	Domestic	RB	Domestic
Length (L)	26.00	26.00	25.85	25.85	19.00	19.00	14.7	14.7	13.6	13.6
Breadth (B)	6.90	6.90	5.02	5.02	4.06	4.06	2.44	2.44	2.06	2.06
Height (H)	3.05	3.05	2.12	2.12	1.68	1.68	1.29	1.29	1.1	1.1
85% H (T)	2.59	2.59	1.80	1.80	1.43	1.43	1.1	1.1	0.94	0.94
LWL	23.93	23.93	22.58	22.58	17.05	17.05	13.23	13.23	12.25	12.25
96% LWL	22.97	22.97	21.68	21.68	16.37	16.37	12.7	12.7	11.76	11.76
LBP	21.44	21.44	21.07	21.07	15.60	15.60	12.36	12.36	11.44	11.44
V_1 (LxBxHx *f*)	300.94	273.59	154.06	137.55	71.28	90.72	25.91	32.39	16.64	21.57
V_2	68.46	68.46	45.44	45.44	17.03	17.03	0	0	0	0
V (V_1 + V_2)	369.40	342.05	199.50	183.00	88.30	107.74	25.91	32.39	16.64	21.57
GT	**92**	**85**	**49**	**45**	**22**	**26**	**6**	**8**	**4**	**5**
f	**0.55**	**0.50**	**0.56**	**0.50**	**0.55**	**0.70**	**0.56**	**0.70**	**0.54**	**0.70**

Table 8. The difference in GT using the same *f* between the real body and the domestic measurement method

Ship Name	Type	GT		Difference (%)	Description
		RB	Domestic		
Ship A	Cargo	92	85	7.61	RB > Domestic
Ship B	Cargo	49	45	8.16	RB > Domestic
Ship C	Fishing Boat	22	26	15.38	RB < Domestic
Ship D	Fishing Boat	6	8	25	RB < Domestic
Ship E	Fishing Boat	4	5	20	RB < Domestic

3.4.1. Comparison of the calculation results of Gross Tonnage (GT)

The GT using the real body calculation and the domestic measurement method is shown in Tables in Table 5 and the weight of the difference between real body calculation and the domestic measurement method is shown in Table 6. As the results, the GT between the real body and the domestic measurement method seems a difference wherein the GT of cargo ship using the real body is higher than the domestic measurement method, in contrast, for the fishing boat, the GT using the real body is smaller than the domestic measurement method. For small fishing boat <7 GT, the difference of the GT is approximately 40% and this is higher value. This matter should be an attention for Government because it relates directly to the fishermen.

On the other hand, by using the volume factor *f* as obtained from the real body, it is further used in the GT calculation of the domestic measurement method as shown in Table 7. Then, the weight of the difference between real body calculation and the domestic measurement method in using the same volume factor *f* obtained from the real body is shown in Table 8. As the comparison result between Table 6 and 8, the GT of the ship cargo is the same difference, however, the difference of the GT for the fishing boat is an average of 12.12%.

3.5. Mathematical equations for determination of volume factor

To determine the volume factor *f*, the correlation between the volume factor *f* with non-dimensional of volume defined by $LBH^{1/3}$ are expressed by using several equations such as linear equation, logarithmic equation, power expression equation, and exponential equation as shown in Figs. 9-12. On the other hand, the coefficient block is used to replace *f* in calculating the GT [15].

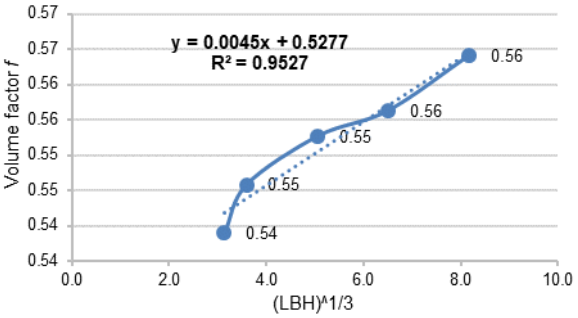

Figure 9. The correlation of the volume factor *f* and $(LBH)^{1/3}$ using linear equation

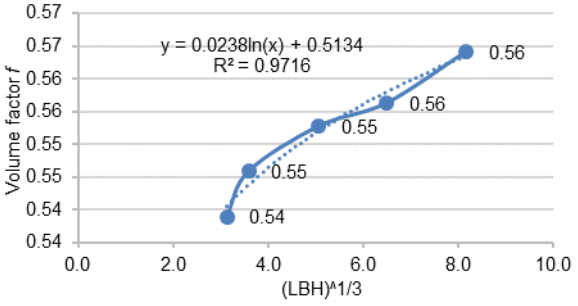

Figure 10. The correlation of the volume factor *f* and $(LBH)^{1/3}$ using logarithmic equation

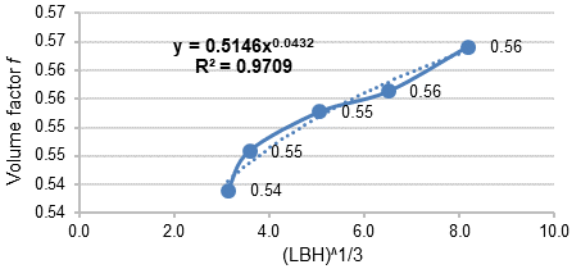

Figure 11. The correlation of the volume factor *f* and $(LBH)^{1/3}$ using power expression equation

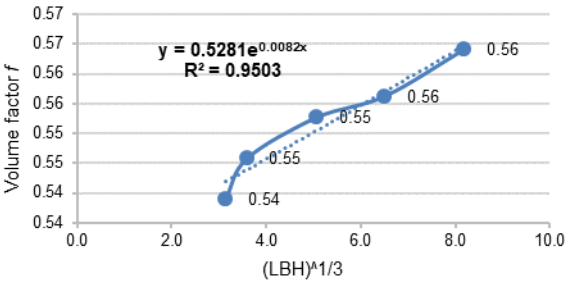

Figure 12. The correlation of the volume factor *f* and $(LBH)^{1/3}$ using exponential equation

Based on Figs. 9-12, the logarithmic equation is the highest correlation between volume factor *f* with $LBH^{1/3}$ due to the determination (R Square) result given the value of 0.9176. By the algorithmic equation, the volume factor *f* can be determined by using the function of $y = 0.238 \log (x) + 0.5134$ or $f = 0.238 \log (LBH)^{1/3} + 0.5134$.

4. Conclusion

This present study was successfully conducted in order to obtain the characteristics of the main dimensions of the traditional wooden ships affected on the GT calculation, the difference of the GT of the traditional wooden boat between the real body and the domestic measurement methods, last but not least the equation in determining the value of the ship volume factor based on the main dimensions of the traditional boat for the calculation of the GT followings.

- The overall ratio of L/B, B/H, and L/H for ship cargo is an average of 3.86, 2.56, and 9.91 respectively. For the fishing boat, the overall ratio of L/B, B/H, and L/H is an average of 5.42, 2.41, and 13.05 respectively. Also, these ratios indicate that traditional wooden ships operated in the Sinjai and Bone Regencies have the quite same of geometry characteristics.
- The GT between the real body and the domestic measurement method seems a difference wherein the GT of cargo ship using the real body is higher than the domestic measurement method, in contrast, for the fishing boat, the GT using the real body is smaller than the domestic measurement method. For small fishing boat <7 GT, the difference of the GT is approximately 40% and this is higher value. This matter should be an attention for Government because it relates directly to the fishermen. This matter should be an attention for Government because it relates directly to the fishermen. Moreover, by using the volume factor *f* as obtained from the real body, the weight of the difference between real body calculation and the

domestic measurement method, the GT of the ship cargo is the same difference, however, the difference of the GT for the fishing boat is an average of 12.12%.

- The correlation between the volume factor *f* with non-dimensional of volume defined by $LBH^{1/3}$ expresses the high correlation. For highest correlation, the logarithmic equation is given the determination (R Square) of 0.9176. By the algorithmic equation, the volume factor *f* can be determined by using the function of $y = 0.238 \log (x) + 0.5134$ or $f = 0.238 \log (LBH)^{1/3} + 0.5134$.

Acknowledgements

We are grateful to the Head of the Class III Sinjai Port Administration Unit Office for his kind help during our research.

References

[1] Pemerintah Kabupaten Bone. Geografi dan Iklim, *Pemerintah Kabupaten Bone*; 2013. accessed at https://bone.go.id/2013/04/26/geografi-dan-iklim/# October 25, 2020.

[2] Naping H, *Laut : Manusia dan Kehidupan*, ed. 1. Makasar: Kaukaba Dipantara; 2017.

[3] Sudjasta B, Suranto PJ, and Putra CES. Analisis Pengukuran Ulang Tonage Kapal Penangkap Ikan Dengan Panjang Kurang Dari 24 Meter, vol. 14, pp. 79–85; 2018.

[4] Peraturan Menteri Perhubungan Republik Indonesia. PM. 8 Tahun 2013 tentang Pengukuran Kapal, Jakarta; 2013.

[5] Arthatiani FY, Peran Penyidik Pegawai Negri Sipil (PPNS) Perikanan dalam Proses Penegakan Hukum Kasus IUU Fishing di Indonesia, *Widyariset*, vol. 17, no. 1, pp. 1–12; 2014.

[6] Garnesia I. Perikanan Tangkap: Masalah Perizinan Tetap Ada, *Tirto.co.id*; 2018. accessed at https://tirto.id/perikanan-tangkap-masalah-perizinan-tetap-ada-c8oN. January 12, 2020.

[7] Biro Komunikasi dan Informasi Publik Kementerian Perhubungan. Ditjen Hubla Jamin Kemudahan Nelayan Lakukan Verifikasi Atau Pengukuran Ulang Kapal Ikan, *Direktorat Jenderal Perhubungan Laut*. accessed at http://dephub.go.id/post/read/ditjen-hubla-jamin-kemudahan-nelayan-lakukan-verifikasi-atau-pengukuran-ulang-kapal-ikan. January 15, 2020

[8] Achmad D. Rancangan pengelolaan perikanan tangkap berbasis sistem registrasi kapal ikan di Provinsi Aceh, Institut Pertanian Bogor; 2012.

[9] Asri S, Firmansyah MR, Wahyuddin, and Djalante AH. Mathematical Model Development to Estimate Gross Tonnage of Ro-Ro Ferry, *Int. J. Eng. Res.*, vol. V5, no. 12, pp. 104–107; 2016, doi: 10.17577/ijertv5is120098.

[10] Asis SA MA , Paroka D, Muhammad AH, Rahman S. Experimental Study on Weather Criterion Applied to South Sulawesi Traditional Wooden Boats, International Conference on Marine Technology; 2020.

[11] Ajisman A. Kearifan Lokal Dalam Pembuatan Kapal Bagan Di Nagari Sungai Nyalo Mudiak Aia Kabupaten Pesisir Selatan 1980-2017, *J. Hist. Cult. Res.*, vol. 6, no. 1, pp. 1–32, 2020, doi: 10.36424/jpsb.v6i1.150.

[12] Kurniawati V, Novita Y, and Kusumanti I. Tingkat Pemanfaatan Material Kayu pada Pembuatan Gading-Gading di Galangan Kapal Rakyat UD. Semangat Untung, Desa Tanah Beru, Bulukumba, Sulawesi Selatan, *Bul. PSP*, vol. 19, no. 3, p. 241743; 2011.

[13] Dariansyah MR, Iskandar BH, Novita Y, Pengajar S. Bentuk Kasko Dan Pengaruhnya Terhadap Kapasitas Volume Ruang Muat Dan Tahanan Kasko, *ALBACORE J. Penelit. Perikan. Laut*, vol. I, no. 3, pp. 265–276; 2017, accessed at https://jurnal.ipb.ac.id/index.php/pspalbacore/article/view/19022. March 09, 2020.

[14] Alham I. Gross Tonage (GT) Hubungannya Dengan Tenaga Penggerak (HP) Pada Kapal Pukat Cincin (Purse Seiner) Di Kabupaten Takalar, Provinsi Sulawesi Selatan, Institut Pertanian Bogor; 2010.

[15] Sunardi, Baidowi A and Yulianto ES. Perhitungan GT Kapal Ikan Berdasarkan Peraturan Di Indonesia Dan Pemodelan Kapal Dengan Dibantu Komputer (Studi Kasus Kapal Ikan Muncar Dan Prigi), vol. 10, no. 2, pp. 141–152; 2019.

EPI International Journal of Engineering
Volume 3, Number 2, August 2020, pp. 172-178
DOI: 10.25042/epi-ije.082020.14

*p*ISSN 2615-5109
*e*ISSN 2621-0541

Study on the Investment Feasibility of the Fishing Boat Considering the Local Wisdom

Syamsul Alam Muchlis[a], Suandar Baso[b,*], Sitti Chairunnisa[c]

[a]Department of Naval Architecture, Engineering Faculty, Hasanuddin, Gowa, Indonesia. Email: alankngejork6@mail.com
[b]Department of Naval Architecture, Engineering Faculty, Hasanuddin, Gowa, Indonesia. Email: s.baso@eng.unhas.ac.id
[c]Department of Naval Architecture, Engineering Faculty, Hasanuddin, Gowa, Indonesia. Email: andi.chairunnisa@yahoo.co.id

Abstract

Indonesia Government, the Ministry of Maritime Affairs and Fisheries, is holding the procurement assistance program for the fishing boat with size from 5 to 30 gross tonnage (GT). In order to succeed in this program, a comprehensive study on a fishing boat is emphasized to be carried out continuously, and then the local wisdom aspect should be considered. This study aims to determine the feasibility of the investment of the fishing boats with the sizes into 12, 21, and 29 GT taking into account the aspect of the local wisdom in the case of Sinjai Regency, South Sulawesi Province, and to determine the weight of local wisdom for the investment of a fishing boat. The investment feasibility was analyzed using the Net Present Value (NPV) and Internal Rate of Return (IRR). In the present results, the three sizes of the fishing boat 12, 21, and 29 GT in Sinjai Regency have met the finacial feasibility. Also, these are suitable sizes to support the fishermen's welfare in Sinjai Regency. For the projection within ten years, the NPV and IRR are for the fishing boat size of 12 GT approximately 823 million rupiahs and 77% respectively, 998 million rupiahs and 54% for 21 GT as well as 979 million rupiahs and 38% for 29 GT. The weight of the local wisdom aspect in the investment of fishing boat is an average of 81.67%, wherein the local wisdom aspect includes the boat hull building, fishing equipment, and labor cost. Also, the weight of the local wisdom aspect for ship operation is an average of 62%, where the local wisdom aspect includes fish recording, maintenance, fish aggregating devices (FADs), and crew salary. For overall, the weight of the local wisdom aspect on the fishing boat building and operation cost are an average of 71.83%.

Keywords: Fishing boat; investment feasibility; internal rate of return; local wisdom; net present value

1. Introduction

Generally, a fishing boat has a wide variety of body forms around the world. The variety of body forms of fishing boats takes into account several aspects such as safety, performance in operation, ease of operation, etc.

The innovation of fishing boat design has been carried out widely. However, the consideration of traditional aspects has been involved in fishing boat design and building by several countries including Indonesia. In Indonesia, the traditional aspect is called traditional content or local wisdom. And the fishing boat is a traditional boat.

Traditional boat design can be improved in order to improve safety and performance, and it is still accepted by a local fisherman after the improvement. The improvement of the traditional fishing boat construction was proposed with model validation [1]. The fishing boat was designed based on local wisdom in Southeast Sulawesi Fishermen [2]. The optimization method of the fishing boat design taking into account local wisdom was proposed [3].

However, the improvement of fishing boat design and building taking into account traditional content affect production cost as well as investment costs. Therefore, the effects must be considered by the shipowner.

Moreover, the investment cost of a fishing boat must be analyzed properly in order to make a business strategy. Correspondingly, financial feasibility has been studied widely by some researchers. Then, the study of the financial feasibility can be a reference for a businessman or other institution. The feasibility of the pole and line fishery was studied in order to compare the level of financial feasibility and determine the level of difference between pole and line fishing businesses [4]. The financial feasibility of the wooden fishing boat in Panggungrejo Subdistrict, Pasuruan, was analyzed and the result fulfills the feasibility value index [5]. The important factors affecting the investment of fishing boats were considered such as vessel age and size, future revenues, operating costs, stock status of the main target species, and the impact of management measures and total fleet size [6].

*Corresponding author. Tel.: +62-852-5562-5397
Jalan Poros Malino km. 6, Bontomarannu, Gowa
Sulawesi Selatan, Indonesia, 92171

On the other hand, the financial feasibility for the business of fishing boat rental was analysed [7]. However, most studies on fishing boat investment, especially traditional boats, do not reveal the effect of the factors of traditional content on investment costs. Consequently, the influence of the traditional content factor can become large or small, nevertheless, this must be considered to decide properly an investment in fishing boats.

Based on the previous explanation, the value of the traditional content or local wisdom factor on the investment feasibility has been investigated in this present study. Through the Indonesian Government, the Ministry of Marine Affairs and Fisheries is holding the assistance program of fishery ship procurement for fishing boat size GT 5 to GT 30. Therefore, the cost components of fishing boat investment considering the local wisdom or traditional content for the boat size 5 to GT 30 GT have been analyzed. The study has been subjected to a fishing boat in Sinjai Regency, South Sulawesi, Indonesia.

The area of the Sinjai Regency consists of land and island. Correspondingly, Sinjai can be considered as one of the regencies in South Sulawesi that has fishery potential. The Sinjai Regency has a coastline length of approximately 28 km with the circumference of the island. Therefore, Sinjai Regency has a possibility for business development in the marine and fisheries sectors.

2. Methodology

The population of the fishing boats was targeted at the location of Lappa Fishing Port (PPI), Sinjai Regency, South Sulawesi Province.

Regarding the data related to the investment feasibility level of fishing vessels, they were collected directly by conducting observation interview, and questionnaire at Lappa Fishing Port (PPI). On observation, the data were collected such as the main particulars and gross tonnages of fishing boats, kinds of fish, the fishing rate per year, and ship operations per year. For the interviews step, the number of fishing boats, potential fish, and a number of fish catches were collected from fishermen, ship owners, and agencies. Also, in this step, the supporting data were needed such as the number of the crew member, time and length of operation, investment cost component, operational cost (fuel oil, lubricating oil, fresh water, and administrative, crew, and other costs), ship repair cost, and ship maintenance cost. Also, the references subjected to the feasibility of the fishing boat investment considering the local wisdom were collected through internet media.

In this present study, the fishing boat sizes are focused on 12 GT, 21 GT, and 29 GT. The population of these fishing boat sizes is large in Sinjai Regency, and then they can be an illustration of the procurement assistance program for the fishing boat 5 to 30 GT held by the Ministry of Maritime Affairs and Fisheries, Indonesia Government. The main particulars and engine of the fishing boats 12 GT, 21 GT, and 29 GT are shown in Table 1.

The local wisdom aspect involved in the fishing boat building cost and operation cost is identified by observation and interview. Then, the weight of the local wisdom is defined by the cost components that are involved in the total cost component divided by the total cost component of the fishing boat building cost and operation cost.

The feasibility of a fishing boat investment is considered based on the financial parameters of Net Present Value (NPV) and Internal Rate of Return (IRR). The followings are the formulas of NPV and IRR [8]. The NPV can be obtained by using the formula as follow:

$$NPV = \left(\sum_{t=0}^{n} \frac{Net\ cash\ flow}{(1+df)^t} \right) - Initial\ investment \quad (1)$$

where *t* is time in year, *n* is the number of time period, and *df* is the discount factor.

The discount factor *df* can be obtaine as follow:

$$df = \sum_{t=0}^{n} \frac{1}{(1 * (1+r)^t)} \quad (2)$$

where *r* is the discount rate.

Then, the IRR can be obtained by using the formula as follow:

$$0 = NPV = \left(\sum_{t=0}^{n} \frac{Net\ cash\ flow}{(1+df)^t} \right) - Initial\ investment \quad (3)$$

The return of the investment cost *Bpi* can be obtained as follow:

$$Bpi = \frac{Net\ cash\ flow}{\sum_{t=1}^{n} \left(\frac{1}{1+df} \right)^t} \quad (4)$$

3. Results and Discussion

3.1. The total investment cost of fishing boat building

Here, the investment cost of a fishing boat building consists of several components wherein it includes several local wisdom aspects that are involved. The investment component and its cost for each fishing boat size are shown in Table 2.

Table 1. Main particulars and engine power of the fishing boats

No	Description	Unit	Ship Size		
			12 GT	21 GT	29 GT
1	Main particulars				
	a. Length overall (Loa)	m	14.90	19.80	20.35
	b. Length between perpendiculars (Lbp)	m	11.52	15.62	16.69
	c. Width (B)	m	3.05	3.9	4.1
	d. Height (H)	m	1.40	1.2	1.9
2	Main engine				
	a. Number	Unit	1	2	2
	b. Power	HP	30	30	30
3	Auxiliary engine				
	a. Number	Unit	1	1	1
	b. Power	HP	30	30	30

Table 2. Total investment cost of the fishing boat building

No	Investment Component	Investment Cost (Rupiah/Rp)		
		12 GT	21 GT	29 GT
1	Hull building and labor	115.000.000	200.000.000	320.000.000
2	Ship engine	21.000.000	51.000.000	60.000.000
3	Fishing equipment	9.000.000	12.000.000	13.000.000
4	Required documents	5.000.000	7.000.000	7.000.000
	Total	150.000.000	270.000.000	400.000.000

Table 3. The results of the analysis of the cost of investment return

Description	12 GT	21 GT	29 GT
Total investment (Rupiah)	150.000.000	270.000.000	400.000.000
Interest rate (%)	6	6	6
Returned costs (Rupiah)	20.380.194	36.684.349	54.347.183
Total returned cost (Rupiah)	268.627.154	483.528.878	716.339.079

Correspondingly, for the investment cost, it is considered to become feasible wherein it can be returned within the age of fishing boat which is approximately ten years. By using the formula of the breakeven point, the returned cost for each fishing boat size within ten years with the interest rate of 6% is shown in Table 3. The returned cost based on the cash flow is Rp. 20.380.194 for 12 GT, Rp. 36.684.349 for 21 GT, and Rp. 54.347.183 for 29 GT. It is obtained by using the integration of the discount rate in ten years.

3.2. Fishing boat operation pattern

The fishing boats sometimes operate outside fishing ground in the sea area of Sinjai's authority such as Jampea, Lombok, and Kupang as shown in Fig.1. Those fishing grounds are nearly the ports of Lombok and Kupang. Therefore, the operation length of the fishing boat is needed for about nine months or called one season.

Furthermore, the round-trip times for Sinjai-Jampea, Sinjai-Kupang, and Sinjai-Lombok as shown in Fig. 1 are considered to determine the operating frequency. Referring to the questionnaire results, the cycle time for the fishing activity includes the times of departure preparation, a port of origin-destination, rest before going to the fishing ground, destination port to the fishing ground, fishing operation, fishing ground to destination port, interval time (due to unloading, fishing sale, and preparation before going to origin port), and destination port to origin port. Based on the cycle time for the fishing activity, the operation frequency within a year for each size of the fishing boat was obtained as shown in Table 4.

Table 4. The frequency of fishing activity per year

No	Route	Number of operating days per year	Activity frequency
1	Sinjai - Jampea	335	23
2	Sinjai – Kupang	305	14
3	Sinjai - Lombok	305	15

(a)

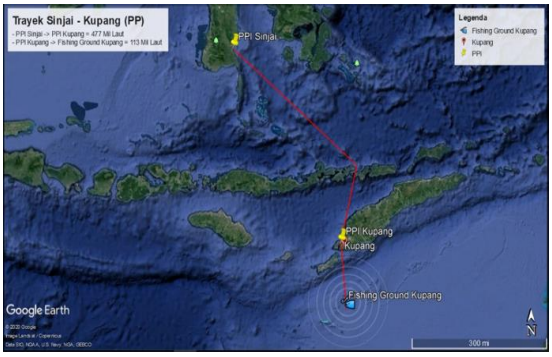

(b)

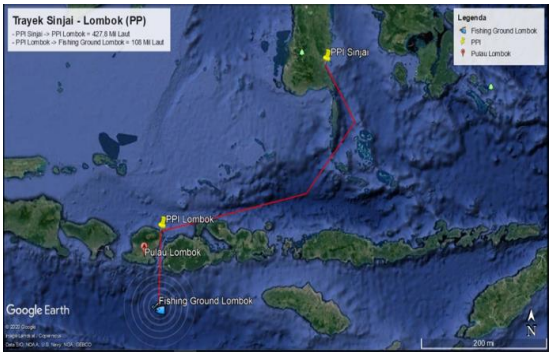

(c)

Figure 1. (a) Round-trip operational pattern for the Sinjai-Jampea route; (b) pattern for the Sinjai-Kupang route; (c) pattern for the Sinjai-Lombok route

3.3. The operation cost of the fishing boat

The annual operation cost of the fishing boat was identified and analyzed as shown in Table 5. Also, the income and expenses costs are shown in Table 5. The expenses cost includes profit-sharing register and operation permit given by the Regional Revenue Office (called Dispenda). Then, the profit-sharing register and operation permits are defined by 10% and 3% of the fish catch seller, respectively. The gross income is defined by the fish catch seller minus the expensive costs. Then, the annual net income is defined by the gross income minus the operation cost.

Table 5. The structure of annual operation, income, and expense costs of the fishing boat

Description	Amount (Rp)		
	12 GT	21 GT	29 GT
Operation cost			
Operating machinery (OM)	42.062.400	39.664.830	39.473.646
Ice box (IB)	24.541.000	23.100.000	33.000.000
Fresh water (FW)	1.725.000	1.050.000	265.000
Provisions (P)	92.000.000	56.000.000	157.500.000
Other services (OS)	1.150.000	700.000	750.000
FADs	500.000	500.000	500.000
Maintenance (M)	5.000.000	10.000.000	15.000000
Total operation cost	166.978.400	131.014.830	248.848.640
Income and expense cost			
Fish catch seller	438.900.000	589.460.000	743.680.000
Operation permit 3%	13.167.000	17.683.800	22.310.400
Profit sharing register 10%	43.890.000	58.946.000	74.368.000
Gross income	381.843.000	512.830.200	647.001.600
Total net income	214.864.600	381.815.370	398.152.960

3.4. Profit sharing scheme based on local wisdom

The scheme of the production sharing had been determined by the government by issuing Law of the Republic of Indonesia Number 16 of 1964 [8], however, the production or profit-sharing in Sinjai Regency has been considered as the local scheme which involves the aspect of the local wisdom. This local scheme of the income sharing is based on the number adjusted to crew members, after equal distribution, each ship owner, crew member, the registrar has a different share, for instance, a fishing boat has a crew number of seventh people, therefore, the income consists of 17 points (sharing factor). These points are shared with the skippers for three points, crew members for six points, and shipowner for eight points. In the income structure, the total net income and sharing fee for each ship size are shown in Table 6. The total net income for the fishing boats 12 GT, 21 GT, and 29 GT are Rp. 214.864.600, Rp. 381.815.370, and Rp. 398.152.370 respectively.

Table 6. The structure of income based on local scheme

No	Description	Fishing boat size		
		12 GT	21 GT	29 GT
1	Total net income (Rp)	214.864.600	381.815.370	398.152.954
2	Sharing factor	13	17	17
3	Number of crew	4	7	7
4	Net basic income (Rp)	16.528.046	22.459.728	23.420.762
5	Ship's master sharing fee (Rp)	49.584.138	67.379.183	70.262.286
6	Crew sharing fee (Rp)	33.056.092	134.758.366	140.524.572
7	Owner sharing fee (Rp)	132.224.369	179.677.821	187.366.096

Table 7. Annual net income after sharing fee

Description	Amount (Rp)		
	12 GT	21 GT	29 GT
Operation cost	166.978.400	131.014.830	248.848.646
Catch sale	438.900.000	589.460.000	743.680.000
Gross income	381.843.000	512.830.200	647.001.600
Net total income	214.864.600	381.815.730	398.152.954
Sharing fee (master and crew)	86.640.230	202.137.549	210.786.858
Net income (after sharing fee)	132.224.369	179.677.821	187.366.096

By using the sharing factor, shipowner based on the fishing boat size 12 GT, 21 GT, and 29 GT gains the income of Rp. 132.224.369, Rp. 179.677.821, and Rp. 187.366.096, respectively. These ownership incomes will be used to analyze investment feasibility for those kinds of fishing boats following.

Based on Table 6, after the deduction of operational costs and income sharing, the net profit a year is shown in Table 7.

3.5. The weight of local wisdom on fishing boat investment

In order to determine the weight of local wisdom on the investment of the fishing boat, the shipbuilding costs and ship operation costs were broken down into the component costs that implicitly involve the local wisdom aspects. Then, the interview and questionnaire were conducted and addressed to the ship owners to understand the local wisdom aspects of the investment cost. The cost components of the shipbuilding investment for each fishing boat size are shown in Fig. 2. Moreover, the weight of the local wisdom aspect involved in the shipbuilding investment for each fishing boat size is shown in Fig. 3.

Based on Fig. 2, the cost component of the boat's hull is greater than other cost components on the shipbuilding investment. The increase of the boat size impacts significantly on the increase of the boat hull cost. Here, the size of the fishing boat 29 GT is a higher shipbuilding investment than other sizes. For the weight of the local wisdom involved in the shipbuilding cost, the boat's hull and fishing gear costs are contributed implicitly higher weight in the shipbuilding cost. Therefore, the weight of the local wisdom involved in the shipbuilding cost for the fishing boat sizes of 12 GT, 21 GT, and 29 GT are approximately 83%, 79%, and 83% respectively. The high weight of the involvement of local wisdom aspects in the fishing boat building is contributed by the hull form including bow shape, type of fishing gear called Penongkol, room layout, and steering system. The form of a fishing boat is generated from the geometry of the local fishing boat, and the room layout is based on the custom of local fishermen. Moreover, the fishing boat was made of wood material, and then it was constructed by using the hereditary tradition. By the high weight, this means that the investment of the fishing boat building is significantly influenced by the local wisdom aspects. Merely, the cost of required documents for the fishing boat and machinery have not a contribution to the local wisdom.

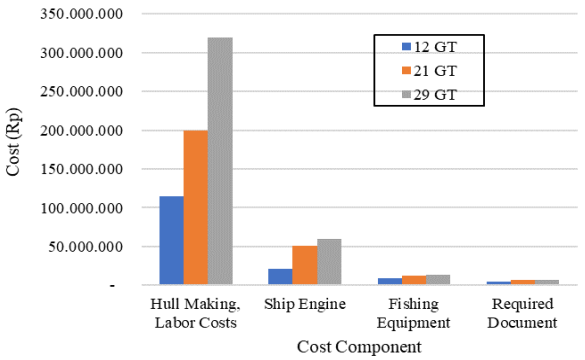

Figure 2. The cost component and its cost of fishing boat building

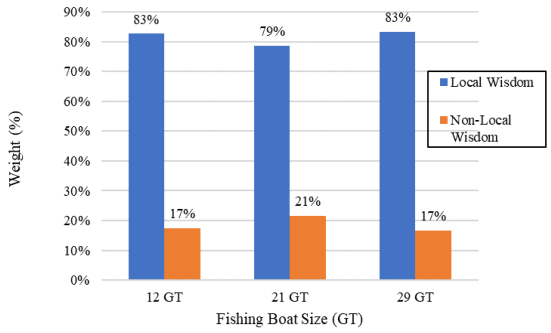

Figure 3. The weight of the of local wisdom on the fishing boat building

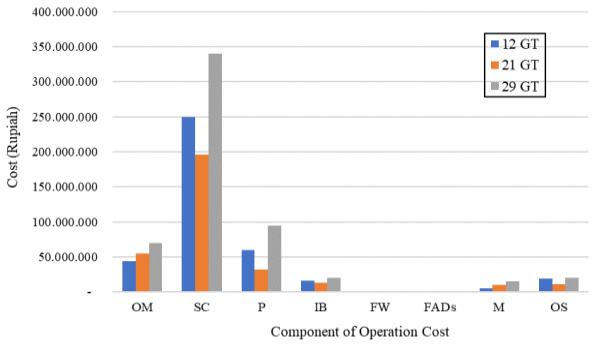

Figure 4. Operation cost of the fishing boat

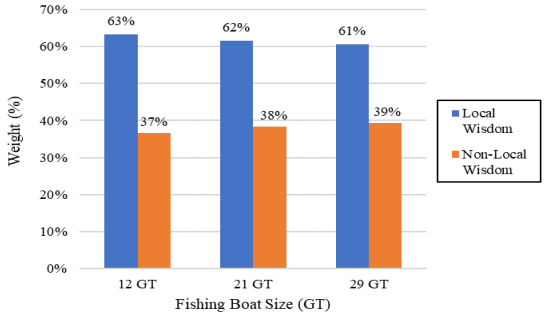

Figure 5. The weight of the of local wisdom on the operation cost

On the other hand, the components of the operation costs of the fishing boat were analyzed and identified by observation and interviewing the fishermen and shipowner. Figure 4 shows the operation cost components per year for each fishing boat size, and the fishermen's salary shows a higher cost than other cost components. As known, the fishermen's salary is influenced by the local scheme of income sharing as explained previously.

By identifying the cost components which involve the local wisdom aspect, the operational cost components of the fish recording, maintenance, fish aggregating devices (FADs), and crew salary are contributed by the value of the local wisdom whereas the costs of freshwater, ice, fuel oil, have not a contribution to the local wisdom. Figure 5 shows the weight of the local wisdom aspect of the operation costs for each fishing boat size. As the result, the weight of the local wisdom aspect contributed to the operation cost of the fishing boat 12 GT, 21 GT, and 29 GT are about 63%, 62%, and 61% respectively. Those weights show a small difference. This means that the increase of the fishing boat size exactly increases the operation cost, however, the weight of the local wisdom contribution to the operation cost is rather constant around the average of 62%.

For the fishing boat investment, the weight of the local wisdom aspect on the fishing boat building and operation cost is 71.83%. For this reason, the Ministry of Maritime Affairs and Fisheries (Indonesia Government) should consider the local wisdom aspect in order to succeed in the procurement assistance program for the fishing boat with its size from 5 to 30 GT.

3.6 Business feasibility based on Net Present Value (NPV)

For the fisheries business, Net Present Value (NPV) as a financial parameter was used to determine the feasibility of investment of the fishing boat sizes 12, 21, and 29 GT. Here, the interest rate was considered 6% by referring to Bank Rakyat Indonesia [9], and the investment period was considered ten years as equal to the ship age. As calculation results, Tables 8 to 10 show the cash flow of Net Present Value (NPV) started one year to ten years for the fishing boat sizes 12, 21, and 29 GT respectively. Based on Tables 8 to 10, the NPV is Rp. 823.182.866 for 12 GT, Rp. 998.784.136 for 21 GT and Rp. 979.030.777 for 29 GT. Overall NPV meets positive (> 0) and this means that overall fishing boat sizes are feasible for the fisheries business that can expect a profit and should consider moving forward with the investment of the fishing boats. Moreover, overall NPV shows within the age of fishing boats can construct a new fishing boat building.

Table 8. The cash flow of the investment feasibility for the fishing boat 12 GT based on Net Present Value (NPV)

Years	Net Income (Rp)	df 6%	PV (Rp)
0	-150.000.000	1.000	-150.000.0000
1	132.224.369	0.943	124.739.971
2	132.224.369	0.890	117.679.218
3	132.224.369	0.840	111.018.130
4	132.224.369	0.792	104.734.085
5	132.224.369	0.747	98.805.740
6	132.224.369	0.705	93.212.963
7	132.224.369	0.665	87.936.757
8	132.224.369	0.627	82.959.205
9	132.224.369	0.592	78.263.401
10	132.224.369	0.558	73.833.397
		NPV	823.182.866

Table 9. The cash flow of the investment feasibility for the fishing boat 21 GT based on Net Present Value (NPV)

Years	Net Income (Rp)	df 6%	PV (Rp)
0	-270.000.000	1.000	-270.000.000
1	171.028.512	0.943	161.347.653
2	171.028.512	0.890	152.214.767
3	171.028.512	0.840	143.598.837
4	171.028.512	0.792	135.470.000
5	171.028.512	0.747	127.802.453
6	171.028.512	0.705	120.568.352
7	171.028.512	0.665	113.743.729
8	171.028.512	0.627	107.305.404
9	171.028.512	0.592	101.231.513
10	171.028.512	0.558	95.501.428
		NPV	998.784.136

Table 10. The cash flow of the investment feasibility for the fishing boat 29 GT based on Net Present Value (NPV)

Years	Net Income/year	df 6%	PV (Present Value)
0	-400.000.000	1.000	-400.000.000
1	187.366.096	0.943	176.760.468
2	187.366.096	0.890	166.755.158
3	187.366.096	0.840	157.316.187
4	187.366.096	0.792	148.411.497
5	187.366.096	0.747	140.010.847
6	187.366.096	0.705	132.085.704
7	187.366.096	0.665	124.609.155
8	187.366.096	0.627	117.555.807
9	187.366.096	0.592	110.901.704
10	187.366.096	0.558	104.624.249
		NPV	979.030.777

3.7. Business feasibility based on Internal Rate of Return (IRR)

Correspondingly, the fishery business was also analyzed by using the parameter of the Internal Rate of Return (IRR). Here, the IRR was used to estimate the profitability of potential investments of the fishing boats that makes the NPV of all cash flows equal to zero in a discounted cash flow analysis (NPV = 0). For the potential investment, Tables 11 to 13 show the cash flow based on IRR from one year to ten years for the fishing boat sizes 12, 21, and 29 GT respectively.

In this case, the overall IRR for the investment of the fishing boat 12 GT, 21 GT and 29 GT is quite high that is 77%, 54%, and 38% respectively. By those IRR results, three sizes of the fishing boats are the prospective investments to support the welfare of fishermen in Sinjai Regency, merely the investment with the highest IRR would probably be considered the best investments which is the fishing boat 12 GT.

Meanwhile, the fishing grounds for these fishing boats are outside the sea authority of Sinjai Regency. This will be a conflict matter for the fishermen, therefore, the fishing area in Sinjai's sea authority should be maintained and conserved for the next future and sustainability of aquaculture activities. According to White et al. [10] stated that coral reefs are a habitat for various types of fish that bring economic benefits to the wider community so that their sustainability is very important. By this effort, the operation cost will be minimized and then the income and investment will be high feasibility.

Table 11. The cash flow of the investment feasibility for the fishing boat 12 GT based on IRR

Years	Net Income (Rp)	df 6%	PV (Rp)
0	-150.000.000	1.000	-150.000.0000
1	132.224.369	0.943	124.739.971
2	132.224.369	0.890	117.679.218
3	132.224.369	0.840	111.018.130
4	132.224.369	0.792	104.734.085
5	132.224.369	0.747	98.805.740
6	132.224.369	0.705	93.212.963
7	132.224.369	0.665	87.936.757
8	132.224.369	0.627	82.959.205
9	132.224.369	0.592	78.263.401
10	132.224.369	0.558	73.833.397
		IRR	77%

Table 12. The cash flow of the investment feasibility for the fishing boat 21 GT based on IRR

Years	Net Income (Rp)	df 6%	PV (Rp)
0	-270.000.000	1.000	-270.000.000
1	171.028.512	0.943	161.347.653
2	171.028.512	0.890	152.214.767
3	171.028.512	0.840	143.598.837
4	171.028.512	0.792	135.470.000
5	171.028.512	0.747	127.802.453
6	171.028.512	0.705	120.568.352
7	171.028.512	0.665	113.743.729
8	171.028.512	0.627	107.305.404
9	171.028.512	0.592	101.231.513
10	171.028.512	0.558	95.501.428
		IRR	54%

Table 13. The cash flow of the investment feasibility for the fishing boat 29 GT based on IRR.

Years	Net Income (Rp)	df 6%	PV (Rp)
0	-400.000.000	1.000	-400.000.0000
1	187.366.096	0.943	176.760.468
2	171.028.512	0.890	166.755.158
3	171.028.512	0.840	157.316.187
4	171.028.512	0.792	148.411.497
5	171.028.512	0.747	140.010.847
6	171.028.512	0.705	132.085.704
7	171.028.512	0.665	124.609.155
8	171.028.512	0.627	117.555.807
9	171.028.512	0.592	110.901.704
10	171.028.512	0.558	104.624.249
		IRR	38 %

4. Conclusion

The study on the investment feasibility of the fishing boats 12 GT, 21 GT, and 29 GT considering the local wisdom aspect in Sinjai Regency was carried out successfully. The weight of the local wisdom aspect and investment feasibility of fishing boats based on NPV and IRR are obtained accordingly.

By using the sharing factor based on the local scheme, shipowner based on the fishing boat size 12 GT, 21 GT, and 29 GT gains the income of Rp. 132.224.369, Rp. 179.677.821, and Rp. 187.366.096, respectively. These ownership incomes are used to analyze investment feasibility for those kinds of fishing boats following.

The weight of the local wisdom involved in the shipbuilding cost for the fishing boat sizes of 12 GT, 21 GT, and 29 GT are approximately 83%, 79%, and 83% respectively. The high weight of the involvement of local wisdom aspects in the fishing boat building is contributed by the hull form including bow shape, type of fishing gear,

room layout, and steering system. In addition, the weight of the local wisdom aspect contributed to the operation cost of the fishing boat 12 GT, 21 GT, and 29 GT are about 63%, 62%, and 61% respectively. Therefore, For the fishing boat investment, the overall weight of the local wisdom aspect on the fishing boat building and operation cost is 71.83%. As the high local wisdom aspect involved in the investment of fishing boats, the Ministry of Maritime Affairs and Fisheries (Indonesia Government) should consider it in order to succeed in the procurement assistance program.

Moreover, the NPV within ten years (the age of fishing boat) with the interest rate of 6% is Rp. 823.182.866 for 12 GT, Rp. 998.784.136 for 21 GT and Rp. 979.030.777 for 29 GT. Overall NPV meet positive (> 0). In addition, the overall IRR for the investment of the fishing boat 12 GT, 21 GT, and 29 GT are quite high that is 77%, 54%, and 38% respectively. Based on those results of NPV and IRR, the fisheries business can expect a profit and should consider moving forward with the investment of the fishing boats. Then, three sizes of the fishing boats are the prospective investments to support the welfare of fishermen in Sinjai Regency.

Acknowledgements

We are grateful to the head of the fish auction in Sinjai Regency, fishing boat owners, and crew members for their kind help during this research that was carried out.

References

[1] Praharsi Y, Jami'in MA, Suhardjito G, Wee HM. Modeling a traditional fishing boat building in East Java, Indonesia. Ocean Eng. 2019; 189:106234.

[2] Santoso AW, Novita Y, Iskandar BH, Baskoro MS. Fishing boat design based local wisdom in Southeast Sulawesi fishermen. American Journal of Software Engineering and Applications, 2020; 9(1):1-18.

[3] Supomo H, Baihaqi L, Pribad TW, Wahidi SI. Design for production and operation for traditional fishing boat based on local wisdom. Marine Techonolgy for Sustainable Development, 2017; II:166–172.

[4] Rinaldi AC, Adhawati SS, Mallawa A. Feasibility of pole-and-line fishery: comparison of milkfish (chanoschanos, forskal) and anchovy (stolephorussp) as Live Bait. Int. J. Environ. Agric. Biotechnol, 2019; 4(5):567–1572.

[5] Pribadi SRW, Ariesta RC, Puspitasari HP. Financial feasibility analysis of wooden fishing vessel in Panggungrejo. Economic and Social of Fisheries and Marine Journal, 2019; 6(2):149–157.

[6] Tidd AN, Hutton T, Kell LT, Padda G. Exit and entry of fishing vessels: an evaluation of factors affecting investment decisions in the North Sea English beam trawl fleet. ICES J. Mar. Sci., 2011; 68(5):961–971.

[7] Rosdianto. Financial Analysis of fishing boat rental business at Kenyamukan Hamlet, District of North Sangatta, Regency of East Kutai, Sumatra. Journal of Disaster, Geography and Geography Education, 2017; 1(1):68-77.

[7] Purba R. Analisis biaya dan manfaat (cost and benefit analysis), Rineka Putra: Jakarta;1997.

[8] Republik Indonesia, Undang-Undang (UU) Nomor 16 Tahun 1964, tentang bagi hasil perikanan, Pemerintah Pusat. Jakarta.

[9] Kur.bri.co.id. Kredit Usaha Rakyat Bank Rakyat Indonesia, retrieved at https://kur.bri.co.id/, August 20, 2020.

[10] White AL, Hale LZ, Renard Y, Cortesi L. Collaborative and community-based management of coral reef: lessons from experience. Kumarian Press, Inc., West Hartford, Connecticut;1994.

EPI International Journal of Engineering
Volume 3, Number 2, August 2020, pp. 179-191
DOI: 10.25042/epi-ije.082020.15

*p*ISSN 2615-5109
*e*ISSN 2621-0541

Factors Related to Visitors' Experience of Orientation and Disorientation at MTC Karebosi Makassar

Musdaria[a,*], Ria Wikantari[b], Afifah Harisah[c]

[a]Architecture Department, Engineering Faculty, Hasanuddin University. Email: riarch2804@gmail.com
[b]Architecture Department, Engineering Faculty, Hasanuddin University. Email: rwikantaria@gmail.com
[c]Architecture Department, Engineering Faculty, Hasanuddin University. Email: harisahhussein@gmail.com

Abstract

Architecture involves the perception of the personal environment and the community in designing to be able to orient users. That perception became the basis for designers to design public buildings. The shopping center is one of the most visited public buildings and often orients and disorients its users. MTC Karebosi is one of the shopping centers in Makassar with the concept of providing primary, secondary, and electronic merchandise needs in one place. The need can be purchased wholesale and retail at affordable prices which makes it one of the alternatives for people to shop in Makassar. As a place to sell wholesale and retail merchandise, the retails laying arrangements are designed to the maximum possible to get a large number of retails in a limited area. As a result, the existing retail looks solid and similar to each other. Because of that, the situation between the corridors to the destination looks similar to each other. These conditions make visitors unable to mark the corridors that pass to the destination so that sometimes visitors experience disorientation. This research aims to determine factors related to the visitor's orientation and disorientation experience and uses survey methods. Data collection uses questionnaires as research instruments. The results revealed that factors related to orientation are spatial aspects, functional aspects, visual aspects, cognitive mapping, and behavior. Factors related to disorientation are spatial aspects, functional aspects, visual aspects, cognitive mapping, behavior, and internal individuals. However, there is one different factor that is the individual internal factor in the disorientation experience whereas orientation is not found. This is because internal factors such as fatigue make it easy for a person to forget and not concentrate so that they experience disorientation.

Keywords: Cognitive mapping; functional and spatial; orientation and disorientation; shopping mall; wayfinding

1. Introduction

The ability of architecture to orient itself and users in space and time has become one of the basic characteristics in the discipline of architecture [1]. Architectural knowledge is closely related to the perception of the designers since each architectural object is designed and used by the subject, i.e. the person [2]. Architecture involves the perception of the personal environment and the community in designing to be able to orient users in buildings. In design, the environmental perception of different groups becomes more important because the users perceived environment and quality are different from the perception of the designer [3]. Therefore, it is important for an architect to understand the environmental perception of society when designing. This is intended so that the results of the building design can be easily understood by the user when looking for the destination of the disorientation experience can be minimized.

Disorientation involves a failed orientation [4]. The inability of architecture to orient itself makes the perceived environment unable to be perceived properly by the user. As a result, the user is unable to orient himself in the space so confusion finds its way and towards its destination. Most subjects rely primarily on architectural elements to find their way and purpose, whereas some subjects seem to rely primarily on sign and message [5].

The shopping center is one of the most visited public buildings and often orients and disorients its users. MTC Karebosi is one of the shopping centers in Makassar with the concept of providing primary, secondary, and electronic merchandise needs in one place. The need can be purchased wholesale and retail at a reasonably priced price that makes it one of the alternatives for people to shop in Makassar. As a place to sell wholesale and retail merchandise, the layout is designed to the maximum possible to get a large number of retails in a limited area. As a result, the existing retail look congested, and the situation between corridors with each other heading to the destination looks similar to each other.

The condition makes visitors disoriented when searching for destinations. In addition to the factors mentioned, there are other factors related to the visitor's orientation and disorientation experience. The problem is the issue in this article is why visitors experience orientation and disorientation when searching for

*Corresponding author. Tel: +6285 2992 13407
Jalan Todoppuli No. 10,
Makassar, Sulawesi Selatan

destinations in MTC Karebosi. The issue is expected to determine the factors related to the orientation and disorientation experience of MTC Karebosi visitors.

2. Literature Review

2.1. Orientation

In the Oxford dictionary [6], orientation is defined as the type of purpose or interest a person or organization has; the act of directing your goals in the direction of a particular thing; a person's basic beliefs or feelings about a particular subject; training or information you provide before starting a new job or course, etc; the direction in which the object is facing. Orientation is a review to determine the right and correct attitude (direction, place, etc.); the underlying view of the mind, attention, or inclination [7].

Schulz [8] states that orientation is a function that allows humans to become homo viators that are part of their nature. Lynch [9] also states that orientation can be an inarticulable memory of a more structured navigational action or mental map or a series of sequences remembered. Orientation is the concept of human consciousness that guides decision-making and action (Kamper in Kling and Kruger [10]).

Based on the understanding, orientation can be interpreted according to context. If it relates to humans then it can be interpreted as a position search by drafting a concept of memory or a structured mental map or a series of sequences that are remembered to make decisions and actions. If it relates to a building according to the context of the architecture then it can be interpreted as the direction in which the object is facing or the object's tendency towards something.

2.2. Spatial orientation

Spatial orientation refers to a process by which a person knows where he or she is towards something [11]. Ohta [12] explained that spatial orientation is considered one of a series of processes that mediate an individual's contact with the physical environment and the implementation of responses in the environment. So spatial orientation is a process that mediates an individual with a static space or environment to know where it is.

Lynch [13] explained that the ability to be able to read signs or symbols is supported by the quality of the environment that has properties:

a. Legibility is the ease to be read or recognized and clarity of information. [13].
b. Imageability is a physical quality that relates to the attributes of identity and structure in mental imagery where that physical quality evokes a strong image in a particular observer. [13].

There are five space-oriented elements. These five elements reinforce the legibility and imageability of an environment when positioning themselves [13], i.e: path, edge, district, node, landmark. Passini in Tanuwidjaja [14] found a similarity to five architectural elements based on Lynch's theory [13] in the study of commercial buildings in Montreal. Passini in Tanuwidjaja [14] divided five architectural elements into oriented processes and found a way, i.e:

a. Pathway

Passini in Tanuwidjaja [14] divides two types of pathways, i.e; horizontal and vertical pathway. Horizontal pathways in the scale of buildings, i.e; corridors while vertical pathways are stairs, escalators, and elevators.

b. Edge

Edge in the scale of the building in the form of a barrier wall that is the outer wall of the building.

c. District

Districts in building scale can be large zones that have similar functions.

d. Node

Nodes in the scale of a building are circulation meetings or meeting areas that are used as gathering places.

e. Landmark

Landmarks in buildings can be empty rooms that have a function as a reference point to know a person's whereabouts, have special features, and the number is not much.

In addition to the architectural elements mentioned above, Passini in Tanuwidjaja [14] also revealed that signage systems are necessary to help orient and process wayfinding to destinations. Gibson [15] divided the signage system into four types, including:

a. Identification signs.

These signs display the name and function of a place or space.

b. Directional signs

These signs show the location of a place, an object, an event in the form of a name, symbol, image, and arrow direction.

c. Orientation signs

These signs offer the user an overview of its surroundings in the form of maps and clues.

d. Regulatory signs

These signs describe something a person may and should not do in a place or space.

2.3. Architectural morphology

Frankl in Ven [16] divided architectural morphology into four categories:

a. Spasial Aspects

This aspect relates to the development of architectural elements that integrate into one unit forming a space and vice versa, from one unit into a separate part.

b. Physical Aspects

This aspect relates to the development of forms that sustain the physical and mass form of the merging of architectural elements.

c. Visual Aspects

This aspect relates to the perception of the user looking at the shape of the architecture from one point of view or different points of view so that it can be viewed in its entirety.

d. Functional Aspects

This aspect relates to the development of architectural forms that govern the organization of space so that it can accommodate functional akivitas and user circulation.

2.4. Orientation functional

The notion of orientation beforehand if the context is related to the building is the tendency towards something. If orientation and functional are combined, it means that the tendency of architectural forms in organizing space so as to accommodate functional activities and circulation of the user. According to Narrel [1], functional orientation is based on several things, i.e:

a. Fixed functional relationships

Architectural elements oriented in relationship to one another and create legibility of form and function [1]. From the clarity of these shapes and functions, architecture creates a fixed functional relationship of shapes and functions so that between elements can create a legible space for shapes and their functions to be able to orient.

b. Static and clear boundaries

Static boundaries are fundamental to understanding of orientation in architecture [1]. Building users will feel more focused on exploring the space if the existing boundaries do not change.

c. Legible identities

Architectural identity is often rooted in materiality and qualities of the building materials that dominate the exterior and interior spaces. Architectural space forming materials affect the clarity of shapes and functions so as to orient the user of the building.

Orientation keeps users in touch with uninhabited places but is still part of the building [17]. Leatherbarrow [17] explains that functional orientation is based on:

a. Clear direction

Direction demands sense by determining and showing one's tendencies. Direction can also mean where the building gives the user directions to its destination.

b. Contrast differentiation

The differentiation of design elements makes destination destinations easier to do. Such is the wide difference for the main circulation in the retail and secondary circulation towards other facilities.

Coleman [18] identified a functional orientation based on his observations of various shopping malls he had seen based on:

a. Special differences

Specific differences can help identify a location or retail so it's easy to see.

b. Individual identity

Identity is required to remember and recognize the specific features a location or retail has when visitors want to come back.

c. Visual access to the outside of the building

To assist orientation such as mallswith long and complex circulation, there are points allowing views to the outside [18].

d. Same entry and exit points

Entry and exit points should be on the same way to assist the costumers’s orientation and to allow them to retrace their route of arrival on departure [18].

e. Clarity of circulation

Clarity of circulation helps users to be able to explore the space easily so that users can linger and head to their destination in a shopping mall.

f. Ease of access

Ease of access can help users to recognize entrances and exits so that users can enter and exit shopping malls without confusion.

2.5. Wayfinding

Wayfinding is a native function of environmental images that involves individual feelings where environmental images are a product of past experience memory and are used to interpret information and guide actions [13]. Wayfinding refers to the cognitive and behavioral abilities of humans and species to find a way from origin to destination [19]. Hunter et al [20] adapted Siegel and White's theory of environmental knowledge sequences in search of roads, namely landmark knowledge, route knowledge, and survey knowledge. route knowledge, and survey knowledge. Landmark knowledge is a search for information in the form of landmarks from the environment that are used as signs.

2.6. Cognitive mapping

Cognitive mapping is essentially everyday human life that is done when traveling then he will imagine: destinations, ways, routes, and locations he is known for [21]. When traveling a human takes and retails the information he obtains consciously or unconsciously. The process of encoding and decoding spatial knowledge is called cognitive mapping, defined as "a process consisting of a series of psychological transformations in which an individual acquires, codes, retails, remembers, and translates information about the relative location and attributes of phenomena in his or her daily spatial environment" (Downs and Stea in Hunter et al. [20]). Figure 1 shows the cognitive mapping formation scheme.

2.7. Cognitive maps

Cognitive maps are mental processes that contain a series of psychological transformations from information received, categorized, or coded, stored, conveyed in a description of a location of phenomena that mark spatial environments or spaces in daily life [21]. Cognitive map as a concept of cognitive mapping [3]. Cognitive maps in

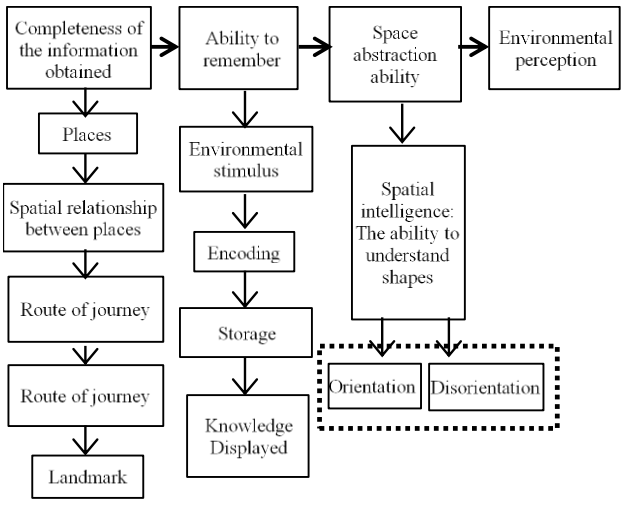

Figure 1. Factors in cognitive mapping [21]

small and medium-sized environments are obtained primarily through direct experience on the go from place to place according to knowledge of the perception of the characteristics of a place [5].

2.8. Perception

Perception is a way of seeing things [4]. This understanding indicates that perception is based on the quality of the human senses to be able to see, hold, feel, and understand. Perception depends on orientation [3]. Without being oriented and located in space and time, organisms cannot see-make hypotheses, gather information from the environment and test this hypothesis (Bruner and Sandström in Rapoport [3]); also can't enjoy the environment.

Human perception involves images (Mann and Berry in Rapoport [3]). In the world of architecture, an image is an imitation or reproduction or a comparison of something [22]. The image of the environment possessed by observers depends on past experiences, current motivations and attitudes [22]. When a human enters a new building, such as a newly built mall, there is an image built based on his experience entering the mall before. If an image of an object is given meaning then the image will become a symbol for the next to be remembered. Symbols are the result of the cognition process; which means an object acquires a connotation (additional understanding) outside of its usefulness [22].

2.9. Architectural perception

Architectural perception is the sense of how something seen [3]. The basic perceptions that are in architectural design [2], i.e:

a. Functional perception
    1) Space function: this approach emphasizes the way space is used in architectural design.
    2) Space location: this approach emphasizes the situation of object location in architectural design.
    3) Space form: this approach emphasizes the shape of objects in architectural design.
b. Persepsi visual
    1) Space restrictions: this approach emphasizes the way space restrictions are designed.
    2) Space order: emphasizes the connection of spaces in architectural design.
c. Structural perception
    1) Space arrangement: this approach emphasizes the arrangement of objects with their environment in architectural design.
    2) Spatial layout: this approach emphasizes the pattern of space in architectural design.

2.10. Environmental perception

Environmental perception is an interpretation of an individual's setting, based on the individual's cultural background, reasoning and experience [23]. Environmental perception is subjective, based on a person's personal view of the environment. Rapoport [3] associates environmental perception with the difference between emic and etic aspects. Emic is how something looks or is perceived by a person or group in a system. Etic is how observers perceive things in the same system.

2.11. Perceived environment

The perceived environment is a product or form of environmental perception of a person or group of people [23]. Perceived environments can be understood as ideas in people's minds based on what is known, expected, imagined, or experienced, and such ideas, which are often manifested in images and schemes [3].

2.12. Disorientation

Etymologically disorientation comes from the word dis- and orientation. According to the Great Dictionary of Indonesia [7] dis means bound form; no, not; separate and inverse or the opposite of. Orientation is a review to determine the right and correct attitude (direction, place, etc.); underlying views of thoughts, concerns or tendencies. So disorientation is a review of determining inappropriate and correct attitudes (direction, place, and so on).

2.13. Spasial disorientation

The terror of being lost comes from the necessity that a mobile organism be oriented in its surroundings [13]. To be oriented it takes a supportive orientation element to be able to determine the position of the building user. Spatial orientation elements according to Lynch [13] are path, edge, district, node, landmark. But if spatial disorientation occurs, then the user does not know the path, edge, district, node, landmark. Users also do not know and use signage.

2.14. Functional disorientation

Based on the determinants of orientation in architecture according to Narrel [1], Leatherbarrow [17], and Coleman [18] that functional orientation is based on some of the things mentioned above. Functional disorientation is based on:

a. Functional relationship are not fixed
b. Dynamic and unclear boundaries
c. Illegibility identities
d. Unclear directions
e. Noncontrast differentiation
f. Differences that are not specific
g. There is individual identity
h. There is visual access to the outside of the building
i. Entry and exit points are not the same
j. Unclearness circulation
k. Difficulty access

3. Reasearch Method

3.1. Research type

The type of research done is quantitative. This type of research is deductive, partial, and dualistis. It is deductive because the concept determination is done at the beginning so that it can be formulated hypothetically. It is partial because quantitative researchers consider that reality is singular and fragmental so that variables can be researched separately and separate unsentisive variables.

Dualistis is the assumption that researchers' interactions with respondents are separate, make distances, and do not influence each other to produce objective research.

3.2. Method

This research method uses the survey method. In survey research, the analysis unit is an individual so one questionnaire is intended for one individual. In this case the individuals analyzed were visitors to MTC Karebosi.

3.3. Research location

As shown in Fig. 2, the research site is located in Indonesia, South Sulawesi province, Makassar city. Precisely located at MTC Karebosi on H. Oemar Said Cokroaminoto street, Nusakambangan street, and Ahmad Yani street. MTC Karebosi consists of nine floors namely two basement floors, six floors of shopping area and one floor for the manager. The shopping area consists of lower ground floor, ground floor, 1st floor, 2nd floor, 3rd floor, and 4th floor.

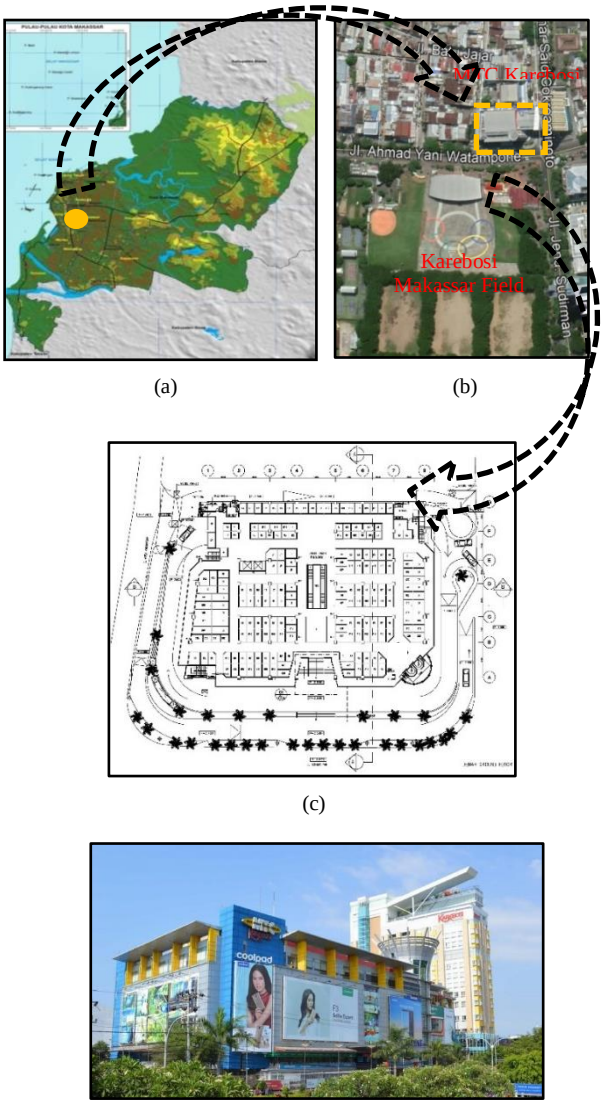

Figure 2. Location under study. (a) Makassar city map, (b) MTC Karebosi location map, (c) MTC Karebosi floor plan, (d) MTC facade

3.4. Sample

The number of MTC populations is unpredictable so to determine the number of samples, researchers did their way with expert formulations. The expert formulation is to determine the number of samples purposive-quota. Purposive sampling with criteria: being inside the MTC or having come to MTC in the past year. Sampling quota is set as much as 60. Existing statistical tests are very effective when applied to samples 30 to 60 (Champion in Indrawan [24]).

3.5. Research data source

a. Primary data

Primary data sources are based on observations, questionnaires, and interviews. Observations were carried out inside MTC karebosi by looking at the condition of exits, escalators, elevators, retails, and corridors. Questionnaires and interviews were conducted to 60 respondents who were in MTC and who had come to MTC in the past year.

b. Secondary data

Secondary data sources in the form of data supporting research from related agencies are MTC karebosi building plans, books related to the research, and the results of publications that support the research.

3.6. Research instruments

Research instruments are tools that researchers use in retrieving data. In this study, the research instruments are:

a. Questionnaire

The questionnaire that is shared is a closed and open questionnaire. The closed questionnaire consists of a list of questions consisting of two answers namely 'yes' and 'no'. The open questionnaire is that respondents are welcome to write down the reasons why answering 'yes' and why answer 'no'

b. Measurement scale

The measurement scale used in this study is guttman scale. This scale has only two answers in the questionnaire: 'yes' and 'no'. A value of 1 is given for the answer 'yes' and a value of 0 for the answer 'no'.

c. Voice recorder

Voice recorder is digital voice recorders are used to record the results of respondents' interviews.

3.7. Research variables

The research variable is a single variable. It consists of only one variable: factors related to the orientation and disorientation of visitors.

3.8. Validity and reliability test

a. Validity test

To test guttman scale validity, first sort questions from easy questions to difficult questions answered by respondents. Questions are sorted by calculating the score value of each question. The score calculation is based on the number of 'yes' answers given by all respondents in each question. The question that has the

highest score is the easiest question and the lowest-scoring question is the hardest question. After that each respondent's error value is calculated and the overall error value was entered into the formula:

$$CR = 1 - \left({}^{e}\!/_{n \times k} \right) \quad (1)$$

where
- CR : Coefficient of Reprodisiability
- e : error value
- n : number of value questions
- k : number of respondents

Next, the data is then calculated again using the Scalability Coefficient (CS) formula. The formula is:

$$CS = 1 - \left({}^{e}\!/_{0.5\left(n \times k\right)} \right) \quad (2)$$

where
- CS : Coefficient of Scalability
- e : error value
- n : number of value questions
- k : number of respondents

The perfect coefficient value for CR is 0.9 and CS is 0.6 [25]. However, in practice to achieve a high coefficient of validity is relatively difficult. If the validity of obtaining a high value then the reliability value will drop. And vice versa. Therefore, coefficients ranging from 0.3 to 0.5 have been able to contribute well to the efficiency of a training institution (Cronbach in Azwar [26]).

b. Reliability test

For guttman scale, reliability test using Kuder-Richardson formula 21 (KR21), i.e:

$$r_i = \frac{k}{k-1}\left(1 - \frac{M\left(k-M\right)}{k\left(st^2\right)}\right) \quad (3)$$

where
- r_i : reliability
- M : mean value
- st^2 : variance of total
- k : number of respondents

The reliability test limit is > 0.6. If reliability has a coefficient < 0.6 is not good, coefficient 0.7 - 0.8 is acceptable, and > 0.8 is good. However, sometimes a not-so-high coefficient can still be considered significant enough, seeing the size of the standard error in measurement is more important because the reliable test is the least variance error [26]. Variance error formula, i.e:

$$s_e = st\sqrt{1 - r_i} \quad (4)$$

where
- s_e : variance of error
- st : variance of score
- r_i : score of reliability

3.9. Data analysis techniques

Descriptive analysis is used to explain factors that affect the orientation and disorientation of MTC visitors. The presentation of data is a percentage table and describes them one by one.

4. Validity and Reliability Test

4.1. Validity

The number of variable error values of related factors (e) is 62. The number of variable questions of related factors (n) amounts to 6 questions. The number of respondents (k) is 60. The value was included in the Coefficient of Reprodisiability (CR) formula.

$$\begin{aligned} CR &= 1 - \left({}^{e}\!/_{n \times k} \right) \\ &= 1 - \left({}^{62}\!/_{6 \times 60} \right) \\ &= 1 - 0.172 \\ &= 0.828 \\ &= 0.83 \end{aligned} \quad (5)$$

The CR value is 0.83 < 0.90, so it is concluded that the variable question of related factors approaches the recommended Coefficient of Reprodisiability (CR) of 0.9. A value of 0.83 is considered satisfactory. After calculating the CR value, the Coefficient of Scalability (CS) value was calculated based on the formula below:

$$\begin{aligned} CS &= 1 - \left({}^{e}\!/_{0.5\left(n \times k\right)} \right) \\ &= 1 - \left({}^{62}\!/_{0.5\left(6 \times 60\right)} \right) \\ &= 1 - \left({}^{62}\!/_{180} \right) \\ &= 0.66 \end{aligned} \quad (6)$$

The CS value is 0.66 > 0.60 so that the variable question of related factors exceeds the recommended Coefficient of Scalability (CS) so that it is considered good.

4.2. Reliability

Reliability test using Kuder Richardson formula 21 (KR21). Before entering values into the formula KR 21 first variance totals and means are calculated based on the total score of each respondent. The number of variable (k) questions is 6. The mean value (M) is 3,717 and the total variance (st2) is 1,636. The value is included in the kr21 formula, i.e:

$$\begin{aligned} r_i &= \frac{k}{k-1}\left(1 - \frac{M\left(k-M\right)}{k\left(st^2\right)}\right) \\ &= \frac{6}{6-1}\left(1 - \frac{3.717\left(6-3.717\right)}{6\left(1.636\right)}\right) \\ &= 1.2\left(1 - 0.864\right) \\ &= 0.162 \\ &= 0.2 \end{aligned} \quad (7)$$

The reliability value is 0.2 < 0.6. These results are considered less good. However, low scores are still considered significant because what determines reliabel questionnaires is the small variance of errors. Error variant values, i.e:

$$\begin{aligned} s_e &= st\sqrt{1-r_i} \\ &= 1.28\sqrt{1-0.2} \\ &= 1.28 \times 0.89 \\ &= 1.132 \end{aligned} \quad (8)$$

The variance error score is 1.132 which means that this value is reliabel.

5. Discussion

A total of 60 respondents were asked questions about orientation and disorientation when searching for escalators when entering, searching for escalators while circling, searching for retails, choosing suitable exits, searching for elevators when entering, and searching for elevators while circling. The destination is considered to be quite representative of the experience most often experienced while in MTC Karebosi when searching for a way. Here's the percentage of visitors who experience orientation and disorientation when searching for destinations depicted in graphic form.

Figure 3 shows that the tendency of visitors to experience orientation is searching for escalators when entering and searching for escalators while circling MTC. When visitors enter the shopping area, escalators tend to be easy for almost all visitors (93.3%). When circling within MTC, escalators are also likely to be easy for almost all visitors (95%).

When searching for a retail and choosing the appropriate exit, the percentage of visitors who experience orientation and disorientation is not too far off. Visitors searching for a retail in MTC were less than half the visitors (56.7%). Disorientated visitors (confusion) searching for a retail were less than half the visitors (43.3%). Meanwhile, visitors who never wrongly chose a suitable exit were less than half the visitors (58.3%). Visitors who once wrongly chose a suitable exit were less than half the visitors (41.7%).

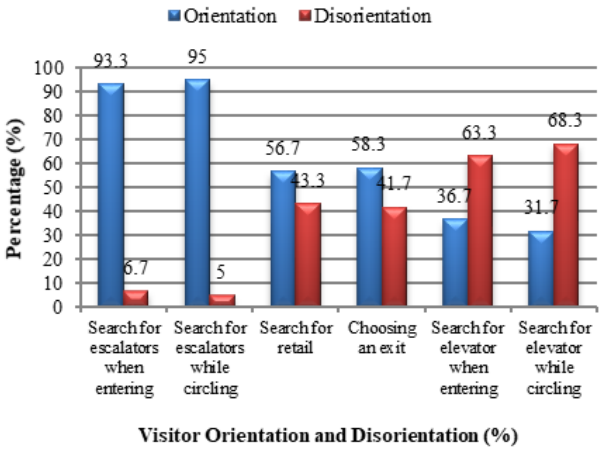

Figure 3. Percentage of visitors who experience orientation and disorientation when searching for destinations.

Furthermore, the percentage of visitors who experience orientation and disorientation when searching for an elevator is quite far. Visitors tend to experience disorientation when searching for elevators when entering or while circling. Visitors who experienced disorientation while searching for an elevator when entering were less than two-thirds of visitors 63.3%). Visitors who experienced orientation while searching for elevators were less than a third of visitors (36.7%). Meanwhile, visitors who experienced disorientation while searching for elevator while circling were less than two-thirds of visitors (68.3%). Visitors who experience orientation when searching for elvators when circling are less than a third of visitors (31.7%).

5.1. Searching for escalator when entering

The escalator is one of the transportation to the upper floors at MTC. Its strategic position makes it easy to find when entering. But there are still disorientations when looking for escalators. Here's why visitors experience orientation and disorientation when searching for escalators when entering Table 1.

a. Orientation

Based on the table above, the reason most visitors experience orientation is because the escalator is visible from the entrance (55%). Then the second most reason is because of the continuous entrance and the escalator is visible (16.7%). Furthermore, because the escalator is seen when go up the basement stairs (15%). The escalator in the middle was the least reason put forward by respondents (6.7%).

The reason visitors are dominated by escalators seen from several entry points illustrates that the position of the escalator is quite strategic. The escalator visible from several entry points is a landmark for MTC as it is visible from several visual points. Escalators as landmarks are part of the spatial orientation element needed for visitor orientation.

Meanwhile, the reason why the escalator is in the middle is the least answer expressed by respondents. MTC in the shape of a cube with the position of the escalator located in the middle of the building makes it easy for visitors to look for escalators upon entry. Its position in the middle is a product of the designer's structural perception of spatial arrangement. The perception makes it easy for visitors to look for escalators because it is in a strategic area that can be reached from various directions and often passed by visitors. This area is also a reference point for visitors to find the desired

Table 1. Reasons and percentage of visitors who experience orientation and disorientation when searching for escalators upon entry

Orientation Reasons	**(%)**	**Disorientation Reasons**	**(%)**
Visible from the entrance	55.0	Enter by elevator, so the escalator is not visible	5.00
The escalator is in the middle	6.7		
From the entrance just keep going and the escalator is visible	16.7	Not visible from the entrance	1.7
Seen while go up the basement stairs	15.0		
Total	93.3	Total	6.7

retail so that the escalator is a landmark in MTC Karebosi which is used as a marker.

b. Disorientation

Based on the table, it appears that visitors who enter use the elevator have difficulty finding escalators because they are not visible (5%). In addition, visitors entering through the front door of Cokroaminoto street also have difficulty finding escalators because the escalator is not visible from the entry point (1.7%). Although the percentage is quite small compared to visitors who experience orientation, this needs to be considered. Escalators and elevators are a means of transportation for visitors, so there needs to be visual access between the two facilities to facilitate visitors.

The reason visitors who have difficulty finding escalators when entering is because it is not visible from the elevator and not visible from the entrance shows that the visual access of visitors is blocked to the escalator. Visitors have difficulty accessing the escalator visually if entering using the elevator because of the elevator that is in the corner. Elevators and escalators are restricted by retails so visitors who enter using the elevator cannot see the presence of escalators. Visitors also have difficulty finding escalators from the entrance from the direction of Cokroaminoto and Nusakambangan streets as it is necessary to walk straight a few meters from the entrance to see the escalator. Rows of retails to pass through make the escalators invisible from the entrance.

5.2. Searching escalators while circling

Visitors who are circling and entering have different situations when searching for escalators. Therefore, the reasons expressed by visitors also vary. Here are the reasons and percentages of reasons visitors experienced orientation and disorientation in Table 2.

a. Orientation

Based on the table above, visitors are more oriented when looking for escalators while circling (95%). The most common reason is that escalators are easy to find when walking around because they are in the middle (75%). The second most reason is because there is ample and empty space around the escalator (6.7%). Then visitors are easy to find escalators when circling because the escalator is visible from several points in the corridor and the corridor always leads to the escalator (5%). The least common reason is that many visitors are seen in the area near the escalator and because the MTC is small (1.7%).

The most reason that most respondents answered was easy to find escalators because the escalator was in the middle. The position of the escalator in the middle facilitates cognitive mapping of visitors due to its memorable location. The second most reason is because there is ample and empty space around the escalator so the escalator is easy to find. This reason clarifies the function of the area as a circulation area and a meeting point of circulation. This relates to the spatial element factor that is the path and node as the marker. Therefore, the importance of a marker around the escalator is different from other circulation lines so as to evoke the visitor's memory of the position of the escalator

Table 2. Reasons and percentage of visitors who experience orientation and disorientation when searching for escalators while circling

Orientation		**Disorientation**	
Reasons	**(%)**	**Reasons**	**(%)**
Escalator in the middle	75.0	The escalator is not visible because many sellers are in the middle of the building	1.7
Many visitors are seen in the area near the escalator	1.7		
Visible from several points in the corridor	5.0	Invisible escalator from the corner of the building	1.7
There is ample and empty space around the escalator	6.7		
Corridors always lead to escalators	5.0	Not all corridors lead to escalators when driving around	1.7
MTC has small size	1.7		
Total	95.0	Total	5.0

The escalator is visible from some point to be the next reason. This reasoning shows that due to its position in the middle makes the escalator visible from several points so it is easy to find when circling. In addition, the corridor also directly leads to the escalator being the next reason. Some corridors are created directly leading to the escalator so that when visitors stand at some point, then the escalator can be seen. The corridor leading to the escalator shows the importance of the path, part of the spatial element to get visitors directly to the destination. It makes visitors not confused looking.

The next reason is that visitors are easy to find escalators when circling because many visitors are seen in the area around the escalator, strengthening the function of the area around the escalator as a meeting circulation and selling place. Visitors who see many visitors gather are associated with seeing the behavior of others as a sign. The behavior strengthens the markers around spatial elements to be recognizable and remembered. Then the reason visitors are easy to find escalators when circling because the size of MTC is small is related to the ability to remember factor owned by each individual. This ability is part of the cognitive mapping process.

b. Disorientation

Visitors who experience disorientation when searching for escalators while circling no more than a twelfth of visitors (5%). The reason visitors experience disorientation is that the escalator is invisible because many sellers in the middle of the building, the escalator is not visible from the corner of the building, and not all corridors are translucent to the escalator (1.7%).

The reason for disorientation is contrary to visitors experiencing orientation. This difference in perception is due to the sometimes fickle MTC situation, especially the situation around escalators. The reason visitors say that escalators are invisible is because many sellers in the middle of the building are related to the absence of visual access of visitors. Large and empty space on escalators is sometimes filled by merchants who rent to sell. The reason for the invisible escalator from the corner of the building is also related to the absence of visual access to visitors. Visitors have difficulty visually accessing the escalator because the view is blocked by rows of retails.

Furthermore, the reason that not all corridors are translucent to the escalator relates to spatial elements in the form of indirect paths pointing to the escalator. The grid-shaped circulation pattern makes the path form a branch so that when misselected the branching path, visitors will have difficulty finding escalators.

5.3. Searching for retail

The retail is the main facility in the shopping center. There are times when visitors want to visit a retail that has been visited before. Here's the percentage of visitors who experience orientation and disorientation when searching for a retail and why presented in Table 3.

a. Orientation

Visitors who were oriented while searching for a retail were less than half the visitors (55%). The most reason is to remember the position of the retail (15%). The second most reason is to remember the position and name of the retail (11.7%). The third most common reason is that the retail is often visited close to the escalator (10%). The fourth most reason is to remember the position and seller of the retail (8.3%). The fifth most reason is to remember the address of the retail block (6.7%). Then the smallest percentage of the reason for visitors is to remember the position and logo of the retail, and remember the position and merchandise (1.7%).

Visitors who experience orientation on the grounds of remembering the position of the retail, are closely related to the ability to remember which is part of cognitive mapping. Visitors who can remember the position of the retail, keep information related to the route that will be passed to the retail to be visited. So is the reason for remembering the retail because it remembers the position and name of the retail, remembers the position and seller of the retail, remembers the block address, remembers the position and logo of the retail, and remembers the position of the retail and the merchandise related to the recall ability. But in this case the unique code by remembering the name, seller, logo, and merchandise is additional information in addition to the position of the retail.

Then the reason for remembering the retail is because the retail is commonly visited adjacent to the escalator, making the escalator as a marker or landmark to mark its position. The presence of landmarks is few in a building so landmarks become reference points that can orient the user. Therefore the placement of retails adjacent to landmarks is very helpful for users to know where they are.

Table 3. The reason and percentage of visitors who experience orientation and disorientation when searching for retails that have been visited before

Orientation		**Disorientation**	
Reason	**(%)**	**Reason**	**(%)**
Remember the block address	6.7	The retails is similar in size, sales, and wall color	15.0
Remember the positions and name of the retail	11.7		
Remember retails positions and logos	1.7	Never come to the same retails	1.7
Remember the positions and seller of the retail	8.3	Corridors to branched retail	10.0
Retails commonly visited close to escalators	10.0	The size of the retails and the corridors that pass through look the same	3.3
		Retails too crowded	6.7
Remember the position of the retails	15.0	The retails is dense and looks similar in size, color, and sales	6. 7
Remember positions and merchandise	1.7	Merchandise sold look similar	1.7
Total	55.0	Total	45.0

b. Disorientation

Visitors who experience disorientation while searching for a retail are less than half the visitors (45%). The most common reason is that the retails that are searched look similar to each other from the size, sales, and color of the walls (15%). The second most reason is the corridor to branch retails (10%). The third most common reason is that retails are too dense and retails are too dense and look similar to each other's size, sales, and wall color (6.7%).

The fourth most common reason is that the size of the retails and the corridors that are passed when searching for a retails look the same (3.3%). Then the least reason put forward by visitors is that the merchandise sold look similar (1.7%). However, there is a reason that visitors never come to the same retail. This cannot be considered disoriented because it has never searched a retail that was visited before.

The reason visitors experience disorientation when searching for a retail because the retail looks similar from the size, sales, and color of the wall is a factor related to the absence of contrasting elements of the retail design with each other. The identity of a retail looks the same, there is no difference that contrasts with each other. This makes visitors unable to obtain information that can be used as a marker to remember the route. Then the reason about the size of the retails and the corridors that are passed looks the same and the merchandise sold look similar is also a functional disorientation factor that is a differentiation that does not contrast.

The reason visitors experience disorientation when searching for a retail is because the corridor to the branched retail describes the corridor line in MTC that forms the grid pattern. Corridor paths with grid patterns form branches at circulation meetings. The branching of the corridor shows that one of the spatial elements is that the path cannot direct visitors. Visitors are confused to choose the right path to find the retail to go to if the line is branched. Furthermore, the reason that the retail is too dense is the designer's functional perception. The functional perception of the designer that produces the design of the retail settings with such a small size gives a solid impression to the user. The retail seems crowded because of the small size of the retail and the squeaking of each other so that visitors can not look for the retail that has been visited.

Table 4. The reason and percentage of visitors who experience orientation and disorientation when choosing the approriate exit

Orientation Reason	**(%)**	**Disorientation Reason**	**(%)**
Memorize the corridors that pass through	15.0	Join the flow of other visitors	6.7
Same entry and exit positions	11.7	The corridor leads to the exit a lot, so it's wrong in	1.7
		Out of focus due to fatigue	1.7
Always pay attention to the signs	1.7	Wrong turn when descending from escalator	3.3
		The retail looks similar and the merchandise is in the corridor so the exit is not visible	3.3
Marking from the escalators position	20.0	Can't remember which floor	8.3
		Elevator position is hard to find	1.7
Remember the position in front of the mobile phone seller	1.7	Follow the escalator path that continues to the lower ground	8. 3
		Can't remember the corridors being passed through and no signage	3.3
The door looks large from the middle of the building	8.3	The door is blocked by the seller's desk	1.7
		The atmosphere of the corridors of each floor looks the same from the height of the ceiling, and the arrangement of the retail	1.7
Total	58.3	Total	41.7

5.4. Choose the appropriate exit

MTC exits are available quite a lot so this sometimes makes visitors experience orientation and disorientation when choosing the desired exit. Table 4 shows why and percentage of visitors who experience orientation and disorientation when choosing the appropriate exit.

a. Orientation

Based on the table above, visitors who experienced orientation when choosing the exit as desired were fewer than half the visitors (58.3%). The most reason visitors experience orientation is because it marks from the position of the escalator (20%). Then the second most reason for memorizing the corridors passed (15%). The third most reason for the same entrance and exit position (11.7%). The fourth most reason is because the door looks large from the center of the building (8.3%). Furthermore, the least reason from respondents is because always pay attention to the signs board and remember the position of the front exit of the mobile phone seller (1.7%).

The reason visitors are that when choosing the appropriate exit by marking the position of the escalator, strengthens the function of the escalator as a landmark. Escalators as landmarks have a strong imageability so the marker is easy to recognize (legibility) and is used as a guide in oriented and finding a way. The reason that visitors can choose the appropriate exit is because memorizing the corridors that pass through is related to the ability to remember. The ability to remember is helped by finding information from around the world to become a marker. The information is stored and becomes knowledge then referenced when the next visit.

The reason for the same entrance and exit position makes it easy for visitors to choose the appropriate exit, showing that the similarity of position when entering and exiting affects the visitor's memory to be oriented. The same entrance and exit positions are part of the consideration in functional orientation. The reason that the door looks large from the center of the building, is related to the size of an object being used as a marker to orient and find a way. Furthermore, the reason for paying attention to signs and remembering the position of the front exit of the mobile phone seller, shows that the importance of a signage and other markers besides signage to be oriented and find a way. Considering the position of the front exit of the mobile phone seller is also part of the ability to remember from the cognitive mapping process.

b. Disorientation

Visitors who experienced disorientation when choosing the exit were less than half the visitors (41.7%). The most reason visitors experience disorientation is because they do not remember which floor and follow the escalator path that continues to the lower floor (8.3%). Then the second most reason for joining the flow of other visitors (6.7%). The third most reason for the wrong turn when descending from the escalator, the retail looks similar and the merchandise is not neatly arranged so that the exit is not visible, and do not know which way to go and no directions (3.3%). Furthermore, the reason with the smallest percentage is because the corridor to the exit is so wrong, the reach becomes out of focus, the elevator position is hard to find, the exit is blocked by the sales desk, and the atmosphere of the corridor of each floor looks the same from the size, height of the ceiling, and the arrangement of the retail (1.7%).

The reason that visitors experience disorientation is because it does not remember which floor and follow the escalator path that continues to the lower floor, related to the lack of ability to remember the position of the exit so do not know the path that is passed to the exit. The second most reason for joining the flow of other visitors, shows the condition of visitors who follow the behavior of other visitors in the hope that the intended destination is in the same location. As a result, the intended exit is wrong because it follows the behavior of other visitors.

The third most reason is because of a wrong turn when descending from the escalator, can not remember the corridor that is passed and there are no signage, and the retail looks similar and the merchandise is in the corridor so the exit is invisible, related to the inability to remember, not knowing the signage, incontrasity of the design elements, and difficulty of visual access to the exit. The reason with the smallest percentage because the corridor to the exit is so much wrong to choose, out of focus due to fatigue, the position of the elevator is hard to find, the exit is blocked by the sales desk, and the atmosphere of the corridor of each floor looks the same from the size, height of the ceiling, and the arrangement of the retail, related to the path of incapable of directing, individual internal factors, invisible elevator position,

difficulty visual access to the exit, and incontrasion of design elements.

5.5. Searching for elevator when entering

The elevator is a means of transportation provided for visitors to visit the desired floor in addition to the escalator. Table 5 explains why visitors and their percentage experience orientation and disorientation when searching for elevator when entering.

a. Orientation

Based on the table above, visitors experience orientation when searching for elevator when entering less than a third of visitors (36.7%). The most reason visitors experience orientation when searching for an elevator when entering is because the elevator is visible from the basement (11.7%). The second most reason is that there are signage to the elevator so that visitors are directed to the elevator (10%). Then the third most reason is because of the memorization of the elevator position (8.3%). The fourth most common reason is because the elevator is visible from the outside (5%). The reason for having the smallest percentage is because many gather in front of the elevator (1.7%).

The reason visitors experience orientation when searching for an elevator when entering is because the elevator is visible from the basement and visible from the outside, related to the ease of visual access. The position of the elevator in the corner of the building is easily visible from the basement because there is a lot of empty space so the visual visitors immediately see the basement in the corner of the building. The elevator is quite good at displaying its image as a vertical means of transport from the basement because the surrounding space that supports the elevator stands out. Then the reason that visitors know the entrance because there are signage to the elevator when entering, related to the signage position is known location so that visitors use it to the elevator. This shows the importance of a signage as an orientation element in finding a way.

The reason visitors know the position of the elevator when entering is because it memorizes the position of the elevator, related to the ability to remember which is part of cognitive mapping. The ability to remember due to the information collected becomes a marker. This marker is then used as a reference so as to form a route to the destination. The next reason visitors experience orientation is because the elevator is visible from the outside, describing part of the situation of the MTC building's skin design that is transparent so that the elevator can be seen from the outside. The position of the elevator makes visitors can access it visually from the outside. Then the reason visitors experience orientation is because many gather in front of the elevator, showing the information obtained by visitors around MTC to find a way by seeing the behavior of others as a sign.

Table 5. Reasons and percentage of visitors who experience orientation and disorientation when searching for elevators when entering

Orientation		**Disorientation**	
Reason	**(%)**	**Reason**	**(%)**
Many gathered in front of the elevator	1. 7	The position is in the corner	6.7
		The path is confusing from the entrance	6.7
Elevator visible from the outside	5.0	Elevator not visible from entrance	38.3
There are signage	10.0	There is no signage to elevator	5.0
Elevator visible from basement	11.7	Not visible from basement stairs	1.7
		Covered by merchandise	1.7
Memorize elevator position	8.3	Covered by retails	3.3
Total	36.7	Total	63.4

b. Disorientation

Visitors who experienced disorientation when searching for elevators while entering were less than a third of visitors (63.3%). This percentage shows that most visitors find it difficult to find an elevator when entering. The most reason visitors experience disorientation when searching for an elevator when entering is because the elevator is not visible from the entrance (38.3%). The second most reason is because of its position in the corner and the confusing path from the entrance (6.7%). The third most reason is because there is no signage to the elevator (5%). The fourth most reason is because elevators are covered by retails (3.3%). Then the reason that has the smallest percentage amount is invisible from basement stairs and elevators covered by merchandise (1.7%).

The reason visitors when searching for an elevator, not visible from the entrance, shows that the position of the elevator is not immediately visible to incoming visitors. The visual perception of the designer wants to expose the elevator by putting it in the corner to be visible from the outside. However, the position is not visible from the entrance so visitors are confused to find the elevator upon entry. Then, the reason visitors that the position of the elevator is in the corner and the path leading to the elevator is confusing from the entrance, describing the position of the elevator that is unknown because it is in the corner. Visitors are confused because they do not find a marker that provides information about which angle the elevator is in. Visitors are also confused because the path is not able to steer so the path is confusing. The reason visitors because there are no signage to the elevator is related to not knowing the signage so visitors do not use signage.

The reason visitors experience disorientation is because elevators are covered by retails, describing the laying of elevators that are not visually accessible. Furthermore, the reason visitors are oriented with the smallest percentage because the elevator is not visible from the basement stairs and the elevator is covered by merchandise due to the position of the elevator that is in the corner and the corridor used to display the merchandise. The position of the elevator in the corner is not visible from the basement stairs located in the middle of the building so it is difficult to find due to the visual perception in designing. Therefore, a designer needs to know the environmental perception of the building user to be a guide in designing. Then, the elevator is covered by merchandise because most sellers put merchandise over the corridor boundary so that visual access is

blocked. This is because the corridor boundaries are dynamic and unclear so sellers use corridors to display merchandise. Therefore, the need to set static and clear corridor boundaries to make visitors oriented indoors.

5.6. Searching for elevator while circling

Previous discussions were discussed about searching an elevator when entering. It appears that the percentage of visitors who experience disorientation is more than those who experience orientation. This discussion will be discussed by visitors who are oriented and oriented when searching for elevators while circling around. Here's why and percentage of visitors in the table below.

a. Orientation

Visitors who experienced orientation when searching for elevator while circling were less than a third of visitors (31.7%). The most reason visitors experience orientation is because of its position in the finished corner when the circumference is visible (20%). The second most reason is because there are signage to the elevator (5%). The third most reason is due to position memorization (3.3%). Then the reason that has the smallest percentage is because MTC is small and the door looks large when roving (1.7%).

The most reason visitors are oriented when searching for an elevator when circling because of its position in the corner so when walking around is seen to be related to the visual access to the elevator when circling. This condition occurs because when circling, visitors browse all parts of the building including the corner of the building so that the elevator is visible and find the elevator.

Table 6. The reason and percentage of visitors who experience orientation and disorientation when searching for elevators while circling

Orientation		**Disorientation**	
Reason	**(%)**	**Reason**	**(%)**
The position is cornered, so when the circumference is visible	20.0	Lots of corridors turns to the elevator so hard to find	5.0
		Because not every corne there is an elevator, so confused which angle	48.3
There are signage to elevator	5.0	There are nosignage to elevator	1.7
Memorize elevator position	3.3	Covered by sales desks and retails	6.7
		Not visible from the middle of the building	3.3
MTC size is small	1.7	The location is not visible from the middle of the building and there are no signage	1.7
The door looks large when circling	1.7	There is no difference in the size of the corridor leading to the elevator with the other corridor so the corridor looks the same	1.7
Total	31.7	Total	68.3

The second most important reason visitors experience orientation is because there are signage to the elevator, showing the importance of a signage to orient the user. Visitors know and use signage because it has legibility properties. The third most reason is due to memorizing the position of the elevator, showing the ability to remember in the cognitive mapping that individuals have so as to imagine the routes that are passed to the elevator.

Then the reason with the smallest percentage of visitors experienced orientation because the size of MTC is small and the elevator door looks large when circling, related to the ability to remember individuals and design elements as markers. The ability to remember makes visitors can imagine the path being melted so feel that the size of MTC is small. Meanwhile, the elevator door that looks large when circling is associated with the design element as a marker. The large elevator door is a marker of the existence of the elevator. When visitors go around and through the elevator, the door can be seen by visitors so that visitors are oriented and know the existence of the elevator.

b. Disorientation

Visitors who experience disorientation when searching for elevators while circling in fewer than two-thirds of visitors (68.3%). This shows that most visitors experience disorientation or confusion searching for an elevator while circling. The reason most visitors experience disorientation is because the position of the elevator is in the corner so confused which angle because not all corners there are elevators (48.3%). The second most reason is because the elevator is covered by sales desks and retails (6.7%). The third most reason is because there are many corridor turns to the elevator so elevators are hard to find (5%). The fourth most reason is because the elevator is not visible from the center of the building (3.3%). Furthermore, the reason that has the smallest percentage is because there are no signage to the elevator, the location of the elevator is not visible from the center of the building and there is no signage, and there is no difference in the size of the corridor leading to the elevator with the other corridor so that the corridor looks the same (1.7%).

The biggest reason is because not every corner there is an elevator so visitors are confused as to which corner the elevator is in, related to the inconsistencies of the design elements. MTC's box-shaped space plan doesn't have a strong image of each corner so visitors don't get markers to distinguish each angle. The second most reason is because elevators are covered by sales desks and retails make visitors disoriented, dealing with visual access difficulties. The corner elevator position and the store setting are quite congested making the elevator blocked by rows of shops. The third most reason is because there are so many corridor turns to the elevator that the elevator is difficult to find, showing the grid pattern in the MTC circulation makes visitors not know the path to the elevator when circling. Circulation patterns in MTC that form grid patterns form branching points making visitors confused to determine the right turn to get to the elevator.

The fourth most reason for the elevator is not visible from the center of the building, describing visual access to the elevator is not visible in a strategic position in the building. The designer's visual perception puts the elevator in the corner so that the elevator can be exposed from the outside. As a result the elevator cannot be seen from the middle of the building. The reason with the smallest percentage is because there are no signage to the elevator, the location of the elevator is not visible from the middle of the building and there are no signage, and there is no difference in the size of the corridor leading to the elevator with the other corridor so that the corridor looks the same makes visitors experience disorientation. The absence of signage to the elevator shows the lack of legibility that signage has so visitors do not know and use existing signage. There is no difference in the size of the corridor leading to the elevator and the other corridor so the corridor looks the same, illustrating the lack of contrast between the corridor leading to the elevator and the other corridor. The lack of contrasting differences between corridors, resulting in corridors that have no legibility. As a result visitors have difficulty finding information that is used as a marker to remember the corridor leading to the elevator.

6. Conclusions and Suggestions

6.1. Conclusions

Based on the results of the research that has been discussed, the following conclusions can be drawn:

a. Factors related to the visitor's orientation experience are: spatial aspects, functional aspects, visual aspects, cognitive mapping, and behavior
b. Factors related to the visitor's disorientation experience are: spatial aspects, functional aspects, visual aspects, cognitive mapping, behavior, and internal individuals.
c. There are five factors in common with orientation and disorientation. However, there is one different factor that is the individual internal factor in the disorientation experience whereas in orientation is not found. This is because internal factors such as fatigue make it easy for a person to forget and not concentrate so that they experience disorientation.

6.2. Suggestions

In connection with the above conclusions, the following suggestions can be outlined:

a. Strengthens the legibility and imageability of spatial elements and functional elements as markers for easy reading or recognition and to evoke strong imagery in individual mental imagery.
b. In addition to the considerations in functional orientation that have been discussed in this study, there are still some other considerations to be used as research materials. Therefore, it is necessary to look for other considerations regarding functional orientation by some experts to see the relationship with spatial orientation.
c. This research was conducted before the pandemic, then further research is needed after the new normal.

References

[1] Narell, Mia Holland. *For Disorientation*. Tesis. Berkeley: University of California; 2016.
[2] Zahnd, Markus. *Pendekatan dalam Perancangan Arsitektur*. Yogyakarta: Kanisius; 2009.
[3] Rapoport, Amos. *Human Aspects of Urban Form: Towards a Man Environment Approach to Urban Form and Design*. Great Britain: Pergamon Press; 1977.
[4] Ahmed, Sara. *Queer Phenomenology: Orientations, Objects, Others*. United States of America: Duke University Press; 2006.
[5] Zube, Ervin H dan Moore, Gary T. *Advanced in Environment, Behavior, and Design*. *Volume 2*. New York: Plenum Press; 1989.
[6] Alan, Evision. *Oxford Learner's Pocket Dictionary*. New York: Oxford University Press; 1983.
[7] Departemen Pendidikan dan Kebudayaan R.I. *Pedoman Umum Ejaan Bahasa Indonesia yang Disempurnakan*. Jakarta: Balai Pustaka; 1975.
[8] Schulz, Christian Norberg. *Genius Loci: Towards a Phenomenology of Architecture*. New York: Rizolli International Publication Inc.; 1979.
[9] Lynch, Kevin. *A Theory of Good City Form*. Cambridge: The MIT Press; 1981.
[10] Kling, Beate dan Kruger Torsten. *Signage: Spatial Orientation*. Munich: Detail; 2013.
[11] Garling, Tommy dan Golledge, Reginald G. *Environmental Perception and Cognition*. Dalam: Zube, Ervin H dan Moore, Gary T (ed). Advances in Environment, Behavior, and Design. Volume 2. New York: Plenum Press; 1989.
[12] Ohta, Russel J. *Spatial Orientation in The Elderly: The Current Status of Understanding*. Dalam: Pick, Herbert L Jr dan Acredolo, Linda P (ed). Spatial Orientation: Theory, Research, and Application. New York: Plenum Press; 1983.
[13] Lynch, Kevin. *The Image of the City*. Cambridge: The MIT Press; 1960.
[14] Tanuwidjaja, Gunawan. Tinjauan Pustaka Wayfinding dan Orientation System, (Online), https://scribd.com/document/86547166/SS-Tinjauan-Pustaka-Way-Finding, 2012.
[15] Gibson, David. *The Wayfinding Handbook*. New York: Princeton Architectural Press; 2009.
[16] Ven, Cornelis van de. *Ruang dalam Arsitektur*. Jakarta: PT. Gramedia Pustaka Mandiri. 1995.
[17] Leatherbarrow, David. Disorientation and Disclosure. *Interstices Under Construction Symposium Unsettled Containers: Aspects of Interiority*, October 8-10th, 2010. University of Auckland, Auckland, New Zealand; 2010. pp 93-104.
[18] Coleman, Peter. *Shopping Environments: Evolution, Planning, and Design*. Italy: Architectural Press; 2006.
[19] Golledge, Reginald G., *Wayfinding Behavior, Cognitive Mapping, and Other Spatial Processes*. London: The Johns Hopkins University Press; 1999.
[20] Hunter, Rebecca H., Anderson, Lynda A., Belza, Basia L. Community Wayfinding: Pathways to Understanding. Switzerland: Springer International Publishing; 2016.
[21] Iskandar, Zulriska. *Psikologi Lingkungan*. Bandung: PT. Refika Aditama; 2016.
[22] Harisah, Afifah dan Masiming, Zulfitria. Persepsi Manusia terhadap Tanda, Simbol, dan Spasial. *Jurnal Smartek*. 2008; 6(1): 29-43.
[23] Haryadi dan Setiawan, B. *Arsitektur Lingkungan dan Perilaku*. Yogyakarta: Proyek Pengembangan Pusat Studi Lingkungan Direktorat Jendral Pendidikan Tinggi Departemen Pendidikan dan Kebudayaan Republik Indonesia; 1995.
[24] Indrawan, Rully dan Yaniawati, Poppy. *Metodologi Penelitian: Kuantitatif, Kualitatif, dan Campuran Untuk Manajemen, Pembangunan, dan Pendidikan*. Bandung: Refika Aditama; 2014.
[25] Dunn dan Rankin. *Scaling Methods*. New Jersey: Lawrence Elbaum; 2004.
[26] Azwar, Saifuddin. *Reliabilitas dan Validitas*. Yogyakarta: Pustaka Pelajar; 2006.

EPI International Journal of Engineering
Volume 3, Number 2, August 2020, pp. 192-199
DOI: 10.25042/epi-ije.082020.16

*p*ISSN 2615-5109
*e*ISSN 2621-0541

The Performance of Floating House Sub Structure in Tempe Lake

Rusdianto[a,*], Nasruddin[b], Hartawan Madeali[c]

[a]Architecture Department, Engineering Faculty, Hasanuddin University. Email:roesdi.a@gmail.com
[b]Architecture Department, Engineering Faculty, Hasanuddin University. Email:nas_junus@yahoo.com
[c]Architecture Department, Engineering Faculty, Hasanuddin University. Email:hartawan@unhas.ac.id

Abstract

This study aims to reveal the lifting power of the bamboo raft in holding the weight of the house on stilts so that it stays floating on the water. This research was conducted on the shores of Lake Tempe, precisely in Laelo Village, Tempe District, Wajo Regency. The method used in this research is a field study to determine the real situation in the field so that the real condition of the floating house is known. Furthermore, calculating the load used on the floating house based on the results of field studies. The final stage of the research is to test the raft lifting capacity of the floating house. The data will be analyzed according to Archimedes' Law, so that it can be seen that the bamboo raft can stay afloat even though it is given an Architectural building as heavy as a simple stilt house. The results of this study revealed that the average number of bamboos used as a raft was 175 stalks, and the mean diameter of bamboos was 7.67 cm or 0.077 m. It is known that the volume of the rod segment cavity is 0.103 m^3, so the total volume between sections on the floating raft on Lake Tempe is 18.058 m^3. The lifting capacity of bamboo rafts is directly proportional to the volume of bamboo joints used as rafts. The experimental test results obtained revealed that the lifting capacity of bamboo per m^3 was 874.51 kg, so the lifting capacity of the bamboo raft in Tempe Lake was 18.058 m^3 x 874.51 kg/m^3 = 15,789.13 kg. While the results of the calculation of the burden of a simple house are known by calculating the house's own load and the living load experienced by the house, and the weight of the house is 9,314.121 kg. With the ability to lift a bamboo raft of 15,789.13 kg, the difference between the lifting capacity of the bamboo raft and the weight of the floating house is 6,475.01 kg. The ideal number of bamboo culms is 129 with a safety factor of 25%. There is an efficient use of 46 bamboo sticks.

Keywords: Floating house; house performance; lower structure

1. Introduction

Tempe Lake is located in three administrative areas, namely Kab. Wajo, Soppeng and Sidrap. Having a large enough area makes Tempe Lake a fishing area by the surrounding community. The people who work as fishermen then set up a residential unit on top of Lake Tempe. This residential unit was established to bring the distance between the house and the fishing work location closer. This house functions as a resting place and a place to store fishing gear equipment, because the intensity of the fishing community in Tempe Lake is longer than on land, even though they already have a house on the mainland.

According to Jumawan [1] the floating house on Lake Tempe was first introduced by fishermen looking for fish in Lake Tempe. The house made by the fishermen is similar to the traditional bugis stilt house. Iskandar [2] stated that people who live on water build houses with structures that can anticipate climate change conditions. Some people use a raft system with wood and bamboo construction, such as those in the Musi River, Palembang, and the Barito River and Mahakam River in Kalimantan and in Lake Tempe, South Sulawesi [3].

In anticipating the climatic and environmental conditions in Lake Tempe, the community chose the raft system in the floating house structure. The system was chosen because the waters of Lake Tempe experience ups and downs according to climatic conditions, namely during the dry season, part of Lake Tempe waters will dry up, and in the rainy season, the lake water will overflow. This raft system is to make it easier for residential units to move according to water level [4]. The displacement of the residential unit follows climate change, during the dry season, when the lake water begins to decrease, the community settles into the middle of the lake, and moves to the shore of the lake during the rainy / flood season, which is when the water rises / overflows.

The floating house structure on Lake Tempe adopts the traditional Bugis stilt house structure, consisting of a lower, middle and upper structure. The uniqueness of this floating house structure is its substructure, which is a raft model made of bamboo. This bamboo raft serves as the

*Corresponding author. Telp. +62-821-9442-9038
Jalan Poros Malino km. 6 Bontomarannu
Gowa, Indonsia 92171

building foundation on it. On top of the raft is placed a house on stilts which has low pillars, the central structure consists of a plank floor, lower tie beam (pattolo riawa), upper tie beam (arateng), floor and wall beams, while the upper structure consists of a roof frame and a covering.

The use of bamboo rafts as a building foundation and being able to withstand the loads on it is something interesting to study, especially in the study of the lifting capacity of bamboo rafts against the loads on it. Therefore, this study intends to reveal the lifting power of the bamboo raft in holding the load of the house on stilts so that it remains floating on the water.

2. Literature Review

2.1. Performance

Kusnadi's menuru performance is something he wants to achieve [5]. Whereas in English, performance is called performance which means action, implementation, performance. The word perform is used when someone performs a task or process skillfully in accordance with existing procedures or conditions.

2.2. Data processing and analysis

Structure is a system, which means a combination or series of various kinds of elements which are assembled in such a way as to become one unified whole. In buildings, structure is defined as a series of main materials (materials) that produce a particular form or form.

Wardhono [6] stated that the structure in building science is a means to transmit the load and the consequences of the use and / or presence of a building on / on the ground. Meanwhile, Schodek [7] said that the study of structure involves understanding the basic principles that show and characterize the behavior of physical objects which are influenced by forces. The structure of the building consists of parts of the building that point to vertical / upright and horizontal / flat lines / planes, as well as sloping lines / planes [8].

2.3. Structure material

The material forming the structure in the building is in the form of building materials that are mixed and arranged in such a way as to become the elements in the structure. As stated by Schodek [7] that an easy approach in classifying structures is based on the type of material (eg wood, steel, or reinforced concrete structures). Knowledge of this material will be felt because of the close relationship between the causes of the structure to deform (as a result of external loads), the material, and the construction method of the structure.

2.4. Stability of the structure

The basic review in planning the structure is to ensure stability under all possible loading conditions. All structures undergo a certain change of shape when loaded. In stable structures, the deformation caused by loads is generally small, and the internal forces arising in the structure have a tendency to return the structure to its original shape when the load is removed. In unstable structures, the deformation caused by loads generally tends to increase as long as the structure is loaded. An unstable structure does not exert internal forces which have a tendency to return the structure to its original shape. Unstable structures are prone to collapse completely and immediately become overburdened [7].

2.5. Stability of the structure

Faoji [9] said the pedestal is a place of placement for support for the construction in continuing the loads working towards the foundation. In construction science there are 3 types of pedestals, namely pinch supports, joint supports and roller supports.

2.5.1. Pinch pedestals

The pinch support is also known as a rigid support which reacts to horizontal and vertical forces and is able to react to torque rotation. On the pinch pedestal, there are 3 variables that can be solved (Rv, Rh and M) as shown in Fig. 1.

2.5.2. Support joints

Joint support or hinge is a pedestal that works like a hinge. Support joints can withstand compressive forces and tensile forces from vertical and horizontal directions. On the pedestal there are two variables that can be solved (Rv and Rh) as shown in Fig. 2

2.5.3. Roller support

A roller support is a pedestal that slides horizontally. The support of the rollers cannot withstand horizontal forces and is only able to withstand the tensile and compression forces vertically. The roller supports also cannot withstand the moment or continue the moment, so that on this pedestal there is only 1 variable to be resolved (Rv). So the roller support has only one reaction force that is perpendicular to the roller as shown in Fig. 3.

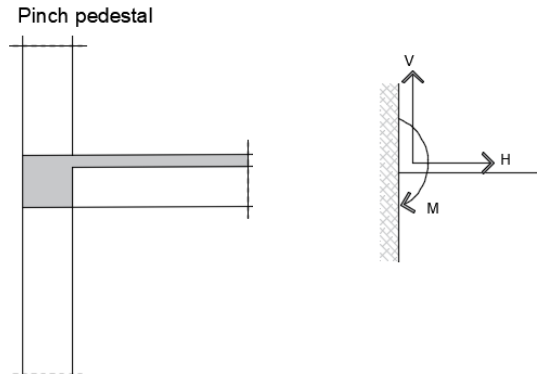

Figure 1. Clip pedestal

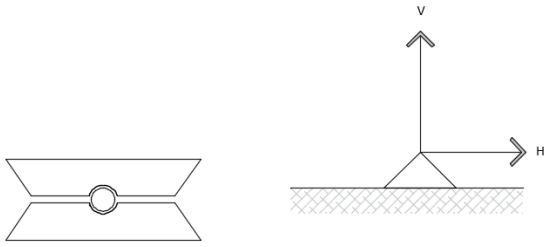

Figure 2. Support joints

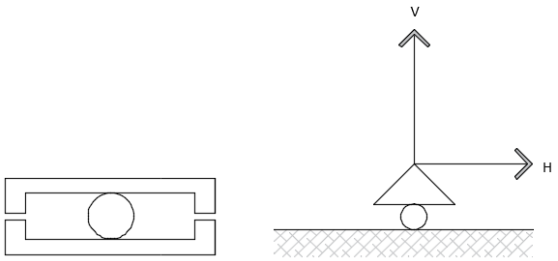

Figure 3. Roll support

2.6. Floating house

A floating house is a house that is above water and is floating, it is not permanent because it can move along with the tides and currents of the water. The existence of a floating house in the Lake Tempe area is an attempt by the community to approach their work location, because they are people who live from the waters in Lake Tempe. The floating house that is occupied is also a temporary house that functions not only for resting but also for storing fishing gear. This is confirmed by Naing [10], that fishing communities also have houses on land, but because fishermen activities in the waters take longer, people tend to live longer on water than on land.

2.7. Floating house

The shape of the floating house on Lake Tempe follows the shape of the Bugis stilt houses in general, which are commonly found in mainland areas. The basic difference between floating houses and houses on land is the base of the building, where the house on the mainland uses an umpak as its base, while the floating house on Lake Tempe uses a series of bamboo arranged to resemble a raft as its base.

The use of a raft as a building base has undergone a process of change according to the development needs of the fishing community at that time. As explained by Naing [11] that initially the community built kalampang (semi-permanent shelter/shelter made of wood/bamboo) as a shelter from heat or rain and a place to store fishing gear.

2.8. Floating house structure

The structure of the floating house on Lake Tempe follows the structure of traditional Bugis houses in general. The traditional Bugis house has a basic structure as stated by Pelras, [9], that the Bugis house has a basic structure consisting of three times three pillars (three long rows of columns and three rows wide) in a rectangular shape with one pole at each corner, and on on each side there is a central pole called the 'navel house' (posi 'ball).

2.9. Floating house structure

The materials used by the Bugis people are local materials that are easily available in the natural environment and vary widely by region. Likewise with the house on stilts on the water, the material used is generally from wood that is easily available around the water.

Types of traditional building materials used by the Bugis are aju betti (bitti wood), aju ippi (ipi wood), aju amara (amara wood), aju sandalwood (sandalwood), aju tippulu (tippulu wood), aju durian (wood durian), aju panasa (wood panasa), aju seppu (iron wood), palm sticks, coconut stems, bamboo, palm sticks, pindang stems, grass leaves and fibers. The use of this material depends on the ability and availability of funds for the home owner.

2.10. Floating house structure

Bamboo is one of the main materials in making floating house rafts in Tempe Lake. this is because bamboo material has long been known by the community, it is very easy to obtain and the price is relatively cheap. Ndale [12] explained that in Indonesia there are more than 13 species of bamboo which are commonly used by the community as building materials. Bamboo types in Indonesia are shown in Table 1.

Bamboo is a type of plant that is included in the Bamboidae which is a member of the grass sub-family, so it grows very fast. In addition, Janssen [13] describes the advantages and disadvantages of using bamboo. The advantages of using bamboo are that bamboo grows very fast and can be cultivated by the population, has good mechanical properties, the process requires simple tools and the outer shell contains a lot of silica which can protect bamboo. While the disadvantages are that bamboo requires preservation to obtain a long term of use, the shape of bamboo stalks is not exactly a cylinder but rather conical and bamboo is flammable.

Furthermore, Ndale [12] explained that bamboo is not prismatic in shape with a narrow cross section at the top, and has an unequal spacing of nodes along the stem. In one bamboo stick consists of the outer skin, outer bamboo, middle bamboo, inner bamboo.

Table 1. Types of bamboo in Indonesia [9]

Local Name	Scientific Name
Thorn bamboo, gesing bamboo, greng bamboo, haur cucuk, pring greng	*Bambusa Spinosa Bluemeana*
Bamboo thorn, pring ori	*Bambusa Bambos Cruce*
Awi krisik, chinese bamboo, pring gendani, pring cendani, bamboo fence	*Bambusa Multiplex Reausech*
Bamboo spotted, jajang ivory, awi koneng	*Bambusa Vulgaris Schrad*
Awi betung, petung bamboo, delin peting, jajang betung, pring petung	*Dendrocalamus Asper (Schult, F) Black ex Heyne*
Andong gombong, awi gombong, awi hideung, black bamboo, pring wulung, pereng sorat	*Gigantochloa Verticillite (Willa) Munro*
Longan bamboo, awi tela, longan bamboo	*Gigantochloa Nigrociliata*
Awi tali, bamboo tali, deling apus, pring tali, Pring Lear	*Gigantochloa Apus*
Awi long rope, awi tela	*Gigantochloa Hasskarlina (kurz) Back ex Heyne*
Pring unceu, chinese bamboo	*Phyllostashyum Aurea*
Awi bunar, awi tamiyang, pring wuluh, reed blowgun	*Schizostashyum Blumei Nees*
Bamboo perling, awi cakeutreauk	*Schizostashyum Zollingeri (Steud) Kurz*
Awi fur	*Schizostashyum Branchycladium Kurz*

2.10.1. Outer skin

The outer skin is the outermost or topmost part, usually green or black. The thickness of the bamboo skin is relatively uniform along the length of the stem, namely ± 1 mm, it is hard and stiff.

2.10.2. Outer bamboo

This part is located under the skin or between the outer and middle skin. The thickness of this section is ± 1 mm, it is hard and stiff.

2.10.3. Middle part

The middle part is located under the outside or between the outside and the inside, also called bamboo meat. The thickness is 2/3 the thickness of bamboo, and it is dense and elastic. For the middle part of the bottom, the fiber is a bit coarse.

2.10.4. The inside of the bamboo

The inside is the bottom part of the thick bamboo, often called the bamboo heart. The nature of the fiber is stiff and breaks easily.

Besides that, Morisco [14], also explained that bamboo has joints and books. Roots will also grow on these segments so that it is possible to multiply the plant from the pieces of each segment, in addition to the rhizome shoots.

Ndale [12], said that the specific gravity of bamboo is the ratio of the weight of bamboo to the weight of a volume of water which is equal to the volume of the bamboo. Furthermore, Handayani [15], said that the density and density of wood or bamboo are factors that will determine its physical and mechanical properties. This is because the density and density of bamboo are determined by the amount of wood substance. Bamboo density ranges from 0.5 - 0.9 gr/cm^3.

2.11. Lifting power in water

According to Archimedes [16], an object that is partially or completely immersed in water or other liquid will experience an upward force equal to the weight of the liquid being moved. The magnitude of this buoyancy depends on the amount of water the object is pushing. The greater the water being pushed, the greater the buoyancy force. When an object is immersed in a liquid, then there is 3 possibilities that occur, namely sinking, floating, and floating.

2.11.1. Submerged object

An object is said to be immersed in liquid if the object's position is always on the bottom where the liquid is as shown in Fig. 4. In submerged objects there are three forces, namely:

W = the object's gravity
Fa = Archimedes style
N = normal force of the plane

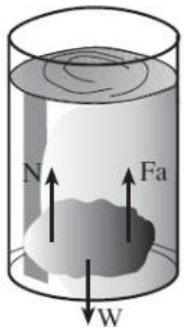

Figure 4. The sunken object [16]

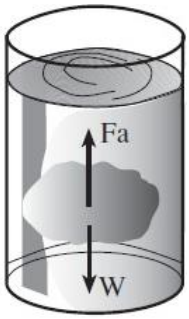

Figure 5. Floating object [16]

In a balanced state, $W = N + Fa$ so that:

$$W > Fa \tag{1}$$

$$m \cdot g > \rho ZC \cdot Vb \cdot g$$
$$\rho b \cdot Vb \cdot g > \rho ZC \cdot Vb \cdot g$$
$$\rho b > \rho ZC$$

where
ρb = density of the object
ρZC = density of the liquid

2.11.2. Floating object

Objects float in liquid when the position of the object is below the surface of the liquid and above where the liquid is as shown in Fig. 5. In floating objects there are two forces, namely *Fa* and *W*, in a balanced state:

$$W = Fa \tag{2}$$

$$\rho b \cdot Vb \cdot g = \rho ZC \cdot Vb \cdot g$$
$$\rho b = \rho ZC$$

2.11.3. Things float

An object floats in a liquid when the position of the object partly appears on the surface of the liquid and partly immersed in the liquid as shown in Fig. 6.

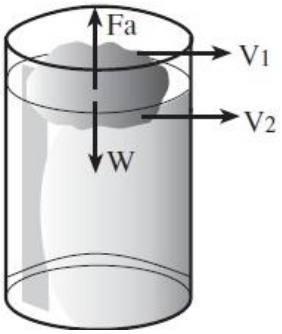

Figure 6. Things float [16]

Floating objects have two forces, namely: Fa and W, in a balanced state, then:

$$W < Fa \quad (3)$$

$$\rho b \cdot Vb \cdot g < \rho ZC \cdot V_2 \cdot g$$

$$\rho b \cdot Vb < \rho ZC \cdot V_2$$

because $Vb < V2$ then $\rho b = \rho ZC$

3. Research Methods

This research was conducted by using field survey methods, literature studies and experimental tests. The variable studied was a bamboo raft in a floating house on Lake Tempe. The research object chosen was a floating house with a simple and natural construction and approaching the shape of a Bugis stilt house. Experimental tests were carried out by making a bamboo raft model that was placed in the water, then gradually given the load on it. Each additional load will affect the water level, so it can be seen the buoyancy force of the bamboo raft. The analysis of buoyancy is based on Archimedes' Law which states that the magnitude of the buoyancy is equal to the weight of the liquid that is being pushed (moved).

4. Results and Discussion

Based on the results of surveys and field observations and interviews with residents, it can be seen that the floating house which is the object of the research has been established for 10 years and has experienced the addition and replacement of bamboo on the raft 3 times gradually, according to the level of damage to the bamboo. The following image shows the shape of the floating house which is the object of research.

The lifting capacity of a bamboo raft to a floating house is based on the ability of a bamboo raft to stay afloat even when given the weight of a simple house. To determine the lifting capacity, this research was carried out by testing the load giving to the bamboo raft.

The raft model made from dried bamboo and cut to a length of 300 cm, then immersed in a water pool with a size of 688x100x70 cm. This pool is filled with water as high as 26 cm. When the bamboo raft is put into a pool filled with water, it floats. This happens because the density of bamboo is less than the density of water. As stated by Ndale, 2013, that the specific gravity of bamboo ranges from 0.5 - 0.9 gr/cm^3. While the specific gravity of water is 1 g/cm^3, meaning that bamboo can float in the water.

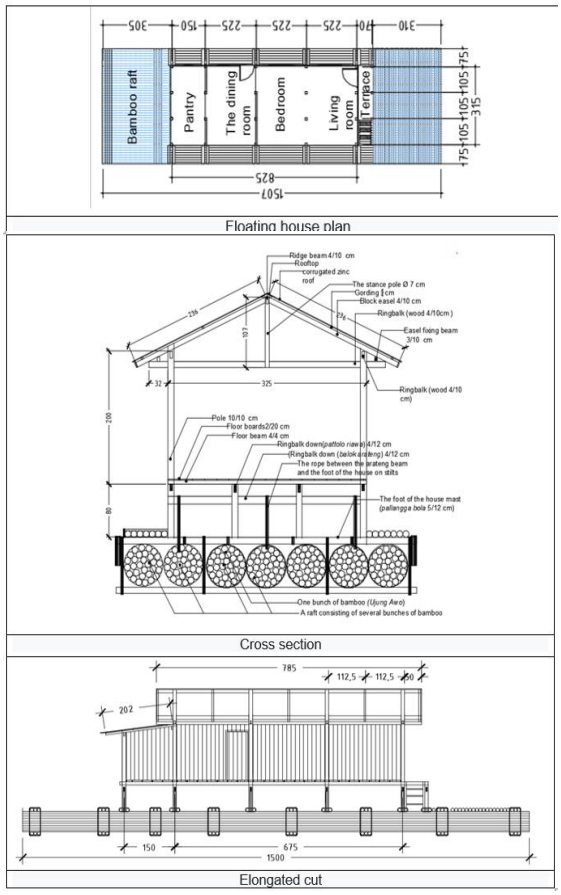

Figure 7. Sketches of floating houses as research objects

The buoyancy of bamboo culms is also influenced by the volume of the cavity between the closed sections of bamboo. Inside the cavity contains air so that it affects the density of the bamboo.

Experimental tests were carried out using 10 pieces of bamboo with a length of 300 cm and the volume of different sections because the diameter of the bamboo was different and so were the lengths of the sections. The calculated segment volume is the volume of the inner and closed cavity, so that water cannot enter. The differences in the volume of these sections are shown in the following table.

Table 2. Results of calculation of cavity volume in experimental bamboo sections

No	Descr.	Bamboo dimensions			
		Inner Dia. of Bamboo (m)	Segments Average Length (m)	No of Segments /Stems	Volume of Segments (m^3)
1	Bamboo 1	0.067	0.484	5	0.009
2	Bamboo 2	0.058	0.463	6	0.007
3	Bamboo 3	0.054	0.495	5	0.006
4	Bamboo 4	0.070	0.435	6	0.010
5	Bamboo 5	0.057	0.328	9	0.008
6	Bamboo 6	0.059	0.482	6	0.008
7	Bamboo 7	0.069	0.502	5	0.009
8	Bamboo 8	0.062	0.458	6	0.008
9	Bamboo 9	0.062	0.326	8	0.008
10	Bamboo 10	0.050	0.486	5	0.005

The ten pieces of bamboo were then formed into a raft, starting from the first 2, 3, 4, to 5. Then the final raft is made of 10 sticks composed of 2 bundles containing 5 bamboo sticks each.

In testing, each raft that was made was placed into a pool that was filled with water. When the raft is placed into a pool filled with water, the water level of the pool rises, which indicates that there is pressure on the pool water. Likewise, when the raft is given loads gradually.

Experiment 1 was carried out using a raft of 2 bamboo sticks (bamboo 1 and 2). When the raft is put into the pool, the water level becomes 0.261 m. Then the raft was given a load of 4.30 kg in stages, then added by 4.24 kg, so that the total load given to the raft of 2 bamboo sticks weighing 8.54 kg was obtained. As a result of the load, the water level changes to 0.262 m at load 1 and 0.263 m after the load is added.

Followed by experiment 2, using a raft of 3 bamboo sticks (bamboo 1, 2 and 3). Then experiment 3 with 4 bamboo stalks, experiment 4 with 5 bamboo sticks and experiment 5 with 10 bamboo sticks consisting of 2 bundles containing 5 bamboo sticks each.

In experiment 5, from the results of the calculations presented in table 1, it is known that the average inner diameter is ± 0.061 m, the length (distance between) sections is ± 0.45 m, the total volume of cavity of the bamboo segment used is 0.077 m^3. The experimental results can be seen in the Fig. 8.

The graph in Figure 8 above shows the change in the water level of the pool after inserting the bamboo raft and adding the load gradually on it. Changes in the water level of the pool depend on the number of bamboos made into the raft and the weight of the loads placed on the raft. The change in the water level of the pool indicates that the more bamboo is made into a raft and the heavier the load is added to the raft, the greater the volume of water pressed. The amount of water volume pressed is influenced by the weight of the bamboo and the additional load on the experimental bamboo raft.

Based on Archimedes' Law which states that when an object is immersed in a liquid, either partially or completely, the object will get a buoyancy (upward force) which is equal to the weight of the liquid being pushed (moved) by the object. This means that any change in the water level in the experimental pool can be said to be the magnitude of the buoyancy force of objects in the water.

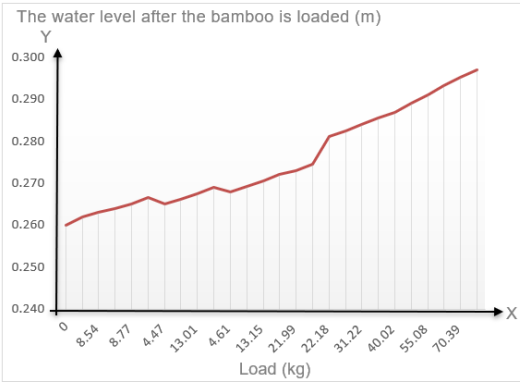

Figure 8. Graph of changes in pool water level

Therefore, in an effort to obtain bamboo lifting capacity, it is necessary to know the volume of water pressed due to the insertion of the bamboo raft into the pool and the load on the raft, because the volume of water pressed is equal to the weight of the bamboo raft and the load given to it.

Table 2 explains that the more bamboo is put into the pond, the greater the volume of water pressed. Likewise, the heavier the load added on the bamboo, the greater the volume of water pressed as shown in Table 3. The volume of water pressed is influenced by the weight of the bamboo raft and the additional load on the raft. The volume of water that is pressed is the difference from the volume of water increase due to the load on the bamboo raft that is inserted into the pond with the volume of pool water before being treated.

Furthermore, to obtain the lifting capacity of the bamboo raft in the above experiment, the difference in the volume of pressed water in each experiment is multiplied by the density of water, where it is known that the density of water is 1 g/cm^3 or 1000 kg/m^3.

Based on the results of the calculations shown in Table 4, it can be seen that from the experimental results, the average lift capacity on a bamboo raft is 874.51 kg/m^3.

Table 3. Results of the calculation of the volume of pressed water

No	Number of bamboo stems	Bamboo raft weight	Load	Volume of water pressed
	Ties (1-2 ties)	(kg)	(kg)	(m^3)
1	2 bamboo sticks (1 bunch)	7.56	4.30	0.00681
		7.56	8.54	0.01110
2	3 bamboo sticks (1 bunch)	13.18	4.30	0.00681
		13.18	8.77	0.01362
		13.18	13.01	0.02384
3	4 bamboo sticks (1 bunch)	19.13	4.47	0.00749
		19.13	8.71	0.01430
		19.13	13.01	0.02384
		19.13	17.62	0.03374
4	5 bamboo sticks (1 bunch)	23.64	4.61	0.00681
		23.64	8.91	0.01984
		23.64	13.15	0.02452
		23.64	17.62	0.03406
		23.64	21.99	0.04019
		23.64	26.48	0.05040
5	10 bamboo sticks (2 bunch)	47.01	22.18	0.04867
		47.01	26.67	0.05108
		47.01	31.22	0.06130
		0.077	35.72	0.07517
		47.01	40.02	0.08053
		47.01	47.60	0.09536
		47.01	55.08	0.10898
		47.01	62.85	0.12464
		47.01	70.39	0.13827
		47.01	75.00	0.14985

Table 4. The results of the calculation of the lifting capacity of bamboo rafts

No	Number of bamboo stems	Urgent volume of water	Bamboo lifting power	Bamboo lifting power is average
		(m^3)	(kg)	(kg/m^3)
1	2 bamboo sticks (1 bunch)	0.00681	6.81	429.21
		0.01110	11.10	699.62
2	3 bamboo sticks (1 bunch)	0.00681	6.81	316.29
		0.01362	13.62	632.59
		0.02384	23.84	1,107.03
3	4 bamboo sticks (1 bunch)	0.00749	7.49	237.30
		0.01430	14.30	453.02
		0.02384	23.84	755.03
		0.03374	33.37	1,057.04
4	5 bamboo sticks (1 bunch)	0.00681	6.81	167.29
		0.01984	14.98	368.03
		0.02452	24.52	602.23
		0.03406	34.06	836.43
		0.04019	40.19	986.98
		0.05040	50.40	1,237.91
5	10 bamboo sticks (2 bunch)	0.04867	40.87	530.34
		0.05108	51.08	662.92
		0.06130	61.30	795.51
		0.07517	71.52	928.09
		0.08053	81.05	1,051.84
		0.09536	95.36	1,237.46
		0.10898	108.98	1,414.24
		0.12464	124.64	1,617.53
		0.13827	138.27	1,794.31
		0.14985	149.85	1,944.57
Lifting power is average				**874.51**

Table 5. Data on bamboo rafts on floating houses in Lake Tempe

No	Description	Volume	Unit
1	The amount of bamboo used	175	stem
2	Length of bamboo in stem	15	m
3	Inner diameter of stem section	8	cm
4	Inner diameter of the middle	9	cm
5	Inner diameter of the end	6	cm
6	The length of the bamboo segment	43	cm
7	The average number of segments in one stem	29	section

Meanwhile, to determine the lifting capacity of the bamboo raft to the floating house in Lake Tempe, it is done by multiplying the total volume of bamboo knots with the average lifting capacity of bamboo per cubic meter. From the field survey conducted at the research location, data is obtained as presented in Table 5.

From the data in Table 5, it is known that the mean diameter of the hollow sections of bamboo is 7.67 cm or 0.077 m and the number of bamboo sections per stick is 29 sections. So the volume of a bamboo segment per stem is 0.77 x 29 = 0.104 m^3. Meanwhile, the total volume of hollow sections of bamboo used in the floating house raft in Tempe Lake is 0.104 m3 x 175 rods = 18.058 m^3. Then the lifting capacity of the bamboo raft in the floating house is 18.058 m^3 x 874.51 kg / m^3 = 15,789.13 kg.

Meanwhile, the results of the calculation of the weight of the house are known by calculating the house's own load and the living load experienced by the house, and the results of the house weight are 9,314.121 kg. With the ability to lift a bamboo raft in a floating house of 15,789.13 kg, the number of bamboo sticks that should be used in making bamboo rafts at floating houses in Lake Tempe are:

$$Jb2 \div BrA = Jb1 \div DaRb \quad (4)$$

$$Jb2 \div 9.314{,}121 \text{ kg} = 175 \div 15.789{,}12 \text{ kg}$$

$$Jb2 = 1.629.971{,}18kg \div 15.789{,}13kg$$

$$Jb2 = 103{,}23 \approx 104 \text{ stem}$$

From the calculation above, it is found that the number of bamboo sticks that should be used in the floating house in Tempe Lake is 104 sticks.

5. Conclusion

The magnitude of this buoyancy depends on the amount of water that is pushed (moved) by the object. Based on the test, it was found that the greater the cavity volume of the bamboo segment, the greater its lifting capacity. Lifting power is obtained by calculating the difference in the volume of water in a pond that has been filled with bamboo and given a load with the volume of water in the pool without any load on the bamboo. Furthermore, the difference in the volume of water pressed is multiplied by the density of the water and divided by the number of stages of giving the load, then the average lifting capacity of bamboo is obtained to be 874.51 kg / m^3.

In the research object, namely the floating house on Lake Tempe, with 175 bamboo rods used as rafts, with an average diameter of 7.67 cm or 0.077 m, the volume between the sections per rod was 0.103 m^3. So the total volume between sections on the floating house raft at Lake Tempe is 0.103 m3 x 175 rods = 18.058 m^3, so that the bamboo raft lift capacity is 18.058 m^3 x 874.51 kg / m^3 = 15,789.13 kg.

Acknowledgements

Thanks are conveyed to the supervisors and thesis examiners, as well as the lecturers and staff at the Department of Architecture, Faculty of Engineering, Hasanuddin University. Especially to parents, wife, children and siblings for all their support and prayers.

References

[1] Jumawan, Faris. 2017. Tempe Lake Fishermen's Residence, Soppeng Regency. Celebes Media Perkasa. Makassar.

[2] Iskandar, Yulindiani. 2010. Local Wisdom in the Completion of Structure and Construction of Raft Houses on the Musi River - Palembang. Lokal Wisdom (Local Wisdom Scientific Online Journal). Volume II, Number 2, pages 37-45, March 2010.

[3] Naing, Naidah. 2009. Traditional Local Wisdom of Fishermen Communities in Floating Settlements on Lake Tempe, South Sulawesi. Lokal wisdom (Local Wisdom Scientific Oline Journal), volume 1, number 1 pages 19-26, March 2009
[4] Naidah. 2011. Moving Settlements in a Floating House System as a Process of Human Adaptation to the Environment in Lake Tempe, South Sulawesi. Postgraduate Dissertation, Sepuluh November Institute of Technology, Surabaya.
[5] Kusnadi. Complete Dictionary of Indonesian Language (latest edition). CV Cahaya Agency. Surabaya.
[6] Wardhono, Uniek Praptiningrum. 2009. Architectural Glossary. Dictionary of Terms in Architecture. Publisher Andi Yogyakarta
[7] Schodek, Daniel L. 1998. Structure. Publisher PT. Refika Aditama. Bandung.
[8] Tangoro, Dwi. 2015. Building Science. High Span and Tall Building Structures. Publisher UI Press. Jakarta.
[9] Faoji, Ahmad, 2018. Comparison of Fixed and Pinned on Structures Power House is Reviewed from Material Efficiency and Costs (Case Study of Peaker Seram PLTMG Project)
[10] Naing, Naidah,2011. Moving Settlements in a Floating House System as a Process of Human Adaptation to the Environment in Lake Tempe, South Sulawesi. Postgraduate Dissertation, Sepuluh November Institute of Technology, Surabaya.
[11] Naing, Naidah,2011. Bugis Floating House. Nusa Cendekia Publisher, printed I, November 2018.
[12] Ndale, Fransiscus. 2013. Sifat Fisik dan Mekanik Bambu sebagai Bahan Konstruksi. Jurnal Teknik Universitas Flores. Volume 7. Nomor 2. Oktober 2013.
[13] Janssen J.J.A., 1980, The Mechanical Properties of Bamboo Used in Cuntruction, 173 – 188. In Lessard, G. & Chouinard, A., Bamboo Research in Asia, IDRC, Canada.
[14] Morisco, 1999, Bamboo Engineering, Nafiri Offset, Yogyakarta.
[15] Handayani, 2007. Bamboo Mechanical Properties Testing. Journal of Civil Engineering and Planning no.1, volume January 9, 2007.
[16] Untoro, Joko. 2009. SMA Physics Smart Books for Grades 1, 2 and 3. Wahyu Media Publisher. Jakarta.